

**IFS DOCUMENTATION – Cy38r1**  
**Operational implementation 19 June 2012**

**PART II: DATA ASSIMILATION**

**Table of contents**

[Chapter 1 Overview](#)  
[Chapter 2 4D variational assimilation](#)  
[Chapter 3 Tangent-linear physics](#)  
[Chapter 4 Background term](#)  
[Chapter 5 Observation operators and observation cost function \( \$J\_o\$ \)](#)  
[Chapter 6 Background, analysis and forecast errors](#)  
[Chapter 7 Gravity-wave control](#)  
[Chapter 8 Diagnostics](#)  
[Chapter 9 Observation processing](#)  
[Chapter 10 Observation screening](#)  
[Chapter 11 Land-surface analysis](#)  
[Chapter 12 Analysis of sea-ice concentration and sea surface temperature](#)  
[Chapter 13 Data flow](#)  
[References](#)

© Copyright 2013

European Centre for Medium-Range Weather Forecasts  
Shinfield Park, Reading, RG2 9AX, England

Literary and scientific copyrights belong to ECMWF and are reserved in all countries. This publication is not to be reprinted or translated in whole or in part without the written permission of the Director. Appropriate non-commercial use will normally be granted under the condition that reference is made to ECMWF. The information within this publication is given in good faith and considered to be true, but ECMWF accepts no liability for error, omission and for loss or damage arising from its use.



# Chapter 1

## Overview

### Table of contents

- [1.1 Introduction](#)
- [1.2 Scientific publications](#)
- [1.3 Brief history of 3D- and 4D-Var in ECMWF operations](#)
- [1.4 Incremental formulation of variational data assimilation](#)

### 1.1 INTRODUCTION

This documentation of 4D-Var serves as a scientific guide to the data assimilation code within ECMWF's Integrated Forecasting System (IFS). The documentation is divided into a number of chapters. This first chapter provides an overview of ECMWF's data assimilation system, a brief history of its evolution and a description of the basic scientific formulation.

The second chapter describes the practical implementation of the multi-resolution incremental method for 4D-Var data assimilation (the multi-resolution version has been used operationally since January 2003, Cy25r3), and the solution algorithm including minimization and preconditioning. The tangent linear physics that is an important part of the variational algorithm is described in [Chapter 3](#). Thereafter follows a description of the background term ([Chapter 4](#)) and a chapter on observation operators and the organisation of observation cost-function calculations for conventional and satellite data ([Chapter 5](#)). [Chapter 6](#) deals with the computation and cycling of background and analysis errors including the recent use of EDA variances. [Chapter 7](#) is on control of gravity waves in the minimization cycle. Diagnostic tools for investigation of the performance of the assimilation system are described in [Chapter 8](#). The modules for observation selection, quality control and screening are described in [Chapter 9](#) and [Chapter 10](#). [Chapter 11](#) describes the land surface analysis, including the screen level parameters, the soil analysis and the snow analysis, [Chapter 12](#) describes the sea surface temperature and sea-ice analysis. Finally [Chapter 13](#) provides summary information about the main unix-scripts and important files, and a schematic of the data flow between the various jobs steps that constitute a data assimilation cycle.

### 1.2 SCIENTIFIC PUBLICATIONS

The scientific description of 3D/4D-Var has been published in a series of papers in the *Quarterly Journal of the Royal Meteorological Society* (QJRMS), in ECMWF workshop proceedings and Technical Memoranda over the years. The incremental formulation was introduced by [Courtier \*et al.\* \(1994\)](#). The ECMWF implementation of 3D-Var was published in a three-part paper by [Courtier \*et al.\* \(1998\)](#), [Rabier \*et al.\* \(1998\)](#) and [Andersson \*et al.\* \(1998\)](#). The original observation operators for conventional data can be found in [Vasiljevic \*et al.\* \(1992\)](#). The methods for assimilation of TOVS radiance data and ERS scatterometer data were developed by [Andersson \*et al.\* \(1994\)](#) and [Stoffelen and Anderson \(1997\)](#), respectively. The pre-operational experimentation with 4D-Var has been documented in three papers by [Rabier \*et al.\* \(2000\)](#), [Mahfouf and Rabier \(2000\)](#) and [Klinker \*et al.\* \(2000\)](#). The background term has been published by [Derber and Bouttier \(1999\)](#), with more recent developments described by [Fisher \(2003\)](#).

Papers of data usage and impact include a study of commercial aircraft data ([Cardinali \*et al.\*, 2003](#)), scatterometer impact ([Isaksen, 1997](#); [Isaksen and Stoffelen, 2000](#); [Isaksen and Janssen, 2004](#)), conventional and satellite humidity data ([Andersson \*et al.\*, 2004](#)), ozone analysis ([Dethof and Holm, 2004](#)), time series of frequent data ([Andersson \*et al.\*, 2001](#)), wind profiler data ([Bouttier, 2001b](#); [Andersson and Garcia-Mendez, 2002](#)), TOVS radiance data ([McNally \*et al.\*, 1999](#)), water-vapour

radiances from geostationary satellites (Munro *et al.*, 2004; Köpken *et al.*, 2004), and the use of high-volume satellite data in general (Thépaut and Andersson, 2003). An more complete overview of data usage at ECMWF is included in the reanalysis review paper by Dee *et al.* (2011).

### 1.3 BRIEF HISTORY OF 3D- AND 4D-VAR IN ECMWF OPERATIONS

3D-Var was implemented in ECMWF operations on 30 January 1996, and was replaced on 25 November 1997 by 4D-Var. The two three-part series of QJRMS papers mentioned above basically describe the two schemes as they were at the time of their implementation. However, there have been very significant developments of the variational data assimilation system during its time in operations. Major code-upgrades have taken place in connection with migrations to new computers. 3D-Var was first implemented on a CRAY C90 shared-memory parallel computer system and was migrated to a distributed-memory Fujitsu VPP700 machine in September 1996 (Dent *et al.*, 1997). Further migrations of the codes took place in May 2000 to a Fujitsu VPP5000, and in March 2003 to an IBM P690, and later in 2004 to an IBM P690+. A history of the evolution of ECMWF super-computing is available at [http://www.ecmwf.int/services/computing/overview/supercomputer\\_history.html](http://www.ecmwf.int/services/computing/overview/supercomputer_history.html). The current IBM implementation of the assimilation system utilizes both shared-memory (OpenMP) and distributed-memory (MPI) parallelism. A general list of changes to the operational forecasting system is available at [http://www.ecmwf.int/products/data/technical/model\\_id/index.html](http://www.ecmwf.int/products/data/technical/model_id/index.html).

The observation handling and data screening modules have also developed rapidly to keep pace with the changing computer environment, and the arrival of new observational data sets. The codes inherited from OI were replaced with new codes at the time of the migration to Fujitsu in 1996. The need for improved parallelism and rapidly increasing data volumes lead to the development of the Observation DataBase (ODB) software (see ODB documentation), facilitating in March 2003 the move to the IBM computers and the introduction of high-spectral resolution satellite data (first AIRS and then IASI in 2009) as well as the use of radio occultation data (GPSRO) in 2008. The quality control, data selection and screening algorithms are described in the paper by Järvinen and Undén (1997), and variational quality control of observations in Andersson and Järvinen (1999). Since 2009 the variational quality control of conventional observations uses the Huber norm (Tavolato and Isaksen, 2010).

One of the most important aspects of a variational assimilation is the specification of background errors. The original formulation of Courtier *et al.* (1998) was replaced in May 1997 by that of Derber and Bouttier (1999). The latter formulation is still used as described in Chapter 4, including more recent improvements such as non-linear balance (January 2003, Cy25r3, Fisher (2003)), wavelet-Jb (April 2005, Cy29r1, Fisher (2006)), introduction of ozone as an analysis variable (Dethof and Holm, 2004) in October 1999 (Cy21r4), the new humidity analysis (Hólm *et al.*, 2002) in October 2003 (Cy26r3), and Jb for GEMS variables (Benedetti and Fisher, 2006). The cycling algorithms for analysis and background errors (Fisher and Courtier, 1995, and Chapter 6) were introduced in 1996. The calibration of background error statistics is since October 1999 based on an ensemble of 3D-Var data assimilations, updated in January 2003 to statistics based on a 4D-Var ensemble (Fisher, 2003). Since May 2011 the Ensemble Data Assimilation (EDA) provides flow dependent background error standard deviations for vorticity on each cycle (Bonavita *et al.*, 2012a).

On the 25th November 1997 6-hourly 4D-Var was introduced operationally, at resolution T213L31, with two iterations of the outer loop: the first at T63L31 with 50 iterations (simplified physics) and the second with 20 iterations (with tangent-linear physics, at same resolution). In April 1998 the resolution was changed to T<sub>L</sub>319 and in June 1998 we revised the radiosonde/pilot usage (significant levels, temperature instead of geopotential) and we started using time-sequences of data (Järvinen *et al.*, 1999), so-called 4D-screening. The data assimilation scheme was extended higher into the atmosphere on 10 March 1999, when the T<sub>L</sub>319L50 model was introduced, which in turn enabled the introduction in May 1999 of ATOVS radiance data (McNally *et al.*, 1999). In October 1999 the vertical resolution of the boundary layer was enhanced taking the number of model levels to a total of L60. In summer 2000 the 4D-Var period was extended from 6 to 12 hours (Bouttier, 2001a), whereas the ERA-40 configuration (Uppala *et al.*, 2005) was built as an FGAT (first guess at the appropriate time) of 3D-Var with a period of 6 hours (Chapter 3). In November 2000, the horizontal resolution of 4D-Var was increased to T<sub>L</sub>511L60, with inner loop resolution enhanced from T63L60 to T<sub>L</sub>159L60 using the linearized semi-Lagrangian scheme. In

February 2006, the horizontal resolution of 4D-Var was increased to T<sub>L</sub>799L91, with inner loop resolution enhanced to T<sub>L</sub>255L91. The horizontal resolution was increased to T<sub>L</sub>1279L91, with unchanged inner loop resolution. The ERA-interim reanalysis also used 12 hour 4D-Var at T<sub>L</sub>255L60 resolution, with T<sub>L</sub>159L60 inner loop resolution [Dee et al. \(2011\)](#).

In January 2003 the 4D-Var solution algorithm was comprehensively revised (in Cy25r4, [Andersson et al., 2003](#)) to take advantage of the efficiency of conjugate gradient minimisation (with pre-conditioning, as introduced one year earlier) and a multi-resolution incremental technique ([Veerse and Thépaut, 1998](#); [Trémolet, 2005](#)). This is the 4D-Var solution algorithm that is presented here in [Chapter 2](#). The early delivery suite was introduced in June 2004 (in Cy28r2, [Haseeler, 2004](#)).

## 1.4 INCREMENTAL FORMULATION OF VARIATIONAL DATA ASSIMILATION

In 3D/4D-Var an objective function  $J$  is minimized. The cost function consists of three terms:

$$J = J_b + J_o + J_q + J_c \quad (1.1)$$

measuring, respectively, the discrepancy with the background (a short-range forecast started from the previous analysis),  $J_b$ , with the observations,  $J_o$ , with the model error,  $J_q$ , and with the slow character of the atmosphere,  $J_c$ . The  $J_q$  term is under active development and is not described further here, but see [Fisher et al. \(2011\)](#). The  $J_c$ -term controls the amplitude of fast waves in the analysis and is described in [Chapter 7](#). It is omitted from the subsequent derivations in this section.

In its incremental formulation ([Courtier et al., 1994](#)), we write

$$J(\delta\mathbf{x}) = \frac{1}{2}\delta\mathbf{x}^T\mathbf{B}^{-1}\delta\mathbf{x} + \frac{1}{2}(\mathbf{H}\delta\mathbf{x} - \mathbf{d})^T\mathbf{R}^{-1}(\mathbf{H}\delta\mathbf{x} - \mathbf{d}) \quad (1.2)$$

$\delta\mathbf{x}$  is the increment and at the minimum the resulting analysis increment  $\delta\mathbf{x}^a$  is added to the background  $\mathbf{x}^b$  in order to provide the analysis  $\mathbf{x}^a$  given by

$$\mathbf{x}^a = \mathbf{x}^b + \delta\mathbf{x}^a \quad (1.3)$$

$\mathbf{B}$  is the covariance matrix of background error while  $\mathbf{d}$  is the innovation vector

$$\mathbf{d} = \mathbf{y}^o - \mathbf{H}\mathbf{x}^b \quad (1.4)$$

where  $\mathbf{y}^o$  is the observation vector.  $\mathbf{H}$  is a suitable low-resolution linear approximation of the observation operator  $H$  in the vicinity of  $\mathbf{x}^b$ , and  $\mathbf{R}$  is the covariance matrix of observation errors. The incremental formulation of 3D/4D-Var consists therefore of solving for  $\delta\mathbf{x}$  the inverse problem defined by the (direct) observation operator  $\mathbf{H}$ , given the innovation vector  $\mathbf{d}$  and the background constraint. The gradient of  $J$  is obtained by differentiating (1.2) with respect to  $\delta\mathbf{x}$  to give

$$\nabla J = (\mathbf{B}^{-1} + \mathbf{H}^T\mathbf{R}^{-1}\mathbf{H})\delta\mathbf{x} - \mathbf{H}^T\mathbf{R}^{-1}\mathbf{d} \quad (1.5)$$

At the minimum, the gradient of the objective function vanishes, thus from (1.5) we obtain the classical result that minimizing the objective function defined by (1.2) is a way of computing the equivalent matrix-vector products given by

$$\delta\mathbf{x}^a = (\mathbf{B}^{-1} + \mathbf{H}^T\mathbf{R}^{-1}\mathbf{H})^{-1}\mathbf{H}^T\mathbf{R}^{-1}\mathbf{d} = \mathbf{B}\mathbf{H}^T(\mathbf{H}\mathbf{B}\mathbf{H}^T + \mathbf{R})^{-1}\mathbf{d} \quad (1.6)$$

where  $\mathbf{B}$  and  $\mathbf{R}$  are positive definite, see e.g. [Lorenc \(1986\)](#) for this standard result.  $\mathbf{H}\mathbf{B}\mathbf{H}^T$  may be interpreted as the square matrix of the covariances of background errors in observation space while  $\mathbf{B}\mathbf{H}^T$  is the rectangular matrix of the covariances between the background errors in model space and the background errors in observation space. 3D-Var uses the observation operator  $\mathbf{H}$  explicitly and statistical models ( $\mathbf{B}$  and  $\mathbf{R}$ ) are required only for describing the statistics of the background errors in model space and the observation error in observation space. Consequently, in 3D/4D-Var it is easy, from an algorithmic point of view, to make use of observations such as TOVS radiances, which have quite a complex dependence on the basic analysis variables. The background term and background error covariance modelling (i.e.  $\mathbf{B}$ ) are described in [Chapter 4](#) and observation operators  $\mathbf{H}$  are described in [Chapter 5](#).



## Chapter 2

# 4D variational assimilation

### Table of contents

- 2.1 Introduction**
- 2.2 Solution algorithm**
  - 2.2.1 The incremental method
  - 2.2.2 The job-steps
  - 2.2.3 Interpolation of trajectory and increments
  - 2.2.4 Pre-conditioning and control variable
  - 2.2.5 Minimization
- 2.3 Top-level controls**
- 2.4 A simulation**
  - 2.4.1 The cost function and its gradient
  - 2.4.2 Interface between control variable and model arrays
- 2.5 The assimilation window**
- 2.6 3D variational assimilation (with the first-guess at appropriate time)**
  - 2.6.1 Introduction
  - 2.6.2 Solution algorithm
  - 2.6.3 Main differences with respect to 4D-Var
  - 2.6.4 Data selection

## 2.1 INTRODUCTION

This part of the documentation covers the top level controls of 4D-Var. It gives a detailed description of the solution algorithm, and the various steps that are performed during a 4D-Var simulation (**SIM4D**). The procedure consists of nested iterations, called inner and outer loops, which communicate through files that either contain meteorological fields, observations, or parameters. The data flow is documented in [Chapter 13](#). The interpolation of model fields to observation points (**OBSHOR**) and the organization of the data in memory (`yomsp`, `yommvo`) is described in [Chapter 5](#). The structure of the computation of the observation cost function and its gradient, managed by the routines **OBSV** and **TASKOB** can also be found in [Chapter 5](#). The background term and the ‘change-of-variable’ operators are explained in [Chapter 4](#).

## 2.2 SOLUTION ALGORITHM

### 2.2.1 The incremental method

The adopted solution algorithm is incremental ([Courtier \*et al.\*, 1994](#)), which allows for considerable flexibility with respect to the computer expense of the various job-steps of the 4D-Var minimisation. In the incremental approach the highest possible resolution is used for the computation of the model trajectory, and for calculating the departures between observations and model, whereas a lower-resolution model (its adjoint and tangent linear) are used for the iterative and relatively costly computation of analysis increments ([Trémolet, 2004](#); [Radnóti \*et al.\*, 2005](#)). The lower-resolution iterations (the inner-loops) can optionally be nested within a set of outer-loop iterations at full resolution ([Trémolet, 2005](#)). Apart from the resolution, the cost of the inner-loops will depend also upon the complexity of the inner-loop model, e.g. the use of simpler or more complete representations of the physical processes ([Janisková \*et al.\*, 2002](#); [Tompkins and Janisková, 2004](#)).

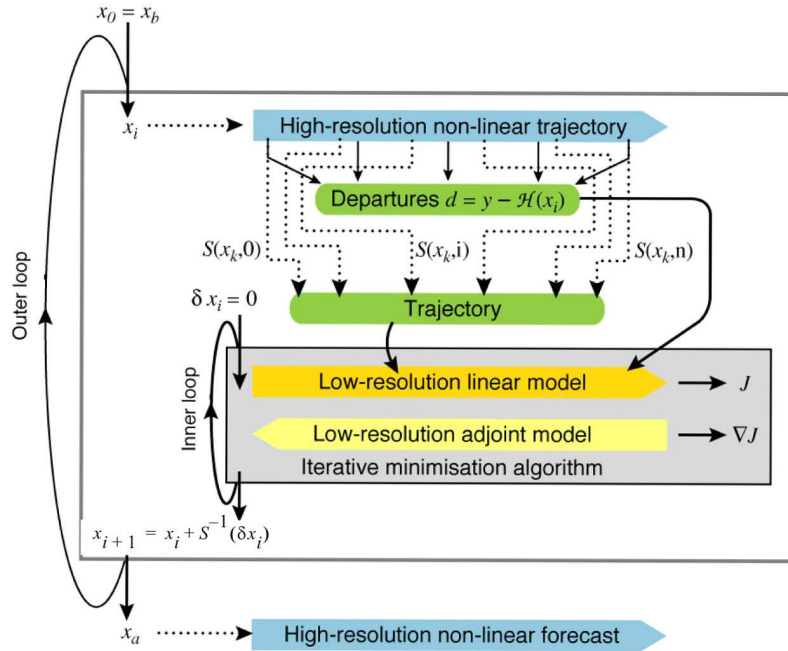


**Figure 2.1** Schematic of the revised 4D-Var solution algorithm implemented in January 2003 (Cy25r4). Outer loops are performed at high resolution (currently T1279) using the full non-linear model. Inner iterations are performed at lower resolution (first T159, then T255) using the tangent-linear forecast model, linearised around a 12-hour succession of model states (‘the trajectory’) obtained through interpolation from high resolution ( $S$  denotes the truncation operator,  $J$  the cost function and  $x$  the atmospheric state vector).

In a further ‘multi-resolution’ extension to the incremental method (Veerse and Thépaut, 1998) the inner-loop resolution is increased with each iteration of the outer-loop. A schematic is shown in Fig. 2.1. In particular, the information about the shape of the cost-function obtained during the early low-resolution iterations provides a very effective pre-conditioner (Chapter 6) for subsequent iterations at higher-resolution, thus reducing the number of costly iterations. The inner-loops can be particularly efficiently minimised using the conjugate gradient method, provided the cost-function is purely quadratic (Fisher, 1998), i.e. the operators involved in the definition of the cost function (the model and the observation operators) are purely linear. For this reason, the inner-loops have been made entirely linear, with the non-linear effects gathered at the outer-loop level. The convergence properties of the outer-loop iterations have been investigated by Trémolet (2005).

### 2.2.2 The job-steps

In the CY37R2 operational configurations the assimilation window is 12-hours long, running from 09–21 UTC to produce the 12 UTC analysis and forecast products, and from 21–09UTC for the 00 UTC production (Haseler, 2004). Several different job steps are performed.

- (i) Comparison of the observations with the background at high resolution to compute the innovation vectors. These are stored in the NCMIFC1-word of the ODB (the observation database) for later use in the minimization. This job step also performs **screening** (i.e. blacklisting, thinning and quality control against the background) of observations (see Chapter 10). The screening determines which observations will be passed for use in the main minimisation. Very large volumes of data are present during the screening run only, for the purpose of data monitoring. The model trajectory is interpolated to the resolution of the next job step and written out.
- (ii) First minimization at low resolution to produce preliminary low-resolution analysis increments, using simplified tangent-linear physics, and tangent-linear observation operators. The eigenvectors



- of the analysis Hessian are computed and these will be used to precondition subsequent inner-loop iterations.
- (iii) Update of the high-resolution trajectory to take non-linear effects partly into account. Observed departures from this new atmospheric state are stored in the ODB and the analysis problem is re-linearized around the updated model state. Variational quality control is computed, and the resulting QC weights will be used in the subsequent minimisation. The updated model trajectory is interpolated to the resolution of the next job step and written out.
  - (iv) Second main minimization at increased resolution with more complete representation of tangent-linear physics. Step (iii) and (iv) are repeated if necessary.
  - (v) Formation of the high-resolution analysis (described below) and a comparison of the analysis with all observations (including those not used by the analysis, for diagnostic purposes).

Each of the job steps is carried out by a different configuration of IFS. They are commonly named as follows.

- (i) **The first trajectory run:** includes a model integration, comparison to observations, and observation screening (quality control and data selection) and is sometimes called **the screening run**. `NCONF = 2`, `LSCREEN = .TRUE`.
- (ii) **The first minimization:** uses simplified physics, typically run at low resolution. This job step includes estimation of analysis and forecast error variances (required for cycling), and calculation of Hessian eigenvectors for pre-conditioning of subsequent minimisation(s). `NCONF = 131`, `LSPHLC = .TRUE.`, `LAVCGL = .TRUE`.
- (iii) **The first trajectory update:** applies the analysis increments obtained in the first minimisations and performs another forecast integration with comparison to observations. This provides a new linearisation state for the next minimisation. `NCONF = 1`, `LOBS = .TRUE`.
- (iv) **The second (and subsequent) minimization:** uses more complete tangent-linear physics, typically higher resolution increments. `NCONF = 131`, `LSPHLC = .FALSE`.
- (v) **Late 4D-start runs:** the analyses (type = an) at the main synoptic hours (00, 06, 12, 18), that fall within the assimilation window, are formed in separate quick job-steps by adding the low-resolution increment to the penultimate high-resolution trajectory of the corresponding time (no forecast integration). See also schematic in [Chapter 13](#).
- (vi) **The final trajectory runs:** carries out verification screening – that is comparison between observations and final analysis. In the final trajectory job-steps with `NUPTRA = 999` the final analysis (type = 4v) is formed ([Bouttier, 2001a](#)), by adding the low-resolution increment to the background (at initial time), and integrating to the analysis times. `NCONF = 1`, `LOBS = .TRUE.`, `NUPTRA = NRESUPD`

The steps (iii) and (iv) are referred to as the second iteration of the *outer loop*, and these can optionally be iterated further to incorporate additional non-linear effects. The trajectory update is not normally done in 3D-Var. The *inner loop* takes place within the main minimization, job steps (ii) and (iv).

### 2.2.3 Interpolation of trajectory and increments

A truncation operator (shown as S in the schematic, [Fig. 2.1](#) above) is required to take the trajectory fields from high to low resolution. This is done using appropriate grid-point interpolations for the surface grid-point fields, whereas upper-air fields are truncated spectrally. Humidity and ozone (and any other grid-point fields) are interpolated in grid-point space to the resolution of the inner loops. Initial time model cloud fields are interpolated to lower resolution using the so-called ‘full-pos’ configuration of IFS. Trajectory cloud fields and trajectory of physical tendencies are generated in a (low resolution) model integration in which the model state is replaced by the interpolated trajectory at each time instance for which it is available. The trajectory handling is managed by the module **TRAJECTORY**.

The spectral and grid-point analysis increments produced by the minimisation are read in by the routine **RDFPINC**. The spectral fields are padded with zeroes for the wave numbers not represented in the inner-loops. The increments for the spectral model variables (vorticity, divergence and logarithm of surface pressure) are added to the background fields. The temperature increments are added to the temperature

of the background (after it has been converted from virtual temperature) and the resulting temperature analysis is converted back to virtual temperature. The humidity and ozone increments are read in as grid-point fields and interpolated to the outer-loop resolution and added to the background. Checks for negative values are applied to humidity and ozone (and trace gasses).

For the 91-level model extension into the mesosphere, it was found that the TL model was unstable in certain situation. This was resolved by introducing smooting of the trajectory fields, if the inner-loop resolution is T255, or higher. This is implemented as a fourth-order diffusion filter applied to the spectral trajectory fields, reducing the amplitude of the shortest wave by a factor five. This is done in `TRAJ_MAIN` just before the fields are written to files in `ifstraj`. The filtering is controlled by the variables `FILTERFACTOR`, `FILTEREXPO`, `FILTERRESOL` in `NAMVAR`, available also in `prepIFS`. In addition, it was found necessary to reduce the amplitude of the analysis increments near the top of the L91 model. They are tapered to zero applying the factor `REDINC`, over the topmost `NLEV_REDINC=4` levels (`NAMJG`), in `RDFPINC`.

#### 2.2.4 Pre-conditioning and control variable

In practice, it is necessary to pre-condition the minimization problem in order to obtain a quick convergence. As the Hessian (the second derivative) of the objective function is not accessible, [Lorenz \(1988\)](#) suggested the use of the Hessian of the background term  $J_b$ . The Hessian of  $J_b$  is the matrix  $\mathbf{B}$ . Such a preconditioning may be implemented either by a change of metric (i.e. a modified inner product) in the space of the control variable, or by a change of control variable. As the minimization algorithms have generally to evaluate several inner products, it was found more efficient to implement a change of variable (under `CHAVAR`, `CHAVARIN`, etc.). Algebraically, this requires the introduction of a variable  $\chi$  such that

$$J_b = \chi^T \chi \quad (2.1)$$

Comparing (1.2) and (2.1) shows that  $\chi = \mathbf{B}^{-1/2} \delta \mathbf{x}$  satisfies the requirement.  $\chi$  thus becomes the *control variable* of the preconditioned problem. This is indeed what has been implemented, as will be explained in [Section 4.2](#). A single-observation analysis with such preconditioning converges in one iteration.

The  $J_b$ -based pre-conditioning is sufficient when the B-term dominates over the observation term of the Hessian. With increasing amounts of observational information, and in cases with locally dense observation coverage, the observation term can be dominant over the background term in defining the shape of the cost-function (its second derivative). The combined Lanczos/conjugate gradient method allows computation of the leading eigenvectors and eigenvalues of the Hessian while solving for the analysis, essentially at no extra cost. This method is fully described in [Chapter 6](#), and it is used for all inner-loop iterations. The Hessian eigenvector information obtained at low resolution is used as preconditioner at subsequent inner-loop iterations at higher resolution. This has been shown to be a very effective way of reducing the number of iterations required at higher inner-loop resolutions.

#### 2.2.5 Minimization

The minimization problem involved in 3D/4D-Var can be considered as large-scale, since the number of degrees of freedom in the control variable is of the order of  $10^7$ . In the case of purely quadratic cost-function (as in operational 4D-Var) the most efficient minimisation is provided by the conjugate gradient algorithm (`CONGRAD` called from `CVA2` and `FORECAST_ERROR`). `Congrad` is preconditioned with the leading Hessian eigenvectors, as described in [Chapter 6](#). The forecast error configuration ([Chapter 6](#), switch `LAVCGL=.TRUE.` in `yomvar`) always uses `CONGRAD`, and otherwise it is activated by the switch `LCONGRAD` in `yomvar`.

For non-quadratic problems, an efficient descent algorithm was provided by the Institut de Recherche en Informatique et Automatique (INRIA, France). It is a variable-storage quasi-Newton algorithm (`M1QN3`) described in [Gilbert and Lemaréchal \(1989\)](#). `M1QN3` uses the available in-core memory to update an approximation of the Hessian of the cost function. In practice, ten updates (`NMUPD`, `namiom`) of this Hessian matrix were used.

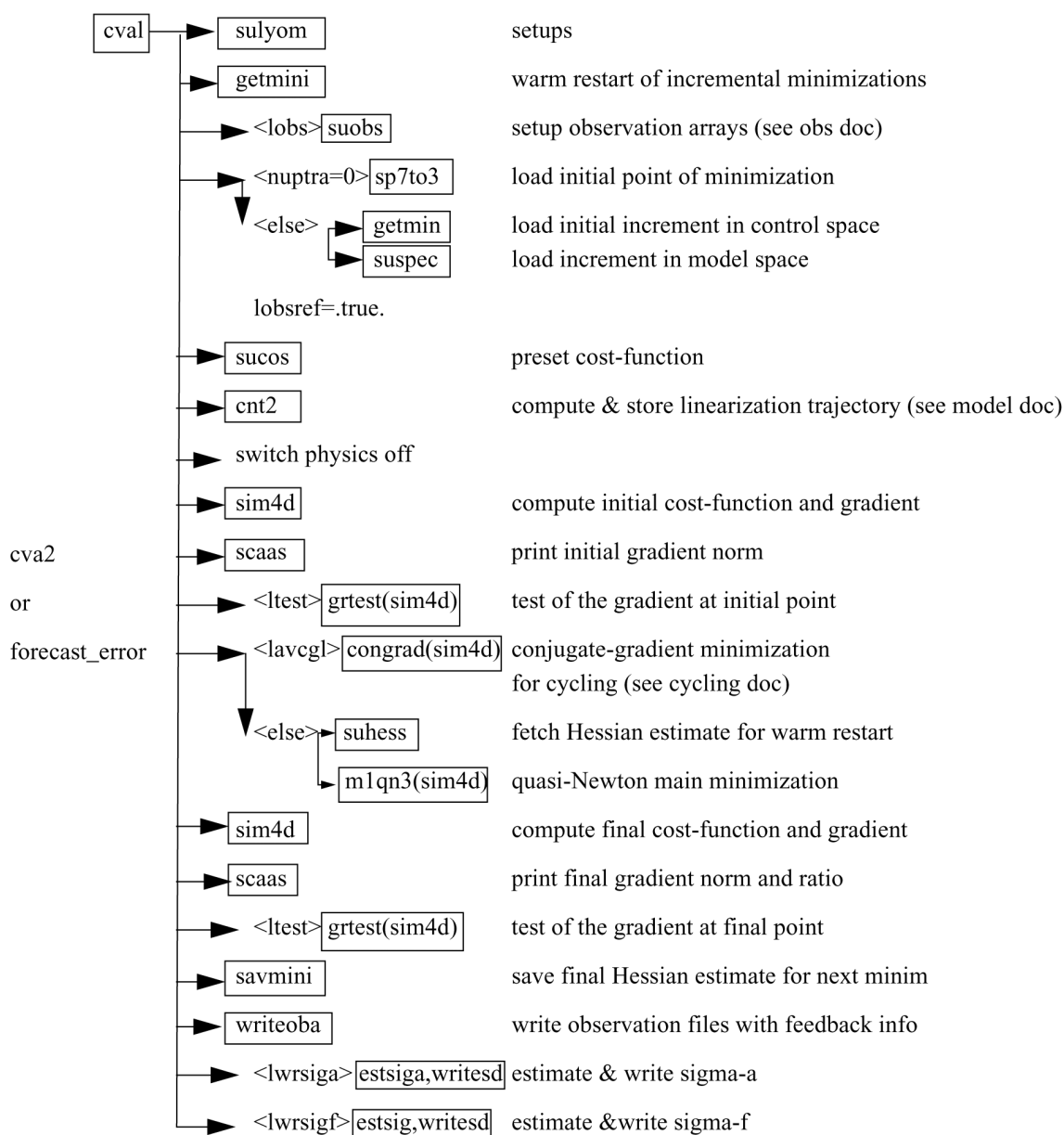


Figure 2.2 Flow diagram for subroutines *CVA1* and *CVA2*.

## 2.3 TOP-LEVEL CONTROLS

The routines *CVA1*, *CVA2* and *FORECAST\_ERROR* control the variational configurations of IFS. The flow diagram of *CVA1* and *CVA2* is shown in Fig. 2.2. The spectral and grid-point first guess fields (FG) have been read in to the SP7-arrays and GP7-arrays (in *YOMSP*) by *SUECGES*, called from *SUJBSTD* within the  $J_b$  setup, see Subsection 4.3.3. At the start of *CVA1* additional setups for the variational configurations are done (*SU1YOM*). The SP3-arrays and GFL-arrays, i.e. the current model state, (in *YOMSP*) are filled by a call to the setup routine *SUINIF* in the routine *SUVAZX*, and only for the first minimisation job-step. For subsequent minimisations the initial state for analysed variables must come from the previous minimisation, i.e. a warm start. This is achieved by getting the control vector *YVAZX* by calling *GETMINI* and performing an inverse change of variables (calling *CHAVARIN*) to transform the control vector to model variables (SP3/SP2-arrays and GFL-arrays). Non-analysed fields (e.g. cloud fields) are read by a call to *SUINIF* earlier in *SUVAZX*.

After minimisation is complete one final simulation is performed in `CVA2` or `FORECAST_ERROR`. This simulation is diagnostic, and characterized by the simulation counter being set to 999, `NSIM4D = NSIM4DL`, `yomvar`. The observation departure from the low-resolution analysis,  $\mathbf{y}^o - H\mathbf{x}_{LR}^a$ , is computed and stored in the NCMIOMN-word of the ODB. Finally at the end of `CVA2` and `FORECAST_ERROR`, respectively, the updated ODB is written to disk, using the routine `WRITEOBA`.

## 2.4 A SIMULATION

### 2.4.1 The cost function and its gradient

A simulation consists of the computation of  $J$  and  $\nabla J$ . This is the task of the routine `SIM4D`, see [Fig. 2.3](#) for the flow diagram. The input is the latest value of the control variable  $\chi$  in the array `VAZX`, computed by `MIQN3`, or `CONGRAD`. First  $J_b$  and its gradient are computed (see [Section 4.2](#)) using

$$\begin{aligned} J_b &= \chi^T \chi \\ \nabla_{\chi} J_b &= 2\chi \end{aligned} \quad (2.2)$$

The gradient of  $J_b$  with respect to the control variable is stored in the array `VAZG` (`YOMCVA`).

- (i) Copy  $\chi$  from `VAZX` to SP3-arrays (`YOMSP`) using the routine `CAIN`.
- (ii) Compute  $\mathbf{x}$ , the physical model variables, using `CHAVARIN` so that

$$\mathbf{x} = \delta\mathbf{x} + \mathbf{x}^b = L\chi + \mathbf{x}^b \quad (2.3)$$

- (iii) `SUBFGS` computes  $\delta\mathbf{x} = \mathbf{x} - \mathbf{x}^g$ , where  $\mathbf{x}^g$  is the guess (not necessarily equal to the background).
- (iv) Perform the direct integration of the linear model, using the routine `CNT3TL`, and compare with observations. See [Section 2.5](#).
- (v) Calculate  $J_o$  for which `OBSV` is the master routine.
- (vi) Perform the adjoint model integration using `CNT3AD`, and observation operators' adjoint.
- (vii) Calculate  $\nabla_{\mathbf{x}} J_o$ , and store it in SP3.
- (viii)  $J_c$  and its gradient are calculated in `COSJC` called from `CNT3AD`, if LJC is switched on (default) in `namvar`.
- (ix) Transform  $\nabla_{\mathbf{x}} J_o + \nabla_{\mathbf{x}} J_c$  to control variable space by applying `CHAVARINAD`.
- (x) Copy  $\nabla_{\chi} J_o + \nabla_{\chi} J_c$  from SP3 and add to  $\nabla_{\chi} J_b$ , already in the array `VAZG`, using `CAIN`.
- (xi) Add the various contributions to the cost function together, in `EVCCOST`, and print to log file using `prtjo`.
- (xii) Increase the simulation counter `NSIM4D` by one.

The new  $J$  and  $\nabla_{\chi} J$  are passed to the minimization algorithm to calculate the  $\chi$  of the next iteration, and so on until convergence (or the maximum number of iterations) has been reached.

### 2.4.2 Interface between control variable and model arrays

The purpose of the routine `CAIN` (the canonical injection) is to identify those parts of the model state that should be included in the variational control variable. This is controlled by on/off switches such as `NVA2D` and `NVA3D` (`yomcva`) initialized in `SUALCTV`. The scalar product used is the one defined by the array `SCALP` (in `yomcva`, set up in the routine `SCALJGS` called from `SUSCAL`), which is 1 if  $m = 0$ , and 2 otherwise. This allows the compression of arrays of the type `VAZX` while using the  $L^2$  norm on the sphere with real fields in spectral space.

The control vector currently consists of four parts, as defined in the module `CONTROL_VECTORS` residing in the `ifsaux` library. Any of the following four parts can be absent.

- (i) The initial-condition control-variables that define the original 4D-Var problem.
- (ii) A representation of model error (for weak-constraint 4D-Var), see [Trémolet \(2003\)](#).
- (iii) The TOVS control vector (`LTOVSCV`), used to estimate surface skin temperature and simplified cloud variables (pressure and fraction) at the radiance field-of-view locations.

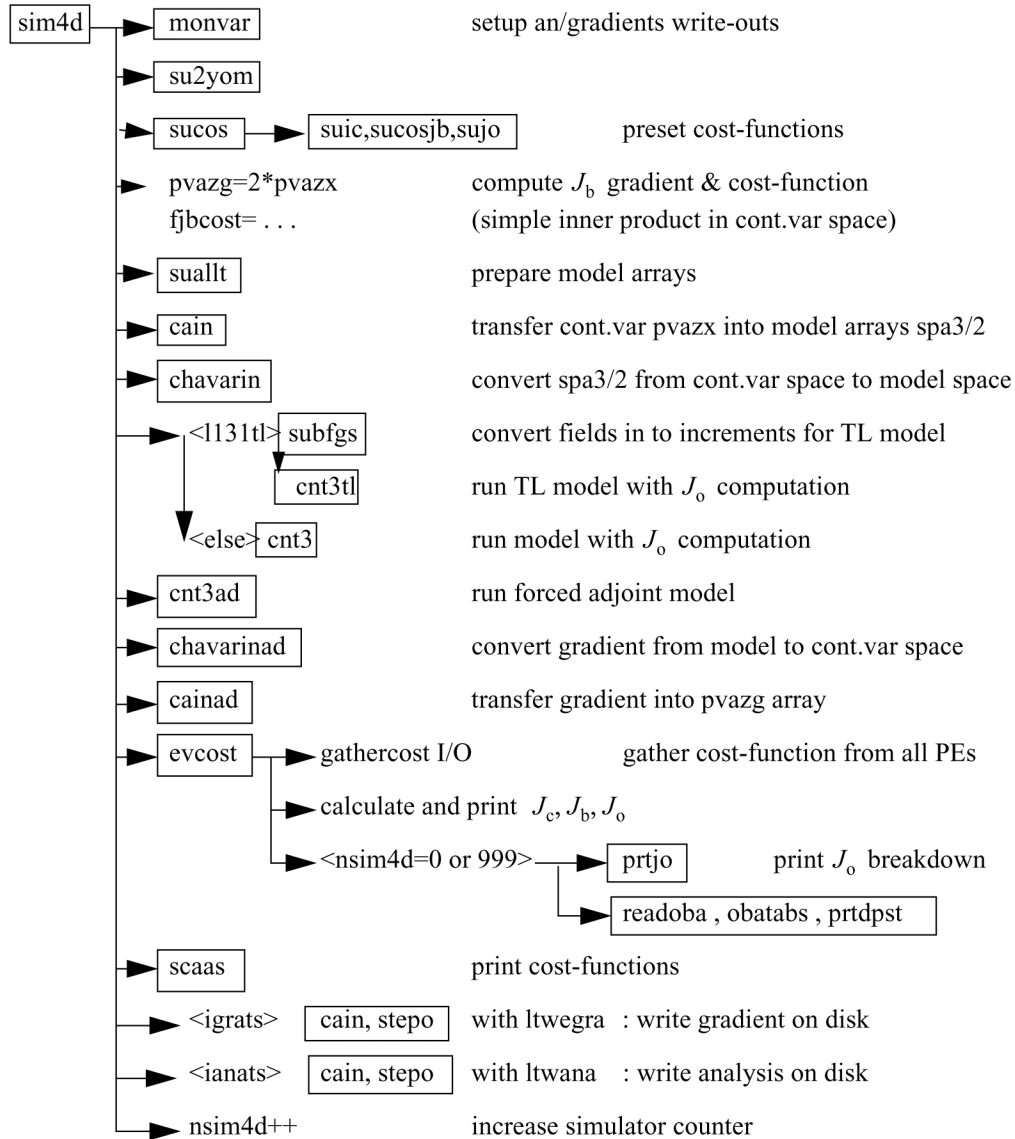


Figure 2.3 Flow diagram for the subroutine *sim4d*.

(iv) Components for the limited-area model ALADIN.

The organisation of elements of the control-vector is now quite flexible and allows for future planned extensions, such as observation bias coefficients (e.g. for radiance data, and wavelet- $J_b$  components).

## 2.5 THE ASSIMILATION WINDOW

In 4D-Var, observations are organized in time-slots (currently half-hourly) as described in the ODB documentation. The cost-function measures the distance between a model trajectory and the available information (background, observations) over an assimilation interval or window. For a 12-hour window, it is either (09 UTC–21 UTC) or (21 UTC–09 UTC), see Haseler (2004). Equation (1.2) (see Chapter 1) is replaced by

$$J(\delta\mathbf{x}) = \frac{1}{2}\delta\mathbf{x}^T\mathbf{B}^{-1}\delta\mathbf{x} + \frac{1}{2}\sum_{i=0}^n(\mathbf{H}_i\delta\mathbf{x}(t_i) - \mathbf{d}_i)^T\mathbf{R}_i^{-1}(\mathbf{H}_i\delta\mathbf{x}(t_i) - \mathbf{d}_i) \quad (2.4)$$

with subscript  $i$  the time index. Each  $i$  corresponds to a half-hour time slot.  $\delta\mathbf{x}$  is as before the increment at low resolution at initial time, and  $\delta\mathbf{x}(t_i)$  the increment evolved according to the tangent linear model

from the initial time to time index  $i$ .  $\mathbf{R}_i$  and  $\mathbf{B}$  are the covariance matrices of observation errors at time index  $i$  and of background errors respectively.  $\mathbf{H}_i$  is a suitable linear approximation at time index  $i$  of the observation operator  $H_i$ . The innovation vector is given at each time step by  $\mathbf{d}_i = \mathbf{y}_i^o - H_i \mathbf{x}^b(t_i)$ , where  $\mathbf{x}^b(t_i)$  is the background propagated in time using the full non-linear model and  $\mathbf{y}_i^o$  is the observation vector at time index  $i$ . If the switch `LTC=.true.` (default is `LTC=.false.`), then SYNOP and DRIBU time sequences of surface pressure and height data are used with serial correlation of observation error, and the observation cost-function computation for those data then spans all time slots. Equation (2.4) therefore needs generalising, as has been done in the paper by Järvinen *et al.* (1999).

A way to account in the final 4D-Var analysis for some non-linearities is to define a series of minimization problems such that

$$\begin{aligned}
 J(\delta \mathbf{x}^n) &= \frac{1}{2} (\delta \mathbf{x}^n + \mathbf{x}^{n-1} - \mathbf{x}^b)^T \mathbf{B}^{-1} (\delta \mathbf{x}^n + \mathbf{x}^{n-1} - \mathbf{x}^b) \\
 &\quad + \frac{1}{2} \sum_{i=0}^n (\mathbf{H}_i \delta \mathbf{x}^n(t_i) - \mathbf{d}_i^{n-1})^T \mathbf{R}_i^{-1} (\mathbf{H}_i \delta \mathbf{x}^n(t_i) - \mathbf{d}_i^{n-1})
 \end{aligned} \tag{2.5}$$

with superscript  $n$  the minimization index.

$\mathbf{x}^{n-1}$  is the current estimate of the atmospheric flow. It is equal to the background for the first minimization.  $\mathbf{d}_i^{n-1} = \mathbf{y}_i^o - H_i \mathbf{x}^{n-1}(t_i)$  is the innovation vector, computed by integrating the model at high resolution from the current estimate.

## 2.6 3D VARIATIONAL ASSIMILATION (WITH THE FIRST-GUESS AT APPROPRIATE TIME)

### 2.6.1 Introduction

3D-Var is a temporal simplification of 4D-Var. The simplest way to implement a 3D-Var within the context of an existing 4D-Var scheme is to replace the tangent-linear (and its adjoint) model integration within the inner loops (as defined in the previous section) by the identity operator (`LIDMODEL = .TRUE.` in `yomtnewt.F90`). This approach has indeed been adopted, as it saves on maintenance of scripts and codes. It is this 3D-Var version that was used for the production of the ERA-40 re-analysis (Uppala *et al.*, 2005) and it was used until 14 March 2006 in ECMWF operations within the so called BC-suite to generate timely boundary conditions for the participating member states.

In this version of 3D-Var as much as possible of the 4D-Var structure is maintained. The available observations, typically over the period of a 6-hour assimilation window, are compared with a model integration at high resolution. The comparison between observation and model is thus performed at the appropriate time: therefore the abbreviation 3D-FGAT (first-guess at appropriate time). This configuration is activated via the switch `LFGAT = .TRUE.` in `namvar.h`.

### 2.6.2 Solution algorithm

The tangent-linear model in 4D-Var evolves the analysis increment over time, within the assimilation window. In 3D-FGAT no such evolution takes place: one static increment is produced. The valid time of this increment is not at the initial time of the window as in 4D-Var, but at the central time. The increment is added to the background field, which forms the analysis at the central time. This has the consequence that a trajectory update from the start of the assimilation window cannot be performed. The 3D-FGAT configuration is therefore based on one single outer-loop without iteration. There are nevertheless two minimisation steps. The first provides analysis error and background error estimates required for cycling, and also pre-conditioning vectors (Hessian eigenvectors) that are used in the second minimisation job-step. The resolution of the first minimisation is typically lower (T42) than for the main one (e.g. T159).

Scatterometer de-aliasing is active and variational quality control is activated approximately halfway into the minimisation, rendering the problem non-linear (and the cost function non-quadratic). The use of conjugate-gradient minimisation is thus prevented. The `M1QN3` algorithm is used instead.

### 2.6.3 Main differences with respect to 4D-Var

The main differences with respect to the standard operational 4D-Var configuration are as follows.

- (i) Variational quality control is carried out within the inner-loop iterations (LQVARQC = .FALSE.).
- (ii) The scatterometer de-aliasing is performed within the inner-loop iterations (LQSCAT = .FALSE.).
- (iii) Use of **M1QN3** instead of conjugate gradient minimisation, due to the cost-function being quadratic.
- (iv) The  $J_c$  term relies on NMI (normal mode initialisation) rather than DFI (Digital filter initialisation) (LJCDFI = .FALSE., LJCNMI = .TRUE.).
- (v) No iteration at outer-loop level.
- (vi) LTRAJHR = .FALSE., which means that the observation operators are linearized around the low-resolution trajectory, which is generated through an integration by the full non-linear model (at the resolution of the minimisation) at the beginning of the minimisation job-step. **CVA1** calls **CNT2** to do this.

### 2.6.4 Data selection

The observational data are stored in time-slots within the ODB (just as in 4D-Var). The data selection criteria are applied in identically the same way as in 4D-Var, allowing time sequences of data to be used also in 3D-FGAT. The 3D scheme is however unable to extract temporal information from the data, and produces an analysis of the temporal average of the FGAT departures. Optionally the screening data selection rules can be applied once for the entire (6-hour) assimilation window, which would pick only the data closest to the analysis centre time. This is called ‘3D-screening’ and was the practice in the original operational 3D-Var configuration.





# Chapter 3

## Tangent-linear physics

### Table of contents

- 3.1 Introduction**
- 3.2 Set-up**
- 3.3 Mixed-phase thermodynamics**
- 3.4 Vertical diffusion**
  - 3.4.1 Upper-air
  - 3.4.2 Surface
  - 3.4.3 Regularization
  - 3.4.4 Flow chart
- 3.5 Subgrid scale orographic effects**
- 3.6 Non-orographic gravity wave drag**
- 3.7 Radiation**
  - 3.7.1 The short-wave radiation scheme
  - 3.7.2 The longwave radiation scheme
  - 3.7.3 Cloud overlap assumptions
  - 3.7.4 Cloud optical properties
- 3.8 Large-scale condensation and precipitation**
  - 3.8.1 Stratiform condensation
  - 3.8.2 Convective contribution
  - 3.8.3 Precipitation formation
  - 3.8.4 Precipitation evaporation
  - 3.8.5 Phase partitioning
  - 3.8.6 Code
  - 3.8.7 Regularization
- 3.9 Moist convection**
  - 3.9.1 Equations for updraught and downdraught
  - 3.9.2 Triggering of moist convection
  - 3.9.3 Entrainment and detrainment
  - 3.9.4 Precipitation formation
  - 3.9.5 Closure assumptions
  - 3.9.6 Flow chart
  - 3.9.7 Regularization
- 3.10 Trajectory management**

### 3.1 INTRODUCTION

The linearized physics describes six processes: vertical diffusion, subgrid-scale orographic effects, non-orographic gravity wave drag, radiation, large-scale condensation/precipitation and convection. In order to prevent spurious unstable perturbations from growing, a number of simplifications have been defined for these schemes with respect to the non-linear physical parametrization schemes (described in Part IV: Physical processes) used in the forecast model. All simplified parametrizations are called in each minimization of 4D-Var.

This text is focused on brief scientific description of the linearized physical parametrization schemes together with some technical aspects. More detailed scientific issues can be found in the mentioned literature references.

### 3.2 SET-UP

The full linearized physics package currently in operational use is activated by setting the following switches in namelist **NAMTRAJP**:

- LEVDIF2 (vertical diffusion),
- LEGWDG2 (subgrid-scale orographic gravity wave drag),
- LEGWMS2 (non-orographic gravity wave drag),
- LERADI2, LERADS, LERADN2 and LERADSW2 (radiation),
- LENCLD2 (large-scale condensation/precipitation),
- LECUMF2 and LECUMFS2 (in namelist **NAMCUMFS**) (moist convection),

In addition, the following switches must be set to `.TRUE.`: **LEPHYS** and **LAGPHY** (also necessary to activate the ECMWF non-linear physics) in namelist **NAEPHY** and **LETRAJP** (to activate storage of the trajectory at  $t - \Delta t$ ) in namelist **NAMTRAJP**.

Tunable parameters of the improved physics (which should not in principle be modified) are defined in **SUPHLI**. The logical **LPHYLIN** (namelist **NAMTLEVOL**) is used to activate the simplifications and/or modifications associated with the linear package in the non-linear physics. This variable is set to `.FALSE.` by default, but is forced to `.TRUE.` before starting tangent-linear (TL) and adjoint (AD) computations in **CNT3TL** and **CNT3AD**. Thus this switch remains `.TRUE.` for the linearized physics called in **EC\_PHYS\_TL** and **EC\_PHYS\_AD**.

### 3.3 MIXED-PHASE THERMODYNAMICS

The thermodynamical properties of the water mixed phase are represented by a differentiable weighting function between  $T_0 = 0^\circ\text{C}$  and  $T_{\text{ice}} = -23^\circ\text{C}$  given by

$$\alpha(T) = \frac{1}{2}[1 + \tanh\{\mu(T - T_{\text{crit}})\}] \quad (3.1)$$

with  $\mu = 0.15$  (**RLPALP1**) and  $T_{\text{crit}} = T_{\text{ice}} + \frac{T_0 - T_{\text{ice}}}{\sqrt{2}}$  (**RLPTRC**).

The tuning parameter  $\mu$  controls the intensity of the smoothing, and the temperature  $T_{\text{crit}}$  has been chosen to give  $\alpha = 0.5$  for the same temperature as in the operational quadratic formulation (see function **FCTTRE**).

This weighting function is used by the large-scale condensation and moist-convection routines.

### 3.4 VERTICAL DIFFUSION

Vertical diffusion applies to wind components, dry static energy and specific humidity. The exchange coefficients in the planetary boundary layer and the drag coefficients in the surface layer are expressed as functions of the local Richardson number (**Louis et al., 1982**). They differ from the operational formulation which uses the Monin–Obukhov length as a stability parameter in stable conditions and a  $K$ -profile approach for convective boundary layers (see the documentation of the ECMWF physics). Analytical expressions are generalized to the situation of different roughness lengths for heat and momentum transfer.

For any conservative variable  $\psi$  (wind components  $u, v$ ; dry static energy  $s$ ; specific humidity  $q$ ), the tendency of its perturbation  $\psi'$  produced by vertical diffusion is

$$\frac{\partial \psi'}{\partial t} = \frac{1}{\rho} \frac{\partial}{\partial z} \left( K(Ri) \frac{\partial \psi'}{\partial z} \right) \quad (3.2)$$

where  $\rho$  is the air density.

In the planetary boundary layer, the exchange coefficient  $K$  is given by

$$K = l^2 \left\| \frac{\partial \mathbf{V}}{\partial z} \right\| f(Ri) \quad (3.3)$$

where  $f(Ri)$  represents the coefficient of the vertical turbulent diffusion which is a function of the Richardson number.

### 3.4.1 Upper-air

#### Stable conditions

In stable conditions ( $Ri > 0$ ), the value of  $f(Ri)$  is computed by assuming a continuous transition from the [Louis \*et al.\* \(1982\)](#) formulation,  $f_{LTG}(Ri)$ , near the surface to the Monin-Obukhov formulation,  $f_{MO}(Ri)$ , further aloft, which reads

$$f(Ri) = \alpha f_{LTG}(Ri) + (1 - \alpha) f_{MO}(Ri) \quad (3.4)$$

with  $\alpha = \exp(-z/z_{\text{trans}})$ . The transition altitude,  $z_{\text{trans}}$ , is set to 300 m for momentum. For heat and moisture, it is set to 150 m for  $z < 1500$  m and to 300 m higher up.

The Louis functions  $f_{LTG}(Ri)$  for momentum and heat/moisture, in the stable case are given by

$$f_{LTG}(Ri) = \begin{cases} \frac{1}{1 + 2bRi(1 + dRi)^{-1/2}} & \text{for momentum} \\ \frac{1}{1 + 2bRi(1 + dRi)^{1/2}} & \text{for heat/moisture} \end{cases} \quad (3.5)$$

with  $b = 5$  and  $d = 1$ .

The Monin-Obukhov stability functions,  $\Phi_{M,H}$ , are used to compute  $f_{MO,M}(Ri) = 1/(\Phi_M^2)$  and  $f_{MO,H}(Ri) = 1/(\Phi_M \Phi_H)$  for momentum and heat/moisture, respectively.

The vertical profile of the mixing length is computed using [Blackadar \(1962\)](#) as

$$l = \frac{\kappa(z + z_0)}{1 + \kappa \frac{(z+z_0)}{\lambda}} \quad (3.6)$$

where  $\lambda$  is the asymptotic mixing length (set to 300 m),  $z_0$  is the roughness length and  $\kappa$  is von Kármán's constant.

#### Unstable conditions

In unstable situations ( $Ri < 0$ ), the computation of  $f(Ri)$  follows [Louis \*et al.\* \(1982\)](#):

$$f(Ri) = \begin{cases} 1 - \frac{2bRi}{1 + 3bc \left( \frac{1}{\sqrt{27}} \right) \left( \frac{l_M}{z+z_{0M}} \right)^2 \sqrt{|Ri|}} & \text{for momentum} \\ 1 - \frac{3bRi}{1 + 3bc \left( \frac{1}{\sqrt{27}} \right) \left( \frac{l_H}{z+z_{0H}} \right)^2 \sqrt{|Ri|}} & \text{for heat/moisture} \end{cases} \quad (3.7)$$

where  $b = 5$  and  $c = 5$ .

The vertical profile of the mixing length in the unstable case also follows [Blackadar \(1962\)](#), but with a reduction in the free atmosphere:

$$l = \frac{\kappa(z + z_0)}{1 + \kappa \frac{(z+z_0)}{\lambda}} \left[ \gamma + \frac{1 - \gamma}{1 + \frac{(z+z_0)^2}{L^2}} \right] \quad (3.8)$$

The asymptotic mixing length  $\lambda_M$  for momentum is set to 150 m, whereas  $\lambda_H = \lambda_M \sqrt{1.5d}$ . The pseudo-depth of the boundary layer is defined by  $L = 4$  km (RLPMIXL), and the reduction factor applied to the mixing length in the free atmosphere is  $\gamma = 0.2$  (RLPBETA) [ $1 \rightarrow \gamma\lambda$  when  $z \gg L$ ].

### 3.4.2 Surface

To parametrize the turbulent fluxes at the surface, the drag coefficients (i.e. the exchange coefficients between the surface and the lowest model level) are computed. The neutral coefficients  $C_{MN}$  and  $C_{HN}$  are written as

$$C_{MN} = \frac{\kappa^2}{\left[\ln\left(\frac{z+z_{0M}}{z_{0M}}\right)\right]^2} \quad \text{and} \quad C_{HN} = \frac{\kappa^2}{\left[\ln\left(\frac{z+z_{0M}}{z_{0M}}\right) \ln\left(\frac{z+z_{0M}}{z_{0H}}\right)\right]} \quad (3.9)$$

The drag coefficients for momentum are computed as

$$C_M = \begin{cases} \frac{1}{1 + \frac{2bRi}{\sqrt{1+dRi}}} C_{MN} & \text{if } Ri > 0 \\ \left(1 - \frac{2bRi}{1 + 3bcC_{MN} \sqrt{\frac{z+z_{0M}}{z_{0M}} |Ri|}}\right) C_{MN} & \text{if } Ri < 0 \end{cases} \quad (3.10)$$

The surface exchange coefficients for dry static energy and specific humidity are

$$C_H = \begin{cases} \frac{1}{1 + 3bRi \sqrt{1 + dRi}} C_{HN} & \text{if } Ri > 0 \\ \left(1 - \frac{3bRi}{1 + 3bcC_{HN} \sqrt{\frac{z+z_{0M}}{z_{0M}} |Ri|}}\right) C_{HN} & \text{if } Ri < 0 \end{cases} \quad (3.11)$$

The empirical coefficients  $b$  (RLPBB),  $c$  (RLPCC) and  $d$  (RLPDD) are set to 5 in SUPHLI.

The same mixed layer parametrization as in the fully-fledged non-linear vertical diffusion scheme is also included (for details, see Part IV: Physical processes - 3.3 The exchange coefficients above the surface and mixed layer).

### 3.4.3 Regularization

Until cycle Cy33r1, perturbations of the exchange coefficients were neglected ( $K' = 0$ ), in order to prevent spurious unstable perturbations from growing in the linearized version of the scheme (Mahfouf, 1999). From Cy33r1 onwards, regularization was introduced for exchange coefficients between upper model levels to include partial perturbations of these coefficients.

### 3.4.4 Flow chart

The simplified diffusion scheme **VDFMANS** can be called from **CALLPAR** when the logical switch for linearized physics **LPHYLIN** is set to **.TRUE.**

The linear versions of the vertical diffusion scheme are called from the drivers **VDFMAINSTL** and **VDFMANSAD**. The ensemble of routines that prepare the surface exchange coefficients and associated surface quantities needed for the solution of the vertical diffusion equations are part of the routine **SURFEXCDRIVERSTL** and **SURFEXCDRIVERSTL**. At this moment the surface arrays are not evolved in time, though the routines are coded for computing perturbations of: the roughness length (**VDFUPDZ0TL**, **VDFUPDZ0AD**), the surface boundary conditions for  $T$  and  $q$  (**VDFSURFTL**, **VDFSURFAD**), the surface exchange coefficients (**VDFEXCSTL**, **VDFEXCSAD**) and the equivalent evapotranspiration efficiency (**VDFEVAPTL**, **VDFEVAPAD**). This can be activated in the future by setting the logical switch **LENOPERT** set to **.FALSE.** in **NAMTRAJP**. The current default version is **.TRUE.** (i.e. no perturbation is required for the surface arrays).

Other computations performed in **VDFMAINSTL** and **VDFMANSAD** involve the calculation of exchange coefficients above the surface layer (**VDFEXCUSTL**, **VDFEXCUSAD**), the solving of the diffusion equations for momentum (**VDFDIFMSTL**, **VDFDIFMSAD**) and dry static energy and moisture (**VDFDIFHSTL**, **VDFDIFHSAD**), as well as the incrementation of tendencies for wind, temperature and specific humidity (**VDFINCRSTL**, **VDFINCRSTL**).

The logical **LEKPERT** in **NAMTRAJP** controls the perturbations of the exchange and drag coefficients. When set to **.FALSE.** (default), the perturbations would be set to 0. In the current 4D-Var computation,

LEKPERT is set to .TRUE., which means that the regularized exchanged coefficients (as described above) are used.

### 3.5 SUBGRID SCALE OROGRAPHIC EFFECTS

Only the low-level blocking part of the operational non-linear scheme developed by [Lott and Miller \(1997\)](#) (see documentation on ECMWF non-linear physics) is taken into account in the tangent-linear and adjoint calculations. The deflection of the low-level flow around orographic obstacles is supposed to occur below an altitude  $Z_{\text{blk}}$  such that

$$\int_{Z_{\text{blk}}}^{2\mu} \frac{N}{|\mathbf{U}|} dz \geq H_{n_{\text{crit}}} \quad (3.12)$$

where  $H_{n_{\text{crit}}}$  is a critical non-dimensional mountain height (GFRCRIT = 0.5),  $\mu$  is the standard deviation of subgrid-scale orography,  $N$  is the vertical stability and  $\mathbf{U}$  is the wind vector.

The deceleration of the wind due to the low-level blocking is given by

$$\begin{aligned} \left(\frac{\partial \mathbf{U}}{\partial t}\right)_{\text{blk}} &= -C_d \max\left(2 - \frac{1}{r}, 0\right) \frac{\sigma}{2\mu} \left(\frac{Z_{\text{blk}} - z}{z + \mu}\right)^{0.5} (B \cos^2 \psi + C \sin^2 \psi) \frac{\mathbf{U}|\mathbf{U}|}{2} \\ &= A(\mathbf{U}|\mathbf{U}|) \end{aligned} \quad (3.13)$$

where

- $C_d$  is the low-level drag coefficient (GWAKE = 1)
- $\sigma$  is the mean slope of the subgrid-scale orography
- $\gamma$  is the anisotropy of the subgrid-scale orography
- $\psi$  is the angle between the low-level wind and the principal axis of topography
- $B = 1 - 0.18\gamma - 0.04\gamma^2$
- $C = 0.48\gamma + 0.3\gamma^2$
- $r = (\cos^2 \psi + \gamma \sin^2 \psi) / (\gamma \cos^2 \psi + \sin^2 \psi)$

Since the final wind tendency produced by the low-level drag parametrization is obtained from the following partially implicit discretization of (3.13)

$$\left(\frac{\partial \mathbf{U}}{\partial t}\right)_{\text{blk}} = -\frac{\beta}{\beta + 1} \frac{\mathbf{U}^{n-1}}{2\Delta t} \quad (3.14)$$

where  $\beta = A|\mathbf{U}^{n-1}|2\Delta t$ , the corresponding perturbation is

$$\left(\frac{\partial \mathbf{U}}{\partial t}\right)_{\text{blk}} = -\frac{\beta'}{(\beta + 1)^2} \frac{\mathbf{U}^{n-1}}{2\Delta t} - \frac{\beta}{\beta + 1} \frac{\mathbf{U}'^{n-1}}{2\Delta t} \quad (3.15)$$

Finally, the local dissipation heating is computed in the same way as in the non-linear scheme, together with the associated perturbation.

The main tangent-linear and adjoint routines, **GWDRAGTL** and **GWDRAGAD**, are called from **CALLPARTL** and **CALLPARAD** respectively. The depth of the low-level blocking layer is determined in **GWSETUPTL** and **GWSETUPAD**, while the low-level blocking effect described by (3.14) is computed at the end of **GWDRAGTL** and **GWDRAGAD**. As mentioned above, the representation of wave breaking is currently not activated in the linearized code by setting the constant RLPDRAG to zero in **SUPHLI**. Note that RLPDRAG is only used when logical LPHYLIN is .TRUE., otherwise GKDRAG is used (set to 0.3 in **SUGWD**).

### 3.6 NON-OROGRAPHIC GRAVITY WAVE DRAG

The non-linear scheme for non-orographic gravity wave (nonorog-gw) ([Orr et al. \(2010\)](#)) has been used operationally in the forecast model since September 2009 (cycle 35R3). Tangent-linear and adjoint versions were developed in order to reduce discrepancies between the full non-linear and linearized versions of

the model. This parametrization scheme is based on [Scinocca \(2003\)](#). The latter is a spectral scheme derived from the [Warner and McIntyre \(1996\)](#) scheme which represents the three basic mechanisms of conservative propagation, critical level filtering, and non-linear dissipation. Since the full non-hydrostatic and rotational wave dynamics considered by [Warner and McIntyre \(1996\)](#) is too costly for operational models, only hydrostatic and non-rotational wave dynamics are employed.

The dispersion relation for a hydrostatic gravity wave in the absence of rotation is

$$m^2 = \frac{k^2 N^2}{\tilde{\omega}^2} = \frac{N^2}{\tilde{c}^2} \quad (3.16)$$

where  $k$ ,  $m$  are horizontal and vertical wavenumbers, while  $\tilde{\omega} = \omega - kU$  and  $\tilde{c} = c - U$  are the intrinsic frequency and phase speed (with  $c$  being the ground based phase speed and  $U$  the background wind speed in the direction of propagation), respectively.

The launch spectrum, which is globally uniform and constant, is given by the total wave energy per unit mass in each azimuth angle  $\phi$  following [Fritts and Nastrom \(1993\)](#) as

$$\tilde{E}(m, \tilde{\omega}, \phi) = B \left( \frac{m}{m_*} \right)^s \frac{N^2 \tilde{\omega}^{-d}}{1 - \left( \frac{m}{m_*} \right)^{s+3}} \quad (3.17)$$

where  $B$ ,  $s$  and  $d$  are constants, and  $m_* = 2\pi L$  is a transitional wavelength. Instead of the total wave energy  $\tilde{E}(m, \tilde{\omega}, \phi)$ , the momentum flux spectral density  $\rho \tilde{F}(m, \tilde{\omega}, \phi)$  is required. This is obtained through the group velocity rule. In order to have the momentum flux conserved in the absence of dissipative processes as the spectrum propagates vertically through height-varying background wind and buoyancy frequency, the coordinate framework  $(k, \omega)$  is used instead of  $(m, \tilde{\omega})$  as shown in [Scinocca \(2003\)](#).

The dissipative mechanisms applied to the wave field in each azimuthal direction and on each model level are critical level filtering and non-linear dissipation. After application of them, the resulting momentum flux profiles are used to derive the net eastward  $\rho \bar{F}_E$  and northward  $\rho \bar{F}_N$  fluxes. The tendencies for the  $(u, v)$  wind components are then given by the divergence of those fluxes obtained through summation of the total momentum flux (i.e. integrated over all phase speed bins) in each azimuth  $\phi_i$  projected onto the east and north directions, respectively:

$$\frac{\partial u}{\partial t} = g \frac{\partial(\rho \bar{F}_E)}{\partial p} \quad (3.18)$$

$$\frac{\partial v}{\partial t} = g \frac{\partial(\rho \bar{F}_N)}{\partial p} \quad (3.19)$$

where  $g$  is the gravitational acceleration and  $p$  is the pressure.

In order to eliminate the artificial noise in TL computations caused by the introduction of this scheme, it was necessary to implement some regularizations. These included rewriting buoyancy frequency computations in the non-linear scheme in height coordinates instead of pressure coordinates and setting increments for momentum flux in the last three spectral elements (high phase speed) of the launch spectrum to zero.

The simplified non-linear version of the non-orographic gravity wave drag scheme can be found in routine [GWDRAG\\_WMSS](#). TL and AD versions of the non-orographic gravity wave drag scheme (routines [GWDRAG\\_WMSSTL](#) and [GWDRAG\\_WMSSAD](#)) are activated by setting `LEGWWMS2` to `.TRUE.` in namelist [NAMTRAJP](#). The schemes would then be used with the prescribed time frequency `GTPHYGWWMS`. The necessary regularizations are activated by setting logical switch `LREGWWMS` in namelist [NAMTRAJP](#).

### 3.7 RADIATION

The radiation scheme solves the radiative transfer equation in two distinct spectral regions. The computations for the longwave (LW) radiation are performed over the spectrum from 0 to  $2820 \text{ cm}^{-1}$ . The shortwave (SW) part of the scheme integrates the fluxes over the whole shortwave spectrum between

0.2 and 4.0  $\mu\text{m}$ . The scheme used for data assimilation purposes must be computationally efficient to be called at each time step and at the full spatial resolution for an improved description of the cloud-radiation interactions during the assimilation period (Janisková *et al.*, 2002).

### 3.7.1 The short-wave radiation scheme

The linearized code for the shortwave radiation scheme has been derived from the ECMWF original non-linear scheme developed by Fouquart and Bonnel (1980) and revised by Morcrette (1991), and which was previously used in the operational forecast model. In this scheme, the photon-path-distribution method is used to separate the parametrization of the scattering processes from that of molecular absorption. Upward  $F_{\text{sw}}^\uparrow$  and downward  $F_{\text{sw}}^\downarrow$  fluxes at a given level  $j$  are obtained from the reflectance and transmittance of the atmospheric layers as

$$F_{\text{sw}}^\downarrow(j) = F_0 \prod_{k=j}^N T_{\text{bot}}(k) \quad (3.20)$$

$$F_{\text{sw}}^\uparrow(j) = F_{\text{sw}}^\downarrow(j) R_{\text{top}}(j-1) \quad (3.21)$$

Computations of the transmittance at the bottom of a layer  $T_{\text{bot}}$  start at the top of atmosphere and work downward. Those of the reflectance at the top of the same layer  $R_{\text{top}}$  start at the surface and work upward. In the presence of cloud in the layer, the final fluxes are computed as a weighted average of the fluxes in the clear sky and in the cloudy fractions of the column as

$$R_{\text{top}} = C_{\text{cloud}} R_{\text{cloud}} + (1 - C_{\text{cloud}}) R_{\text{clear}} \quad (3.22)$$

$$T_{\text{top}} = C_{\text{cloud}} T_{\text{cloud}} + (1 - C_{\text{cloud}}) T_{\text{clear}} \quad (3.23)$$

In the previous equations,  $C_{\text{cloud}}$  is the cloud fractional coverage of the layer within the cloudy fraction of the column (depending on the cloud-overlap assumption).

The non-linear version of the shortwave radiation scheme (described in details in section IV: Physical processes - 2.2. The pre-Cy32r2 shortwave radiation scheme) used six spectral intervals with transmission functions derived from a line-by-line code (Dubuisson *et al.*, 1996).

The non-linear scheme is reasonably fast for application in 4D-Var and has, therefore, been linearized without a priori modifications. The only modification with respect to the non-linear model is using two spectral intervals with transmission functions (instead of six intervals used in the former operational non-linear model) in order to reduce the computational cost.

### 3.7.2 The longwave radiation scheme

The longwave radiation scheme, operational in the ECMWF forecast model until June 2000, was a band emissivity type scheme (Morcrette, 1989). This scheme has been replaced by the Rapid Radiation Transfer Model (RRTM: (Mlawer *et al.*, 1997) in June 2000. The complexity of the RRTM scheme for the longwave part of the spectrum makes accurate computations expensive. In the variational assimilation framework, the former operational scheme (Morcrette, 1989) has been linearized. In this scheme, the longwave spectrum from 0 to 2820  $\text{cm}^{-1}$  is divided into six spectral regions. The transmission functions for water vapour and carbon dioxide over those spectral intervals are fitted using Padé approximations on narrow-band transmissions obtained with statistical band models (Morcrette *et al.*, 1986). Integration of the radiation transfer equation over wavenumber  $\nu$  within the particular spectral regions gives the upward and downward fluxes.

The incorporation of the effects of clouds on the longwave fluxes follows the treatment discussed by (Washington and Williamson, 1977). The scheme calculates first upward and downward fluxes ( $F_0^\uparrow(i)$  and  $F_0^\downarrow(i)$ ) corresponding to a clear-sky atmosphere. In any cloudy layer, the scheme evaluates the fluxes assuming a unique overcast cloud of emissivity unity, i.e.  $F_n^\uparrow(i)$  and  $F_n^\downarrow(i)$  for a cloud present in the  $n$ th layer of the atmosphere. The fluxes for the actual atmosphere are derived from a linear combination of the fluxes calculated in the previous steps with some cloud overlap assumption in the case of clouds present in several layers. Let  $N$  be the number of model layers starting from the top of atmosphere to

the bottom,  $C_i$  the fractional cloud cover in layer  $i$ , the cloudy upward  $F_{lw}^\uparrow$  and downward  $F_{lw}^\downarrow$  fluxes are expressed as:

$$F_{lw}^\uparrow(i) = (1 - CC_{N,i})F_0^\uparrow(i) + \sum_{k=i}^N (CC_{i,k+1} - CC_{i,k})F_k^\uparrow(i) \quad (3.24)$$

$$F_{lw}^\downarrow(i) = (1 - CC_{i-1,0})F_0^\downarrow(i) + \sum_{k=1}^{i-1} (CC_{i,k+1} - CC_{i,k})F_k^\downarrow(i) \quad (3.25)$$

where  $CC_{i,j}$  is the cloudiness encountered between any two levels  $i$  and  $j$  in the atmosphere computed using a certain overlap assumption.

In the case of semi-transparent clouds, the fractional cloudiness entering the calculations is an effective cloud cover equal to the product of the emissivity ( $\varepsilon_{cld}$ ) due to condensed water and gases in the layer by the horizontal coverage of the cloud cover. This is the so called effective emissivity approach. The detailed description of this longwave radiation scheme can be found in Section IV - Physical processes (2.2. The pre-Cy22r3 longwave radiation scheme).

To reduce a computational cost of the linearized longwave radiation for data assimilation, the transmission functions are only computed for H<sub>2</sub>O and CO<sub>2</sub> absorbers (though the version taking into account the whole spectrum of absorbers is also coded). The cloud effects on LW radiation are only computed to the level defined by the current cloud top height.

### 3.7.3 Cloud overlap assumptions

Cloud overlap assumptions must be made in atmospheric models in order to organize the cloud distribution used for radiation and precipitation/evaporation computations. A cloud overlap assumption of some sort is necessary to account for the fact that clouds often do not fill the whole grid box. The maximum-random overlap assumption (originally introduced in [Geleyn and Hollingsworth, 1997](#)) is used operationally in the ECMWF model ([Morcrette, 2000](#)). Adjacent layers containing cloud are combined by using maximum overlap to form a contiguous cloud and discrete layers separated by clear-sky are combined randomly as

$$CC_{i,j} = 1 - (1 - C_i) \prod_{k=i+1}^{j-1} \left[ \frac{1 - \max(C_k, C_{k-1})}{1 - C_{k-1}} \right] \quad (3.26)$$

where  $CC_{i,j}$  is cloudiness encountered between any levels  $i$  and  $j$  in the atmosphere and  $C_k$  is the cloud fraction of the layer  $k$  located between levels  $k$  and  $k + 1$ .

### 3.7.4 Cloud optical properties

Considering the cloud-radiation interactions, it is not only the cloud fraction or cloud volume, but also cloud optical properties that matter. In the case of shortwave radiation, the cloud radiative properties depend on three different parameters: the optical thickness  $\delta_c$ , the asymmetry factor  $g_c$  and the single scattering albedo  $\overline{\omega_c}$ . They are derived from [Fouquart \(1987\)](#) for the water clouds, and [Ebert and Curry \(1992\)](#) for the ice clouds. The optical thickness  $\delta_c$  is related to the cloud liquid/ice water amount  $u_{LWP}$  by :

$$\delta_c = u_{LWP} \left( a_i + \frac{b_i}{r_e} \right) \quad (3.27)$$

where  $a_i$  and  $b_i$  are defined from [Ebert and Curry \(1992\)](#) for ice particles and are set to respectively 0 and 3/2 for water particles. The mean effective radius of the size distribution of the cloud water droplets is defined by  $r_e$ . For water clouds,  $r_e$  is set to 13  $\mu\text{m}$  over oceans and to 10  $\mu\text{m}$  over continents. When ice cloud optical properties were initially introduced in the radiation code, the effective radius was set to 40  $\mu\text{m}$ . However, observations indicate that the effective radius of ice crystals increases with temperature, usually attributed to accretion from falling crystals. In the current scheme, account is taken of this by using the diagnostic formulation of [Ou and Liou \(1995\)](#):

$$r_e = 326.3 + 12.42 \times T_i + 0.197 \times T_i^2 + 0.0012 \times T_i^3 \quad (3.28)$$



where  $T_i = \min(T, -23^\circ\text{C})$ . The effective radius is then limited within the interval 30–60  $\mu\text{m}$ .

In the two spectral intervals of the shortwave scheme, the asymmetry factor  $g_c$  is fixed to 0.865 and 0.910, respectively and  $\omega_c$  is given as a function of  $\delta_c$  following [Fouquart \(1987\)](#):

$$\bar{\omega}_{c1} = 0.9999 - 5 \times 10^{-4} \exp(-0.5\delta_c) \quad (3.29)$$

$$\bar{\omega}_{c2} = 0.9988 - 2.5 \times 10^{-3} \exp(-0.05\delta_c) \quad (3.30)$$

These cloud shortwave radiative parameters have been fitted to in-situ measurements of stratocumulus clouds ([Bonnell \*et al.\*, 1983](#)).

The optical properties of ice clouds are expressed as:

$$\bar{\omega}_i = c_i - d_i r_e \quad (3.31)$$

$$g_i = e_i + f_i r_e \quad (3.32)$$

where the coefficients are derived from [Ebert and Curry \(1992\)](#).

Cloud longwave optical properties are represented by the emissivity  $\varepsilon_{cld}$  related to the condensed water amount and by the condensed water mass absorption coefficient  $k_{abs}$ . The emissivity  $\varepsilon_{cld}$  is related to the condensed water amount by:

$$\varepsilon_{cld} = 1 - \exp(-k_{abs} u_{LWP}) \quad (3.33)$$

where  $k_{abs}$  is the condensed water mass absorption coefficient obtained following [Smith and Shi \(1992\)](#) for the water clouds and [Ebert and Curry \(1992\)](#) for the ice clouds.  $u_{LWP}$  is the condensed water path.  $k_{abs}$  depends upon the water phase (ice or water) and upon temperature. A spectral dependency can also be included.

Linearized shortwave and longwave radiation schemes are activated using the logical switch `LERADSN2=.TRUE.` in the namelist `NAMTRAJP`.

To use the tangent-linear (TL) and adjoint (AD) versions of the shortwave radiation scheme, `LERADSW2` should be set to `.TRUE.` in `NAMTRAJP`. The default value is set to `.FALSE.`. To decrease a computational cost of the shortwave radiation in data assimilation, the number of spectral intervals is reduced to two (six intervals are used in the forecast model) during minimization. The number of spectral intervals `NSW` is changed in `CVA1`. This change also requires to read several parameters for two spectral intervals. This is done in set-up routines `SUSWN`, `SUCLOPN` and `SUAERSN`.

The TL/AD longwave radiation scheme can be activated by setting `LERADLW2=.TRUE.` in the namelist `NAMTRAJP` (the default value is `.FALSE.`). To use a time/memory optimized version of the code, additional set-up (requirement for the shorter loops inside of `NPROMA` by setting `LOPTLWPR=.TRUE.` and definition of the number of loops inside of `NPROMA`, currently `NLOOPLW=3`) should also be included in `NAMTRAJP`. For further optimization, cloud effects on the longwave radiation are only computed to the certain level determined from the cloud top height. This is activated by `LWLCLHR=.TRUE.` in `NAMTRAJP`. Using this optimization, computational cost is decreased, but TL and AD results are not bit reproducible. If reproducibility is required in 4D-Var (`LREPRO4DVAR=.TRUE.`) the switch `LWLCLHR` is automatically set to `.FALSE.`. The same can be achieved by using default value for `LWLCLHR`, which is `.FALSE.`.

The linearized radiation schemes are called from `RADINATL` and `RADINAAD`, where the computation of radiation fluxes is performed. Tendencies produced by the linearized longwave and shortwave radiation are computed in `RADHEATTL` and `RADHEATAD`. All those routines are called from `CALLPARTL` and `CALLPARAD`, respectively.

`RADLSWTL` and `RADLSWAD` are the drivers for the computation of the solar and thermal fluxes by calling specialized routines for shortwave radiation (`SWTL` and `SWAD`) and for longwave radiation (`LWTL` and `LWAD`).

### 3.8 LARGE-SCALE CONDENSATION AND PRECIPITATION

The original version of the simplified diagnostic large-scale cloud and precipitation scheme currently used in the minimization of 4D-Var is described in [Tompkins and Janisková \(2004\)](#). This scheme replaced the much simpler large-scale precipitation parametrization of [Mahfouf \(1999\)](#), which was used in operations until Cy33r1.

The physical tendencies of temperature and specific humidity produced by moist processes on the large-scale can be written as

$$\frac{\partial q}{\partial t} = -\mathcal{C} + E_{\text{prec}} + \mathcal{D}_{\text{conv}} \quad (3.34)$$

$$\frac{\partial T}{\partial t} = L(\mathcal{C} - E_{\text{prec}} - \mathcal{D}_{\text{conv}}) + L_f(\mathcal{F} - \mathcal{M}) \quad (3.35)$$

where  $\mathcal{C}$  denotes large-scale condensation (negative if evaporation),  $E_{\text{prec}}$  is the moistening due to the evaporation of precipitation and  $\mathcal{D}_{\text{conv}}$  is the detrainment of cloud water from convective clouds.  $\mathcal{F}$  and  $\mathcal{M}$  correspond to the freezing of rain and melting of snow, respectively.  $L$  and  $L_f$  are the latent heats of vaporisation/sublimation and fusion, respectively.

#### 3.8.1 Stratiform condensation

The subgrid-scale variability of humidity is assumed to be represented by a uniform distribution with half width  $W$ . Condensation inside the model gridbox occurs whenever gridbox mean relative humidity,  $RH$ , exceeds a critical threshold,  $RH_{\text{crit}}$ . The half width of the distribution is given by

$$W = q_{\text{sat}} \{1 - RH_{\text{crit}} - \kappa(RH - RH_{\text{crit}})\} \quad (3.36)$$

The critical relative humidity threshold,  $RH_{\text{crit}}$ , is assumed to be dependent on reduced pressure  $\sigma = p/p_{\text{surf}}$ , through

$$RH_{\text{crit}} = 0.7\sigma(1 - \sigma)(1.85 + 0.95(\sigma - 0.5)) \quad (3.37)$$

$\kappa$  is a coefficient that reduces the width of the uniform distribution when  $RH$  increases and it also depends on  $\sigma$  as

$$\kappa = \max(0, 0.9(\sigma - 0.2)^{0.2}) \quad (3.38)$$

Equation (3.36) together with the assumption of a uniform distribution yields the following relationships for stratiform cloud cover,  $C_{\text{strat}}$ , and cloud condensate specific ratio,  $q_{\text{c}}^{\text{strat}}$ :

$$C_{\text{strat}} = 1 - \sqrt{\frac{1 - RH}{1 - RH_{\text{crit}} - \kappa(RH - RH_{\text{crit}})}} \quad (3.39)$$

$$q_{\text{c}}^{\text{strat}} = q_{\text{sat}} C_{\text{strat}}^2 \{ \kappa(1 - RH) + (1 - \kappa)(1 - RH_{\text{crit}}) \} \quad (3.40)$$

where  $q_{\text{sat}}$  is the saturation specific humidity.

Figure [Fig. 3.1](#) displays the variations of stratiform cloud cover,  $C_{\text{strat}}$ , as a function of relative humidity for various settings of parameter  $\kappa$ .

#### 3.8.2 Convective contribution

The impact of convective activity on large-scale clouds, which is particularly important in the tropics and mid-latitude summers, is accounted for through the detrainment term coming out of the convection scheme (see [Section 3.9](#)). The additional cloud cover,  $C_{\text{conv}}$ , and cloud condensate,  $q_{\text{c}}^{\text{conv}}$ , resulting from convection are computed as

$$C_{\text{conv}} = (1 - C_{\text{strat}}) \left\{ 1 - \exp\left(\frac{-\delta_{\text{u}} M_{\text{u}} \Delta t}{\rho \Delta z}\right) \right\} \quad (3.41)$$

$$q_{\text{c}}^{\text{conv}} = \delta_{\text{u}} M_{\text{u}} q_{\text{l}}^{\text{u}} \frac{\Delta t}{\rho \Delta z} \quad (3.42)$$

where  $\delta_{\text{u}}$  (unitless),  $M_{\text{u}}$  (in  $\text{kg m}^{-2} \text{s}^{-1}$ ) and  $q_{\text{l}}^{\text{u}}$  (in  $\text{kg kg}^{-1}$ ) are the detrainment rate, mass flux and cloud liquid water content in the convective updraught, respectively.  $\Delta t$  and  $\Delta z$  denote the model time step and model layer depth, while  $\rho$  is the air density.

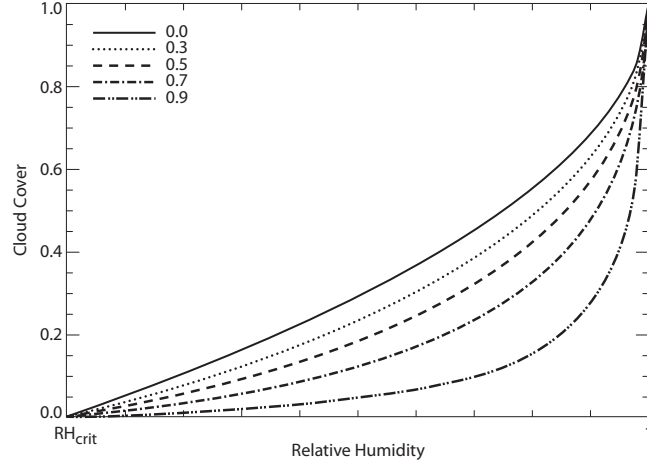


**Figure 3.1** Stratiform cloud cover,  $C_{\text{strat}}$ , as a function of grid-box mean relative humidity for various values of parameter  $\kappa$  (see top left legend). Relative humidity ranges between  $RH_{\text{crit}}$  and unity (i.e. grid box is entirely saturated).

### 3.8.3 Precipitation formation

The formation of precipitation from cloud condensate,  $q_c$ , is parameterized according to Sundqvist *et al.* (1989). The corresponding tendency writes

$$\left(\frac{\partial q_c}{\partial t}\right)_{\text{prec}} = -C_0 q_c \left\{ 1 - \exp \left[ - \left( \frac{q_c}{C q_c^{\text{crit}}} \right)^2 \right] \right\} \quad (3.43)$$

where  $C = C_{\text{strat}} + C_{\text{conv}}$  is used to obtain in-cloud condensate amounts. The critical cloud water threshold,  $q_c^{\text{crit}}$  is set to  $3 \times 10^{-4} \text{ kg kg}^{-1}$  if precipitation evaporation is activated,  $6 \times 10^{-4} \text{ kg kg}^{-1}$  otherwise. The conversion factor  $C_0$  is set to  $3.33 \times 10^{-4} \text{ s}^{-1}$ . Note that the Bergeron-Findeisen mechanism and collection processes are disregarded in the current version of the simplified scheme.

In the code, the new cloud water content after precipitation formation is calculated as

$$q_c^{\text{new}} = q_c \exp(-D) \quad (3.44)$$

where the quantity  $D$  is computed as

$$D = C_0 \Delta t \left\{ 1 - \exp \left[ - \left( \frac{q_c}{C q_c^{\text{crit}}} \right)^2 \right] \right\} \quad (3.45)$$

It is worth noting that precipitation formed from cloud liquid water at temperatures below the freezing point is assumed to freeze instantly, which corresponds to term  $\mathcal{F}$  in (3.35).

### 3.8.4 Precipitation evaporation

The scheme partially accounts for the overlap of precipitation with the subgrid clear-sky distribution of humidity fluctuations (uniformly distributed). Precipitation evaporation computations are based on the mean specific humidity,  $\overline{q_{\text{prec}}^{\text{clr}}}$ , in the clear-sky portion through which precipitation is falling, denoted  $f_{\text{prec}}^{\text{clr}}$ . Consistent with the maximum overlap assumption made in the calculations of total cloud cover and precipitation fraction, it is hypothesized that  $f_{\text{prec}}^{\text{clr}}$  corresponds to the moistest part of the uniform distribution, as illustrated in Fig. 3.2.

From this, one can show that

$$\overline{q_{\text{prec}}^{\text{clr}}} = q_{\text{sat}} - \frac{f_{\text{prec}}^{\text{clr}} (q_{\text{sat}} - \bar{q})}{(1 - C)^2} \quad (3.46)$$

where  $\bar{q}$  denotes the gridbox mean specific humidity.

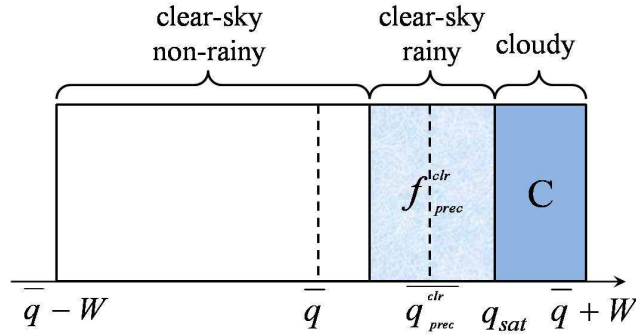


**Figure 3.2** Illustration of the uniform distribution of specific humidity over the model grid box with various quantities referred to in the text.

Precipitation evaporation is parameterized following Kessler (1969):

$$\left(\frac{\partial q}{\partial t}\right)_{\text{evap}} = f_{\text{prec}}^{\text{clr}} \beta (q_{\text{sat}} - \overline{q_{\text{prec}}^{\text{clr}}}) \quad (3.47)$$

where  $\beta$  is given by

$$\beta = 5.44 \times 10^{-4} \left\{ \left(\frac{p}{p_{\text{surf}}}\right)^{\frac{1}{2}} \frac{P_{\text{clr}}}{5.9 \times 10^{-3} f_{\text{prec}}^{\text{clr}}} \right\}^{0.577} \quad (3.48)$$

where  $P_{\text{clr}}$  denotes precipitation in the clear-sky fraction of the grid box. Equation (3.47) is solved implicitly to take into account the reduction of  $q_{\text{sat}}$  due to evaporative cooling, which yields the moistening associated to precipitation evaporation:

$$E_{\text{prec}} = \frac{f_{\text{prec}}^{\text{clr}} \beta \Delta t (q_{\text{sat}} - \overline{q_{\text{prec}}^{\text{clr}}})}{1 + \beta \Delta t \left[ 1 + \frac{L_v}{c_p} \frac{\partial q_{\text{sat}}}{\partial T} \right]} \quad (3.49)$$

Finally, the loss of precipitation through evaporation (in  $\text{kg m}^{-2} \text{ s}^{-1}$ ) is simply expressed as  $\Delta P_{\text{evap}} = -E_{\text{prec}} \Delta p / (g \Delta t)$ .

### 3.8.5 Phase partitioning

A simple diagnostic partitioning based on temperature is used to separate cloud condensate into liquid and ice. The liquid water fraction,  $\alpha_l$ , is calculated as

$$\alpha_l = \begin{cases} 0.545 \times \tanh [0.17(T - 266.41) + 1] & \text{if } T < 273.15 \text{ K} \\ 1 & \text{if } T \geq 273.15 \text{ K} \end{cases} \quad (3.50)$$

### 3.8.6 Code

The computations performed in the simplified large-scale cloud and precipitation scheme are performed in subroutine **CLOUDST**, which is called from the main physics routine **CALLPAR**. **LENCLD2** (namelist **NAMTRAJP**) is the main switch that activates this simplified scheme in non-linear and linearized (tangent-linear and adjoint) integrations. The switch **LEVAPLS2** (namelist **NAMTRAJP**) controls the activation of the precipitation evaporation computations (default setting is **.FALSE.**). The tangent-linear and adjoint versions of the scheme are **CLOUDSTTL** and **CLOUDSTAD**, respectively.

#### SET-UP OF PARAMETERS

Defined in subroutines **SUCLDP** and **SU0PHY**.

### 3.8.7 Regularization

Special care had to be taken to avoid the spurious growth of some perturbations in the tangent-linear and adjoint versions of the simplified large-scale cloud and precipitation code. Problematic perturbations

are artificially reduced, as described below. Switch LREGCL should be set to `.TRUE.` in namelist `NAMTRAJP` to activate these regularizations in the linearized code. In the following, the prime symbol is employed to denote perturbations.

#### CLOUDSTTL/CLOUDSTAD:

- After (3.39):  $C'_{\text{strat}} = C'_{\text{strat}} \times \begin{cases} -1.2 C_{\text{strat}} + 0.94 & \text{if } 0.2 < C_{\text{strat}} < 0.7 \\ 0.1 & \text{if } 0.7 \leq C_{\text{strat}} < 0.95 \\ 0.1 \sqrt{(1 - C_{\text{strat}})/(1 - 0.95)} & \text{if } C_{\text{strat}} \geq 0.95 \end{cases}$
- $D'$  is scaled by 0.01 in autoconversion of cloud water to precipitation (3.45).

### 3.9 MOIST CONVECTION

The original version of the simplified mass-flux convection scheme currently used in the minimization of 4D-Var is described in Lopez and Moreau (2005). It replaced the much simpler convective parametrization of Mahfouf (1999), which was used in operations until Cy33r1. Through time, the original scheme from Lopez and Moreau (2005) has been updated so as to gradually converge towards the full convection scheme used in high-resolution 10-day forecasts (see Chapter 6 of Part IV). The transport of tracers by convection has also been added.

The physical tendencies produced by convection on any conservative variable  $\psi$  (dry static energy, wind components, specific humidity, cloud liquid water) can be written in a mass-flux formulation as Betts (1997)

$$\frac{\partial \psi}{\partial t} = \frac{1}{\rho} \left[ (M_u + M_d) \frac{\partial \psi}{\partial z} + D_u(\psi_u - \psi) + D_d(\psi_d - \psi) \right] \quad (3.51)$$

The first term on the right hand side represents the compensating subsidence induced by cumulus convection on the environment through the mass flux,  $M$ . The other terms accounts for the detrainment of cloud properties in the environment with a detrainment rate,  $D$ . Subscripts  $u$  and  $d$  refer to the updraughts and downdraughts properties, respectively. Evaporation of cloud water and precipitation should also be added in (3.51) for dry static energy,  $s = c_p T + gz$ , and specific humidity,  $q$ .

#### 3.9.1 Equations for updraught and downdraught

The equations describing the evolution with height of the convective updraught and downdraught mass fluxes,  $M_u$  and  $M_d$  (units  $\text{kg m}^2 \text{s}^{-1}$ ), respectively, are

$$\frac{\partial M_u}{\partial z} = (\epsilon_u - \delta_u) M_u \quad (3.52)$$

$$\frac{\partial M_d}{\partial z} = -(\epsilon_d - \delta_d) M_d \quad (3.53)$$

where  $\epsilon$  and  $\delta$  respectively denote the entrainment and detrainment rates (in  $\text{m}^{-1}$ ). A second set of equations is used to describe the evolution with height of any other characteristic,  $\psi$ , of the updraught or downdraught, namely

$$\frac{\partial \psi_u}{\partial z} = -\epsilon_u(\psi_u - \bar{\psi}) \quad (3.54)$$

$$\frac{\partial \psi_d}{\partial z} = \epsilon_d(\psi_d - \bar{\psi}) \quad (3.55)$$

where  $\bar{\psi}$  is the value of  $\psi$  in the large-scale environment.

In practice, (3.52) and (3.53) are solved in terms of  $\mu = M/M_u^{\text{base}}$ , where  $M_u^{\text{base}}$  is the mass flux at cloud base (determined from the closure assumptions as described further down).  $\mu$  is equal to 1 at cloud base for the updraught and is set to  $-0.3$  at the Level of Free Sinking (LFS) in the case of the downdraught. The LFS is assumed to be the highest model level (below the level of minimum moist static energy) where a mixture of equal parts of cloud and saturated environmental air at the wet-bulb temperature becomes negative buoyant with respect to the environmental air. In other words, LFS corresponds to the starting level of the downdraught. The solution profiles of  $\mu$  values are eventually multiplied by  $M_u^{\text{base}}$  to obtain the final mass-flux profiles.

### 3.9.2 Triggering of moist convection

The determination of the occurrence of moist convection in the model is based on whether a positively buoyant test parcel starting at each model level (iteratively from the surface and upwards) can rise high enough to produce a convective cloud and possibly precipitation. Shallow convection is first tested for by considering a parcel rising from the lowest model level. New test parcels starting from model levels of increasing altitude are then considered to identify deep convection, this time. This procedure is repeated until deep convection is found or until the departure altitude of the parcel reaches about 15 km.

The initial characteristics of the test parcel originating from the lowest model level (to test for shallow convection) are derived from surface sensible and latent turbulent heat fluxes ( $J_s$  and  $J_q$ , respectively). The initial vertical velocity of the test parcel is assumed to be equal to the convective-scale vertical velocity,  $w_*$ , defined as

$$w_* = 1.2 \left( u_*^3 - 1.5 \frac{gz\kappa}{\bar{\rho}T} \left[ \frac{J_s}{c_p} + 0.608 \bar{T} \frac{J_q}{L_v} \right] \right) \quad (3.56)$$

where  $\kappa=0.4$  is the von Karman constant and the friction velocity  $u_*$  is set to a constant value of  $0.1 \text{ m s}^{-1}$ .

Following [Jakob and Siebesma \(2003\)](#), the temperature excess,  $\Delta T_u$ , and moisture excess,  $\Delta q_u$ , of the test parcel with respect to the environment are prescribed as

$$\Delta T_u = -1.5 \frac{J_s}{\bar{\rho}c_p w_*} \quad \text{and} \quad \Delta q_u = -1.5 \frac{J_q}{\bar{\rho}L_v w_*} \quad (3.57)$$

For a test parcel initiated higher than the lowest model level (i.e. deep convection test), its initial vertical velocity is arbitrarily set to  $1 \text{ m s}^{-1}$ , while its temperature and moisture excesses are assumed to be

$$\Delta T_u = 0.2 \text{ K} \quad \text{and} \quad \Delta q_u = 1 \times 10^{-4} \text{ kg kg}^{-1} \quad (3.58)$$

Furthermore, in the lowest 60 hPa of the atmosphere that typically correspond to the mixed-layer depth over oceanic regions, the updraught values of the dry static energy and moisture at the departure level  $k$  are initialized as  $s_k^u = \tilde{s}_k + c_p \Delta T_u$ , where the tilde symbol represents a 50 hPa layer average, instead of  $s_k^u = \bar{s}_k + c_p \Delta T_u$  as for departure levels above the 60 hPa mixed-layer.

If convection is found for the parcel initiated from the lowest level, it is classified as shallow convection if cloud depth is lower than 200 hPa. If convection is found for a parcel initiated above the lowest model level, it is classified as deep convection provided cloud depth exceeds 200 hPa. A grid point affected by both shallow and deep convection is treated as deep convection. Note that mid-level convection is not distinguished from deep convection.

### 3.9.3 Entrainment and detrainment

#### Updraught

Entrainment rate ( $\epsilon_u$ ) in the updraught is split into turbulent and organized components by writing  $\epsilon_u = \epsilon_u^{\text{turb}} + \epsilon_u^{\text{org}}$ . Both parts consist of constant parameters that are modulated by humidity conditions in the environment, in terms of relative humidity,  $\overline{RH}$ , and saturation specific humidity,  $\overline{q_{\text{sat}}}$ .

The constant parameters for turbulent and organized entrainment are:

$$\epsilon_{0_u}^{\text{turb}} = \begin{cases} 0.8 \times 10^{-4} \text{ m}^{-1} \text{ (ENTRPEN2)} & \text{for deep convection} \\ 3 \times 10^{-4} \text{ m}^{-1} \text{ (ENTRSCV2)} & \text{for shallow convection} \end{cases} \quad (3.59)$$

$$\epsilon_{0_u}^{\text{org}} = \begin{cases} 0.8 \times 10^{-4} \text{ m}^{-2} \text{ s}^2 \text{ (ENTRORG2)} & \text{for deep convection} \\ 0 & \text{for shallow convection} \end{cases} \quad (3.60)$$

The final entrainment rates in the updraught, to be used in (3.52)-(3.55), are computed as

$$\epsilon_u^{\text{turb}} = \epsilon_{0u}^{\text{turb}} \times 4 \times \min\left(1, \frac{\overline{q_{\text{sat}}}}{q_{\text{sat}}^{\text{base}}}\right) \quad (3.61)$$

$$\epsilon_u^{\text{org}} = \begin{cases} g\epsilon_{0u}^{\text{org}} [1.0 - \min(\overline{RH}, 1)] & \text{for } z = z_{\text{base}} \\ g\epsilon_{0u}^{\text{org}} [1.3 - \min(\overline{RH}, 1)] \min\left(1, \left(\frac{\overline{q_{\text{sat}}}}{q_{\text{sat}}^{\text{base}}}\right)^3\right) & \text{for } z > z_{\text{base}} \\ 0 & \text{otherwise} \end{cases} \quad (3.62)$$

In each layer,  $\epsilon_u^{\text{org}} \Delta z$  is limited to a maximum value of 0.4. Also note that organized entrainment is always zero for shallow convection.

Detrainment in the updraught is assumed to occur inside the convective cloud only where updraught vertical gradient of kinetic energy ( $\partial w_u^2 / \partial z$ ) and buoyancy are negative (i.e. usually in the upper part of the convective cloud). The corresponding detrainment rate,  $\delta_u$ , between model levels  $k+1$  and  $k$  is given by

$$\delta_u = \max\left(1.2\epsilon_{0u}^{\text{turb}}, 1 - \frac{(w_u^2)_k}{(w_u^2)_{k+1}}\right) \quad (3.63)$$

Any remaining updraught mass flux is supposed to be detrained at the level where  $w_u$  vanishes.

#### Downdraught

For all types of convection, the entrainment rate in the downdraught is set to a constant value:

$$\epsilon_d = \begin{cases} 2 \times 10^{-4} \text{ m}^{-1} \text{ (ENTRDD2)} & \text{for } z_{\text{topde}} \leq z \leq z_{\text{LFS}} \\ 0 & \text{elsewhere} \end{cases} \quad (3.64)$$

where subscript *topde* denotes the model level corresponding to the top of the 60 hPa atmospheric layer just above the surface.

Detrainment in the downdraught is defined as

$$\delta_d = \begin{cases} \frac{1}{z_{\text{topde}}} \frac{M_d^{\text{topde}}}{M_d} & \text{for } z < z_{\text{topde}} \\ \epsilon_d & \text{for } z_{\text{topde}} \leq z \leq z_{\text{LFS}} \\ 0 & \text{for } z > z_{\text{LFS}} \end{cases} \quad (3.65)$$

This formulation ensures a downward linear decrease of downdraught mass flux to zero at the surface.

#### Special case of momentum

To describe momentum exchange between the updraught and the environment, the entrainment rate is specified as a linear combination of the entrainment and detrainment rates that are applied to all other variables (as given in (3.61), (3.62) and (3.63))

$$\epsilon_u^{\text{mom}} = \begin{cases} \epsilon_u + 2\delta_u & \text{in all types of convection} \\ \epsilon_u + 3\delta_u & \text{at the top three levels of deep convective cloud} \\ 0 & \text{otherwise} \end{cases} \quad (3.66)$$

### 3.9.4 Precipitation formation

The formation of precipitation from the cloud water contained in the updraught ( $q_l^u$ ) is parameterized according to Sundqvist *et al.* (1989). The corresponding tendency writes:

$$\left(\frac{\partial q_l^u}{\partial z}\right)_{\text{prec}} = -C_0 C_{\text{BF}} q_l^u \left\{ 1 - \exp\left[-\left(\frac{q_l^u}{q_l^{\text{crit}}}\right)^2\right] \right\} \quad (3.67)$$

where the critical cloud water threshold,  $q_l^{\text{crit}}$  is set to  $5 \times 10^{-4} \text{ kg kg}^{-1}$ . Conversion factors  $C_0$  and  $C_{\text{BF}}$  (Bergeron-Findeisen mechanism) are given by:

$$C_0 = \frac{1.5 \times 10^{-3}}{0.75 w_u} \quad (3.68)$$

$$C_{\text{BF}} = \begin{cases} 1 + 0.5 \sqrt{\min(T_{\text{BF}} - T_{\text{ice}}, T_{\text{BF}} - T_u)} & \text{if } T_u < T_{\text{BF}} \\ 1 & \text{if } T_u \geq T_{\text{BF}} \end{cases} \quad (3.69)$$

where  $w_u$  and  $T_u$  are the vertical velocity and the temperature of the updraught, and  $T_{\text{ice}}=250.16 \text{ K}$  ( $-23^\circ\text{C}$ ) and  $T_{\text{BF}}=268.16 \text{ K}$  ( $-5^\circ\text{C}$ ).

In the code, (3.67) is integrated over each model layer during the updraught ascent. The new cloud water content in the updraught at a given model level  $k$  after precipitation formation is expressed as a function of the initial updraught cloud water content at model level  $k+1$  and of the additional amount of condensate ( $Cond$ ) produced by convection during the ascent from levels  $k+1$  to  $k$  (by convention, model level number increases downwards):

$$(q_l^u)_k = (q_l^u)_{k+1} \exp(-D) + Cond \frac{1 - \exp(-D)}{D} \quad (3.70)$$

where the quantity  $D$  is computed as

$$D = C_0 C_{\text{BF}} \Delta z \left\{ 1 - \exp \left[ - \left( \frac{(q_l^u)_{k+1}}{q_l^{\text{crit}}} \right)^2 \right] \right\} \quad (3.71)$$

It is worth noting that precipitation formed from cloud liquid water at temperatures below the freezing point is assumed to freeze instantly.

### 3.9.5 Closure assumptions

One needs to formulate so-called closure assumptions to compute the convective updraught mass-flux at cloud base,  $M_u^{\text{base}}$ , from quantities that are explicitly resolved by the model.

#### Deep convection

The closure is based on the balance between the convective available potential energy ( $CAPE$ ) in the subgrid-scale updraught and the total heat release ( $HEAT$ ) in the resolved larger-scale environment.  $CAPE$  and  $HEAT$  are computed as vertical integrals over the depth of the convective cloud as

$$CAPE = \int_{\text{cloud}} g \left( \frac{T_v^u - \overline{T_v}}{\overline{T_v}} - q_l^u \right) dz \quad (3.72)$$

$$HEAT = \int_{\text{cloud}} \left( \frac{1}{c_p \overline{T}} \frac{\partial \overline{s}}{\partial z} + 0.608 \frac{\partial \overline{q}}{\partial z} \right) (\mu_u + \mu_d) \frac{g}{\rho} dz \quad (3.73)$$

where  $T_v$  denotes virtual temperature. Finally, the cloud-base mass flux for deep convection situations is given by:

$$M_u^{\text{base}} = \frac{CAPE}{HEAT \times \tau} \quad (3.74)$$

where  $\tau$  is an adjustment timescale (in seconds), which is expressed as

$$\tau = (1 + 264/n_T) H_{\text{cld}} / \overline{w_u} \quad (3.75)$$

In (3.75),  $\overline{w_u}$  is the updraught vertical velocity averaged over the cloud depth,  $H_{\text{cld}}$ , and  $n_T$  if the spectral truncation.

#### Shallow convection



The closure assumption links the moist-energy excess at cloud base,  $\delta h_{\text{base}}$ , to the moist-energy convergence inside the sub-cloud layer (SCL),  $\delta h_{\text{SCL}}$ . The two latter quantities are defined as

$$\delta h_{\text{base}} = \left[ c_p(T_u - \bar{T}) + L_v(q^u + q_l^u - \bar{q}) \right]_{\text{base}} \quad (3.76)$$

$$\delta h_{\text{SCL}} = \int_{\text{SCL}} \left( c_p \frac{\partial \bar{T}}{\partial t} + L_v \frac{\partial \bar{q}}{\partial t} \right) \frac{dp}{g} \quad (3.77)$$

Eventually, the cloud-base mass flux for shallow convection is given by:

$$M_u^{\text{base}} = \frac{\delta h_{\text{SCL}}}{\delta h_{\text{base}}} \quad (3.78)$$

### 3.9.6 Flow chart

The computations performed in the simplified cumulus convection scheme are performed in the subroutines shown in Fig. 3.3. LECUMFS and LECUMFS2 are the two main switches to activate this simplified convection scheme in non-linear and linearized (tangent-linear and adjoint) integrations, respectively (namelist **NAMCUMFS**).

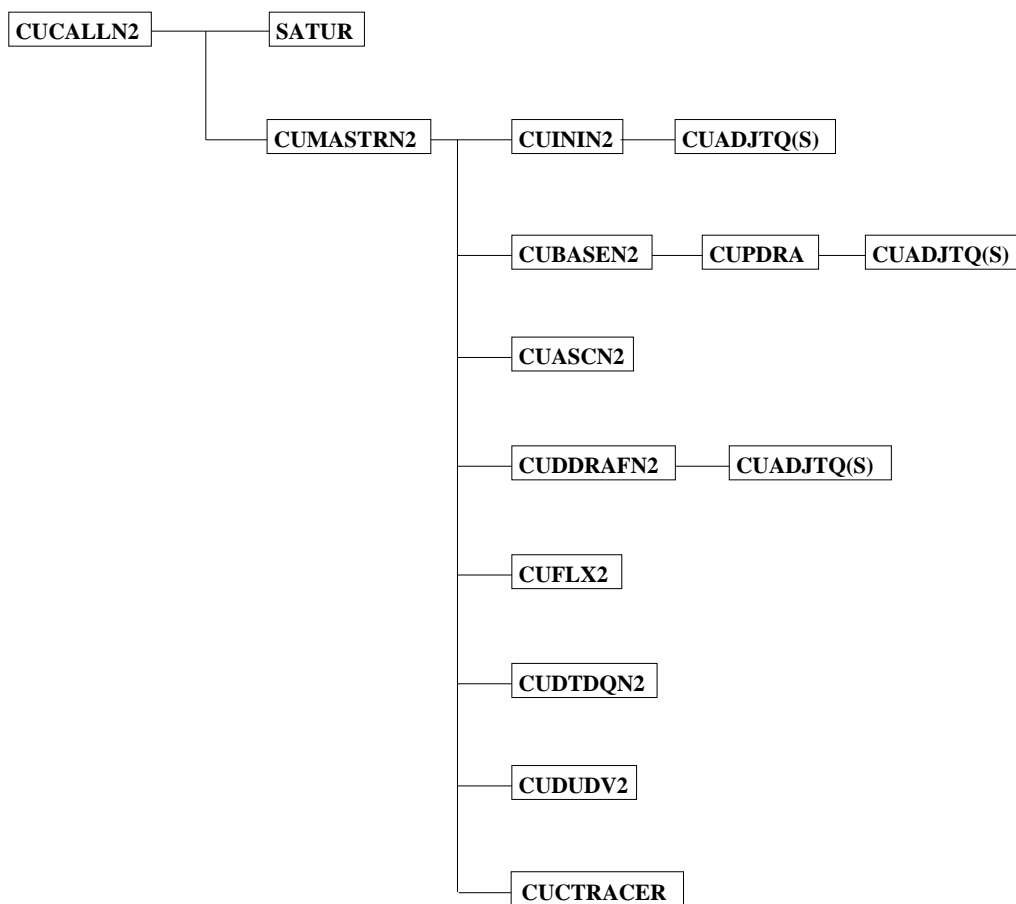


**Figure 3.3** Structure of the simplified convection scheme for data assimilation.

**CUCALLN2**: Provides interface of routines for cumulus parametrization. It is called from **CALLPAR** and returns updated tendencies of  $T$ ,  $q$ ,  $u$ ,  $v$  and chemical tracers, as well as convective precipitation rates.

**CUMASTRN2**: Master routine for convection scheme. Also performs the convective closure and computes the momentum transport by convective draughts.

**CUININ2**: Initializes variables for convection scheme (including vertical interpolation to half model levels).

**CUBASEN2:** Triggering of convective updraught. Calculates condensation level and sets updraught base variables and first-guess cloud type.

**CUPDRA:** Computes preliminary updraught ascent to evaluate convective cloud top and base heights.

**CUASCN2:** Calculates actual ascent in updraught.

**CUDDRAF2:** Calculates the downdraught descent.

**CUFLX2:** Calculates final convective fluxes and surface precipitation rates taking into account of melting/freezing and the evaporation of falling precipitation.

**CUDTDQN2:** Calculates the tendencies of  $T$  and  $q$  from convection.

**CUDUDV2:** Calculates the tendencies of  $u$  and  $v$  from convection.

**CUCTRACER2:** Calculates the tendencies of tracer fields due to the transport by convection.

EXTERNALS

**SATUR:** Computes saturation specific humidity.

**CUADJTQS:** Calculates super/sub-saturation and adjusts  $T$  and  $q$  accordingly.

All subroutines listed above have tangent-linear and adjoint versions with extension TL and AD, respectively. Of course, in the adjoint code, the calling order of the subroutines shown in [Fig. 3.3](#) is reversed.

SET-UP OF PARAMETERS

Defined in subroutine **SUCUM2** called from **SUPHEC**.

### 3.9.7 Regularization

Special care had to be taken to avoid the spurious growth of some perturbations in the tangent-linear and adjoint versions of the simplified convection code. In most cases, problematic perturbations are artificially reduced or even set to zero, as described below for each affected routine. Switch **LREGCV** should be set to **.TRUE.** in namelist **NAMCUMFS** to activate these regularizations in the linearized code. In the following, the prime symbol is employed to denote perturbations.

**CUMASTRN2TL/AD:**

- $(\delta h_{\text{base}})'$  is multiplied by 0.1 in computation of  $M_{\text{u}}^{\text{base}}$  for shallow convection.
- $(M_{\text{u}}^{\text{base}})'$  is scaled by 0.2 in test whether  $\delta h_{\text{SCL}}/(\delta h_{\text{base}})^2 > 10^3$ .
- $(M_{\text{u}}^{\text{base}})'$  is scaled by 0.25 for both deep and shallow convection.

**CUBASEN2TL/AD:**

- $w'_* = 0$  if  $w_* < 0.5 \text{ m s}^{-1}$  (convective-scale velocity).
- Buoyancy perturbation is scaled by 0.35 in updraught initialization.

**CUASCN2TL/AD:**

- $(\epsilon_{\text{u}}^{\text{org}})'$  is scaled by 0.1.
- $(\frac{w_{\text{u}}^2(k)}{w_{\text{u}}^2(k+1)})'$  is set to 0 in organized detrainment computations.
- $w'_{\text{u}}$  is set to 
$$\begin{cases} 0 & \text{if } w_{\text{u}} < 0.1 \text{ m s}^{-1} \\ 0.1 \times w'_{\text{u}} & \text{if } w_{\text{u}} \geq 0.1 \text{ m s}^{-1} \end{cases}$$
- $(\frac{q_{\text{sat}}}{q_{\text{base}}})'$  is set to 0 in turbulent entrainment computations.

- Buoyancy perturbation is scaled by 0.33 in updraught computations.

#### CUPDRATL/AD:

- Buoyancy perturbation is scaled by 0.33 in updraught computations.

#### SUCUMF2:

- Mass-flux limiter, RMFCFL2, is set to 1 to avoid instabilities in implicit solver.

### 3.10 TRAJECTORY MANAGEMENT

The ECMWF physics uses the tendencies from the dynamics and variables at  $t - \Delta t$  as input to compute the tendencies of a given process (represented by the operator P) for a prognostic variable  $\psi$ . Therefore

$$\frac{\psi^{n+1} - \psi_u^{n-1}}{2\Delta t} = P(\psi_u^{n-1}) \quad (3.79)$$

where the variable  $\psi_u$  has already been updated by the dynamics and by the previous physical processes (which are called in the following order: radiation; vertical diffusion; subgrid-scale orographic effects; moist convection; large-scale condensation).

Thus

$$\psi_u^{n-1} = \psi^{n-1} + \left( \frac{\partial \psi}{\partial t} \right)_{\text{dyn}} + \left( \frac{\partial \psi}{\partial t} \right)_{\text{phys}} \quad (3.80)$$

In (3.79), if the operator P is non-linear, its linearization around the basic state  $\psi_u^{n-1}$ , will require to store the model state at time step  $n - 1$  (trajectory at  $t - \Delta t$ ) as well as the tendencies produced by the dynamics  $(\partial\psi/\partial t)_{\text{dyn}}$ . The physical tendencies from the previous processes  $(\partial\psi/\partial t)_{\text{phys}}$ , require an additional call to the non-linear routines in the adjoint computations (**CALLPARAD**) and a local storage of the partial tendencies.

The storage of the trajectory at  $t - \Delta t$  is performed in **EC\_PHYS** by the routine **STORE\_TRAJ\_PHYS** called before the driver of the ECMWF physics **CALLPAR**. Fields are stored in grid-point space in an array **TRAJ\_PHYS**. This array is allocated in the module **TRAJ\_PHYSICS**, where also the number of the fields to be stored is defined.

The following three-dimensional fields are stored.

- (i) **For the atmosphere:** the prognostic variables (wind components, temperature, specific humidity) and their tendencies produced by adiabatic processes, the vertical velocity, the long-wave fluxes and the solar transmissivity.
- (ii) **For the soil:** the prognostic variables for temperature and moisture content (used to compute the surface fluxes from the trajectory in the linear vertical-diffusion scheme).
- (iii) **For the tiles (i.e. vegetation (surface cover) types):** u- and v-stress, surface sensible heat flux, surface evaporation and skin temperature.

A number of two-dimensional fields used at time step  $t - \Delta t$  need to be stored: surface pressure, surface fluxes, skin temperature, skin reservoir, snow reservoir, roughness lengths (mainly for the vertical diffusion).

The preliminary computations (pressure and geopotential at full and half model levels, astronomy parameters) are performed in **EC\_PHYS\_TL** and **EC\_PHYS\_AD** before calling the driver of the tangent-linear physics **CALLPARTL** or the driver of the adjoint physics **CALLPARAD**, and after reading the trajectory fields from **GET\_TRAJ\_PHYS**.



# Chapter 4

## Background term

### Table of contents

- 4.1 Introduction**
- 4.2 Description of the algorithm**
  - 4.2.1 The wavelet correlation matrix and gridpoint variances
  - 4.2.2 The multivariate error correlations between variables: ‘balance’
  - 4.2.3 The univariate variable transform: ‘gaussianization’
- 4.3 Implementation**
  - 4.3.1 The  $J_b$  information structure: SPJB\_VARS\_INFO
  - 4.3.2 User input
  - 4.3.3 Input files
  - 4.3.4 Initial setup
  - 4.3.5 Change of variable

### 4.1 INTRODUCTION

The background term described in [Courtier \*et al.\* \(1998\)](#) was replaced in May 1997 by a new formulation by [Bouttier \*et al.\* \(1997\)](#), and replaced again in April 2005 by a wavelet-based covariance model ([Fisher \(2004\)](#), [Fisher \(2003\)](#)). The two older formulations are still part of the IFS but will not be described in this documentation.

### 4.2 DESCRIPTION OF THE ALGORITHM

We use the following notation.

- (i)  $\mathbf{B}$  is the assumed background error covariance matrix.
- (ii)  $\delta\mathbf{x} = (\delta\zeta, \delta\eta, \delta(T, p_{\text{surf}}), \delta q, \delta o_3, \dots)^T$  is the low-resolution analysis increment (i.e. model field departures from the background) of vorticity, divergence, temperature and surface pressure, specific humidity, ozone mass mixing ratio and  $\dots$ , on model levels.
- (iii) A tilde  $\tilde{\cdot}$  denotes a univariate transform of the increments with more Gaussian error statistics than the original increments.
- (iv) A subscript  $\cdot_u$  denotes a multivariate transform of the increments with less correlated error statistics than the original increments. Dynamic and other balance relationships are included here.

The incremental variational analysis problem, (1.2) of [Chapter 1](#), is rewritten in the space defined by the change of variable  $\delta\mathbf{x} = \mathbf{L}\chi$  ([Section 1.4](#)) where  $\mathbf{L}$  satisfies  $\mathbf{L}\mathbf{L}^T = \mathbf{B}$  so that  $J_b$  takes a simple form. In operational practice, the initial point of the minimization is either the background (in which case  $\delta\mathbf{x} = \chi = 0$ ) or the control vector saved from an earlier minimization. The minimization is carried out in the space of  $\chi$ . At the end of the minimization, the analysis increments are reconstructed in model space by  $\delta\mathbf{x} = \mathbf{L}\chi$ . In order to compare with observations,  $\mathbf{x}$  is reconstructed using (2.4), in each simulation. Thus the variational analysis can be performed using only transformations from minimization space to model space ([CHAVARIN](#)). The transformation from model space to minimization space is never required. In particular,  $\mathbf{L}$  is not required to be invertible, and may even be rectangular. This is the case in the “wavelet”  $J_b$  formulation described here, where the dimension of the control vector is considerably larger than the dimension of the model state vector.

The background-error covariance matrix  $\mathbf{B}$  is implied by the design of  $\mathbf{L}$ , which currently has the form

$$\mathbf{L} = \mathbf{K}\mathbf{L}_u \quad (4.1)$$

where  $\mathbf{K}$  is a balance and variable transform operator going from the set of variables  $\delta\tilde{\mathbf{x}}_u$  to the model variables  $\delta\mathbf{x}$ .

The  $\mathbf{L}_u$  operator defines the covariance matrix for  $\delta\tilde{\mathbf{x}}_u$  as

$$\mathbf{B}_u = \mathbf{L}_u\mathbf{L}_u^T \quad (4.2)$$

So far, the formulation is quite general. Now, we restrict  $\mathbf{L}_u$  to a simple form and choose a particular balance and variable transform operator  $\mathbf{K}$ .

The covariance matrix  $\mathbf{B}_u$  is assumed to be block-diagonal, with no correlation between the parameters, so that

$$\mathbf{B}_u = \begin{bmatrix} \mathbf{C}_\zeta & 0 & 0 & 0 & 0 & 0 \\ 0 & \mathbf{C}_{\eta_u} & 0 & 0 & 0 & 0 \\ 0 & 0 & \mathbf{C}_{(T,p_{\text{surf}})_u} & 0 & 0 & 0 \\ 0 & 0 & 0 & \mathbf{C}_{q_u} & 0 & 0 \\ 0 & 0 & 0 & 0 & \mathbf{C}_{o3} & 0 \\ 0 & 0 & 0 & 0 & 0 & \ddots \end{bmatrix} \quad (4.3)$$

The matrix  $\mathbf{L}_u$  is similarly block-diagonal, with diagonal blocks  $\mathbf{L}_\zeta$ ,  $\mathbf{L}_{\eta_u}$ ,  $\mathbf{L}_{(T,p_{\text{surf}})_u}$ ,  $\mathbf{L}_{q_u}$ ,  $\mathbf{L}_{o3}$ , (etc.). However, these sub-matrices are rectangular. Each sub-matrix is treated identically in the code, except for differences in the coefficients used to describe the covariances, so we will consider just one sub-matrix,  $\mathbf{L}_\zeta$ .

#### 4.2.1 The wavelet correlation matrix and gridpoint variances

The “wavelet”  $J_b$  formulation was devised to allow both spatial and spectral variation of the horizontal and vertical covariances of background error. Only a brief description is given here. The reader is referred to [Fisher \(2004\)](#) for a mathematical justification of the method, and also to [Fisher \(2003\)](#).

Simultaneous spatial and spectral variation of horizontal and vertical covariances is achieved by dividing the control vector up into several parts, each of which corresponds to a band of total spherical wavenumbers,  $n$ . For each band, the elements of the control vector are arranged on a linear reduced Gaussian grid that is appropriate to the spectral truncation corresponding to the highest wavenumber in the band. The wavenumber bands overlap, with the result that exactly two bands use linear grids corresponding to the full model resolution. The cutoff wavenumber decreases by approximately a factor of  $\sqrt{2}$  for each subsequent band and the number of gridpoints reduces by a factor of two, so that the total number of elements of the control vector is approximately three times larger than a gridpoint representation of the model fields.

Information about the vertical and horizontal correlations is stored in the form of sets of vertical covariance matrices. There is one set of matrices for each wavenumber band, and for each band the symmetric square-roots of these matrices are stored on a horizontal grid that is somewhat coarser than the grid used for the band’s control vector elements.

The transformation of the control vector to model space, represented by  $\mathbf{L}_\zeta$ , consists of the following steps. First, for each wavenumber band, each vertical column of the grid is multiplied by the square-root of the covariance matrix (from the set corresponding to the wavenumber band) that is nearest to the grid column. Next, the control vector elements are transformed to spectral space. Since the wavenumber bands overlap, there are now more than one (in fact, exactly two) sets of spectral coefficients for each spherical wavenumber,  $n$ . These sets of coefficients are combined in a weighted sum to give a conventional spectral description of the model fields. For each wavenumber, the sums of squares of the weights is equal to one. In fact, the weights are the square-roots of triangle functions that decay to zero towards the boundaries of each wavenumber band, and take the value one at the centre of the band. As a result, the vertical covariance associated with each wavenumber is effectively linearly interpolated between the covariance

matrices defined for each band, and the horizontal covariance is defined by a piecewise-linear function of  $n$ .

The final step of the transformation  $\mathbf{L}_\zeta$  is to transform the spectral fields to the model grid, and to multiply by the assumed standard deviations of background error.

#### 4.2.2 The multivariate error correlations between variables: ‘balance’

The operator  $\mathbf{K}$  first applies a multivariate ‘balance’ operator to obtain variables with less correlated errors, and then a univariate variable transform is applied to obtain variables with more Gaussian error statistics. The multivariate part of  $\mathbf{K}$  currently accounts for dynamic balance in spectral space (nonlinear balance and quasi-geostrophic omega equation) and thermodynamic balance between humidity and temperature in gridpoint space (moist-adiabatic relationship in cloud covered fraction of gridbox). In general, any multivariate error correlations will be included here.

##### (a) Dynamic balance in spectral space

After the control variable has been multiplied by the background error standard deviations, the contribution due to dynamic balances is added back in spectral space, currently defined by the following transformations for temperature, surface pressure and divergence only:

$$\begin{aligned}\delta(T, p_{\text{surf}}) &= \mathbf{N}\delta\zeta + \mathbf{P}\delta\eta_{\text{u}} + \delta(T, p_{\text{surf}})_{\text{u}} \\ \delta\eta &= (\mathbf{M} + \mathbf{Q}_2)\delta\zeta + \delta\eta_{\text{u}} + \mathbf{Q}_1\delta(T, p_{\text{surf}})\end{aligned}\quad (4.4)$$

The matrix blocks  $\mathbf{M}$ ,  $\mathbf{N}$ ,  $\mathbf{P}$ ,  $\mathbf{Q}_1$  and  $\mathbf{Q}_2$  are in general not invertible, however the balance operator  $\mathbf{K}$  is. The  $\mathbf{M}$ ,  $\mathbf{N}$  and  $\mathbf{P}$  operators used to define balance have a restricted algebraic structure.  $\mathbf{M}$  and  $\mathbf{N}$  are both the product of a so-called horizontal balance operator  $H$  and vertical balance operators  $M$ ,  $N$  such that

$$\begin{aligned}\mathbf{M} &= MH \\ \mathbf{N} &= NH\end{aligned}\quad (4.5)$$

The  $H$  operator is a block-diagonal matrix of identical horizontal operators transforming the spectral coefficients of vorticity, independently at each level, into an intermediate variable  $P_{\text{b}}$  which is a kind of linearized mass variable. The horizontal operators in  $H$  are defined analytically as linearized versions of the non-linear balance equation:

$$\nabla^2 P_{\text{b}} = (f + \zeta) \times v_{\psi} + \frac{1}{2} \nabla(v_{\psi} \cdot v_{\psi}) \quad (4.6)$$

where  $v_{\psi} = \mathbf{k} \times \nabla\psi$  is the rotational wind.

This equation is simplified, by treating model levels as if they were pressure levels, and is linearised about the background state to provide a linear equation for increments in  $P_{\text{b}}$  as a function of vorticity increments.

The matrices  $\mathbf{Q}_1$  and  $\mathbf{Q}_2$  are also defined analytically, as simplified and linearised versions of the quasi-geostrophic omega equation:

$$\left( \sigma \nabla^2 + f_0^2 \frac{\partial^2}{\partial p^2} \right) \omega' = -2 \nabla \cdot \mathbf{Q} \quad (4.7)$$

(Here,  $\mathbf{Q}$  is the Hoskins’ Q-vector: a function of temperature and rotational wind.)

Once again, model levels are treated as if they were pressure levels, and the stability parameter,  $\sigma$  is assumed to be a function of pressure. This allows the equation to be separated into a set of small tri-diagonal systems that can be solved non-iteratively to give divergence increments as a linear function of vorticity and temperature increments.

The  $M$ ,  $N$  and  $\mathbf{P}$  operators all have the same structure: block-diagonal, with one full vertical matrix per spectral component. The vertical matrices depend only on the total wavenumber  $n$ , and are calculated by linear regression. (For example, in the case of the operator  $N$ , the regression is between  $\delta\mathbf{P}$  and  $\delta(T, p_{\text{surf}})$ .)

Calibration of the statistically-derived operators of the balance operator is performed outside the IFS using programs developed by Francois Bouttier.

(b) *Thermodynamic balance in gridpoint space*

The contribution to humidity coming from the thermodynamic relation with temperature is now added back in gridpoint space,

$$\delta\tilde{q} = \delta\tilde{q}_u + Q_{qT} \frac{q^b}{q_s(T^b)} \frac{L}{R_v(T^b)^2} \delta T \quad (4.8)$$

where  $\delta\tilde{q} = \delta q/q_s(T^b)$  (see below),  $q_s(T^b)$  is the saturation specific humidity at the background temperature  $T^b$ ,  $L$  is the latent heat for mixed phase and  $R_v$  is the gas constant for water vapour. This relationship between humidity and temperature changes is derived from the Clausius-Clapeyron equation which gives the heat generated by a given phase-change of water vapour in clouds. The coefficient  $Q_{qT}$  is determined by a statistical regression as function of the background relative humidity  $rh^b$  and model level.  $Q_{qT}$  starts from zero in cloud free grid boxes, estimated as  $rh^b$  below about 80% relative humidity, and goes to unity as  $rh^b$  approaches 1. The regression coefficient  $Q_{qT}$  does resemble a simplified statistical model of cloud cover. The humidity-temperature balance is put to zero in supersaturated (wrt mixed phase) areas and in the stratosphere (determined by a tropopause diagnosed from the background fields).

The statistical regression for obtaining  $Q_{qT}$  is performed outside the IFS using programs developed by Elías Hólm.

### 4.2.3 The univariate variable transform: ‘gaussianization’

The last step is to transform any variables that have been ‘gaussianized’ back to the model variables. Currently only humidity has been transformed to another variable to obtain more Gaussian error statistics,

$$\delta q = q_s(T^b) \delta\tilde{q} \quad (4.9)$$

For the other variables  $\delta T = \delta\tilde{T}$ , etc. It is important to note that this is a linear transform in the inner loops, whereas a non-linear transform may really be what is required to account for the non-Gaussianity at this stage. The non-linear aspect of the transform is dealt with at the outer loop level in the variational framework, see Hólm *et al.* (2002) for a discussion.

## 4.3 IMPLEMENTATION

### 4.3.1 The $J_b$ information structure: SPJB\_VARS\_INFO

The  $J_b$  code is required to be sufficiently flexible to allow the incorporation of new variables, and to allow the choice of analysed variables to differ from the choice of model variables. This is achieved through a separation of the arrays used by  $J_b$  from the model arrays, and is controlled by a “structure” (Fortran derived type) containing information about the  $J_b$  variables: SPJB\_VARS\_INFO. This structure is ubiquitous throughout the  $J_b$  code.

SPJB\_VARS\_INFO is defined in YOMJG, and is a one-dimensional array with one element for each analysed variable. Analysed variables may be either three-dimensional (for example, vorticity) or two-dimensional (e.g. surface pressure).

Each element of SPJB\_VARS\_INFO is a structure with the following elements:

- IGRIBCODE
- IGRIBCODE\_FCE
- IPT
- IPTJB
- IPTFCE
- IPTBG
- L\_IN\_SPA3
- L\_IN\_SPA2



- L\_IN\_SPGFL
- L\_IN\_GPGFL
- COR\_STRING

The first two elements give the GRIB parameter codes used to identify the variable and the corresponding background error fields. These may be different since, for fields involved in the balance operator, IGRIBCODE\_FCE refers to the unbalanced component of the field, whereas IGRIBCODE refers to the full (balanced plus unbalanced) field.

The elements IPT, IPTJB, IPTFCE and IPTBG are indexes into various arrays. IPT indicates which field in the model's SPA3, SPA2, SPGFL or GFL arrays corresponds to the analysed variable. IPTJB provides an index into the (spectral)  $J_b$  arrays, SPA3JB and SPA2JB. IPTFCE locates the variable in the forecast-error array FCEBUF, and IPTBG locates the corresponding background fields in SP7A3, GP7A3 or SP7A2.

Four logical flags, L\_IN\_SPA3, L\_IN\_SPA2, L\_IN\_SPGFL and L\_IN\_GPGFL, show where in the model's various arrays the variable is stored. These flags are used in conjunction with the element IPT to locate the model's equivalent of the analysed variable.

The final element of SPJB\_VARS\_INFO is a character string. This is used to match the variable with the covariance matrices in the input file "wavelet.cv".

### 4.3.2 User input

The initial setup of  $J_b$  is performed by **SUJB**. The user can input, via NAMJG, the number of analysed variables (N\_SPJB\_VARS). GRIB parameter codes for these variables (M\_GRIBCODES) and for the corresponding background error fields (M\_GRIBCODES\_FCE), and also the character strings that identify the corresponding covariance matrices (C\_COR\_STRINGS), are input via NAMJBCODES.

These inputs are sufficient for **SUJB** to construct the information structure, SPJB\_VARS\_INFO. The correspondence between analysis fields and model fields is derived by looking up the grib code of the analysed variable in the model's GMV and GFL structures. If none of the inputs is specified, the analysis defaults to 6 variables: vorticity, divergence, temperature, surface log-pressure, humidity and ozone.

Background error statistics for wavelet  $J_b$  may be calculated by setting LJBWSTATS to TRUE. In this case, the code expects to read a large set of background states as spectral GRIB fields. The states are expected to be produced by an analysis ensemble with N\_BGMEMBERS members and covering N\_BGDATES dates. Inter-member differences are calculated for each date, and the statistics of background error are calculated from this set of differences. (Statistics may be calculated using the "NMC method" by regarding, for example, a set of 48-hour forecasts as member 1, and a set of 24-hour forecasts as member 2.) The filename for each state is constructed as a six-character prefix (CINBGSTATES) followed by a string of the form "mXXX\_dYYY", where XXX is in the range 1...N\_BGMEMBERS, and YYY is in the range 1...N\_BGDATES.

Calculation of the statistics is performed in **SUJBWAVGEN** and associated subroutines. At the end of the calculation, a file called "wavelet.cv" is written, and the code stops a little inelegantly with an abort message. Note that calculation of the  $J_b$  statistics is largely single-threaded.

### 4.3.3 Input files

The IFS requires three input files to define  $J_b$ . The covariance matrices that define the vertical and horizontal correlations are read from "wavelet.cv". This file also contains power spectrum information which is used to determine global mean vertical profiles of standard deviations of background error. Coefficients for the balance operator are read from "stabal96.bal", and standard deviations of background error are read from "errgrib".

### 4.3.4 Initial setup

**SUJBWAVELETO** determines the number of wavenumber bands and their wavenumber boundaries by reading header information from the statistics file "wavelet.cv". Next, the spherical transforms and grid

layouts corresponding to the cutoff wavenumbers for each band are defined by a call to **SUJBWAVTRANS**. This information is stored in the structure **GRID\_DEFINITION** (**YOMWAVELET**).

Some allocation of arrays is carried out in **SUALGES**, and the control vector is allocated in **SUALCTV**. Coefficients for the humidity variable and for the balance operators are initialised by **SUJBCHVAR** and **SUJBBAL**, respectively.

Most of the setup for “wavelet  $J_b$ ” is performed by **SUJBWAVELET** and **SUJBWAVVALLO**. The main tasks are to read the input file, which contains the symmetric square-roots of the vertical covariance matrices. To reduce the size of the input file, each matrix has an associated “skyline”, which identifies the first and last element in each row (or column, since the matrices are symmetric) that is significantly different from zero. Only the matrix elements between these limits are stored in the file.

In addition to the covariance matrices, the input file also contains power-spectrum information about the analysed variables. This is used to construct global-mean profiles of background error standard deviation.

The covariance matrices are stored in the structure **WAVELET\_VCORS**, together with information about their grid layout.

The final part of the  $J_b$  setup is to read the background fields (**SUECGES**), and to initialise the standard deviations of background error (**SUINFCE**).

#### 4.3.5 Change of variable

The change of variable, **CHAVARIN**, implicitly defines the background error covariance model. It consists of three steps: **CVAR2IN** implements multiplication of control vector by the matrix denoted **L** in [Section 4.2](#). The transformed variables are inserted into the model’s arrays by **JBTOMODEL**. This may involve spectral transforms, since the  $J_b$  variables are all spectral, whereas model variables may be held as gridpoint fields. Finally, the background state is added to the model fields by **ADDBGS**.

The control vector for the minimization contains several components besides those related to  $J_b$ . Within **CVAR2IN** all these components are handled, and the  $J_b$  components are dealt with by a call to **CVAR3IN**. In **CVAR3IN** a call to **SQRTBIN** applies the vertical and horizontal correlations (**JGCORI**) and multiplies by the standard deviations of background error (**CVARGPTL**). The next step in **CVAR3IN** is to apply the dynamic balance operator via calls to **BALNONLINTL**, **BALVERT** and **BALOMEGATL**. The final step in **CVAR3IN** is a call to **JBCHVARI** which includes the humidity related thermodynamic balance and ‘gaussianization’ change of variable.

Note that **CVARGPTL** calls **TRANSINV\_WAVELET** and **TRANSDIR\_WAVELET** to perform the spectral transforms required to convert variables between spectral and gridpoint representations. Here these routines implement *spectral* transforms using the information stored in **GRID\_DEFINITION**. They do not implement wavelet transforms.

**JGCORI** calls **JBVCOR\_WAVELETIN** once for each band of wavenumbers to perform the main part of the wavelet  $J_b$  change of variable. **JBVCOR\_WAVELETIN** has three steps. First, each column of the control vector is multiplied by the square-root of a vertical covariance matrix. This is performed by **JBVCORG**. Next, the gridpoint fields are transformed to spectral space by a call to **TRANSDIR\_WAVELET**. The coefficients are multiplied by the appropriate weights by **WAVXFORM**, and the weighted coefficients are added into the arrays **PSPA3JB** and **PSPA2JB**.

The calls to **JBVCORG** are the most expensive part of the wavelet  $J_b$  code. The calls are performed within an Open-MP loop over **NPROMA** blocks. For each grid column and each analysis variable, the nearest covariance matrix is identified by a call to **JBMATINTERP**, and the column is multiplied by the square-root of the covariance matrix. A considerable saving of computational time is achieved by taking into account the fact that elements outside the matrix “skyline” (see above) are known to be zero.

## Chapter 5

# Observation operators and observation cost function ( $J_o$ )

### Table of contents

- 5.1 Introduction**
  - 5.1.1 Data selection controls, and the interface to the blacklist
- 5.2 Horizontal interpolation to observation points**
  - 5.2.1 Method
  - 5.2.2 Storage in GOM-arrays
  - 5.2.3 Variable numbers and association with observation operators
  - 5.2.4 Organization in observation sets
  - 5.2.5 Cost function
  - 5.2.6  $J_o$  tables
  - 5.2.7 Correlation of observation error
- 5.3 Variational quality control**
  - 5.3.1 Description of the method
  - 5.3.2 Implementation
- 5.4 Variational bias correction**
  - 5.4.1 Variational estimation of the bias parameters
  - 5.4.2 Modular implementation
- 5.5 Observation operators – general**
- 5.6 The observation operator for conventional data**
  - 5.6.1 Geopotential height
  - 5.6.2 Wind
  - 5.6.3 Humidity
  - 5.6.4 Temperature
- 5.7 Satellite radiance operators**
  - 5.7.1 Common aspects for the setup of nadir radiance assimilation
  - 5.7.2 Clear-sky nadir radiances and overcast infrared nadir radiances
  - 5.7.3 All-sky nadir radiances
  - 5.7.4 Cloud affected infrared radiances
  - 5.7.5 Clear-sky limb radiances
- 5.8 Other satellite observation operators**
  - 5.8.1 Atmospheric Motion Vectors
  - 5.8.2 Thicknesses
  - 5.8.3 Gas retrievals
  - 5.8.4 Scatterometer winds
  - 5.8.5 GPS Radio Occultation bending angles
- 5.9 Surface observation operators**
  - 5.9.1 Vertical interpolation
  - 5.9.2 Surface values of dry static energy
  - 5.9.3 Transfer coefficients
  - 5.9.4 Two-metre relative humidity

## 5.1 INTRODUCTION

The observation operators provide the link between the analysis variables and the observations (Lorenc, 1986; Pailleux, 1990). The observation operator is applied to components of the model state to obtain the model equivalent of the observation, so that the model and observation can be compared. The operator  $H$  in (1.4) signifies the ensemble of operators transforming the control variable  $\mathbf{x}$  into the equivalent of each observed quantity,  $\mathbf{y}^o$ , at observation locations. The 3D/4D-Var implementation allows  $H$  to be (weakly) non-linear, which is an advantage for the use of satellite radiance data, scatterometer data with aliased wind direction, cloud and precipitation data, for example. In this chapter we define the content of each of the IFS observation operators and the associated controls for all data used in 3D/4D-Var. The calculation of departures and the  $J_o$  costfunction are also described.

The IFS observation operators are generic in the sense that the same routine is often used for several different data types. For example, the radiance operator (RTTOV) simulates measurements from a large number of satellite radiometers (microwave and infrared), and the temperature operator (PPT) is used for TEMP, AIREP, and other data types and it is also used to provide input to RTTOV. Similarly the routine PPQ is used for interpolation of specific humidity to given pressures, but it can also be used for any other atmospheric mixing ratio constituents, such as ozone and carbon dioxide. Note that many of the PP-routines were developed for the model's pressure-level post-processing package and are used also in that context.

In Table 10.2 there is a list of the observing systems currently used by 4D-Var in ECMWF's operational data assimilation suite. The table also indicates important restrictions on data usage and thinning of data. The observation errors are also given in Chapter 10. In 4D-Var, the evolving model state is compared to the available observations at the correct time, currently at half-hourly intervals. These intervals are called *time-slots*. The Observation Data Base (see ODB documentation) holds the observations organized by time slots. If there are multiple reports from the same fixed observing station within a time slot then the data nearest the analysis time are selected for use in the analysis. Some thinning is applied for satellite data and other moving platforms reporting frequently. The thinning rules are applied to each time slot, separately. The thinning, quality control and data selection tasks are performed in the *screening* job step of 4D-Var – it is described in Chapter 10.

### 5.1.1 Data selection controls, and the interface to the blacklist

Most data selection criteria are coded in so called *blacklist files*, written in a convenient, readable blacklist language (see the Blacklist Documentation, Järvinen *et al.*, 1996). The blacklist mechanism is very flexible and allows nearly complete control of which data to use/not use in the assimilation. The 'monthly blacklist' is the part of the blacklist that is based on operational data monitoring results, and it is maintained by the Meteorological Operations Section. The blacklist is consulted in the screening job. The interface is set up in BLINIT, in such a way that a number of named items from the header (Table 5.1) and body (Table 5.2) parts of the observation report can be passed to the blacklist software. Depending on the blacklisting criteria flags are communicated to the routine BLACK, and those are written to the ECMA ODB data base. Blacklist-rejected data are subsequently excluded from the CCMA ODB and will not be present in the minimisation job steps. Data selection rules should be coded in the blacklist files whenever possible rather than in the IFS code itself. The operational blacklist history is kept in an archive.

Classes of data can also be switched on and off using the NOTVAR array in NAMJO, however it is preferable to use the blacklist mechanism for this purpose. The second dimension in this array is the observation type. The first dimension is the variable number (NVAR, see below). The elements of the NOTVAR array can take either of two values: 0, means that the data will be used; -1, means that the data will not be used.

## 5.2 HORIZONTAL INTERPOLATION TO OBSERVATION POINTS

### 5.2.1 Method

Currently it is assumed that each observation equivalent can be computed from a single vertical profile of model data. That is, it is assumed that each observation operator can be written as  $H = H_v H_h(\mathbf{x})$  where

**Table 5.1** Header variables for the ifs/blacklist interface.

Index	Name	Description
1	OBSTYP	observation type
2	STATID	station identifier
3	CODTYP	code type
4	INSTRM	instrument type
5	DATE	date
6	TIME	time
7	LAT	latitude
8	LON	longitude
9	STALT	station altitude
10	LINE_SAT	line number (atovs)
11	RETR_TYP	retrieval type
12	QL1	quality indicator 1
13	QL2	quality indicator 2
14	QL3	quality indicator 3
15	MODORO	model orography
16	LSMASK	land-sea mask (integer)
17	RLSMASK	land-sea mask (real)
18	MODPS	model surface pressure
19	MODTS	model surface temperature
20	MODT2M	model 2-metre temperature
21	MODTOP	model top level pressure
22	SENSOR	satellite sensor indicator
23	FOV	field of view index
24	SATZA	satellite zenith angle
25	NANDAT	analysis date
26	NANTIM	analysis time
27	SOE	solar elevation
28	QR	quality of retrieval
29	CLC	cloud cover
30	CP	cloud top pressure
31	PT	product type
32	SONDE_TYPE	sonde type
33	SPECIFIC	amsua specific
34	SEA_ICE	model sea ice fraction

**Table 5.2** Body variables for the ifs/blacklist interface.

Index	Name	Description
1	VARIAB	variable name
2	VERT_CO	type of vertical coordinate
3	PRESS	pressure, height or channel number
4	PRESS_RL	reference level pressure
5	PPCODE	synop pressure code
6	OBS_VALUE	observed value
7	FG_DEPARTURE	first guess departure
8	OBS_ERROR	observation error
9	FG_ERROR	first-guess error
10	WINCHAN_DEP	window channel departure
11	OBS_T	observed temperature

$H_h$  is horizontal interpolation of model data to the location of the observation.  $H_h$  is performed for all observations within a time-slot directly after the corresponding model time step has been performed. The output of  $H_h$  is a vertical profile of model data for each observation location. These profiles are stored in a data structure called GOM-arrays, and used later in the vertical part of the observation operator  $H_v$  performed in HOP, called from OBSV. Recently, two-dimensional GOM-arrays have been developed, to permit horizontal integration as required for limb-sounding and radio-occultation data. The orientation of the two-dimensional GOM-arrays (e.g. one vertical plane per observation) is then determined by the satellite viewing geometry. The  $H_v$  operator for those data receive the vertical plane of model data as input.

**COBSLAG** is the master routine for the horizontal interpolation of model data to observation points. It is called after the inverse spectral transform in **SCAN2MDM**, and after the so-called *semi-Lagrangian buffers* have been prepared by **COBS** and **SLCOMM2**, see the flow diagram in Fig. 5.1. The interpolation code is shared with the semi-Lagrangian advection scheme of the dynamics. The buffers contain a *halo* of gridpoints big enough to enable interpolation to all observations within the grid-point domain belonging to the processor. **COBSLAG** calls **OBSHOR** which does the following.

- (i) Performs the interpolation, using **SLINT**.
- (ii) Message-passes the result to the processors where the corresponding observations belong, and copies the model data at observation points to the so-called GOM-arrays (**GOMS**, described below) using the routine **MPOBSEQ**.

There are three methods of horizontal interpolation.

- (i) **LAIDDIOPS**: 12-point bi-cubic interpolation, used for all upper-air fields (if **NOBSHOR** = 203) except clouds.
- (ii) **LAIDDIOPS**: Bi-linear interpolation, used for surface fields.
- (iii) **LAIDLIC**: Nearest gridpoint, used for cloud parameters.

The interpolation method for the upper-air fields can be switched to bi-linear by specifying **NOBSHOR** = 201 in **namobs**. The default is **NOBSHOR** = 203 (bi-cubic) for the trajectory jobs, but **NOBSHOR** = 201 (bi-linear) in the minimisation jobs. Lists of interpolation points and weights are prepared by the routine **LASCAW**. In 4D-Var bi-cubic interpolation is used at high resolution (i.e. in the trajectory runs), and bi-linear is used at low resolution (i.e. in the main minimization). The interpolation is invoked once per 4D-Var time slot.

The adjoint (**OBSHORAD**) follows the same general pattern but gets further complicated by the fact that the gradient from several observations may contribute to the gradient at a given gridpoint. The summation of gradients is done in the same order, irrespective of the number of processors, as reproducibility is desired (strictly speaking, overall 4D-Var reproducibility is only ensured if the so called reproducibility switch is ON. This adds to computational cost, and the default is OFF). Tables for managing this are prepared in **MKGLOBSTAB**.

### 5.2.2 Storage in GOM-arrays

There are two types of GOM arrays, one-dimensional GOM arrays which contain vertical profiles of model values at observation points and two-dimensional GOM arrays which contain a set of vertical profiles of model values. There are namelist-switches (in **NAMGOM**) to control which upper-air model variables that will appear in the GOM-arrays and whether to use one or two-dimensional GOM arrays. The control is at the observation type level.

The setup of the GOM structures are done in routine **SUGOMS** and the data structures can all be found in module **GOMS**

The trajectory GOM5 arrays (identical to GOM) are allocated in the case that tangent linear observation operators are used. They are to hold the trajectory interpolated to the observation locations, and in that case the GOM-arrays hold the perturbations.

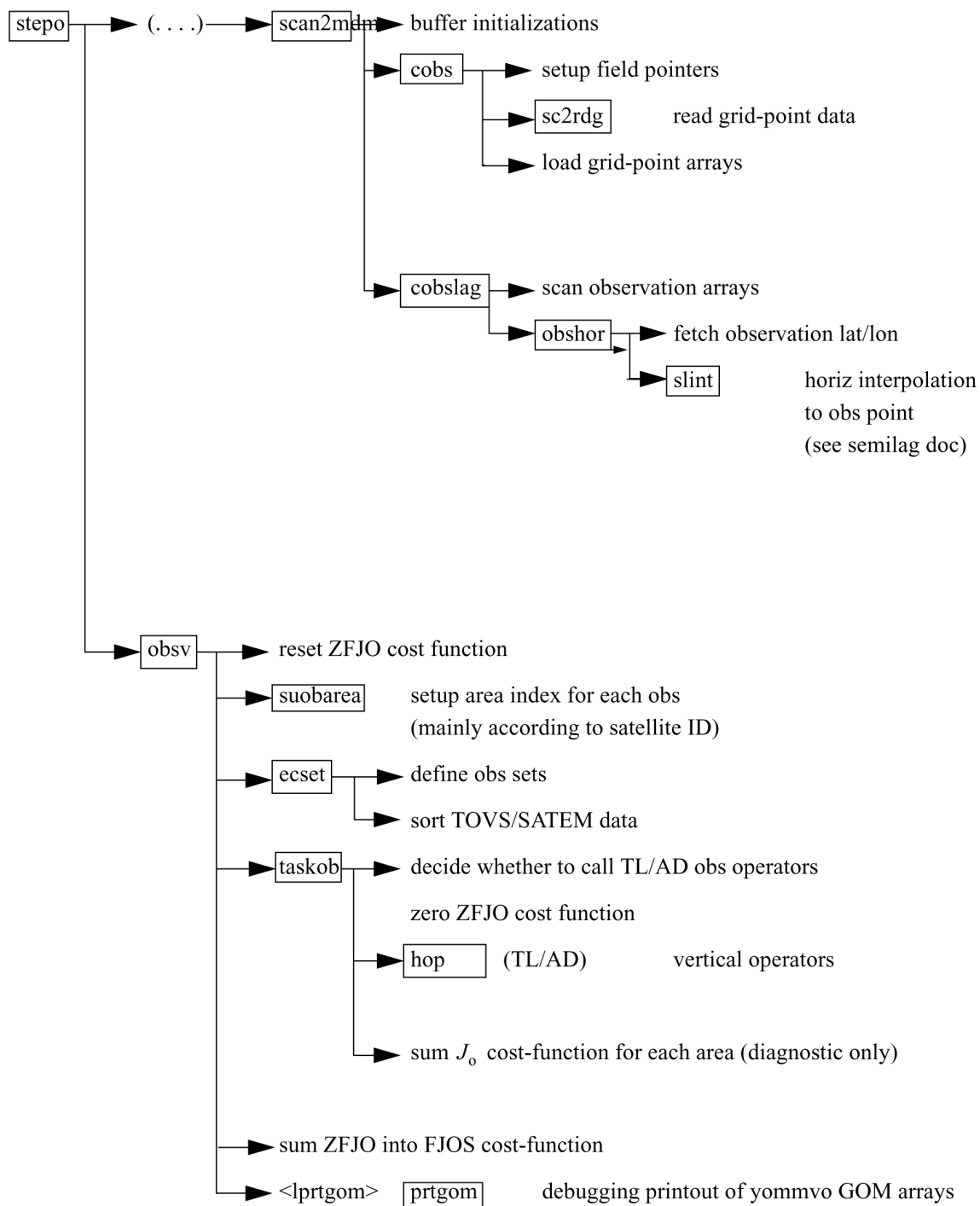


Figure 5.1 Flow diagram for subroutines *scan2mdm* and *obsv*.

At the end of the adjoint observation operators the GOM-arrays are zeroed and overwritten by the gradient (in **PREINTAD**).

The r.m.s. of the GOM arrays is printed (by **PRTGOM**) if the switch **LPRTGOM** = **.TRUE.**, (in **YOMOBS**). The default is that the print is switched on. It can be located in the log file by searching for ‘RMS OF GOM’. The printing is done from **OBSV**, (i) when the GOM arrays contain the background interpolated to the observation points, (ii) when it contains  $\nabla J_o$  of the first simulation, (iii) when it contains first TL perturbations after the initial call to the minimizer and (iv) when it contains  $\nabla J_o$  at the final simulation.

### 5.2.3 Variable numbers and association with observation operators

In the ODB each observed value is associated with a vertical position (‘press’ with pointer **MDBPPP**, given in terms of pressure, height or channel number) and a variable number (‘varno’ with pointer **MDBVNM**). The defined variable numbers are listed in the array **NVNUMB** as described in the ODB documentation. The variable number indicates which physical quantity has been observed. Each observed quantity is linked to an IFS observation operator (in **HVNMTLT**). In the case there is no corresponding observation operator in IFS, no observation equivalent will be computed, and the observation will be rejected from further processing. Each available observation operator has been given a number (**NVAR**) and a short name (**CVAR\_NAME**, three characters), set in **YOMCOSJO**.

There are currently **JPXVAR** = 25 operator names defined: U, U10, DD, FF, H, H2, T, Z, DZ, LH, T2, TS, RAD, SN, RR, PS, CC, CLW, Q, FFF, S0, X, PWC, TO3 and TCW, numbered sequentially in **NVAR**. Each number can be referenced by variables such as **NVAR\_U**(= 1), **NVAR\_U10**(= 2) and so on. Based on the ODB variable number for each observation, which has been associated with an observation-operator number and name, **HOP** calls the appropriate observation operator routine. For example, observations with ODB variablenumber = **NVNUMB**(8), will in **HVNMTLT** be associated with **NVAR\_T** = 7 and **CVAR\_NAME**(7) = ‘T’, and **HOP** will thus call the subroutine **PPT**.

In the log file **CVAR\_NAME** is used to label entries in the  $J_o$ -table. The  $J_o$ -table shows the  $J_o$ -values for each observation sub-type, for each observation operator (**NVAR**). RMS of observation error and background error are also shown. See [Subsection 5.2.6](#).

### 5.2.4 Organization in observation sets

The vertical observation operators are vectorized over **NMXLEN** (**yomdimo**) data. To achieve this the data first have to be sorted by type and subdivided into sets of lengths not exceeding that number. **NMXLEN** is currently set to 511, in **SUDIMO**. The observation sets may span several 4D-Var time slots, as the input to the observation operators is the GOM-arrays which have been pre-prepared for all time slots during the tangent linear model integration. However, in the current operational context this is not the case, as **OBSV.F90** is called once per time slot. Furthermore, on the current IBM machines long vector loops are not very important for performance, our IBMs being scalar machines.

The organization of the sets is done in **ECSET** and **SMTOV** and the information about the sets is kept in **yomobset**. Radiance observation sets (e.g. **ATOVS**, **AIRS**, **SSMI/S**) must not contain data from more than one instrument. That is to say that inside **HOP**, **HOPTL** and **HOPAD** (and routines called from there) data from several instruments are not mixed – different instrument are handled in separate calls. This is controlled by sorting according to the area-parameter, which for radiance data is an indicator of satellite ID and instrument, prior to forming the sets. The area-parameter is determined in **SUOBAREA**, and is irrelevant for the observation processing for all data other than the radiance data.

### 5.2.5 Cost function

The master routine controlling the calls to the individual observation operators is called **HOP**. This routine deals with all different types of observations.

The **HOP/HOPTL/HOPAD** routines are called from **TASKOB/TASKOBTL/TASKOBAD** (called from **OBSV/OBSVTL/OBSVAD**) in a loop over observation sets. The data type of each set is known from the information in tables such as **MTYPOB(KSET)** stored in **yomobset**.



**Table 5.3** Association between variable numbering and observation operator routines. The *CVAR-NAMEs* also appear in the printed  $J_o$ -table in the log-file.

NVAR	CVAR_NAME	Observation operator routine	Description
1	U	PPUV	Upper air wind components
2	U10	PPUV10M	10-metre wind components
3	DD		Wind direction
4	FF	PPUV	Wind speed
5	H	PPRH	Relative humidity
6	H2	PPRH2M	2-metre relative humidity
7	T	PPT	Temperature
8	Z	PPGEOP	Geopotential
9	DZ	PPGEOP	Thickness
10	LH	PPRH	Layer mean RH (M-France)
11	T2	PPT2M	2-metre temperature
12	TS		Surface temperature (M-France)
13	RAD	RADTR/RADTR_ML	Radiance data
14	SN		Snow (M-France)
15	RR		Rain rate (M-France)
16	PS	PPPS	Surface pressure
17	CC	PPTCC	Cloud cover
18	CLW	PPCLW	Cloud liquid water
19	Q	PPQ	Specific humidity
20	FFF	PPUV10M	10-metre wind speed
21	S0		Sigma_0
22	X		Reserved
23	PWC	PPPWC	Layer water content or TCWV
24	TO3	PPPWC	Layer ozone content
25	TCW		Layer cloud water content
26	RFL	REFLSIM	Radar reflectivity
27	APD	GPSZEN_DELAY	GPS total zenith delay
28	RO	GPSRO_OP	GPS radio occultation
29	HLS	RTL_HOP_ID	Limb sounding radiance
30	AOD	AOD_OP	Aerosol optical depth
31	LRA		unknown

The following describes **HOP**//**HOPTL**/. The adjoint **HOPAD** follows the reverse order.

- (i) First prepare for vertical interpolation using the routine **PREINT**. Data on model levels are extracted from the GOM-arrays (**GOMS**). Pressures of model levels are computed using **GPPRE**. Help arrays for the vertical interpolation are obtained (**PPINIT**) and  $T^*$  and  $T_0$  are computed (**CTSTAR**).  $T^*$  and  $T_0$  are later used for extrapolation of temperature below the model's orography, [Subsection 5.6.1](#). The routine **PREINTS** deals with model surface fields needed for the near-surface observation operators and **PREINTR** deals with those fields that are specific to the radiance observation operators.
- (ii) The observation array is then searched to see what data is there. The 'body' of each observation report is scanned for data, and the vertical coordinate and the variable-number for each datum is retained in tables (**ZVERTP** and **IVNMRQ**). These tables will later constitute the 'request' for model equivalents to be computed by the various observation operators. Tables of pointers to data ('body' start addresses) and counters are stored (arrays **IPOS** and **ICMBDY**).
- (iii) Then the forward calculations are performed. There is an outer loop over all known 'variable numbers'. If there are any matching occurrences of the loop-variable number with the content of **IVNMRQ**, then the relevant observation operator will be called. A variable-number and an observation operator are linked by a table set up in the routine **HVNMTLT**. The interface routines **PPOBSA** (upperair) and **PPOBSAS** (surface) are used, which in turn call **PPFLEV** and the

individual operator routines. For radiance data the interface is **RADTR** which calls the radiative transfer code.

- (iv) In **HDEPART**, calculate the departure  $\mathbf{z}$  as

$$\mathbf{z} = \mathbf{y}^o - H\mathbf{x} + (\mathbf{y}^o - H\mathbf{x}_{\text{HR}}^b) - (\mathbf{y}^o - H\mathbf{x}_{\text{LR}}^b) \quad (5.1)$$

where the two terms in brackets have been computed previously: the first one in the high resolution trajectory run and the second one in the LOBSREF call, described in [Section 2.2](#).

If LOBSTL then  $\mathbf{z}$  is

$$\mathbf{z} = \mathbf{y}^o - \mathbf{H}\delta\mathbf{x} + (\mathbf{y}^o - H\mathbf{x}_{\text{HR}}^b) - \mathbf{y}^o \quad (5.2)$$

which simplifies to what has been presented in [Section 1.4](#).

The TOVS radiance bias correction is also carried out at this point by subtracting the bias estimate (kept in the NCMTORB-word of ODB) from the calculated departure.

Finally the departure is divided by the observation error  $\sigma_o$  (NCMFOE in ODB) to form the *normalized departure*.

- (v) Departures of correlated data are multiplied by  $\mathbf{R}^{-1}$ , see [Subsection 5.2.7](#). The division by  $\sigma_o$  has already taken place in **HDEPART**, so  $\mathbf{R}$  at this point is in fact a correlation (not a covariance) matrix.
- (vi) The cost function is computed in **HJO**, as

$$J_o = \mathbf{z}^T \mathbf{z} \quad (5.3)$$

for all data, even for SCAT data when LQSCAT = .TRUE., as in current 4D-Var with quadratic cost-function. When LQSCAT = .FALSE. (as in current 3D-Var configuration) the SCAT cost function combines the two ambiguous winds (subscripts 1 and 2) in the following way (also in **HJO**),

$$J_{\text{SCAT}} = \left[ \frac{J_1^4 J_2^4}{J_1^4 + J_2^4} \right]^{1/4} \quad (5.4)$$

These expressions for the cost function are modified by variational quality control, see [Section 5.3](#). The cost-function values are store in two tables, as detailed in [Subsection 5.2.6](#).

- (vii) **HJO**, also stores the resulting *effective departure* in the NCMIOM0-word of ODB, for reuse as the input to the adjoint. The effective departure is the normalized departure after the effects of (vertical) observation error correlation and quality control have been taken into account,  $\mathbf{z}_{\text{eff}} = \mathbf{z}^T \mathbf{R}^{-1} [\mathbf{QC}_{\text{weight}}]$ , where the QC-weight will be defined below, [Section 5.3](#).

We have now reached the end of the forward operators. In the adjoint routine **HOPAD** some of the tasks listed above have to be repeated before the actual adjoint calculations can begin. The input to the adjoint (the effective departure) is read from the ODB. The expression for the gradient (with respect to the observed quantity) is then simply

$$\nabla_{\text{obs}} J_o = -2\mathbf{z}_{\text{eff}} / \sigma_o \quad (5.5)$$

which is calculated in **HOPAD** for all data. The gradient of  $J_{\text{SCAT}}$  is much more complicated and is calculated in a separate section of **HOPAD**. The adjoint code closely follows the structure of the direct code, with the adjoint operators applied in the reverse order.

### 5.2.6 $J_o$ tables

There are two different tables for storing the  $J_o$  values. One is purely diagnostic (JOT, yomcosjo.h), and is used for producing the printed  $J_o$  tables in the log-file (**PRTJO** called rom **EVCOST**). JOT is a FORTRAN90 derived type with items containing cost function value, data count, observation error, background error and codetype, for each observation type and for each observed variable (as defined by NVAR above).

The actual  $J_o$ -table is called FJOS (**yomcosjo**). FJOS is indexed by the absolute observation number, iabnob = MABNOB(jobs,kset), so that the contributions from each individual observation can be summed up in a predetermined order (in **EVCOST**), to ensure reproducibility, irrespective of number of processors and tasks.

### 5.2.7 Correlation of observation error

The observation error is assumed uncorrelated (i.e. the matrix  $\mathbf{R}$  is diagonal) for all data. Optionally, by setting `LTC=.true.`, time-sequences of SYNOP/DRIBU surface pressure and height data (Järvinen *et al.*, 1999) will be time correlated. There used to be code for vertical correlation of observation error for radiosonde geopotential data and SATEM thicknesses, but these were removed in Cy21r2. Similar can easily be reintroduced again in a later cycle, provided the correlation acts on data within a single report (vertical or inter-channel correlation).

The serial correlation for SYNOP and DRIBU data is modelled by a continuous correlation function  $ae^{-b(t_1-t_2)^2}$  where  $a = \text{RTCPART} = 0.3$  and  $b = \text{RTCEFT} = 6.0$  hours, under the switch `LTC (namjo)`. The remaining fraction  $1 - a$  of the error variance is assumed uncorrelated (see `COMTC`).

When  $\mathbf{R}$  is non-diagonal, the ‘effective departure’  $\mathbf{z}_{\text{eff}}$  is calculated by solving the linear system of equations  $\mathbf{z}_{\text{eff}}\mathbf{R}$  for  $\mathbf{z}_{\text{eff}}$ , using LAPACK routines SPOTRF (Choleski decomposition) and SPOTRS (backwards substitution), as is done in `COMTC`.

## 5.3 VARIATIONAL QUALITY CONTROL

The variational quality control, VarQC, has been described by Andersson and Järvinen (1999). It is a quality control mechanism which is incorporated within the variational analysis itself. A modification of the observation cost function to take into account the non-Gaussian nature of gross errors, has the effect of reducing the analysis weight given to data with large departures from the current iterand (or preliminary analysis). Data are not irrevocably rejected, but can regain influence on the analysis during later iterations if supported by surrounding data. VarQC is a type of buddy check, in that it rejects those data that have not been fitted by the preliminary analysis (i.e. the current state vector), often because it conflicts with surrounding data.

### 5.3.1 Description of the method

The method is based on Bayesian formalism. First, an *a priori* estimate of the probability of gross error  $P(G)_i$  is assigned to each datum, based on study of historical data. Then, at each iteration of the variational scheme, an *a posteriori* estimate of the probability of gross error  $P(G)_f$  is calculated (Ingleby and Lorenc, 1993), given the current value of the iterand (the preliminary analysis). VarQC modifies the gradient (of the observation cost function with respect to the observed quantity) by the factor  $1 - P(G)_f$  (the QC-weight), which means that data which are almost certainly wrong ( $P(G)_f \approx 1$ ) are given near-zero weight in the analysis. Data with a  $P(G)_f > 0.75$  are considered ‘rejected’ and are flagged accordingly, for the purpose of diagnostics and feedback statistics, etc.

The normal definition of a cost function is

$$J_o = -\ln p \quad (5.6)$$

where  $p$  is the probability density function. Instead of the normal assumption of Gaussian statistics, we assume that the error distribution can be modelled as a sum of two parts: one Gaussian, representing correct data and one flat distribution, representing data with gross errors. We write

$$p_i = N_i[1 - P(G_i)] + F_iP(G_i) \quad (5.7)$$

where subscript  $i$  refers to observation number  $i$ .  $N$  and  $F$  are the Gaussian and the flat distributions, respectively, given by

$$N_i = \frac{1}{\sqrt{2\pi}\sigma_o} \exp\left[-\frac{1}{2}\left(\frac{y_i - Hx}{\sigma_o}\right)^2\right] \quad (5.8)$$

$$F_i = \frac{1}{L_i} = \frac{1}{2l_i\sigma_o} \quad (5.9)$$

The flat distribution is defined over an interval  $L_i$  which in (5.9) has been written as a multiple of the observation error standard deviation  $\sigma_o$ . Substituting (5.7) to (5.9) into (5.6), we obtain after rearranging

the terms, an expression for the QC-modified cost function  $J_o^{\text{QC}}$  and its gradient  $\nabla J_o^{\text{QC}}$ , in terms of the normal cost function  $J_o^{\text{N}}$

$$J_o^{\text{N}} = \frac{1}{2} \left( \frac{y_i - Hx}{\sigma_o} \right)^2 \quad (5.10)$$

$$J_o^{\text{QC}} = -\ln \left( \frac{\gamma_i + \exp[-J_o^{\text{N}}]}{\gamma_i + 1} \right) \quad (5.11)$$

$$\nabla J_o^{\text{QC}} = \nabla J_o^{\text{N}} \left( 1 - \frac{\gamma_i}{\gamma_i + \exp[-J_o^{\text{N}}]} \right) \quad (5.12)$$

$$\nabla J_o^{\text{QC}} = \nabla J_o^{\text{N}} w_i \quad (5.13)$$

where

$$w_i = 1 - \frac{\gamma_i}{\gamma_i + \exp[-J_o^{\text{N}}]} \quad (5.14)$$

$$\gamma_i = \frac{P(G_i)/(2l_i)}{[1 - P(G_i)]/\sqrt{2\pi}} \quad (5.15)$$

### 5.3.2 Implementation

The *a priori* information, i.e.  $P(G)_i$  and  $l_i$ , is set during the screening, in the routine **DEPART**, and stored in the NCMFGC1 and NCMFGC2-words of the ODB. Default values are set in DEFGRUN, and can be modified by the namelist namjo. VarQC can be switched on/off for each observation type and variable individually using LVARQC, or it can be switched off all together by setting the global switch LVARQCG = .FALSE.. Since an as good as possible ‘preliminary analysis’ is needed before VarQC starts, it is necessary to perform part of the minimization without VarQC, and then switch it on.

**HJO** computes  $J_o^{\text{QC}}$  according to (5.11) and the QC-weight,  $w_i$ , according to (5.14).

The 3D-Var assimilation system (Chapter 3) can handle non-quadratic cost functions because it is using the **M1QN3** minimization routine. This allows VarQC to be activated after NITERQC (40 by default) iterations during the minimization process. The 4D-Var assimilation system (Chapter 2) by default use a conjugate gradient minimization method that requires a strictly quadratic cost function. So in 4D-Var we use a quadratic formulation of VarQC, controlled by LQVARQC (default .TRUE.).

In the non-quadratic formulation the QC-weight,  $w_i$ , (5.14) is updated for each simulation based on the normalized departure values calculated from the latest model state. However, to obtain a strictly quadratic cost function the QC-weight is not allowed to change during the minimisation process, because the cost function shape would then change. Also, when LQVARQC = .TRUE. it is not possible to activate VarQC in the middle of the minimisation process, i.e. NITERQC MUST be zero, because this would otherwise introduce a sudden jump in the cost function. Therefore, in 4D-Var assimilations VarQC is not applied during the first outer-loop but only for the second (and possibly subsequent) outer-loop iteration(s).

The quadratic VarQC implementation satisfies the quadratic constraint by calculating the QC-weight,  $w_i$ , based on the high resolution trajectory fields and using this constant weight during the next minimisation step. The cost function value is increased/reduced for each simulation during the minimisation by a factor  $w_i^*$  (norm\_dep\_LR-norm\_dep\_HR), linearized in the vicinity of the high resolution cost function at norm\_dep\_HR. For the minimisation the most important input is the modification of the gradient by the weight  $w_i$ . During the trajectory run the high resolution departure is stored in ROBODY(...,MDBIFC1(NUPTRA+1)) in **HDEPART**. For each simulation during the next minimisation step the high resolution departure is read and normalized by the final observation error in **HJO** HJO loop 1.3.2. This is used as input to the VarQC weight calculations (loop 1.5.3–1.5.4 in **HJO**). It is assured that the same weight is used for each simulation in the minimisation if LLQVARQC\_MIN = .TRUE., because ZFJOS\_HR(JOBS,JBODY) is constant during the minimisation. The cost function value is calculated like  $Jo\_varqc\_LR = Jo\_varqc\_HR + w_i^*(norm\_dep\_LR-norm\_dep\_HR)$ .

The *a posteriori* probability of gross error is stored in the ODB and passed to BUFR feedback. Storing in ODB is done at the final simulation of the last minimisation if LQVARQC = .F., but done during the

final trajectory run if `LQVARQC = .TRUE.` in order to use the updated final trajectory for calculating the QC-weight based on final high-resolution analysis values. This is done in `HJO` – see [Subsection 5.2.5](#).

Variational quality control for time correlated observations: The same method as above is (by default) applied for time correlated observations (`LTC = .TRUE.`). Here the high resolution departure values are required for all the time correlated observations. This is achieved by storing the normalized high resolution departures in the array `RTCNDPHR` in `HJO` and reading them in `COMTC`. They are then copied to local array `ZTCNDPHR_W` and then used instead of the low resolution departures in the calculation (overwriting `ZOM1DEP_W` by high resolution values).

## 5.4 VARIATIONAL BIAS CORRECTION

Variational bias correction (VarBC, [Dee \(2004\)](#)) of observations was first introduced into the IFS in Cy31r1. VarBC works by including additional degrees of freedom (bias parameters) in the observational term of the 4D-Var cost function to account for possible systematic errors in selected observations and/or observation operators. The systematic errors (or biases) are represented by linear predictor models, which can be formulated separately for different groups of observations.

Configuration of the VarBC system involves specifications of:

- observation classes:** types of observations subject to VarBC (e.g. clear-sky radiances; aircraft temperatures)
- data groups:** subsets within each class that share the same bias model (e.g. individual radiance channels; reports from specified aircraft types)
- bias predictors:** information used to explain the bias in a given data group (e.g. layer thickness; scan position; solar elevation)

The bias correction  $b$  for an observation belonging to data group  $j$  is defined as

$$b = \sum_{i=0}^{N^j-1} \beta_i^j p_i^j \quad (5.16)$$

where the  $p_i^j$  are the  $N^j$  bias predictors associated with the group. The bias parameters  $\beta_i^j$  are adjusted by the variational analysis. By convention  $p_0 \equiv 1$ , representing a globally constant component of bias, but the other predictors can be flexibly defined. They may depend on properties of the observed atmospheric column, on the state of the instrument, or on any other available information.

If  $N^g$  is the number of data groups, then the total number  $N^p$  of bias parameters to be estimated is

$$N^p = \sum_{j=1}^{N^g} N^j \quad (5.17)$$

The number  $N^j$  of predictors used for each data group is typically between 1 and 10. As of Cy36r1, the number  $N^g$  of data groups subject to variational bias correction is approximately  $10^3$ , and the total number  $N^p$  of bias parameters used for this purpose is slightly less than  $10^4$ .

### 5.4.1 Variational estimation of the bias parameters

Including the bias parameter vector  $\beta = \{\beta_i^j, i = 1, \dots, N^j; j = 1, \dots, N^g\}$  in the variational analysis replaces equation (1.2) by

$$J(\delta\mathbf{x}, \delta\beta) = \frac{1}{2} \delta\mathbf{x}^T \mathbf{B}^{-1} \delta\mathbf{x} + \frac{1}{2} \delta\beta^T \mathbf{B}_\beta^{-1} \delta\beta + \frac{1}{2} (\mathbf{H}\delta\mathbf{x} + \mathbf{b}(\beta) - \mathbf{d})^T \mathbf{R}^{-1} (\mathbf{H}\delta\mathbf{x} + \mathbf{b}(\beta) - \mathbf{d}) \quad (5.18)$$

where  $\delta\beta = \beta - \beta^b$  with  $\beta^b$  a prior estimate, usually the result of the previous analysis cycle. The matrix  $\mathbf{B}_\beta$  controls the adaptivity of the bias parameter estimates. We use a diagonal  $\mathbf{B}_\beta$  with elements

$$\sigma_{\beta_i^j}^2 = (\sigma^j)^2 / M^j, \quad i = 1, \dots, N^j; \quad j = 1, \dots, N^g \quad (5.19)$$

where  $\sigma^j$  is an estimate of the error standard deviation for a typical observation in group  $j$ , and  $M^j$  is a positive integer. This formula effectively provides the same weight to the prior estimate for  $\beta_i^j$  as it would to  $M^j$  newly available observations.

The number  $M^j$  in (5.19) is a stiffness parameter for the bias estimates associated with a data group. It should be interpreted as the minimum sample size required to allow significant adjustment of the estimates by VarBC. For satellite observations, the number of data per analysis cycle is typically much larger than the number of bias parameters to be estimated. The background term in that case does not strongly affect the bias estimates unless  $M^j$  is extremely large. For data groups with typically small sample sizes, such as station data, the effect of the stiffness parameter  $M^j$  is mainly to control the time scale over which bias estimates are allowed to vary.

Preconditioning of the joint minimisation problem (5.18) is based on a separately defined change-of-variable for the bias control parameters, and is described in Dee (2004).

#### 5.4.2 Modular implementation

VarBC was originally designed to handle clear-sky radiance data only, with data groups consisting of individual channels for all available satellite sensors. The code was completely rewritten for Cy35r2 to facilitate implementation of bias corrections for other types of observations. The new design is modular, with separate code modules for different observation classes. All information needed by VarBC that is specific to the observations contained in a class is handled by the corresponding class module. This includes, for example, the exact definition of a data group, the choice of predictors for each group, the option for initialising bias parameters for new groups, specification of the stiffness parameters, and various other configuration choices.

The following class modules are included in Cy36r1:

<code>varbc_rad</code>	clear-sky radiance data
<code>varbc_allsky</code>	all-sky radiance data
<code>varbc_to3</code>	ozone layer concentrations (MACC ozone, greenhouse gases, and aerosol optical depth available in Cy36r4)
<code>varbc_tcwv</code>	total column water vapour data from MERIS
<code>varbc_airep</code>	temperature reports from aircraft (available in Cy36r4)

Several generic modules provide functions that are essentially independent of the type of data involved. These are:

<code>varbc_setup</code>	to configure VarBC, administer VarBC data structures, set up preconditioning, provide I/O functions
<code>varbc_pred</code>	to evaluate predictors
<code>varbc_eval</code>	to evaluate the bias models, including TL and AD

Communication between the various class-dependent code modules on the one hand and the generic modules on the other is accomplished by assigning a unique key to each data group within a class. This key is a character string created by the class module, which encodes into the key whatever information it needs in order to uniquely identify the observations for that group. In the case of satellite radiance data, for example, the key contains the satellite id, sensor number, and channel number associated with the group. Only the class module needs to be able to decode the key. The generic modules communicate with the class modules simply by reference to the keys. VarBC assigns a unique integer (index) to each key, and requests the class modules to store this index in the ODB at `varbc_idx@body`. From that point on, the IFS recognises observations that are subject to VarBC simply by the presence of a positive VarBC index, and handles all VarBC-related operations in essentially the same way, independently of the type of data involved, by reference to its VarBC index.

Each class module must have the following public interfaces to serve the generic code modules ("`varbc_XXX`" denotes the class module name):

<code>varbc_xxx_config</code>	to configure itself
<code>varbc_xxx_groups</code>	to identify the available data groups in its class
<code>varbc_xxx_groupdescr</code>	to provide a printable description for a data group
<code>varbc_xxx_varbcix</code>	to store the assigned varbc indices for all its data groups in the ODB
<code>varbc_xxx_pred</code>	to provide configuration parameters needed to define and/or initialise the bias predictor models
<code>varbc_xxx_min</code>	to provide configuration parameters for the minimisation

## 5.5 OBSERVATION OPERATORS – GENERAL

The operator  $H$  is subdivided into a sequence of operators, each one of which performs part of the transformation from control variable to observed quantity.

- (i) The inverse change of variable (**CHAVARIN**) converts from control variables to model variables.
- (ii) The inverse spectral transforms put the model variables on the model's reduced Gaussian grid (controlled by **SCAN2MDM**).
- (iii) A 12-point bi-cubic or 4-point bi-linear horizontal interpolation, similar to the semi-lagrangian interpolation routines described elsewhere, gives vertical profiles of model variables at observation points (controlled by **COBS**, **COBSLAG**). The surface fields are interpolated bi-linearly to avoid spurious maxima and minima. The three steps (i) to (iii) are common to all data types. Thereafter follows steps (iv) and (v).
- (iv) Vertical integration of, for example, the hydrostatic equation to form geopotential, and of the radiative transfer equation to form radiances (if applicable).
- (v) Vertical interpolation to the level of the observations.

The vertical operations depend on the variable. The vertical interpolation is linear in pressure for temperature (**PPT**) and specific humidity (**PPQ**), and it is linear in the logarithm of pressure for wind (**PPUV**). The vertical interpolation of geopotential (**PPGEOP**) is similar to wind (in order to preserve geostrophy) and is performed in terms of departures from the ICAO standard atmosphere for increased accuracy (**Simmons and Chen, 1991**, see [Section 5.6](#)). The current geopotential vertical interpolation together with the temperature vertical interpolation are not exactly consistent with hydrostatism. A new consistent and accurate vertical interpolation has been devised by Météo-France, which may be important for intensive use of temperature information. The new routines have been tested by ECMWF and as the results were not unambiguously positive the new routines have not yet been adopted – and they are not described in this documentation. In the meantime, the old routines are still used (switch `LOLDPP = .TRUE.` in `namct0`), under the names **PPT\_OLD**, **PPGEOP\_OLD** and **PPUV\_OLD**, with tangent linear **PPTTL\_OLD**, **PPGEOPTL\_OLD** and **PPUVTL\_OLD** and adjoint **PPTAD\_OLD**, **PPGEOPAD\_OLD** and **PPUVAD\_OLD**.

The vertical interpolation operators for SYNOP 10-metre wind (**PPUV10M**) and 2-metre temperature (**PPT2M**) match an earlier version of the model's surface layer parametrization. The vertical gradients of the model variables vary strongly in the lowest part of the boundary layer, where flow changes are induced on very short time and space scales, due to physical factors such as turbulence and terrain characteristics. The vertical interpolation operator for those data takes this into account following Monin–Obukhov similarity theory. Results using such operators, which follow **Geleyn (1988)** have been presented by **Cardinali et al. (1994)**. It was found that 2-metre temperature data could not be satisfactorily used in the absence of surface skin temperature as part of the control variable, as unrealistic analysis increments appeared in the near-surface temperature gradients. The Monin–Obukhov based observation operator for 10-metre wind, on the other hand, is used for all surface winds (SYNOP, DRIBU, TEMP, PILOT and SCAT), where interpolation is not confined to only 10 m, but is performed to the actual observation height (in practise ranging from 4 to 10 m).

Relative humidity is assumed constant in the lowest model layer to evaluate its 2-metre value (**PPRH2M**), see [Subsection 5.9.4](#). Model equivalents of total column water vapour data are obtained by vertical integration of  $q$  (in **GPPWC** and **PPPWC**). The routine **PPPWC** is also used for vertical integration of GEMS/MACC trace gasses. Observation operators exist for precipitable water content (also using **PPPWC**) and thicknesses (**PPGEOP**).

The variational analysis procedure requires the gradient of the objective function with respect to the control variable. This computation makes use of the adjoint of the individual tangent linear operators, applied in the reverse order. The details regarding observation operators for conventional data can be found in [Vasiljevic et al. \(1992\)](#), [Courtier et al. \(1998\)](#), and in the following sections.

## 5.6 THE OBSERVATION OPERATOR FOR CONVENTIONAL DATA

### 5.6.1 Geopotential height

The geopotential at a given pressure  $p$  is computed by integrating the hydrostatic equation analytically using the ICAO temperature profile and vertically interpolating  $\Delta\phi$ , the difference between the model level geopotential and the ICAO geopotential ([Simmons and Chen, 1991](#)). The ICAO temperature profile is defined as

$$T_{\text{ICAO}} = T_0 - \frac{\Lambda}{g}\phi_{\text{ICAO}} \quad (5.20)$$

where  $T_0$  is 288 K,  $\phi_{\text{ICAO}}$  is the geopotential above 1013.25 hPa and  $\Lambda$  is 0.0065 K m<sup>-1</sup> in the ICAO troposphere and 0 in the ICAO stratosphere (the routine **PPSTA**). The ICAO tropopause is defined by the level where the ICAO temperature has reached 216.5 K (**SUSTA**). Using this temperature profile and integrating the hydrostatic equation provides  $T_{\text{ICAO}}$  and the geopotential  $\phi_{\text{ICAO}}$  as a function of pressure (**PPSTA**). We may then evaluate the geopotential  $\phi(p)$  at any pressure  $p$  following

$$\phi(p) - \phi_{\text{surf}} = \phi_{\text{ICAO}}(p) - \phi_{\text{ICAO}}(p_{\text{surf}}) + \Delta\phi \quad (5.21)$$

where  $p_{\text{surf}}$  is the model surface pressure and  $\phi_{\text{surf}}$ , the model orography.  $\Delta\phi$  is obtained by vertical interpolation from the full model level values  $\Delta\phi_k$ . The interpolation is linear in  $\ln(p)$  up to the second model level (**PPINTP**) and quadratic in  $\ln(p)$  for levels above it (**PPITPQ**, see below). Following [Simmons and Burridge \(1981\)](#) the full model level values are obtained by integrating the discretized hydrostatic equation using the routine **GPGE0** of the forecast model to give

$$\Delta\phi_k = \sum_{j=L}^{k+1} R_{\text{dry}}(T_{v_j} - T_{\text{ICAO}_j}) \ln\left(\frac{p_{j+1/2}}{p_{j-1/2}}\right) + \alpha_k R_{\text{dry}}(T_{v_k} - T_{\text{ICAO}_k}) \quad (5.22)$$

with

$$\alpha_k = 1 - \frac{p_{k-1/2}}{p_{k+1/2} - p_{k-1/2}} \ln\left(\frac{p_{k+1/2}}{p_{k-1/2}}\right)$$

for  $k > 1$  and  $\alpha_1 = \ln(2)$ .

#### (a) Quadratic vertical interpolation near the top of the model

Above the second full level of the model, the linear interpolation (**PPINTP**) is replaced by a quadratic interpolation in  $\ln p$ , performed in the routine **PPITPQ** using

$$z(\ln p) = a + b(\ln p) + c(\ln p)^2 \quad (5.23)$$

where  $a$ ,  $b$  and  $c$  are constants determined so that the above equation fits the heights at the top levels ( $k = 1, 2$  and  $3$ ). The interpolation formula is

$$\phi(\ln p) = z_2 + \frac{(z_2 - z_1)(\ln p - \ln p_2)(\ln p - \ln p_3)}{(\ln p_2 - \ln p_1)(\ln p_1 - \ln p_3)} - \frac{(z_2 - z_3)(\ln p - \ln p_1)(\ln p - \ln p_2)}{(\ln p_2 - \ln p_3)(\ln p_1 - \ln p_3)} \quad (5.24)$$

where 1, 2 and 3 refer to levels  $k = 1, 2$  and  $3$ , respectively.

#### (b) Below the model's orography

The extrapolation of the geopotential below the model's orography is carried out as follows: Find  $T^*$  (surface temperature) by assuming a constant lapse rate  $\Lambda$ , from the model level above the lowest model



level (subscript  $l - 1$ ), see the routine **CTSTAR**, using

$$T^* = T_{l-1} + \Lambda \frac{R_{\text{dry}}}{g} T_{l-1} \ln \frac{p_{\text{surf}}}{p_{l-1}} \quad (5.25)$$

$$T^* = \frac{\{T^* + \max[T_y, \min(T_x, T^*)]\}}{2} \quad (5.26)$$

Find the temperature at mean sea level,  $T_0$  (also in **CTSTAR**) from

$$T_0 = T^* + \Lambda \frac{\phi_{\text{surf}}}{g} \quad (5.27)$$

$$T_0 = \min[T_0, \max(T_x, T^*)] \quad (5.28)$$

where  $T_x$  is 290.5 K and  $T_y$  is 255 K. The geopotential under the model's orography is (in **PPGEOP**) calculated as

$$\phi = \phi_{\text{surf}} - \frac{R_{\text{dry}} T^*}{\gamma} \left[ \left( \frac{p}{p_{\text{surf}}} \right)^\gamma - 1 \right] \quad (5.29)$$

where  $\gamma = \frac{R_{\text{dry}}}{\phi_{\text{surf}}} (T_0 - T_{\text{surf}})$ .

### 5.6.2 Wind

In **PPUV** a linear interpolation in  $\ln p$  (**PPINTP**) is used to interpolate  $u$  and  $v$  to the observed pressure levels up to the second full model level, above which a quadratic interpolation is used (**PPITPQ**, see [Subsection 5.6.1](#)). Below the lowest model level wind components are assumed to be constant and equal to the values of the lowest model level.

### 5.6.3 Humidity

Specific humidity  $q$ , relative humidity  $U$  and precipitable water content  $PWC$  are linearly interpolated in  $p$ , in **PPQ**, **PPRH** and **PPPWC**, respectively. Upper air relative humidity data are normally not used, but could be used, if required. The use of surface relative humidity data is described in [Subsection 5.9.4](#).

#### (a) Saturation vapour pressure

The saturation vapour pressure  $e_{\text{sat}}(T)$  is calculated using Tetens's formula given by

$$e_{\text{sat}}(T) = a_1 \exp^{a_3 \left( \frac{T - T_3}{T - a_4} \right)} \quad (5.30)$$

using FOEEWM (mixed phases, water and ice) in the model and FOEEWMO (water only) for observations. The use of water-phase only is in accordance with the WMO rules for radiosonde and synop reporting practices. Note that these statement functions compute  $(R_{\text{dry}}/R_{\text{vap}})e_{\text{sat}}(T)$ , with the parameters set according to [Buck \(1981\)](#) and the AERKi formula of [Alduchov and Eskridge \(1996\)](#), i.e.  $a_1 = 611.21$  hPa,  $a_3 = 17.502$  and  $a_4 = 32.19$  K over water, and for FOEEWM  $a_3 = 22.587$  and  $a_4 = -0.7$  K over ice, with  $T_3 = 273.16$  K. Furthermore in FOEEWM the saturation value over water is taken for temperatures above 0°C and the value over ice is taken for temperatures below -23°C. For intermediate temperatures the saturation vapour pressure is computed as a combination of the values over water  $e_{\text{sat}(\text{water})}$  and  $e_{\text{sat}(\text{ice})}$  according to the formula

$$e_{\text{sat}}(T) = e_{\text{sat}(\text{ice})}(T) + [e_{\text{sat}(\text{water})}(T) - e_{\text{sat}(\text{ice})}(T)] \left( \frac{T - T_i}{T_3 - T_i} \right)^2 \quad (5.31)$$

with  $T_3 - T_i = 23$  K.

#### (b) Relative humidity

In **GPRH** relative humidity  $U$  is computed from

$$U = \frac{pq \frac{R_{\text{vap}}}{R_{\text{dry}}}}{\left[ 1 + \left( \frac{R_{\text{vap}}}{R_{\text{dry}}} - 1 \right) q \right] e_{\text{sat}}(T)} \quad (5.32)$$

and then in **PPRH** interpolated to the required observed pressure levels (using **PPINTP**). Below the lowest model level and above the top of the model is  $U$  assumed to be constant. Saturation vapour pressure is calculated using FOEEWMO if **GPRH** has been called from the observation operator routines, and using FOEEWM if called from the model post processing.

(c) *Precipitable water*

In **GPPWC** precipitable water is calculated as a vertical summation from the top of the model by

$$PWC_k = \frac{1}{g} \sum_{i=1}^k q_i (p_i - p_{i-1}) \quad (5.33)$$

and then in **PPPWC** interpolated to the required observed pressure levels (using **PPINTP**).  $PWC$  is assumed to be zero above the top of the model. Below the model's orography  $PWC$  is extrapolated assuming a constant  $q = q_l$ .

(d) *Specific humidity*

Specific humidity  $q$  is in **PPQ** interpolated to the required observed pressure levels (using **PPINTP**). Below the lowest model level and above the top of the model is  $q$  assumed to be constant and equal to  $q_l$  and  $q_1$ , respectively.

#### 5.6.4 Temperature

Temperature is interpolated linearly in pressure (**PPINTP**), in the routine **PPT**. Above the highest model level the temperature is kept constant and equal to the value of the highest model level. Between the lowest model level and the model's surface the temperature is interpolated linearly, using

$$T = \frac{(p_{\text{surf}} - p)T_l + (p - p_l)T^*}{p_{\text{surf}} - p_l} \quad (5.34)$$

Below the lowest model level the temperature is extrapolated by

$$T = T^* \left[ 1 + \alpha \ln \frac{p}{p_{\text{surf}}} + \frac{1}{2} \left( \alpha \ln \frac{p}{p_{\text{surf}}} \right)^2 + \frac{1}{6} \left( \alpha \ln \frac{p}{p_{\text{surf}}} \right)^3 \right] \quad (5.35)$$

with  $\alpha = \Lambda R_{\text{dry}}/g$ , for  $\phi_{\text{surf}}/g < 2000$  m, but  $\alpha$  is modified for high orography to  $\alpha = R_{\text{dry}}(T'_0 - T^*)/\phi_{\text{surf}}$ , where

$$T'_0 = \min(T_0, 298) \quad (5.36)$$

for  $\phi_{\text{surf}}/g > 2500$  m, and

$$T'_0 = 0.002[(2500 - \phi_{\text{surf}}/g)T_0 + (\phi_{\text{surf}}/g - 2000) \min(T_0, 298)] \quad (5.37)$$

for  $2000 < \phi_{\text{surf}}/g < 2500$  m. If  $T'_0 < T^*$  then  $\alpha$  is reset to zero. The two temperatures  $T^*$  and  $T_0$  are computed using (5.25) to (5.28).

## 5.7 SATELLITE RADIANCE OPERATORS

The majority of satellite data assimilated currently is radiances. Radiances, rather than retrieved products, are assimilated directly (Andersson *et al.*, 1994), wherever possible. The current operational configuration uses clear level-1C radiances from a number of sensors, including ATOVS (McNally *et al.*, 1999), AIRS, IASI, ATMS, as well as geostationary water vapour clear-sky radiances (Munro *et al.*, 2004). Clear, cloudy and precipitation-affected microwave imager radiances from TMI, SSMI/S, WINDSAT are monitored or assimilated using an all-sky approach, and a parallel datastream of AMSU-A data is sent through the all-sky route for monitoring purposes too (though AMSU-A is actively assimilated using the normal clear-sky route). Hence there are currently two routes in the IFS to assimilate satellite radiances, one for normal clear-sky radiances and totally overcast infrared radiances, and one for all-sky microwave radiances.

The first route, i.e. the one for all clear-sky radiances, as well as for totally overcast infrared radiances, uses the radiative transfer operator on model profiles interpolated to observation locations. The processing within 3D/4D-Var of satellite data assimilated through this route follows the same general layout as that of conventional data.

The second route uses the radiative transfer operator on model profiles at model grid point locations, and associates the output with any observations within that model grid box. This assimilation route differs considerably from that used for conventional observations. The route is currently only used for all-sky microwave radiances.

For the nadir radiances, the observation operators for both routes are different flavours of the RTTOV radiative transfer model (Saunders and Matricardi, 1998; Matricardi *et al.*, 2001), currently using RTTOV version 10.

### 5.7.1 Common aspects for the setup of nadir radiance assimilation

The operational radiance assimilation shares the following setup aspects for both radiance assimilation routes. The datasets are distinguished by a satellite ID, a sensor ID, and a codetype. The latter is used to distinguish clear-sky (codetype=210=NGTHRb) or all-sky radiances (codetype=215=NSSMI).

The main set-up routine for radiances is **SURAD**. It recognises BUFR satellite IDs (call to **GETSATID**), reads RTTOV coefficient files (call to **RTSETUP**), and builds a “satellite group table” containing information on which satellite groups are present.

#### (a) Satellite identifiers and sensors

Satellite identifiers are dealt with in the routine **GETSATID**, called from **SURAD**. The ODB contains the identifiers as given in the original BUFR messages. Lists of identifiers for which data exist in any given ODB are prepared in the routine **SURAD**. The routine **GETSATID** matches those BUFR satellite identifiers with the platform and satellite numbers used by the RT-code (e.g. platform 1, satellite 10 for NOAA-10). New satellite IDs need to be defined in **GETSATID**, but the id-conversion tables can also be modified through the namelist **NAMSATS**.

The various types of radiance data in the IFS are also classified by sensor. Each satellite sensor is assigned a number, defined in the module **YOMSATS**. The sensor number is used as index to various tables containing observation errors, BgQC thresholds, VarQC parameters, the  $J_o$ -table **JOT**, etc. See the routine **DEFRUN**.

#### (b) Satellite group table

Various satellite-related indices are gathered in the routine **SURAD** in the FORTRAN90 data structure called the ‘satellite group table’, **satgrp\_t** (defined in **YOMSATS**). The table contains elements such as the satellite ID, the sensor ID, the codetype, a sequence number for addressing the transmittance coefficients (**rtcoef\_pos**), the number of channels, a channel number list, etc. The various satellite-related indices are universally determined across all processors. There is one entry in the satellite group table per satellite, sensor, and codetype. A list of all the satellite groups that were found in the ODBs can be found in the *ifstraj* output by searching for **SATGRP**.

#### (c) Radiative transfer coefficients, pressure levels and validation bounds

Various preparations for RTTOV calculations are set-up in the call to **RTSETUP** from **SURAD**. This includes reading of the various coefficient files required by RTTOV. The files can be found under `/home/rd/rdx/data/38r1/sat/rttov`. There is one file with the prefix *rtcoef\_* containing coefficients for the general clear-sky radiative transfer for each instrument and satellite, and files with prefix *scldcoef\_* used for a parametrization of cloud scattering effects for some infrared sensors. Both types of files are read via a call to **RTTVI** (in the **satrad** library) which also communicates other settings from the RTTOV code in the **satrad** library to the IFS side. Only the files that are required are read, i.e. only the files for which observations are present (for the clear-sky coefficients) or for which data is present and the calculation of cloudy radiances is requested through switching the flags **LCLD\_RTCALC\_SCREEN** or

LCLD\_RTCALC\_ASSIM on in the module **SATS\_MIX** for the respective sensor. A third type of RTTOV coefficient files (prefix *mietable\_*) is required for RTTOV\_SCATT computations in the all-sky system (see 5.7.3), read via a call to **MWAVE\_SETUP** under **RTSETUP**.

If the interpolation to RTTOV pressure levels is performed on the IFS side (rather than inside RTTOV, see 5.7.2), the list of the NLSAT = 44 fixed pressure levels is stored in arrays in **SATS\_MIX**. They are read in the satrad project from the transmittance coefficient file, called via the route of **SURAD** and **RTSETUP**. **RTSETUP** similarly obtains (from RTTOV) lists of temperature, humidities and ozone limits indicating the valid range of the RT transmittance regression. The RT code is not reliable in conditions beyond these limits. The IFS uses just one set of fixed pressure levels, reference or limit profiles (rather than having instrument dependent ones), and the ones that are read last are used. The reference pressure levels and limit profiles are only used if the interpolation to RTTOV pressure levels is performed in the IFS before the call to RTTOV instead of using the internal RTTOV interpolation (see 5.7.2), and the number of levels is fixed to NLSAT = 44.

If the interpolation to RTTOV pressure levels is performed inside RTTOV (the default behaviour at ECMWF, see 5.7.2), the transmittance coefficient file for different sensors can use any number of fixed pressure levels, and the number can be different for different sensors.

### 5.7.2 Clear-sky nadir radiances and overcast infrared nadir radiances

#### (a) Radiance observation errors and bias correction

Observation errors for 1C radiances are written to the ODB in a call to **RADICOB** (from **HRETR**). They are set by sensor and channel in the routine **DEFRUN**, variable ROERR\_RAD1C.

The bias correction is performed through variational bias correction, see section Section 5.4. The VarBC class is called “rad”, and the class-specific routines for the generic VarBC code are in the module **VARBC\_RAD**. For most sounding radiances, the predictors used consist of four layer-thicknesses derived from the First Guess (as defined in **VARBC\_PRED**), but some window channels do not include such air mass predictors to avoid aliasing of cloud information into the bias correction. Also, AMSU-A channel 14 is assimilated without a bias correction, in order to anchor the stratospheric temperature analysis. Without such an anchor, the variational bias corrections tend to drift to unrealistic values as a result of model biases. This is done at script level, through the namelist NAMVARBC\_RAD.

#### (b) Surface emissivity

Microwave (**EMIS\_MW\_N**) and infrared (**EMIS\_IR**) surface emissivities are set during the screening phase in **RADICEMIS** (called from **HRETR**) and stored in the ODB for later use by RTTOV. Setting the emissivity to values outside the range of 0 and 1 prompts the calculation of surface emissivity within RTTOV, using FASTEM (Deblonde and English, 2001) for the microwave and ISEM-6 (Sherlock, 1999) for the infrared. This is done for all microwave and infrared radiances over sea.

For microwave radiances over land, several options exist to specify the surface emission, following the methods described in Karbou *et al.* (2006). The surface emissivity can be specified through an atlas, or it can be dynamically retrieved from window channel observations and FG estimates of skin temperature and atmospheric profiles, or the skin temperature can be retrieved given an emissivity atlas value and FG estimates of atmospheric profiles. Default choices are made by sensor in **SUEMIS\_CONF** (including which channel is used for the last two options) and can be overwritten through the namelist **NAMEMIS\_CONF** or controlled through the preIFS switch AMSU\_LAND in the Satellites window in the case of AMSU-A/B/MHS. For the two options with dynamic retrieval of emissivity or skin temperature, the required radiative transfer calculations are performed in the routine **satrat/rttov/ifs/rttov\_ec** when called from **HRETR** via **RADTR** or **RADTR\_ML** (see also next section). The atlas values and the retrieved emissivities or skin temperatures are written to the ODB, and used as fixed input in subsequent calls to RTTOV. If atlas values are required, these are read in the routine **DEFRUN**. The default for AMSU-A/B/MHS over land is to use the dynamic retrieval of surface emissivity, using an evolving emissivity atlas to quality-control the retrieved emissivities.

For AMSU-A/B/MHS a Kalman Filter is used to produce an evolving emissivity atlas from past dynamically retrieved emissivity values, as summarised in Krzeminski *et al.* (2009). The atlas is updated using the programs `EMISKF_UPDATE_AMSUA`, `EMISKF_UPDATE_AMSUB`, and `EMISKF_UPDATE_MHS` in the satrad project (together with `emiskf*` and `kfgrid*` routines that can be found in the `emiss` directory of the satrad project). These programs access the ODB and read the required retrieved emissivity values. Routine `EMISKF_INIT` specifies the resolution of the atlas and other configuration settings. Routine `EMISKF_INIT_SENSOR` is used to read the atlas values, `EMISKF_UPDATE_ATLAS` to update the emissivity parametrization, and `EMISKF_WRITE_SENSOR` to output the updated atlas. The cycling of the atlas information is done through the files `emiskf.cycle*` which are stored as tar-ball in ECFS. The routine `EMISKF_INIT_SENSOR` is also used to read the atlas under `DEFRUN` during the application stage in the screening run. If no atlas is available a “coldstart” is performed, setting the atlas values and their errors to pre-specified values.

(c) *Calling the radiative transfer model*

The radiative transfer model RTTOV is called from the general observation operator routine `HOP`. More details on RTTOV can be found in Eyre (1991), updated by Saunders and Matricardi (1998).

RTTOV performs optical depth calculations on a number of fixed pressure levels, as specified in the `rtcoef_` coefficient file mentioned earlier. RTTOV includes the option to provide the atmospheric profile input either on this set of fixed pressure levels or on a set of different and variable pressure levels. In the latter case, RTTOV will perform the required interpolation internally, using an interpolation that provides smoother gradients than a simple linear interpolation. If this option is used, the radiative transfer computations are also performed on the input user levels, rather than the fixed RTTOV pressure levels.

The IFS allows the user to either perform the interpolation to the RTTOV pressure levels before the call to RTTOV on the IFS side, or to provide the model data on the model fields and use the RTTOV internal interpolation. The choice is done via the flag `LRTTOV_INTERPOL` in the module `SATS_MIX`. The default for ECMWF is to use the RTTOV internal interpolation, so the flag is set to `.True.`

Depending on the setting of `LRTTOV_INTERPOL`, the routine `HOP` will perform different tasks:

In case `LRTTOV_INTERPOL` is set to `.False.`, `HOP` interpolates the model profiles of temperature, humidity and ozone ( $T$ ,  $q$ , and  $oz$ ) to the NLSAT(= 44) RT levels ( $\dot{T}$  and  $\dot{q}$ ) and calls the interface `RADTR` to the RT code RTTOV. The standard routines `PPT` and `PPQ` are used to carry out the vertical interpolation, and they are called through the `PPOBSA` interface, as usual. Various radiance preparations are performed in the routine `HRADP`. For the purpose of radiance calculations  $T_{2m} = T_l$  (the lowest model level temperature) and  $q_{2m} = \dot{q}_{NLSAT}$  (specific humidity at the lowermost of the RT pressure levels). These quantities represent a very shallow layer of air near the surface and contribute little to the calculated radiances – it was not considered necessary to use `PPT2M` and `PPRH2M` (Section 5.9) in this context. In order to make the radiance cost function continuous in  $p_{surf}$  it was necessary to ensure that  $\dot{T}$  and  $\dot{q}$  approach  $T_{2m}$  and  $q_{2m}$  as the pressure on any of the RT levels approaches  $p_{surf}$ . This is done in a section of `HRADP`. The routine `RADTR` checks that the input model profile is within the valid range of the transmittance regression, and re-sets the values to the limit values if they fall outside these validity bounds.

In case `LRTTOV_INTERPOL` is set to `.True.` (the default), `HOP` will call RTTOV via the routine `RADTR_ML` and profile information will be input to RTTOV on `NFLEVG+1` levels. These correspond to the `NFLEVG` model levels with an additional level set at the model’s surface pressure, for which the temperature, humidity, and other gas concentration values are taken from the lowest model level. A check against the validity bounds of the RTTOV transmittance parametrization is in this case done within RTTOV (routine `SATRAD/RTTOV/MAIN/RTTOV_CHECKINPUT.F90`), for the optical depth calculations only (switch `APPLY_REGRESSION_LIMITS` in `SATRAD/MODULE/RTTOV_CONST.F90`). Various radiance preparations are again performed in a modified version of `HRADP`, `HRADP_ML`.

In either case, the routine `HOP` constructs a list of requested channel numbers for each report from the observation array, and only model radiances for exactly those channels are then requested from the RT-code. The routines `RADTR` or `RADTR_ML` packets the profiles into chunks of work of an appropriate

maximum size for the RT-code (currently set to 8 in `SATRAD/MODULE/mod_cparam.F90`). The RT packet size has been communicated to IFS in the call to `RTSETUP`. The output is radiances for the channels requested.

The tangent linear `HOPTL` and the adjoint `HOPAD` follow the same pattern as `HOP`. In both the TL and the adjoint  $\dot{T}$  and  $\dot{q}$  have to be recomputed before the actual tangent linear and adjoint computations can start. The pointers to the radiance data in the observation array are obtained just as it was done in the direct code.

(d) *Skin-temperature ‘sink-variable’ at satellite FOVs*

In the case of 1C, or ‘raw’ radiance data, as used since May 1999 (McNally *et al.*, 1999) surface skin temperature is retrieved by 3D/4D-Var at each field of view, if the switch `LTOVSCV` is on (default is on), in namelist `NAMVAR`. This is done for all infrared and microwave satellite sensors and instruments. The handling of the skin temperature retrieval at the radiance FOVs is performed in the routine `HRADP/HRADPTL/HRADPAD`, called from `HOP/HOPTL/HOPAD`. The background skin temperature is provided by the model trajectory integration, and a background error of 1 K/5 K is assigned over sea/land, respectively (stored in `TOVSCVER`, module `YOMSATS`). The gradient with respect to the skin temperature obtained from `RTTOV` is temporarily stored in the `TOVSCVX` array and later transferred to its location in the distributed control vector (Chapter 2). The next iteration of the minimisation provides updated skin temperature increments (also stored in `TOVSCVX`) that are used by `RTTOVTL` in subsequent iterations. The outer-loop iterations result in a new linearisation state, stored in `TOVSCVX5`. All the skin-temperature-related information at FOV locations that needs to be passed between job-steps, reside in the ODB, in the satellite predictors table. This approach has been adopted for  $\text{CO}_2$  retrieval at AIRS FOVs (Engelen *et al.*, 2004).

### 5.7.3 All-sky nadir radiances

Observations from microwave imagers and sounders can be assimilated using an all-sky approach which unifies clear-sky, cloudy, and precipitation-affected radiances in one observation operator, using `RTTOV-SCATT` for the radiative transfer, which is capable of modelling the effects of multiple scattering from hydrometeors. The microwave imagers `TMI` and `SSMIS` are actively assimilated. `WINDSAT` and `SSM/I` are passively monitored, as are channels 1-5 of `AMSU-A`. Observations are assimilated or monitored only over oceans, and only for latitudes equatorward of  $60^\circ$  ( $40^\circ$  for `AMSU-A`).

All-sky observations follow a path through the IFS code that is slightly different from that for clear-sky radiance observations, though the observation operator does now run under `HOP` rather than under the model physics, as previously. However, the observation operator requires a number of diagnostic variables (e.g. precipitation flux and fraction) that come from the moist physics parametrizations and require a model timestep to have been run before they can be made available in observation space. These fields are generated in `CALLPAR`, stored in the `GFL` arrays and interpolated to observation space like any other model field required by an observation operator, using the `GOM` arrays. The main difference is that there is no interpolation: the observation operator gets the model profile at the grid point closest to the observation.

All-sky assimilation can be switched on in PrepIFS by means of switches for individual sensors, e.g. `LSSMI`, `LAMSRE`, `LTMI`, `LSSMIS` etc. For all-sky `AMSU-A`, which runs in parallel to the clear-sky assimilation, there is a separate switch `LAMSUA_ALLKSY`. Comprehensive scientific documentation of the all-sky approach can be found in Bauer *et al.* (2010), Geer *et al.* (2010), Geer and Bauer (2011b), Geer and Bauer (2011a).

(a) *Preprocessing*

Observations are received in BUFR format and are pre-processed by `SCRIPTS/GEN/premwimg`, which calls a number of fortran programs:

`SATRAD/PROGRAMS/bufr_screen_ssmi_1d` and `bufr_screen_amsre_1d` perform a preliminary screening, removing observations over land and checking for any unrealistic brightness temperatures. `AMSR-E` observations are re-assigned to the BUFR subtype 127, which is that of `SSM/I`. Later, this is

used to identify the observations as part of the all-sky path by giving them codetype 215 (see [ODB/CMA2ODB/bufr2cmat\\_new](#)).

[SATRAD/PROGRAMS/bufr\\_grid\\_screen](#) is called to do superobbing. Based on the final inner loop resolution, typically T255, observations are binned onto the Gaussian grid. This brings the relatively high observation resolution of microwave imagers (up to 10 km) down to roughly the scale of clouds in the IFS model. The superobbing is done by computing the numerical mean of all BUFR fields, except longitude and latitude, which are taken to be those of the grid-point, and the observation time, which comes from the last observation meaned. This program also allows a further thinning of the data by keeping only observations associated with grid points at every  $n$ th longitude and  $m$ th latitude.

#### (b) *Observation operator*

Code for the all-sky observation operator is prefixed by ‘mwave’ and located either in [IFS/MWAVE](#) or [SATRAD/MWAVE](#). The observation operator wrapper [IFS/MWAVE/mwave\\_wrapper](#) is called from [IFS/OP\\_OBS/hop](#) or its TL or adjoint. The same wrapper function is called whether in direct, TL or AD mode, and the required TL or AD functionality is driven by optional arguments. Lower down, there are separate observation operator routines for each mode: ([IFS/MWAVE/mwave\\_obsop](#), [mwave\\_obsop\\_tl](#) or [mwave\\_obsop\\_ad](#)). In the screening trajectory, [IFS/MWAVE/mwave\\_screen](#) is called instead. Inputs to the observation operator are the profiles of model variables (passed in via a structure of `mwave_phys_type`) and any observation-related information (passed via a structure of `mwave_rad_type`). The observation-related information has been read from the ODB by [IFS/MWAVE/mwave\\_get](#), [mwave\\_get\\_tl](#) or [mwave\\_get\\_ad](#). Outputs from the observation operator (such as the simulated brightness temperatures, and the observation error) are returned in a similar way and are written to the ODB by [IFS/MWAVE/mwave\\_put](#) or [mwave\\_put\\_tl](#). This approach is slightly different to that of other observation operators and is a result of the code’s former location in the model physics.

The main function of the observation operator code in [IFS/MWAVE](#) and [SATRAD/MWAVE](#) is simply to provide the correct inputs and initialisations to run [RTTOV\\_SCATT](#). However, there is code for quality control, to produce diagnostic output, and to determine the observation error, which is not constant, but a function of hydrometeor amount, as described in [Geer and Bauer \(2011b\)](#). VarQC ([Section 5.3](#)), VarBC ([Section 5.4](#)), blacklisting and background quality control (all in [Chapter 10](#)) are done largely as for other radiance observations. The internal IFS thinning routines are completely bypassed, however, because a suitable thinning has already been achieved during the superobbing.

A number of initialisation tasks are performed in [IFS/MWAVE/mwave\\_setup](#), including reading the namelist [NAMMWAVE](#) for configuration flags. An array of `mwave_ids` structures is created, one for each satellite and sensor combination that will pass through the all-sky operators. In this private table are stored things like the instrument zenith angle, observation error specifications, and the ID numbers used in the rest of the IFS (e.g. sensor, satellite and bufr IDs).

#### (c) *External files*

Observation error definitions for completely clear and completely cloudy skies are stored in files with names like `mwave_error_<satellite>_<instrument>.dat`. These are read by [IFS/MWAVE/mwave\\_setup](#).

Some configuration options are specified in the [NAMMWAVE](#) namelist in [SCRIPTS/GEN/ifsmim](#) and [ifstraj](#).

#### (d) *Diagnostics*

The consistency of the TL and adjoint operators can be tested by setting `ldmwave_test = .true.` in the [NAMMWAVE](#) namelist in the [SCRIPTS/GEN/ifsmim](#) script. This causes [IFS/MWAVE/mwave\\_obsop\\_test](#) to be called during the minimisation with the real TL input values for each observation. The results of the test are written to the IFS logfiles, prefixed by ‘MWAVE\_OBSOP\_TEST AD:’. The first number gives the TL / AD inaccuracy in multiples of machine precision. Typically this should be substantially less than 100 but it will go over 1000 for a few observations.

A number of diagnostics are stored in the ODB in the `allsky` or `allsky_body` table:

**DATUM\_TBFLAG** - This is a bitfield which records quality control decisions for the all-sky observations. It is an additional diagnostic on top of the usual status and event flags, and it only records decisions made internally in the all-sky observation operator. A value of 1 indicates an OK observation; all other values indicate rejection. However, even if the observation is considered OK by the all-sky observation operator, it may subsequently be rejected by the other IFS screening processes (e.g. blacklisting, thinning, VarQC, background QC), so always check the ‘`status@hdr`’ and ‘`status@body`’ too. Binary arithmetic can be used to decipher the `tbflag` bitfield. For example, if  $\text{DATUM\_TBFLAG} = 33 = 2^5 + 2^0$ , that means bits 5 and 0 have been set. Bit 5 indicates contamination by sea-ice.  $2^0$  is equal to 1; this would have indicated “OK” if no other bit had been set. The full structure of the `DATUM_TBFLAG` bitfield is described in [IFS/MODULE/yommwave](#).

**DATUM\_TBCLOUD** - this is a bitfield recording the status of diagnostic cloud and rain identification tests performed on observed and simulated brightness temperatures by [IFS/OP\\_OBS/mwimager.cloud](#) and further documented in the code and in [Geer et al. \(2008\)](#). The bitfield structure is documented in [IFS/MODULE/yommwave](#). The lowest 2 bits give the results of the FG cloud test. With AND representing the bitwise boolean operator,  $(\text{DATUM\_TBCLOUD AND } 2) / 2$  will give the result of the test for cloud in the FG, with 1 indicating a cloudy scene.  $(\text{DATUM\_TBCLOUD AND } 1) / 1$  will give the result for the observation.

There are also a number of diagnostics relating to FG and analysis model state. These are valid at the time and location of the observation, giving information that is not otherwise archived. These values include the surface rain and snow rate, in  $\text{kg m}^{-2} \text{ s}^{-1}$ , and the total columns of water vapour, cloud water, cloud ice, rain and snow, in  $\text{kg m}^{-2}$ .

#### 5.7.4 Cloud affected infrared radiances

For infrared data from HIRS, AIRS and IASI simplified cloud parameters (cloud top pressure and effective cloud fraction) are estimated for each field of view. Background values are computed during the screening in routine [CLOUD\\_ESTIMATE](#) using a method described in [McNally \(2009\)](#). If the scene is diagnosed as overcast (i.e. cloud fraction equal to 1) then all channels are used (that would be used in a completely clear scene) and the cloud parameters become additional elements of the local control vector (as skin temperature). This is done by default, but can be disabled by setting the switch `LCLDSINK` to false in namelist `NAMVAR`. The cloud top pressure is assigned an error (`CTOPBGE` in `YOMVAR` currently equal to 5 hPa) but the cloud fraction is effectively fixed. The handling of the estimated cloud parameters is then performed in the routine [HRADP/HRADPTL/HRADPAD](#), called from [HOP/HOPTL/HOPAD](#). The gradient with respect to the cloud parameters is obtained from `RTTOV` (`TOVSCVX` array) and it is later transferred to its location in the distributed control vector ([Chapter 2](#)). The next iteration of the minimisation provides updated cloud parameter increments (also stored in `TOVSCVX`) that are used by `RTTOVTL` in subsequent iterations. The outer-loop iterations result in a new linearisation state, stored in `TOVSCVX5`. All the cloud parameter information at FOV locations that needs to be passed between job-steps, resides in the ODB, in the satellite predictors table.

If the scene is not diagnosed as overcast, only channels flagged as clear are assimilated and the cloud parameters are essentially inactive.

#### 5.7.5 Clear-sky limb radiances

Assimilation of clear-sky limb radiances has been implemented in the IFS for experimental purposes. The radiances are assimilated using the `RTLIMB` radiative transfer model which is an extension of `RTTOV` to the limb geometry. Details of the radiative transfer model and the assimilation of limb radiances can be found in [Bormann et al. \(2005\)](#); [Bormann and Healy \(2006\)](#); [Bormann and Thépaut \(2007\)](#); [Bormann et al. \(2007\)](#). Many aspects have been primarily developed for the assimilation of MIPAS limb radiances; the assimilation of radiances from other sensors is likely to require additional coding.

Limb radiances fall under obstype 10 “Limb observations”, codetype 251. The general approach mirrors that used for clear-sky nadir radiances, i.e., the assimilation uses spatially interpolated vertical profile(s)



of model variables. However, setup routines, the radiative transfer code, and the interface routines are different from the clear-sky nadir radiance assimilation.

The routine `SULIMB` sets up a limb group table (defined and stored in module `YOMLIMB`), for each satellite, sensor, and codetype, along the lines of the satellite group table set up in `SURAD`. Limb radiances are treated together with GPS radio occultation observations here. `SULIMB` calls the routine `RTL_SETUP` which includes the interface routine to the satrad library to read the `RTLIMB` coefficient files. Note that in contrast to the setup for nadir radiances, the code is set up to use fixed pressure levels, reference and limit profiles that are specific to the RT-coefficient files. This information is stored in the limb group table. `RTL_SETUP` also reads a channel selection file into the channel selection structure `Y_LIMB_CHAN_SEL` in the module `YOMLIMB`. Observation errors and constant, channel-specific biases are also read here from auxillary files and stored in dedicated variables `YOMLIMB`.

Setting of observation errors and biases and screening of clear-sky limb radiances is performed from `HRETR` in the routines `RTL_OBERROR` and `RTL_SCREEN`. The latter applies the channel selection previously stored in `Y_LIMB_CHAN_SEL` in module `YOMLIMB`, and it performs cloud screening.

The actual assimilation happens in the routine `HOP` and its tangent linear and adjoint. `HOP` calls the routine `RTL_HOP_1D` which performs the following tasks: it interpolates the model profiles in the vertical to the fixed pressure levels (using the standard interpolation routines), does a simple extrapolation above the model top if required (based on a fixed mesospheric lapse rate for temperature, and holding humidity or ozone constant), and it checks the model profiles against the validity limits provided with the `RTLIMB` coefficient file. Finally, `RTL_HOP_1D` calls `RTLIMB_HAT` to enter the satrad library and perform the radiance computations.

The routine `RTL_HOP_1D` is used when local horizontal homogeneity is to be assumed for the radiative transfer computations. Alternatively, the radiative transfer computations can take the horizontal structure in the limb-viewing plane into account by providing a series of profiles covering the limb-viewing plane. In this case, profiles provided by `PREINT2D` are used, and the routine `RTL_HOP_2D` is called from `HOP` instead of `RTL_HOP_1D`. The two-dimensional facility is switched on by specifying `NOBSPROFS(10) > 1` for obstype 10 in the namelist `NAMNPROF`. Note that this means GPS radio occultation bending angles present in the assimilation will also take horizontal structure into account.

## 5.8 OTHER SATELLITE OBSERVATION OPERATORS

Non-radiance satellite data are assimilated through various other observation operators, using model profiles interpolated to observation locations. Different operators are called from `HOP`, depending on the variable identifier of the observation. Dedicated observation operators exist, for instance, for scatterometer ambiguous surface winds (Stoffelen and Anderson, 1997; Isaksen and Janssen, 2004), or SATEM thicknesses and PWC (Kelly and Pailleux, 1988; Kelly *et al.*, 1991).

### 5.8.1 Atmospheric Motion Vectors

Groups of AMVs (aka SATOBs) are set up in the routine `SUAMV`, one group per satellite, computational method, and codetype. The information is stored in the satob group table, residing in the module `YOMSATS`.

The group table also specifies what type of observation operator is to be used for the particular group (entry `obs_oper`). The default used in operations is to assimilate all AMVs as single-level wind observations (Tomassini *et al.*, 1998; Bormann *et al.*, 2003), much in the same way as conventional data, using the same interpolation routine. Other options are treating AMVs as layer averages, with weights defined, for instance, by a boxcar weighting function.

### 5.8.2 Thicknesses

The pressures of layer bounds (top T, and bottom B) are found (in `HOP`) by scanning the observation array for thickness data. The geopotential for the top and the bottom of the layer are computed, using `PPGEOP` (Section 5.6), and the thickness is given by the difference  $\phi_T - \phi_B$ .

### 5.8.3 Gas retrievals

Retrievals of atmospheric species such as ozone or water vapour are used in the form of integrated layers bounded by a top and bottom pressure which are given as a part of the observation. The same observation operator is used as for precipitable water (PPPWC, Section 5.5). The same concept is applied to all data, whether it is total column data (like TOMS and GOME ozone data or MERIS total column water vapour) or data with higher vertical resolution (like SBUV). For ozone, variational bias correction is implemented (see Section 5.4, class name “to3”, module VARBC\_TO3). SBUV data is currently used as anchor for the variational bias correction of ozone and therefore assimilated without bias correction.

### 5.8.4 Scatterometer winds

In HOP, the observation array is scanned for SCAT data. For ERS-2 and ASCAT normally two ambiguous pairs of  $u$ -component and  $v$ -component observations are found at each SCAT location – with directions approximately 180 degrees apart. QuikSCAT can have 2, 3 or 4 ambiguous winds. Up to the first NSCAWSOLMAX (4 by default, adaptable through the namelist NAMSCC) wind solutions are accepted. In case only one ambiguity is found, the report is rejected. If LQSCATT = .TRUE. (the default, modifiable through the namelist NAMJO), the normal quadratic  $J_o$  will be used. In this case only the SCAT wind nearest to the high resolution background will be used (which is determined in a section of HOP). For winds that are not closest to the first guess or analysis, global datum event flag 9, respectively 10 is set (see Table 9.40). For the latter case datum status is set to rejected as well (Table 9.39). When LQSCATT = .FALSE, the two first winds are used and the ambiguity removal takes place implicitly through a special SCAT cost-function, (5.4), in HJO (Stoffelen and Anderson, 1997). In that case for QuikSCAT the most likely wind (highest *a priori* probability) and its most opposing ambiguity are selected.

Routine PPUV10M (Section 5.9) is like SYNOP, SHIP and DRIBU wind, also used also for SCAT data. Difference is that (in case account is taken for ocean current) the relative wind rather than the absolute wind is returned (not active in the operational suite, though), and the evaluation of equivalent-neutral wind rather than the real wind (which latter includes for scatterometer data undesired stability effects; operational since November 2011).

In the adjoint (SURFACAD) there is a separate section of HOP for the calculation of the  $\nabla_{\text{obs}} J_{\text{SCAT}}$ .

### 5.8.5 GPS Radio Occultation bending angles

The subroutine GPSRO\_OP is called in HOP and it simulates GPS radio occultation bending angles using the one-dimensional model outlined in Healy and Thépaut (2006). The subroutine evaluates a profile of bending angles,  $\alpha$  as function of impact parameter,  $a$ , at each observation location by evaluating the integral

$$\alpha(a) = -2a \int_a^\infty \frac{\frac{d \ln n}{dx}}{(x^2 - a^2)^{1/2}} dx \quad (5.38)$$

where  $n$  is the refractive index and  $x = nr$ , the product of the refractive index and  $r$ , a radial coordinate value. The pressure, temperature, specific humidity and geopotential on the model levels (ZPRESF5, ZTF5, ZQF5 and ZGEOPF5, respectively) produced by PREINT (see Subsection 5.6.1) are the inputs to GPSRO\_OP. The observation operator calculates the refractivity (defined as  $N = 10^{-6}(n - 1)$ ) on the full model levels using the pressure, temperature and specific humidity profiles. It then converts the geopotential heights to geometric heights and then radius values. The bending angle integral is evaluated assuming that the refractivity,  $N$ , varies exponentially between the model levels.

The bending angle observation errors are set in GPSRO\_OBERROR, which is called in HRETR. Entries in the JO tables are set in SULIMB.

The routine GPSRO\_OP is used when local horizontal homogeneity is to be assumed for the bending angle computations. Alternatively, the ray-tracing can take the horizontal structure in the limb-viewing plane into account by providing a series of profiles covering the limb-viewing plane. In this case, profiles provided by PREINT2D are used, and the routine GPSRO\_2DOP is called from HOP instead of GPSRO\_OP. The 2d facility is switched on by specifying NOBSPROFS(10) > 1 for obstype 10 in the namelist NAMNPROF.

Note that this means any limb radiances present in the assimilation will also take horizontal structure into account.

## 5.9 SURFACE OBSERVATION OPERATORS

Preparations for the vertical interpolation of surface data is done in **PREINTS** (see [Subsection 5.2.5](#)). Here dry static energy (**SURBOUND**), Richardson number, drag coefficients and stability functions (**EXCHCO**) are computed. For scatterometer data, information on equivalent neutral 10-metre wind is directly fetched from the physics package (via the GOM arrays) which is preprocessed in routine **EXCHCO\_VDF**. The actual vertical interpolation is performed in **PPOBSAS**, which embraces routines for 10-metre vector-wind components (**PPUV10M**), 2-metre temperature (**PPT2M**) and 2-metre relative humidity (**PPRH2M**).

### 5.9.1 Vertical interpolation

For wind and temperature an analytical technique ([Geleyn, 1988](#)) is used to interpolate values between the lowest model level and the surface. It is based on Monin–Obukhov theory in which simplified versions of stability functions  $\phi_M$  and  $\phi_H$  are used. The following equations are to be integrated:

$$\frac{\partial \mathbf{u}}{\partial z} = \frac{\mathbf{u}_*}{\kappa(z+z_0)} \phi_M \left( \frac{z+z_0}{L} \right), \quad (5.39)$$

$$\frac{\partial s}{\partial z} = \frac{s_*}{\kappa(z+z_0)} \phi_H \left( \frac{z+z_0}{L} \right), \quad (5.40)$$

$$L = \frac{c_p T u_*^2}{g \kappa s_*}, \quad (5.41)$$

were  $\mathbf{u}$ ,  $s$  are wind and energy variables,  $\mathbf{u}_*$ ,  $s_*$  are friction values,  $u_* = |\mathbf{u}_*|$ , and  $\kappa = 0.4$  is von Kármán's constant. Note that  $\mathbf{u}$  denotes the vector wind relative to a surface current  $\mathbf{u}_0$ ,

$$\mathbf{u} = \mathbf{u}_a - \mathbf{u}_0, \quad (5.42)$$

with  $\mathbf{u}_a$  the wind in the absolute (model) frame. In default configuration (global variable LECURR is false) surface current is zero, in which case the distinction between absolute and relative wind is irrelevant.

The temperature is linked to the dry static energy  $s$  by

$$s = c_p T + \phi \quad (5.43)$$

$$c_p = c_{p\text{dry}} \left[ 1 + \left( \frac{c_{p\text{vap}}}{c_{p\text{dry}}} - 1 \right) q \right]. \quad (5.44)$$

The neutral surface exchange coefficient at the height  $z$  is defined as

$$C_N = \left[ \frac{\kappa}{\ln \left( \frac{z+z_0}{z_0} \right)} \right]^2, \quad (5.45)$$

where  $z_0$  is the surface roughness length. Drag and heat coefficients are defined as

$$C_M = \frac{u_*^2}{[u(z)]^2}, \quad (5.46)$$

$$C_H = \frac{u_* s_*}{u(z)[s(z) - \tilde{s}]}, \quad (5.47)$$

where  $u(z) = |\mathbf{u}(z)|$  and  $\tilde{s}$  is the dry static energy at the surface. Details on the estimation of the roughness length and transfer coefficients can be found in [Subsection 5.9.3](#).

For convenience the following quantities are introduced:

$$B_N = \frac{\kappa}{\sqrt{C_N}}, \quad B_M = \frac{\kappa}{\sqrt{C_M}}, \quad B_H = \frac{\kappa \sqrt{C_M}}{C_H}. \quad (5.48)$$

For stable conditions the (simplified) stability function is assumed

$$\phi_{M/H} = 1 + \beta_{M/H} \frac{z}{L}, \quad (5.49)$$

and integration of (5.39) and (5.40) from 0 to  $z_1$  (the lowest model level) leads to values for relative wind  $\mathbf{u}(z)$  and static energy  $s(z)$  at observation height  $z$ :

$$\mathbf{u}(z) = \frac{\mathbf{u}(z_1)}{B_M} \left[ \ln \left( 1 + \frac{z}{z_1} (e^{B_N} - 1) \right) - \frac{z}{z_1} (B_N - B_M) \right], \quad (5.50)$$

$$s(z) = \tilde{s} + \frac{s(z_1) - \tilde{s}}{B_H} \left[ \ln \left( 1 + \frac{z}{z_1} (e^{B_N} - 1) \right) - \frac{z}{z_1} (B_N - B_H) \right]. \quad (5.51)$$

In unstable conditions the stability function is chosen as

$$\phi_{M/H} = \left( 1 - \beta_{M/H} \frac{z}{L} \right)^{-1} \quad (5.52)$$

and the vertical profiles for relative wind and dry static energy are then given by

$$\mathbf{u}(z) = \frac{\mathbf{u}(z_1)}{B_M} \left[ \ln \left( 1 + \frac{z}{z_1} (e^{B_N} - 1) \right) - \ln \left( 1 + \frac{z}{z_1} (e^{B_N - B_M} - 1) \right) \right], \quad (5.53)$$

$$s(z) = \tilde{s} + \frac{s(z_1) - \tilde{s}}{B_H} \left[ \ln \left( 1 + \frac{z}{z_1} (e^{B_N} - 1) \right) - \ln \left( 1 + \frac{z}{z_1} (e^{B_N - B_H} - 1) \right) \right]. \quad (5.54)$$

In case the influence of stability is neglected, the following equivalent-neutral wind profile  $\mathbf{u}_n(z)$  is obtained:

$$\mathbf{u}_n(z) = \frac{\mathbf{u}(z_1)}{B_M} \ln \left( 1 + \frac{z}{z_1} (e^{B_N} - 1) \right). \quad (5.55)$$

For wind, the relevant routine **PPUV10M** embodies this method of [Geleyn \(1988\)](#) to estimate vector wind components at observation height  $z$  from provided lowest model level wind  $\mathbf{u}(z_1) = \mathbf{u}_a(z_1) - \mathbf{u}_0$ . For scatterometer data, by default, relative wind (5.50), (5.53) is returned, while for all other data the wind in the absolute frame is evaluated:

$$\mathbf{u}_a = \mathbf{u} + \mathbf{u}_0. \quad (5.56)$$

For scatterometer data, by default equivalent-neutral wind (5.55) is returned. In case non-neutral wind is to be assimilated (operational before November 2010), a variable LSCATT\_NEUTRAL is to be set to false.

The temperature at observation height  $z = 2$  m is evaluated in **PPT2M**. It is obtained from  $s$  as

$$T(z) = s(z) - \frac{zq}{c_p}, \quad (5.57)$$

where  $s$  is interpolated according to (5.51) and (5.54).

The vertical interpolation relies on estimates for coefficients  $B_M, B_N$  for wind, and on coefficients  $B_H, B_N$  and dry static energy at the surface  $\tilde{s} = \tilde{s}(T_{\text{surf}}, q = 0)$ . These are provided in the routines **EXCHCO**, **EXCHCO\_VDF** and **SURBOUND**, and are described in the following two subsections.

### 5.9.2 Surface values of dry static energy

To determine the dry static energy at the surface we use (5.43) and (5.44) where the humidity at the surface is defined by

$$\tilde{q} = q(z = 0) = h(C_{\text{snow}}, C_{\text{liq}}, C_{\text{veg}}) q_{\text{sat}}(T_{\text{surf}}, p_{\text{surf}}) \quad (5.58)$$

where, according to [Blondin \(1991\)](#),  $h$  is given by

$$h = C_{\text{snow}} + (1 - C_{\text{snow}})[C_{\text{liq}} + (1 - C_{\text{liq}})\bar{h}] \quad (5.59)$$

with

$$\bar{h} = \max \left\{ 0.5 \left( 1 - \cos \frac{\pi \vartheta_{\text{soil}}}{\vartheta_{\text{cap}}} \right), \min \left( 1, \frac{q}{q_{\text{sat}}(T_{\text{surf}}, p_{\text{surf}})} \right) \right\} \quad (5.60)$$

where  $\vartheta_{\text{soil}}$  is the soil moisture content and  $\vartheta_{\text{cap}}$  is the soil moisture at field capacity (2/7 in volumetric units). Equation (5.59) assigns a value of 1 to the surface relative humidity over the snow covered and wet fraction of the grid box. The snow-cover fraction  $C_{\text{snow}}$  depends on the snow amount  $W_{\text{snow}}$  so that

$$C_{\text{snow}} = \min \left( 1, \frac{W_{\text{snow}}}{W_{\text{snow}_{\text{cr}}}} \right)$$

where  $W_{\text{snow}_{\text{cr}}} = 0.015$  m is a critical value. The wet skin fraction  $C_{\text{liq}}$  is derived from the skin-reservoir water content  $W_{\text{liq}}$  by

$$C_{\text{liq}} = \min \left( 1, \frac{W_{\text{liq}}}{W_{\text{liq}_{\text{max}}}} \right),$$

where

$$W_{\text{liq}_{\text{max}}} = W_{\text{layer}_{\text{max}}} \{ (1 - C_{\text{veg}}) + C_{\text{veg}} A_{\text{leaf}} \}$$

with  $W_{\text{layer}_{\text{max}}} = 2 \times 10^{-4}$  m being the maximum amount of water that can be held on one layer of leaves, or as a film on bare soil,  $A_{\text{leaf}} = 4$  is the leaf-area index, and  $C_{\text{veg}}$  is the vegetation fraction.

### 5.9.3 Transfer coefficients

Comparing the (5.39) and (5.40) integrated from  $z_o$  to  $z + z_o$  with (5.45) to (5.47),  $C_M$  and  $C_H$  can be analytically defined:

$$\frac{1}{C_M} = \frac{1}{\kappa^2} \left[ \int_{z_o}^{(z+z_o)} \frac{\phi_M(z'/L)}{z'} dz' \right]^2 \quad (5.61)$$

$$\frac{1}{C_H} = \frac{1}{\kappa^2} \left[ \int_{z_o}^{(z+z_o)} \frac{\phi_M(z'/L)}{z'} dz' \int_{z_o}^{(z+z_o)} \frac{\phi_H(z'/L)}{z'} dz' \right] \quad (5.62)$$

Because of the complicated form of the stability functions, the former integrals have been approximated by analytical expressions, formally given by (coded in **EXCHCO**)

$$\begin{aligned} C_M &= C_N f_M \left( Ri, \frac{z}{z_o} \right) \\ C_H &= C_N f_H \left( Ri, \frac{z}{z_o} \right) \end{aligned} \quad (5.63)$$

where  $C_N$  is given by (5.45). The bulk Richardson number  $Ri$  is defined as

$$Ri = \frac{g \Delta z \Delta T_v}{c_p T_v |\Delta u|^2} \quad (5.64)$$

where  $T_v$  is the virtual potential temperature. The functions  $f_M$  and  $f_H$  correspond to the model instability functions and have the correct behaviour near neutrality and in the cases of high stability (Louis, 1979; Louis *et al.*, 1982).

(i) *Unstable case*  $Ri < 0$

$$f_M = 1 - \frac{2bRi}{1 + 3bcC_N \sqrt{\left(1 + \frac{z}{z_o}\right)(-Ri)}}, \quad (5.65)$$

$$f_H = 1 - \frac{3bRi}{1 + 3bcC_N \sqrt{\left(1 + \frac{z}{z_o}\right)(-Ri)}}, \quad (5.66)$$

with  $b = c = 5$ .

(ii) *Stable case*  $Ri > 0$

$$f_M = \frac{1}{1 + 2bRi/\sqrt{(1 + dRi)}}, \quad (5.67)$$

$$f_M = \frac{1}{1 + 3bRi/\sqrt{(1 + dRi)}}, \quad (5.68)$$

with  $d = 5$ .

(a) *Extraction of stability information from the ECMWF surface-layer physics*

The estimation of transfer coefficients as described above (Louis, 1979; Louis *et al.*, 1982) does not overlap well with the stability as evaluated in the full nonlinear surface layer physics parametrization, for two reasons. First, the method of Louis (1979); Louis *et al.* (1982) does not correspond anymore with the presently used parametrization. And second, the estimation of the neutral exchange coefficient (5.45) uses (for technical reasons) a roughness length  $z_0$  that is based on climatology, rather than on the actual roughness. Over oceans this embraces a value of  $z_0 = 1\text{mm}$ , which is typically one order of magnitude too high. The effect on the estimation on 10-metre wind appears to be negligible, however, for 10-metre equivalent neutral wind (used for scatterometer data) and wind at 4 or 5 metre height (typical buoy observation height) a systematic effect can be observed (Hersbach, 2010a).

As an alternative, the information on stability can be extracted from the 10-metre equivalent neutral wind  $u_n$  as evaluated in **SPPCFLMOD** in the ECMWF surface-layer physics, which is activated by a switch `LVDFTRAJ=true`. In that case, over the ocean roughness length  $z_0$  is estimated from  $u_n$  and the ocean-wave Charnock parameter  $\alpha$ , by an approximate solution (Hersbach, 2011) of the following set of implicit equations (coded in **ZOSEA**):

$$z_0 = \alpha_M \frac{\nu}{u_*} + \alpha \frac{u_*^2}{g}, \quad (5.69)$$

$$u_n = \frac{u_*}{\kappa} \log(1 + z_{10}/z_0). \quad (5.70)$$

Here  $z_{10} = 10\text{ m}$ ,  $\alpha_M = 0.11$ ,  $\kappa = 0.4$  is the Von Kármán constant,  $g = 9.80665\text{ ms}^{-2}$  is the gravitational acceleration, and  $\nu = 1.5 \times 10^{-5}\text{ m}^2\text{ s}^{-1}$  the kinematic viscosity.

The coefficient  $C_N$  is, again evaluated by (5.45), but now using the improved estimate of  $z_o$ , while coefficient  $C_M$  for momentum is given by (**EXCHCO\_VDF**):

$$C_M = B_M^2/\kappa, \quad B_M = \log(1 + z_{10}/z_0) \|\mathbf{u}(z_1)\|/u_n. \quad (5.71)$$

In the operational configuration this method is only used for the assimilation of scatterometer wind. For other observables, the method of Louis (1979); Louis *et al.* (1982) (`LVDFTRAJ=false`) is used. Routine **EXCHCO\_VDF** does not provide an estimate for the coefficient  $C_H$  for heat.

#### 5.9.4 Two-metre relative humidity

In **GPRH** relative humidity is computed according to (5.32). The relative humidity depends on specific humidity, temperature and pressure ( $q$ ,  $T$  and  $p$ , respectively) at the lowest model level. It is constant in the surface model layer, see **PPRH2M**.

## Chapter 6

# Background, analysis and forecast errors

### Table of contents

- [6.1 Nomenclature](#)
- [6.2 Input and ‘massaging’ of background errors](#)
- [6.3 Diagnosis of background-error variances](#)
- [6.4 Calculation of eigenvalues and eigenvectors of the Hessian](#)
- [6.5 The preconditioner](#)
- [6.6 Calculation of analysis-error variances](#)
- [6.7 Calculation of forecast-error variances](#)
- [6.8 Diagnosis of background-error variances through the EDA](#)

### 6.1 NOMENCLATURE

The calculation of standard deviations of background errors is unfortunately an area of confusing nomenclature. “Standard deviations of background error” is quite a mouthful, so they are generally referred to simply as ‘background errors’ (likewise for standard deviations of analysis errors and forecast errors). Although inaccurate, this nomenclature has been adopted in the following for the sake of brevity.

A second source of confusion is that the terms ‘background error’ and ‘forecast error’ are often used interchangeably. This confusion has even crept into the code, where the buffer which contains the standard deviations of background error is called FCEBUF. Such confusion is clearly unwise when discussing their calculation. In the following, we describe the processing of error variances during a single analysis cycle. The term ‘background error’ will be used exclusively to refer to the standard deviations of background error used in the background cost function. The background errors are an input to the analysis. The term ‘forecast error’ will refer to an estimate of the standard deviation of error in a short-term forecast made from the current analysis. The forecast errors are calculated by inflating an estimate of the standard deviation of analysis error, and are an output from the analysis system. They provide background errors for the *next* analysis cycle.

### 6.2 INPUT AND ‘MASSAGING’ OF BACKGROUND ERRORS

Background errors for use in  $J_b$  are initialised by a call to `SUINFCE`. This is part of the  $J_b$  set-up, which is described in [Subsection 4.3.3](#).

As with most of the  $J_b$  code, the structure `SPJB_VARS_INFO`, described in [Subsection 4.3.1](#), is important. At the beginning of `SUINFCE`, this structure is examined to determine which variables are present in  $J_b$ , and to locate the corresponding profiles of globally-averaged background error. Next, a call to `IO_INQUIRE` is made to determine which fields are present in the input file (filename `errgrib`), and to find details of their grid resolution, etc.

The fields of background error are read by a call to `IO_GET`, and interpolated to the model’s horizontal grid using `SUHIFCE`.

Vertical interpolation requires knowledge of the background surface pressure. In addition, one method of constructing humidity background errors requires knowledge of background values of specific humidity and temperature. So, background fields in grid space are obtained either by a call to `GET_TRAJ_GRID`, or by transforming the corresponding spectral fields.

Before the vertical interpolation takes place, the locations of the different  $J_b$  variables within the background error array FCEBUF are found by a set of calls to the internal subroutine **LOOKUP**, which interrogates SPJB\_VARS\_INFO.

The large loop “VARIABLE\_LOOP” in **SUINFC** loops over the fields of the input file. Each field is interpolated onto model levels by a call to **SUVIFCE** (unless it is a surface field), and either stored in FCEBUF or used to construct a field in FCEBUF. (For example, if background errors for vorticity are not available in the input file, they are constructed by scaling zonal wind errors.)

Background errors for the humidity variable are treated as a special case, and generated after the main loop over variables by a call to **SUSHFCE**. The calculation of background errors for humidity is described in [Subsection 4.3.4](#).

Next, one of two routines is called. **SUMDFCE** calculates a vertically averaged ‘pattern’ of background error. This is required if the background errors are to be represented as a product of a vertical profile of global mean error and a horizontal pattern. The pattern is stored in FGMWNE. (Note in particular that **SUMDFCE** is called if horizontally-constant background errors are requested by setting LCFCE. In this case, all elements of FGMWNE are set to one.)

Alternatively, **SUPRFCE** is called to calculate global mean profiles of the input background errors. This is the default. The profiles are stored in FCEIMN.

The final step in processing the background errors is performed by **SUSEPFCE**. This modifies the background errors in one of two ways. If separable background errors have been requested, the contents of the background error buffer are replaced by the product of the vertical profile stored in FCEMN and the horizontal pattern stored in FGMWNE. Otherwise, the background errors for each variable at each level are multiplied by the ratio of the corresponding elements of FCEMN and FCEIMN. The result of this operation is to adjust the global mean profiles of background error to match those stored in FCEMN.

### 6.3 DIAGNOSIS OF BACKGROUND-ERROR VARIANCES

Background error variances for use in  $J_b$  and for observation first guess checks can be computed in two distinct ways. If an Ensemble of Data Assimilations (EDA) is available, background errors can be directly diagnosed from the EDA background forecasts as described in [section 6.8](#). EDA-derived errors will be used if the logical switch LEDA\_ERRORS\_IN is true. Otherwise they can be estimated by subroutine **BGVECS**, which is called from **FORECAST\_ERROR**. One of two methods may be employed, depending on whether NBGVECS is equal to, or greater than, zero. In either case, the estimated variances of background error are stored in the analysis error buffer, ANEBUF (in **YOMANEB**).

If NBGVECS is zero, then background errors for variables which are explicitly present in the background error buffer, FCEBUF, are copied into ANEBUF and squared. Errors for those variables whose background errors are defined implicitly through the change of variable are estimated using simple scaling of appropriate explicit errors. This scaling is performed by a call to **ESTSIGA**.

If NBGVECS is non-zero, then the variances of background error are estimated using randomization. This method assumes that the change of variable transforms the background error covariance matrix into the identity matrix. A sample of NBGVECS vectors drawn from a multi-dimensional Gaussian distribution with zero mean and identity covariance matrix is generated by calls to **RANDOM\_CTLVEC**. These vectors are transformed to the space of physical variables by **CHAVARIN**. The transformed variables form a sample drawn from the distribution of background errors. A call to **STEPOTL** (‘0AA00A000’) transforms each vector to gridpoint space and accumulates the sums of squares in ANEBUF. In addition, observation operators are applied to the random variables to generate samples of background error in terms of radiance, for example. The sums of squares of these observation-space variables are also accumulated to provide estimates of background error in observation space.

Finally, the sums of squares of random vectors are divided by the number of vectors by a call to **SCALEAE** to provide a somewhat noisy estimate of the variances of background error actually used in the analysis. Noise may be filtered by a call to **FLTBGERR**, which transforms the variances to spectral coefficients, multiplies each coefficient by  $\cos^2(\min((n/\text{NBGTRUNC}), 1)\pi/2)$ , and then transforms to grid space. The



default is to filter with a very large value of `NBGTRUNC`. Effectively, the background errors are simply spectrally truncated. It is highly recommended that the filtering is performed, since it prevents a grid-scale numerical instability which occurs when the error growth model introduces spatial features which cannot be resolved by the spectral control variable.

Flow-dependent background errors, valid at the end of the window may be generated by setting `LBGM` (`namvar`) to `TRUE`. In this case, the tangent linear model is used to propagate each of the random background vectors to the end of the analysis window. The eigenvectors of the analysis Hessian (see the next section) are also propagated in time, by a call to `CNT3TL` from `XFORMEV`. For the normal case, `LBGM` is false, and background and analysis errors are estimated at the beginning of the analysis window, and propagated using the simple error-growth model described in section 6.7.

The background errors diagnosed by `BGVECS` may be written out for diagnostic purposes by setting `LWRISIGB`. The errors are written by a call to `WRITESD` (called from `FORECAST_ERROR`).

## 6.4 CALCULATION OF EIGENVALUES AND EIGENVECTORS OF THE HESSIAN

The second stage in the calculation of analysis errors is to determine eigenvalues and eigenvectors of the Hessian of the cost function. This is done using a combined Lanczos and conjugate-gradient algorithm, `CONGRAD`, called from `CVA1` under the control of `LAVCGL`. The reader is referred to Fisher (1998, ECMWF Seminar proceedings pp364-385) for a detailed description of the `CONGRAD` algorithm. Note that `CONGRAD` requires that the cost function is strictly quadratic.

`CONGRAD` starts by transforming the initial control variable and gradient to a space with Euclidian inner product. Typically, this transformation is simply a multiplication by `YRSCALPSQRT`, but may also involve preconditioning via calls to `PRECOND`. The transformed initial gradient is normalized to give the first Lanczos vector. The Lanczos vectors are stored in the array `YLZCGLWK`.

Each iteration of the conjugate-gradient/Lanczos algorithm starts by calculating the product of the Hessian and the latest search direction. This is calculated as  $J''d = [\nabla J(x_0 + d) - \nabla J(x_0)]$ , where  $d$  is a vector of unit length. This finite difference formula is exact, since the cost function is quadratic.

The main iteration loop calculates the sequence of gradients, and the sequence of coefficients according to the the Lanczos recurrence. The sequence of control vectors that partially minimize the cost function is not explicitly generated. Thus, unlike e.g. `M1QN3`, the control vectors passed to `SIM4D` do not lie on a path towards the minimum, and the gradients returned by `SIM4D` do not, in general, decrease as the minimization proceeds. The optimal control vector and the corresponding gradient can, however, be determined as a linear combination of the Lanczos vectors.

In general, only the gradient is calculated at each iteration. It is required in order to monitor the convergence of the minimization. Optionally, by setting `L_CHECK_GRADIENT`, the optimal point is also calculated, and an additional call to `SIM4D` is made to evaluate the true gradient at the optimal point. This is useful as a means of checking the assumption of linearity on which the algorithm is based. However, it doubles the cost of the minimization.

The Lanczos algorithm produces a sequence of coefficients, which are stored in the arrays `ZDELTA` and `ZBETA`. These correspond to the diagonal and sub-diagonal of a symmetric tri-diagonal matrix. The calculation of the optimal point and the corresponding gradient require the solution of a linear system involving this matrix. This is performed by the internal subroutine `PTSV`, which is a simple interface to the LAPACK routine `SPTSV`. In addition, the eigenvalues of the tri-diagonal matrix are approximations to eigenvalues of the Hessian of the cost function. These approximate eigenvalues are calculated every iteration, together with bounds on their accuracy. As soon as the leading eigenvalue has converged sufficiently, it is monitored to check that it does not increase. This provides a sensitive test that the algorithm is behaving correctly. Any increase in the leading eigenvalue provides an early indication of failure (for example, due to a bad gradient) and the algorithm is immediately terminated. The calculation is not aborted, since the test detects the failure of the algorithm before the converged eigenvalues and eigenvectors become corrupted.

A call to **PREDICT\_RUNTIME** is made every iteration. This subroutine attempts to predict how many iterations will be required to minimize the cost function, and how long this is likely to take. These predictions are written to STDERR.

After the last iteration, the converged eigenvectors of the Hessian are calculated by calling **WREVECS**. Note that the criterion used to decide which eigenvalues have converged is relaxed at this stage to  $\|J''\mathbf{v} - \lambda\mathbf{v}\| < \varepsilon\|\mathbf{v}\|$ , where  $\varepsilon$  is given by EVBCGL. The default value for EVBCGL is 0.1.

Next, if required, upper and lower bounds for  $N - p^T(J'')^{-1}p$  (where  $N$  is the dimension of the control vector) and  $-p^T \log_2[(J'')^{-1}]p$  are calculated using the algorithm of Golub and Meurant (1994). These quantities may be used to evaluate the information content of the analysis using the switch L\_INFO\_CONTENT.

Finally, **CONGRAD** calculates the the optimal control vector and gradient as a linear combination of the Lanczos vectors, and transforms them from the Euclidian space used internally to the usual space of the control variable.

## 6.5 THE PRECONDITIONER

**CONGRAD** allows the use of a preconditioner. The preconditioner is a matrix which approximates the Hessian matrix of the cost function. The preconditioner used in **CONGRAD** is a matrix of the form

$$\mathbf{I} + \sum_{i=1}^L (\mu_i - 1) \mathbf{w}_i \mathbf{w}_i^T \quad (6.1)$$

where the vectors  $\mathbf{w}_i$  are orthogonal. The pairs  $\{\mu_i, \mathbf{w}_i\}$  are calculated in **PREPPCM**, and are intended to approximate some of the eigenpairs (i.e. eigenvalues and associated eigenvectors) of the Hessian matrix of the cost function. They are calculated as follows.

A set of  $L$  vectors,  $\mathbf{u}_i$ , is read in using **READVEC**. These vectors may be in the space of the control vector (if LEVECCNTL is true), or in model space (if LEVECCNTL is false). In the latter case, the vectors are transformed to control space by calls to **CHAVAR**.

The vectors (transformed, if necessary to control space) are assumed to satisfy

$$\mathbf{I} - \sum_{i=1}^L \mathbf{u}_i \mathbf{u}_i^T \approx (J'')^{-1} \quad (6.2)$$

Vectors which meet this criterion can be written out from an earlier forecast error calculation by setting LWRIEVEC.

The input vectors are not necessarily orthogonal, whereas the preconditioner requires a set of orthogonal vectors. Let us denote by  $\mathbf{U}$  the matrix whose columns are the vectors  $\mathbf{u}_i$ . A sequence of Householder transformations is now performed to transform  $\mathbf{U}$  to upper triangular. Let us represent this sequence of Householder transformations by the matrix  $\mathbf{Q}$ . Then  $\mathbf{QU}$  is upper triangular, which means that  $(\mathbf{QU})(\mathbf{QU})^T$  is zero except for an  $L \times L$  block in the top left hand corner.

It is clear that  $(\mathbf{QU})(\mathbf{QU})^T$  has only  $L$  non-zero eigenvalues. Moreover, the non-zero eigenvalues are the eigenvalues of the  $L \times L$  block matrix, and the eigenvectors of  $(\mathbf{QU})(\mathbf{QU})^T$  are the eigenvectors of the block matrix, appended by zeroes. These eigenvalues and eigenvectors are calculated by a call to the LAPACK routine SSYEV.

Now, since  $\mathbf{Q}$  is an orthogonal matrix, we have  $\mathbf{QQ}^T = \mathbf{I}$ . So, we may write (6.2) as

$$\mathbf{I} - \mathbf{Q}^T (\mathbf{QU})(\mathbf{QU})^T \mathbf{Q} \approx (J'')^{-1} \quad (6.3)$$

Let us denote the eigenpairs of  $(\mathbf{QU})(\mathbf{QU})^T$  by  $\{\rho_i, \mathbf{v}_i\}$ . Then we may write (6.3) as

$$\mathbf{I} - \sum_{i=1}^L \rho_i (\mathbf{Q}^T \mathbf{v}_i) (\mathbf{Q}^T \mathbf{v}_i)^T \approx (J'')^{-1} \quad (6.4)$$

The orthogonality of  $\mathbf{Q}$  and the orthonormality of the eigenvectors  $\mathbf{v}_i$ , means that the vectors  $\mathbf{Q}^T \mathbf{v}_i$  are orthonormal. They are, in fact, the required vectors,  $\mathbf{w}_i$  of the preconditioner matrix.

Inverting (6.4) gives

$$\mathbf{I} - \sum_{i=1}^L \frac{1}{\rho_i} \mathbf{w}_i \mathbf{w}_i^T \approx \mathbf{J}'' \quad (6.5)$$

Defining  $\mu_i = 1 - 1/\rho_i$  gives the required approximation to the Hessian matrix.

The preconditioner vectors are sorted in decreasing order of  $\mu_i$ , and all vectors for which  $\mu_i < 1$  are rejected. These vectors cannot be good approximations to eigenvectors of the Hessian matrix, since the eigenvalues of the Hessian matrix are all greater than or equal to one. A final refinement to the calculation is to reduce large values of  $\mu_i$  to a maximum of R\_MAX\_CNUM\_PC (typically 10). This was found to be necessary in practice to avoid ill-conditioning the minimization.

The numbers  $\mu_i$  are stored in RCGLPC. The vectors,  $\mathbf{w}_i$  are stored in YVCGLPC, and the total number of preconditioner vectors is stored in NVCGLPC.

Application of the preconditioner is straightforward, and is performed by subroutine PRECOND. This routine can also apply the inverse, the symmetric square root, or the inverse of the symmetric square root of the preconditioner matrix. Application of the latter matrices relies on the observation that if

$$\mathbf{M} = \mathbf{I} + \sum_{i=1}^L (\mu_i - 1) \mathbf{w}_i \mathbf{w}_i^T \quad (6.6)$$

with orthonormal  $\mathbf{w}_i$ , then the expressions for  $\mathbf{M}^{-1}$ ,  $\mathbf{M}^{1/2}$  and  $\mathbf{M}^{-1/2}$  result from replacing  $\mu_i$  in (6.6) by  $1/\mu_i$ ,  $\sqrt{\mu_i}$  and  $1/(\sqrt{\mu_i})$  respectively.

## 6.6 CALCULATION OF ANALYSIS-ERROR VARIANCES

The eigenvectors and eigenvalues of the Hessian matrix calculated by CONGRAD are passed to XFORMEV, which uses them to estimate the analysis-error variances.

The first step is to undo any preconditioning. If preconditioning has been employed, then the eigenvectors and eigenvalues produced by CONGRAD provide an approximation to the preconditioned Hessian,  $\mathbf{M}^{-1/2} \mathbf{J}'' \mathbf{M}^{-1/2}$ , of the form

$$\mathbf{M}^{-1/2} \mathbf{J}'' \mathbf{M}^{-1/2} \approx \mathbf{I} + \sum_{i=1}^K (\lambda_i - 1) \mathbf{v}_i \mathbf{v}_i^T \quad (6.7)$$

Multiplying to the left and right by  $\mathbf{M}^{1/2}$ , gives

$$\mathbf{J}'' \approx \mathbf{M} + \sum_{i=1}^K (\lambda_i - 1) (\mathbf{M}^{1/2} \mathbf{v}_i) (\mathbf{M}^{1/2} \mathbf{v}_i)^T \quad (6.8)$$

Substituting for the preconditioner matrix from (6.6), gives the following

$$\mathbf{J}'' \approx \mathbf{I} + \sum_{i=1}^{L+K} \mathbf{s}_i \mathbf{s}_i^T \quad (6.9)$$

where

$$\mathbf{s}_i = \begin{cases} (\mu_i - 1)^{1/2} \mathbf{w}_i & \text{for } i = 1 \dots L \\ (\lambda_{i-L} - 1)^{1/2} \mathbf{M}^{1/2} \mathbf{v}_{i-L} & \text{for } i = L + 1 \dots L + K \end{cases} \quad (6.10)$$

Note that the resulting approximation to the Hessian is not expressed in terms of eigenvalues and eigenvectors. Consequently, inversion of the approximation must be performed using the Sherman–Morrison–Woodbury formula. Let  $\mathbf{S}$  be the matrix whose columns are the vectors  $\mathbf{s}_i$ . Then, according to

the Sherman–Morrison–Woodbury formula, the inverse of the approximate Hessian matrix is

$$(J'')^{-1} \approx \mathbf{I} - \mathbf{S}(\mathbf{I} + \mathbf{S}^T \mathbf{S})^{-1} \mathbf{S}^T \quad (6.11)$$

The matrix  $(\mathbf{I} + \mathbf{S}^T \mathbf{S})$  has dimension  $(L + K) \times (L + K)$ . This matrix is constructed, and its Cholesky decomposition is calculated using the LAPACK routine SPOTRF. This gives a lower triangular matrix  $\mathbf{C}$  such that

$$(J'')^{-1} \approx \mathbf{I} - (\mathbf{S}\mathbf{C}^{-1})(\mathbf{S}\mathbf{C}^{-1})^T \quad (6.12)$$

The matrix  $(\mathbf{S}\mathbf{C}^{-1})$  is calculated by back-substitution.

The final stage in the calculation of the analysis errors is to transform the columns of the matrix  $(\mathbf{S}\mathbf{C}^{-1})$  to the space of model variables by applying the inverse change of variable, **CHAVARIN**. This gives the required approximation to the analysis error covariance matrix

$$\mathbf{P}_a \approx \mathbf{B} - \mathbf{V}\mathbf{V}^T \quad (6.13)$$

where  $\mathbf{V} = \mathbf{L}^{-1} \mathbf{S}\mathbf{C}^{-1}$ , and where  $\mathbf{L}^{-1}$  represents the inverse of the change of variable. The columns of  $\mathbf{V}$  may be written out (e.g. for diagnostic purposes, or to form the preconditioner for a subsequent minimization) by setting LWRIEVEC. The columns of  $\mathbf{V}$  are then transformed to gridpoint space, and their sums of squares (i.e. the diagonal elements of  $\mathbf{V}\mathbf{V}^T$  in gridpoint space) are subtracted from the variances of background error which were stored in ANEBUF before the minimization by **BGVECS**.

The analysis errors are calculated as the difference between the background errors and a correction derived from the eigenvectors of the Hessian. If the background errors are underestimated, there is a danger that the correction will be larger than the background error, giving negative variances of analysis error. This is unlikely to happen if the background errors are estimated using randomization, or for variables whose background errors are explicitly specified in the background cost function, but is possible for variables such as temperature whose background errors are not explicitly specified. To guard against this eventuality, if NBGVECS is zero, then the variances of analysis error for variables whose background errors are not explicit are estimated by applying a scaling to the explicit variables by a call to **ESTSIGA** from **CVA1**. The variances are then converted to standard deviations and written out by a call to **WRITESD**.

## 6.7 CALCULATION OF FORECAST-ERROR VARIANCES

The analysis errors are inflated according to the error growth model of **Savijärvi (1995)** to provide estimates of short-term forecast error. This is done by a call to **ESTSIG**.

The error growth model is

$$\frac{d\sigma}{dt} = (a + b\sigma) \left( 1 - \frac{\sigma}{\sigma_\infty} \right) \quad (6.14)$$

Here,  $a$  represents growth due to model errors,  $b$  represents the exponential growth rate of small errors, and  $\sigma_\infty$  represents the standard deviation of saturated forecast errors. The growth due to model error is set to 0.1 times the global mean background error per day. The exponential growth rate,  $b$ , is set to 0.4 per day.

The saturation standard deviations are calculated as  $\sqrt{2}$  times the standard deviation of each field. The standard deviations have been calculated for each month from the re-analysis dataset. **ESTSIG** reads these climatological error fields from file ‘stdev\_of\_climate’ by calling **READGRIB**, and interpolates them in the horizontal and vertical using **SUHIFCE** and **SUVIFCE**. The climatological errors may also be artificially increased in the tropics under the control of LFACHRO. If climate standard deviations are not available for any field, they are estimated as 10 times the global mean background error for the field.

The error growth model is integrated for a period of NFGFCLEN hours. The integration is done analytically using the expression given by **Savijärvi (1995)**. Two precautions are taken in integrating the error growth model. First, negative analysis-error variances are set to zero. Second, the growth rate due to model error is limited to a sensible value with respect to the saturation errors. This was found to be necessary to prevent numerical problems when calculating specific humidity errors for the upper levels of the model.

**ESTSIG** overwrites the contents of ANEBUF with the estimated variances of forecast error. The variances are converted to standard deviations and written out by **WRITESD**.

## 6.8 DIAGNOSIS OF BACKGROUND-ERROR VARIANCES THROUGH THE EDA

The EDA consists of an ensemble of 10 independent lower-resolution 4D-Var assimilations (T399L91 with two inner loops at T95 and T159) that differ by the explicit perturbation of the observations, the sea-surface temperature and the model physics, plus 1 control 4D-Var which runs without any perturbation. The reason for running an EDA is that it can be shown ( [Isaksen \*et al.\* \(2010\)](#)) that if the perturbations to the observations, model evolution and boundary conditions are properly chosen, the EDA analysis and background spread will provide realistic estimates of analysis and background errors standard deviations.

In the EDA, for each observation, perturbations are defined by randomly sampling a Gaussian distribution with zero mean and standard deviation equal to the estimate of the observation error standard deviation. Sea surface temperature fields are also perturbed, with correlated patterns as currently used in the Seasonal Forecasting System ( [Vialard \*et al.\* \(2005\)](#)). To simulate the impact of model uncertainty, the stochastically perturbed parametrization tendency (SPPT) scheme is used; this perturbs the total parametrized tendency of physical processes (more details can be found in part V of this document).

The EDA background mean and standard deviations are computed in the **enda\_pp** family which runs after completion of the EDA background forecasts family. The first task of the **enda\_pp** family is **ens\_stats\_members**, where the EDA background fields are retrieved from storage and necessary pre-processing operations are carried out. These include the computation of fields which are not archived from the EDA run (Geopotential Height, Relative Humidity, Radiative Radiances for a selection of sensors). The **ens\_stats\_members** task is split into a number of sub-tasks (**ens\_stats\_mem**) equal to the size of the EDA in order to parallelize the computations on the different EDA members.

Task **ens\_stats\_gather** computes the ensemble mean and standard deviations of the EDA background fields. These fields are stored as grib files of type 'em' and 'es' of stream 'enda', respectively.

Task **ens\_fetch\_fields** gathers the operational analysis fields needed for the calibration step of the EDA standard deviations. This is performed in task **ens\_cal**, where the calibration coefficients of the EDA background variances are computed by **Spread\_Skill\_Time\_Avg**. Variance Calibration is performed against the ECMWF operational analysis separately for each parameter, model level and geographical region (Northern Extra-Tropics, Tropics, Southern Extra-Tropics).

Variance calibration is done to ensure that EDA background variance matches the mean squared difference of the EDA background mean and the corresponding operational analysis. In order to have a large enough statistical sample and to reduce time variability, the calibration is computed using the latest 10 sets of EDA backgrounds and operational analysis verifying at the same time.

The last job in the **enda\_pp** family is **ens\_errors**. If the logical switch LENS\_CAL is true the EDA background variances computed in **ens\_stats** are calibrated by **Ens\_Spread\_Cal** using the coefficients computed in **ens\_cal**. The calibrated variances are then transformed to a spectral representation and filtered by **Spectral\_Filter** in order to eliminate the sampling noise. The filtering procedure is based on [Bonavita \*et al.\* \(2012b\)](#). Finally the filtered spectral variances are transformed back to a gridpoint representation, converted to standard deviations and stored as grib files of type 'ses' of stream 'enda'.



# Chapter 7

## Gravity-wave control

### Table of contents

- [7.1 Introduction](#)
- [7.2 Normal-mode initialization](#)
- [7.3 Computation of normal modes](#)
  - [7.3.1 Vertical modes](#)
  - [7.3.2 Horizontal modes and help arrays](#)
- [7.4 Implementation of NMI](#)
- [7.5 Computation of  \$J\_c\$  based on NMI](#)
- [7.6 Digital filter initialization](#)
- [7.7 Implementation of DFI as a weak constraint in 4D-Var](#)

### 7.1 INTRODUCTION

In 3D-Var, gravity-wave control is achieved via a penalty term  $J_c$  based on the techniques of normal-mode initialization (NMI), in 4D-Var a weak constraint digital filter is used.

[Section 7.2](#) provides a brief overview of NMI techniques, together with references to scientific papers in which further details can be found. [Section 7.3](#) describes the computation of normal modes and related arrays. [Section 7.4](#) documents the implementation of nonlinear NMI in 3D- and 4D-Var, while [Section 7.5](#) describes the computation of  $J_c$  based on NMI. [Section 7.6](#) gives an overview of digital filter initialization techniques while [Section 7.7](#) describes its implementation as it is used in the 4D-Var assimilation system.

### 7.2 NORMAL-MODE INITIALIZATION

If the model equations are linearized about a state of rest, the solutions can (with a certain amount of arbitrariness) be classified into ‘slow’ (Rossby) and ‘fast’ (gravity) modes. This classification defines two mutually orthogonal subspaces of the finite-dimensional vector space containing the model state  $\mathbf{x}$ . Thus, the model state can be written as

$$\mathbf{x} = \mathbf{x}_R + \mathbf{x}_G \tag{7.1}$$

where  $\mathbf{x}_R$  is the ‘slow’ component and  $\mathbf{x}_G$  the ‘fast’ component. *Linear* NMI consists of removing the fast component altogether ( $\mathbf{x}_G = 0$ ). Since the model is nonlinear, a much better balance is obtained by setting the *tendency* of the fast component to zero ( $\dot{\mathbf{x}}_G = 0$ ); it is this balance condition which *nonlinear* NMI seeks to impose.

Nonlinear NMI was first demonstrated by [Machenhauer \(1977\)](#), in the context of a spectral shallow-water model. For a multi-level model, the first stage in the modal decomposition is a vertical transform; each vertical mode then has its own set of horizontal slow and fast modes (for the shallower vertical modes, all the corresponding horizontal modes can be considered as ‘slow’). In the case of a multi-level spectral model using the ECMWF hybrid vertical coordinate the details may be found in the report by [Wergen \(1987\)](#), which also describes techniques for taking into account forcing by physical (non-adiabatic) processes and the diurnal and semi-diurnal tidal signals. Although these options are still coded in the IFS, they are no longer used operationally at ECMWF and will not be described in this documentation.

Implicit normal mode initialization ([Temperton, 1988](#)) is based on the observation that, except at the largest horizontal scales, the results of NMI can be reproduced almost exactly without computing the

horizontal normal modes at all. The calculation reduces to solving sets of elliptic equations. In the case of a spectral model (Temperton, 1989), these sets of equations are tridiagonal in spectral space. The IFS code includes the option of ‘partially implicit NMI’, in which the initialization increments are computed using the full ‘explicit’ NMI procedure for large horizontal scales while the remaining increments at smaller horizontal scales are computed using the simpler implicit procedure.

## 7.3 COMPUTATION OF NORMAL MODES

### 7.3.1 Vertical modes

The vertical normal modes depend on the number of levels in the model and on their vertical distribution. They also depend on the choice of reference temperature SITR (assumed isothermal) and reference surface pressure (SIPR). The vertical modes used by the initialization routines are also used in the semi-implicit scheme for the forward integration of the model. The computation of  $J_b$  and  $J_c$  also uses the vertical normal modes, but for these purposes different values of SITR and SIPR may be selected. Thus the vertical modes are computed both in **SUDYN** and **SUSINMI**, the latter being used especially in 4D-Var where it is necessary to alternate between applications using different choices of SITR and SIPR. The vertical modes are computed by first calling **SUBMAT** to set up a vertical structure matrix and then calling an eigenvalue/eigenvector routine **EIGSOL** (at the end of **SUDYN**, it calls routine **RG** in the auxiliary library). After reordering and normalization, the eigenvectors (vertical modes) are stored in the matrix **SIMO**, while the corresponding eigenvalues (equivalent depths) are stored in the array **SIVP**. The inverse of **SIMO** is computed and stored in **SIMI**.

### 7.3.2 Horizontal modes and help arrays

The horizontal normal modes depend on the equivalent depths (see above) and the chosen spectral truncation **NXMAX**. For ‘explicit’ NMI, **NXMAX** is equal to the model’s spectral truncation **NSMAX**. Normally, ‘partially implicit NMI’ is chosen by setting the switch **LRPIMP** to **.TRUE**. In this case the explicit NMI increments are used only up to spectral truncation **NLEX** (21 by default) but in order to blend the explicit and implicit increments smoothly, explicit increments are computed up to a slightly higher resolution. By default,  $\text{NXMAX} = \text{NLEX} + 5$ .

For most applications of the NMI procedure in the operational suite, it is considered that the larger horizontal scales are best left uninitialized (they include, for example, atmospheric tidal signals and large-scale tropical circulations driven by diabatic processes). To cater for this option there is another logical switch, **LASSI** (‘adiabatic small-scale initialization’), which sets to zero all the initialization increments for total wavenumbers up to **NFILTM** (= 19 by default). Since only the small-scale increments are used, the NMI can be completely implicit: **NLEX** is set to 0 and there is no need to calculate the ‘explicit’ horizontal normal modes.

All the horizontal-normal-mode computations are carried out only for the first **NVMOD** vertical modes. By default,  $\text{NVMOD} = 5$ .

The horizontal modes are computed by calling **SUMODE3**. In turn, **SUMODE3E** computes the explicit modes and their frequencies while **SUMODE3I** computes the ‘help’ arrays required to invert the tridiagonal systems encountered in implicit NMI.

## 7.4 IMPLEMENTATION OF NMI

Nonlinear NMI can be invoked by calling **NNMI3**. This is no longer applied by default in IFS, now all gravity-wave control during the assimilation process is done through the penalty term or digital filter. But significant parts of the NMI code is still used for this, as described in Section 7.5. Model tendencies are computed by calling **STEPO** to perform one (forward) timestep. The tendencies are then supplied to **MO3DPRJ** which computes the required increments, using the ‘explicit’ (Machenauer) or the ‘implicit’ scheme (or both, after which the results are merged). The increments are added to the original spectral fields and the process is iterated **NITNMI** (by default 2) times.



## 7.5 COMPUTATION OF $J_c$ BASED ON NMI

In the notation of (7.1), the penalty term  $J_c$  is defined by

$$J_c = \varepsilon \|(\dot{\mathbf{x}} - \dot{\mathbf{x}}_b)_G\|^2 \quad (7.2)$$

where  $\varepsilon$  is an empirically chosen weighting factor,  $\mathbf{x}$  is the current state of the control variable and  $\mathbf{x}_b$  is the background. The norm  $\|\cdot\|^2$  is based on a weighted sum of squares of spectral coefficients. Only the first NVMOD vertical modes are included in the evaluation of (7.2).

$J_c$  is computed by calling the routine **COSJC**. Control passes through **JCCOMP** to **NMIJCTL**, where  $J_c$  is evaluated by calling **STEPO** twice, then projecting the differences in the tendencies on to the gravity modes via **MO3DPRJ**, and finally computing  $J_c$  in **NMICOST**.

## 7.6 DIGITAL FILTER INITIALIZATION

Digital filter initialization consists in removing high frequency oscillations from the temporal signal represented by the meteorological fields. A general description of digital filter initialization can be found in Lynch (1993). It can be implemented as a strong constraint by filtering the model fields at the beginning of each forecast or as a weak constraint as described in Gustafsson (1992) and Gauthier and Thépaut (2001).

Time oscillations exceeding a cut-off frequency  $\omega_c = (2\pi)/T_c$  can be filtered by applying a digital filter to a time series  $f_k = f(t_k)$  for  $f_k = k\Delta t$ ,  $\Delta t$  being the timestep. This proceeds by doing a convolution of  $f(t)$  with a step function  $h(t)$  so that

$$f \bullet h(t_N) = \sum_{k=-\infty}^{\infty} h_k f_{N-k}$$

The step function  $h_k$  is found to be

$$h_k = \frac{\sin(\omega_c k \Delta t)}{k\pi}$$

In practice, the convolution is restricted to a finite time interval of time span  $T_s$ . We can write  $T_s = 2M\Delta t$  and

$$f \bullet h(t_0) = \sum_{k=-M}^M \alpha_k f_k$$

with  $\alpha_k = -h_{-k}$ . This truncation introduces Gibbs oscillations which can be attenuated by introducing a Lanczos window which implies that the weights  $\alpha_k$  are defined as  $\alpha_k = -h_{-k} W_k$  with

$$W_k = \frac{\sin((k\pi)/(M+1))}{(k\pi)/(M+1)}$$

An alternative which is used at ECMWF has been proposed by Lynch (1997) to use a Dolph–Chebyshev window in which case

$$W_k = \frac{1}{2M+1} \left[ 1 + 2r \sum_{m=0}^M T_{2M}(x_0 \cos \theta_m/2) \cos m\theta_k \right] \quad (7.3)$$

where  $1/x_0 = \cos(\pi\Delta t)/\tau_s$ ,  $1/r = \cosh(2M \operatorname{acosh} x_0)$ ,  $\theta_k = (k2\pi)/M$  and  $T_{2M}$  is the Chebyshev polynomial of degree  $2M$ . The time span of the window is chosen so that  $\tau_s = M\Delta t$ .

## 7.7 IMPLEMENTATION OF DFI AS A WEAK CONSTRAINT IN 4D-VAR

In the context of 4D-Var data assimilation, the digital filter is used as a weak constraint. A penalty term is added to the cost function and replaces the NMI based penalty term. The implementation is based

on [Gauthier and Thépaut \(2001\)](#). The filtered increments are calculated as

$$\delta\bar{\mathbf{X}}(t_{N/2}) = \sum_{k=0}^N \alpha_k \delta\mathbf{X}(t_k)$$

where  $N$  is the number of time steps in the minimisation and delta represents increments.

During each integration of the tangent linear model in the inner loop of the 4D-Var, the digital filter is applied to the increments and the partial sum accumulated by [EDIGFIL](#). This gives a filtered increment valid at the mid-point of the assimilation window (arrays RACCSPA2 and RACCSPA3). The value of the non-filtered increment valid at the same time is also stored by [ECOPSP](#) in arrays RSTOSPA2 and RSTOSPA3. These routines are called in [CNT4TL](#) each time-step.

The adjoint model integration calculates the gradient in [EDIGFILAD](#). The gradient is obtained by a single backward integration of the adjoint model. The adjoint calculations associated with the digital filter is a virtually cost free addition to the adjoint observation cost function calculations.

The filtering weights used by the digital filter are calculated during the setup phase by [SUEFW](#). The default is to use a Dolph–Chebyshev non-recursive filter ( $NTPDFI = 4$ , see equation (7.3))

The weak constraint term which is added to the cost function is the moist energy norm of the departure between those two states times a weight factor. All these computations are conducted in spectral space and applied to the spectral fields. The default mode at ECMWF is to redefine the norm so the digital filter is only applied to divergence ( $LDIVONLY = .TRUE.$ ). A larger weight factor ( $ALPHAG = 100.$ ) is in that case used in the weak constraint term.

The norm of the departure is computed in two steps. In [EVJCDFI](#), the difference between RACCSPA2/RACCSPA3 and RSTOSPA2/RSTOSPA3 is computed and multiplied with  $ALPHAG$  for the subset of wave numbers and vertical levels associated with each processor. The cost contribution is calculated for each wavenumber and vertical level using the specified norm. The contributions for all wavenumbers, levels and variables are gathered on each processor by [GATHERCOST2](#) and the total cost contribution is summed in array  $RSUMJCDFI$  for each variable and level. Finally, in [EVCOST](#), the contributions from each variable and level are added to obtain the value of the penalty term.

# Chapter 8

## Diagnostics

### Table of contents

- 8.1 Introduction**
  - 8.1.1 Influence matrix diagnostic in 4D-Var
  - 8.1.2 How to compute the observation influence (OI)
- 8.2 Observational influence for a DA scheme**
  - 8.2.1 Linear statistical estimation in numerical weather prediction
  - 8.2.2 Approximate calculation of self-sensitivity in a large variational analysis system
- 8.3 Gradient test**
- 8.4 The 24-hour forecast error contribution to observations (FEC)**

## 8.1 INTRODUCTION

### 8.1.1 Influence matrix diagnostic in 4D-Var

The influence matrix is used in ordinary least-squares applications for monitoring statistical multiple-regression analyses. Concepts related to the influence matrix provide diagnostics on the influence of individual data on the analysis, the analysis change that would occur by leaving one observation out, and the effective information content (degrees of freedom for signal) in any sub-set of the analysed data. The corresponding concepts have been derived in the context of linear statistical data assimilation in numerical weather prediction. An approximate method to compute the diagonal elements of the influence matrix (the self-sensitivities or observation influence) has been developed for a large-dimension variational data assimilation system (the 4D-Var system of ECMWF).

### 8.1.2 How to compute the observation influence (OI)

In prepIFS, experiment type ‘an’ task ‘forecast error handling’, the logical switch LANOBS=on will allow the OI computation for all observation assimilated. OI is saved in ODB in an\_sens\_obs.

A Fortran program is available to compute the DFS (Degree of Freedom for Signal) and OI. The program output is a Table that can be imported in XL for graphical display. Geographical maps and time series for all the assimilated observations are produced by OBSTAT.

## 8.2 OBSERVATIONAL INFLUENCE FOR A DA SCHEME

### 8.2.1 Linear statistical estimation in numerical weather prediction

Data assimilation systems for NWP provide estimates of the atmospheric state  $\mathbf{x}$  by combining meteorological observations  $\mathbf{y}$  with prior (or background) information  $\mathbf{x}_b$ . A simple Bayesian Normal model provides the solution as the posterior expectation for  $\mathbf{x}$ , given  $\mathbf{y}$  and  $\mathbf{x}_b$ . The same solution can be achieved from a classical *frequentist* approach, based on a statistical linear analysis scheme providing the best linear unbiased estimate (Talagrand, 1997) of  $\mathbf{x}$ , given  $\mathbf{y}$  and  $\mathbf{x}_b$ . The optimal GLS solution to the analysis problem (see Lorenc, 1986) can be written

$$\mathbf{x}_a = \mathbf{K}\mathbf{y} + (\mathbf{I}_n - \mathbf{K}\mathbf{H})\mathbf{x}_b \quad (8.1)$$

The vector  $\mathbf{x}_a$  is the ‘analysis’. The gain matrix  $\mathbf{K}(n \times p)$  takes into account the respective accuracies of the background vector  $\mathbf{x}_b$  and the observation vector  $\mathbf{y}$  as defined by the  $n \times n$  covariance matrix  $\mathbf{B}$  and

the  $p \times p$  covariance matrix  $\mathbf{R}$ , with

$$\mathbf{K} = (\mathbf{R}^{-1} + \mathbf{H}^T \mathbf{R}^{-1} \mathbf{H})^{-1} \mathbf{H}^T \mathbf{R}^{-1} \quad (8.2)$$

Here,  $\mathbf{H}$  is a  $p \times n$  matrix interpolating the background fields to the observation locations, and transforming the model variables to observed quantities (e.g. radiative transfer calculations transforming the models temperature, humidity and ozone into brightness temperatures as observed by several satellite instruments). In the 4D-Var context introduced below,  $\mathbf{H}$  is defined to include also the propagation in time of the atmospheric state vector to the observation times using a forecast model.

Substituting (8.2) into (8.1) and projecting the analysis estimate onto the observation space, the estimate becomes

$$\hat{\mathbf{y}} = \mathbf{H} \mathbf{x}_a = \mathbf{H} \mathbf{K} \mathbf{y} + (\mathbf{I}_p - \mathbf{H} \mathbf{K}) \mathbf{H} \mathbf{x}_b \quad (8.3)$$

It can be seen that the analysis state in observation space ( $\mathbf{H} \mathbf{x}_a$ ) is defined as a sum of the background (in observation space,  $\mathbf{H} \mathbf{x}_b$ ) and the observations  $\mathbf{y}$ , weighted by the  $p \times p$  square matrices  $\mathbf{I} - \mathbf{H} \mathbf{K}$  and  $\mathbf{H} \mathbf{K}$ , respectively.

In this case, for each unknown component of  $\mathbf{H} \mathbf{x}$ , there are two data values: a real and a ‘pseudo’ observation. The additional term in (8.3) includes these pseudo-observations, representing prior knowledge provided by the observation-space background  $\mathbf{H} \mathbf{x}_b$ . From (8.3), the analysis sensitivity with respect to the observations is obtained

$$\mathbf{S} = \frac{\partial \hat{\mathbf{y}}}{\partial \mathbf{y}} = \mathbf{K}^T \mathbf{H}^T \quad (8.4)$$

Similarly, the analysis sensitivity with respect to the background (in observation space) is given by

$$\frac{\partial \hat{\mathbf{y}}}{\partial (\mathbf{H} \mathbf{x}_b)} = \mathbf{I} - \mathbf{K}^T \mathbf{H}^T = \mathbf{I}_p - \mathbf{S} \quad (8.5)$$

We focus here on the expressions (8.4) and (8.5). The influence matrix for the weighted regression DA scheme is actually more complex, but it obscures the dichotomy of the sensitivities between data and model in observation space.

The (projected) background influence is complementary to the observation influence. For example, if the self-sensitivity with respect to the  $i$ th observation is  $S_{ii}$ , the sensitivity with respect the background projected at the same variable, location and time will be simply  $1 - S_{ii}$ . It also follows that the complementary trace,  $\text{tr}(\mathbf{I} - \mathbf{S}) = p - \text{tr}(\mathbf{S})$ , is not the  $df$  for noise but for background, instead. That is the weight given to prior information, to be compared to the observational weight  $\text{tr}(\mathbf{S})$ . These are the main differences with respect to standard LS regression. Note that the different observations can have different units, so that the units of the cross-sensitivities are the corresponding unit ratios. Self-sensitivities, however, are pure numbers (no units) as in standard regression. Finally, as long as  $\mathbf{R}$  is diagonal,  $0 \leq S_{ii} \leq 1$  is assured, but for more general non-diagonal  $\mathbf{R}$ -matrices it is easy to find counter-examples to that property.

Inserting (8.1) into (8.4), we obtain

$$\mathbf{S} = \mathbf{R}^{-1} \mathbf{H} (\mathbf{B}^{-1} + \mathbf{H}^T \mathbf{R}^{-1} \mathbf{H})^{-1} \mathbf{H}^T \quad (8.6)$$

As  $(\mathbf{B}^{-1} + \mathbf{H}^T \mathbf{R}^{-1} \mathbf{H})$  is equal to the analysis error covariance matrix  $\mathbf{A}$ , we can also write  $\mathbf{S} = \mathbf{R}^{-1} \mathbf{H} \mathbf{A} \mathbf{H}^T$ .

### 8.2.2 Approximate calculation of self-sensitivity in a large variational analysis system

In a optimal variational analysis scheme, the analysis error covariance matrix  $\mathbf{A}$  is approximately the inverse of the matrix of second derivatives (the Hessian) of the cost function  $J$ , i.e.  $\mathbf{A} = (\mathbf{J})^{-1}$  (Rabier and Courtier, 1992). Given the large dimension of the matrices involved,  $\mathbf{J}$  and its inverse cannot be computed explicitly. Following Fisher and Courtier (1995) we use an approximate representation of the Hessian based on a truncated eigen-vector expansion with vectors obtained through the Lanczos algorithm. The calculations are performed in terms of a transformed variable  $\mathbf{P}$ ,  $\mathbf{P} = \mathbf{L}^{-1}(\mathbf{x} - \mathbf{x}_b)$ , with  $\mathbf{L}$

chosen such that  $\mathbf{B}^{-1} = \mathbf{L}^T \mathbf{L}$ . The transformation  $\mathbf{L}$  thus reduces the covariance of the prior to the identity matrix. In variational assimilation  $\mathbf{L}$  is referred to as the change-of-variable operator (Courtier *et al.*, 1998).

$$\mathbf{J}''^{-1} \simeq \mathbf{B} - \sum_{i=1}^M \frac{1 - \lambda_i}{\lambda_i} (\mathbf{L}v_i)(\mathbf{L}v_i)^T \quad (8.7)$$

The summation in (8.7) approximates the variance reduction  $\mathbf{B} - \mathbf{A}$  due to the use of observations in the analysis.  $(\lambda_i, v_i)$  are the eigen-pairs of  $\mathbf{A}$ . In ECMWF's operational data assimilation system, the variances of analysis error are computed according to this method. The variances are inflated to provide estimates of short-term forecast (background) error variances to be used as background errors in the next analysis cycle (Fisher, 1996). The Hessian eigen-vectors are also used to precondition the minimization (Fisher and Andersson, 2001). The computed eigen-values are not used to minimize the cost function but only to estimate the analysis covariance matrix. It is well known, otherwise, that the minimization algorithm is analogous to the conjugate-gradient algorithm. Because the minimum is found within an iterative method, the operational number of iterations is sufficient to find the solution (with required accuracy) but does not provide a sufficient number of eigen-pairs to estimate the analysis-error variances.

The diagonal of the background error covariance matrix  $\mathbf{B}$  in (8.7) is also computed approximately, using the randomisation method proposed by Fisher and Courtier (1995). From a sample of  $N$  random vectors  $\mathbf{u}_i$  (in the space of the control-vector), drawn from a population with zero mean and unit Gaussian variance, a low-rank representation of  $\mathbf{B}$  (in terms of the atmospheric state variables  $\mathbf{x}$ ) is obtained by

$$\mathbf{B} = \frac{1}{N} \sum_{i=1}^N (\mathbf{L}u_i)(\mathbf{L}u_i)^T \quad (8.8)$$

This approximate representation of  $\mathbf{B}$  has previously been used by Andersson *et al.* (2000) to diagnose background errors in terms of observable quantities, i.e.  $\mathbf{H}\mathbf{B}\mathbf{H}^T$ .

Inserting (8.7) and (8.8) into (8.6) we arrive at an approximate method for calculating  $\mathbf{S}$ , that is practical for a large dimension variational assimilation (both 3D and 4D-Var). This is given by

$$\mathbf{S} = \mathbf{R}^{-1} \mathbf{H} \left[ \frac{1}{N} \sum_{i=1}^N (\mathbf{L}u_i)(\mathbf{L}u_i)^T + \sum_{i=1}^M \frac{1 - \lambda_i}{\lambda_i} (\mathbf{L}v_i)(\mathbf{L}v_i)^T \right] \mathbf{H}^T \quad (8.9)$$

Only the diagonal elements of  $\mathbf{S}$  are computed and stored in ODB – that is, the analysis sensitivities with respect to the observations, or self-sensitivities  $S_{ii}$ . The cross-sensitivity  $S_{ij}$  for  $i \neq j$ , that represents the influence of the  $j$ th observation to the analysis at the  $i$ th location, is not computed. Note that the approximation of the first term is unbiased, whereas the second term is truncated such that variances are underestimated. For small  $M$  the approximate  $S_{ii}$  will tend to be over-estimates. For the extreme case  $M = 0$ , (8.9) gives  $\mathbf{S} = \mathbf{R}^{-1} \mathbf{H}\mathbf{B}\mathbf{H}^T$  which in particular can have diagonal elements larger than one if elements of  $\mathbf{H}\mathbf{B}\mathbf{H}^T$  are larger than the corresponding elements of  $\mathbf{R}$ . The number of Hessian vectors operationally computed is  $M = 40$  and the number of random  $\mathbf{B}$  vectors is  $N = 50$ .

In general, in the operational system, 15% of the global influence is due to the assimilated observations in any one analysis, and the complementary 85% is the influence of the prior (background) information, a short-range forecast containing information from earlier assimilated observations. About 25% of the observational information is currently provided by surface-based observing systems, and 75% by satellite systems.

Low-influence data points usually occur in data-rich areas, while high-influence data points are in data-sparse areas or in dynamically active regions. Background error correlations also play an important role: High correlation diminishes the observation influence and amplifies the importance of the surrounding real and pseudo observations (prior information in observation space). Incorrect specifications of background and observation error covariance matrices can be identified, interpreted and better understood by the use of influence matrix diagnostics for the variety of observation types and observed variables used in the data assimilation system.

Self-sensitivities cannot be larger than one (they are bounded in the interval zero to one) but, because of the small number of eigenpair we can compute,  $S_{ii}$  can be greater than one. Approximations in both of the two terms of (8.9) contribute to the problem. In the second term the number of Hessian eigen-vectors is truncated to  $M$ . The term is therefore underestimated, and  $S_{ii}$  will tend to be over-estimated. The degree of over-estimation depends on the structure of the covariance reduction matrix  $\mathbf{B-A}$ .

For an analysis in which observations lead to strongly localised covariance reduction (such as the humidity analysis with its short co-variance length scales  $\sim 180$  km, and large observational impacts) a large  $M$  is required to approximate  $\mathbf{B-A}$  accurately. The approximate computation is mostly affecting the self-sensitivities close to the upper bound leaving the self-sensitivities  $< 0.7$  almost unaffected.

To conclude, the self-sensitivity provides a quantitative measure of the observation influence in the analysis. In robust regression, it is expected that the data have similar self-sensitivity (sometimes called leverage) – that is, they exert similar influence in estimating the regression line. Disproportionate data influence on the regression estimate can have different reasons: First, there is the inevitable occurrence of incorrect data. Second, influential data points may be legitimately occurring extreme observations. However, even if such data often contain valuable information, it is constructive to determine to which extent the estimate depends on these data. Moreover, diagnostics may reveal other patterns e.g. that the estimates are based primarily on a specific sub-set of the data rather than on the majority of the data. In the context of 4D-Var there are many components that together determine the influence given to any one particular observation. First there is the specified observation error covariance  $\mathbf{R}$ , which is usually well known and obtained simply from tabulated values. Second, there is the background error covariance  $\mathbf{B}$ , which is specified in terms of transformed variables that are most suitable to describe a large proportion of the actual background error covariance. The implied covariance in terms of the observable quantities is not immediately available for inspection, but it determines the analysis weight given to the data. Third, the dynamics and the physics of the forecast model propagate the covariance in time, and modify it according to local error growth in the prediction. The influence is further modulated by data density. Low influence data points occur in data-rich areas while high influence data points are in data-sparse regions or in dynamically active areas. Background error correlations also play an important role. In fact, very high correlations drastically lessen the observation influence in favour of background influence and amplify the influence of the surrounding observations.

With the approximate method used here, out-of-bound self-sensitivities occur if the Hessian representation based on an eigen-vector expansion is truncated, especially when few eigen-vectors are used. However, this problem affects only a small percentage of the self-sensitivities computed in this study, and in particular those that are closer to one. Remaining values greater than one can be due to large background to observation error ratio, which is one factor that is known to contribute towards ill-conditioning and poor convergence of the 4D-Var algorithm.

### 8.3 GRADIENT TEST

If `LTEST = .TRUE.` a gradient test will be performed both before and after minimization. This is done by the routine `GRTEST`. In the gradient test a test value  $t_1$  is computed as the ratio between a perturbation of the co-t-function and its first-order Taylor expansion using

$$t_1 = \lim_{\delta\chi \rightarrow 0} \frac{J(\chi + \delta\chi) - J(\chi)}{\langle \nabla J, \delta\chi \rangle} \quad (8.10)$$

with  $\delta\chi = -\alpha \nabla J$ . Repeatedly increasing  $\alpha$  by one order of magnitude, printing  $t_1$  at each step should show  $t_1$  approaching one, by one order of magnitude at a time, provided  $J(\chi)$  is approximately quadratic over the interval  $[\chi, \chi + \delta\chi]$ . The near linear increase in the number of 9's in the print of  $t_1$  over a wide range of  $\alpha$  (initially as well as after minimization) proves that the coded adjoint is the proper adjoint for the linearization around the given state  $\chi$ .

The behaviour of the cost function in the vicinity of  $\chi$  in the direction of the gradient  $\nabla J$  is also diagnosed by several additional quantities for each  $\alpha$ . The results are printed out on lines in the log-file starting

with the string 'GRTEST:'. To test the continuity of  $J$ , for example, a test value  $t_0$  is computed with

$$t_0 = \frac{J(\chi + \delta\chi)}{J(\chi)} - 1 \quad (8.11)$$

and printed. For explanation of other printed quantities see the routine **GRTEST** itself. A range of additional test was introduced in Cy28r2.

#### 8.4 THE 24-HOUR FORECAST ERROR CONTRIBUTION TO OBSERVATIONS (FEC)

For information about the FEC computation see:

<http://datasvc.ecmwf.int/twiki/bin/view/Main/DiagnosticsToolsDataAssimilation>.





## Chapter 9

# Observation processing

### Table of contents

<b>9.1</b>	<b>Basic principles</b>
<b>9.2</b>	<b>Main MKCMARPL tasks and functions</b>
9.2.1	Basic observation processing setup
9.2.2	Invoking, initializing and controlling the MKCMARPL
9.2.3	MKCMARPL
9.2.4	Basic observation handling routines
<b>9.3</b>	<b>Observation types, subtypes and code types</b>
9.3.1	BUFR observation types and subtypes
9.3.2	ODB observation and code types
9.3.3	Mapping between ODB and BUFR observation types, code types and subtypes
<b>9.4</b>	<b>Variables</b>
9.4.1	Observed variables
9.4.2	Derived variables
9.4.3	Adjusted variables
9.4.4	Codes for variables
<b>9.5</b>	<b>Observation error statistics</b>
9.5.1	Persistence observation error
9.5.2	Prescribed observation errors
9.5.3	Derived observation errors
9.5.4	Final (combined) observation error
9.5.5	Overview over METEOSAT and GEOS imager CSR in the ECMWF archives
9.5.6	Thinning and screening prior to insertion into the assimilation
<b>9.6</b>	<b>Definitions</b>
9.6.1	Observation characteristics: instrument specification and retrieval type
9.6.2	Vertical coordinate: pressure, satellite ID and level ID codes
9.6.3	ODB report status: events, flags and codes
9.6.4	Datum status: events, RDB and analysis flags

## 9.1 BASIC PRINCIPLES

The ECMWF Data Assimilation Observation Processing System prior to Cy26r1 (April 2003) was roughly split in two parts.

- (i) Non-IFS observation processing modules.
- (ii) IFS integrated observation processing module.

Originally, the main difference in function between these two parts was based on whether information about a field (e.g. first guess) was required or not. Thus, the observation processing functions for which field information was not required were dealt with by the non-IFS modules, whereas the IFS itself dealt with those observation processing functions for which field information was needed.

The non-IFS observation processing came in two main parts.

- (i) Preparation and massaging of input BUFR data.
- (ii) Creation of two data structure; one acceptable by the IFS as input and the other one for archiving purposes (observation feedback).

The first part of the non-IFS observation processing, which is still intact, consists of a number of modules: **PRE1CRAD** (further split by instrument type), **PREOBS**, **PREOBS\_WAVE**, **PREGEOS**, **PREREO3** and **PRESCAT**. Without going into too many details here, the main theme for all of them is to prepare input BUFR data in an appropriate form for further processing. This also involves performing preliminary data thinning. As such, this part is preserved even after the major change which occurred with Cy26r1.

The second part of the non-IFS observation processing consisted of two modules: **OBSPROC** and **OBSORT**. The main task of **OBSPROC** was to prepare input BUFR data in a form to be used by the analysis, whereas **OBSORT** dealt with any issues related to parallel computing. In this context **OBSORT** was not doing anything on its own; it was normally called by **OBSPROC** to ensure efficient parallelisation. During an analysis cycle **OBSPROC** is executed twice: just before and just after the IFS. The task before the IFS, called **MAKECMA** or for short **MKCMA**, performed a number of observation processing functions.

- (i) Read in and crack input BUFR data.
- (ii) Carry out preliminary data checks.
- (iii) Perform necessary variable changes.
- (iv) Assign observation errors.
- (v) Create CMA data structure recognised by the IFS.
- (vi) Etc.

On the other hand the task of **OBSPROC** just after the IFS, called **FEEDBACK**, was to create BUFR feedback. This was done by appending the input BUFR data with analysis-related information (departures, flags, events, etc.).

Cy26r1 saw a major revision in this area. Observation processing modules **OBSPROC** and **OBSORT**, as well as the CMA observation data structure, have been phased out. Hence, **MKCMA** and **FEEDBACK** tasks as we knew them were made obsolete. However, a new data structure, the ODB, as well as two new observation processing modules (**BUFRTOODB** and **ODTTOBUFR**) have been introduced. Most of the observation processing functions earlier performed by the **MKCMA** task within **OBSPROC** have now been included in the IFS. It is only purely BUFR related processing functions that have now been taken over by **BUFRTOODB** and **ODTTOBUFR**.

- **BUFRTOODB**, together with **MERGEODB**, runs just before the IFS and is called **MAKEODB**. Effectively what it does is to read input BUFR data and create initial ODB which is formally acceptable by the IFS.
- **ODTTOBUFR** together with **MATCHUP** runs just after the IFS and is called **ODB2BUFR**.

Both **MAKEODB** and **ODB2BUFR** have been developed and are handled by the Operations Department.

The **OBSORT** observation processing functions have now almost entirely been incorporated into the ODB software.

As mentioned earlier most of the observation processing functions of **OBSPROC** are now integrated in the IFS. These newly integrated IFS observation processing functions are now known as “MAKE CMA REPLACEMENT” or for short **MKCMARPL**.

Here we will mostly concentrate on the IFS integrated observation processing whereas the other parts of the ECMWF documentation will deal with the remaining aspects of observation processing.

## 9.2 MAIN MKCMARPL TASKS AND FUNCTIONS

### 9.2.1 Basic observation processing setup

In order to perform the observation processing functions, a number of basic observation processing setups are carried out at the very beginning of initialising the IFS. This is done by calling several routines in addition to all other routines needed to setup the IFS (see [Fig. 9.1](#)).

- Program **MASTER** calls **CNT0** which in turn calls **SU0YOMA**.
- **SU0YOMA** calls (among other routines) **SUOAF** from which **SUCMOCTP**, **SUEVENTS**, **SUCODES**, **SUFLTXT** and **SUCMA** are called. **SUCMOCTP** defines the ODB observation types and code types, and **SUEVENTS**, **SUCODES** and **SUFLTXT** define analysis events, various codes used and flags naming conventions.
- **SUCMA** calls **SUCMAF** which then calls several subroutines: **SUCMAD1**, **SUCMAD2**, **SUCMAHFP**, **SUCMAHOP**, **SUCMBDFP** and **SUCMBDTP**. These routines define the structure of ODB Data Descriptor Records (DDRs) as well as the ODB packing patterns (bit structure) employed for header and body respectively.

### 9.2.2 Invoking, initializing and controlling the MKCMARPL

The MKCMARPL run is initiated by the **MKCMARPL** subroutine (see [Fig. 9.2](#)). This routine is only invoked in the SCREENING run of the IFS. It is called, together with some of its additional setup routines via subroutine **SUOBS**. The additional setup routines called at this level are: **SUANCT**, **DEFRUN**, **SULIM**, **SULEVLAY**, **SUSATRET**, **SUVNMB**, **SUSCRE0**, **SUOBSORT**, **SETCOM**, **DEPERERR**, **SUERRORS**, **INIERSCA**.

- **MKCMARPL** is namelist driven and in **DEFRUN** a logical variable **LMKCMARPL** is defined. By default **LMKCMARPL** = **.TRUE**. but it can be overwritten via namelist **NAMOBS**. Furthermore, many other parameters and switches are defined in **DEFRUN** and some of them can also be overwritten via namelists.
- **SUANCT** and **SULIM** define some additional analysis constants and limits.
- **SULEVLAY** and **SUSATRET** define analysis related level/layer and satellite retrieval parameters, respectively.
- **SUVNMB** declares variable numbers.
- **SUSCRE0**, **SUOBSORT** and **SETCOM** define flag limits, identify ambiguous moving platforms, initialise observation sorting, and provide some general observation common variables.
- **DEPERERR** and **SUERRORS** deal with observation error statistics definitions. **SUERRORS** calls **SUPERERR** to define observation persistence errors and **SUOBSERR** to define prescribed observation errors.
- **INIERSCA** deals with initialising **SCATT** processing.

The next step is to find out if it is a SCREENING run and if so to check if it is a MKCMARPL run as well. In the case of a MKCMARPL run all aspects of the observation processing before the screening are dealt with by calling **MKCMARPL** (more about it in [Subsection 9.2.3](#)). After **MKCMARPL** has finished there are several ways to proceed. These depend on the status of **LMKCMARPLO** and **LRPLSWAPOUT** logical switches (**NAMOBS** namelist). If **LRPLSWAPOUT** = **.TRUE**. the ODB is swapped out and if **LMKCMARPLO** = **.TRUE**. the ODB is written out and the run terminated. Both of these options are not normally used and their use is for diagnostics/debugging purposes. Once the **MKCMARPL** work has been completed the remainder of **SUOBS** will execute as before. Thus, calls to **WRITEOBA**, **WINDAUX**, **OBATABS**, **SUAMV**, **SURAD**, **SULIMB**, **SUOBAREA**, **MKGLOBSTAB** and **SUREO3** are issued.

In the context of operational running, the **MKCMARPL** related switches are set:

```
LMKCMARPL = .TRUE.  LRPLSWAPOUT = .FALSE.  LMKCAMRPLO = .FALSE.
```

### 9.2.3 MKCMARPL

The main purpose of **MKCMARPL** is to control the IFS observation pre-processing. Observation pre-processing at this stage is done in groups of observations. At the moment there are six groups:

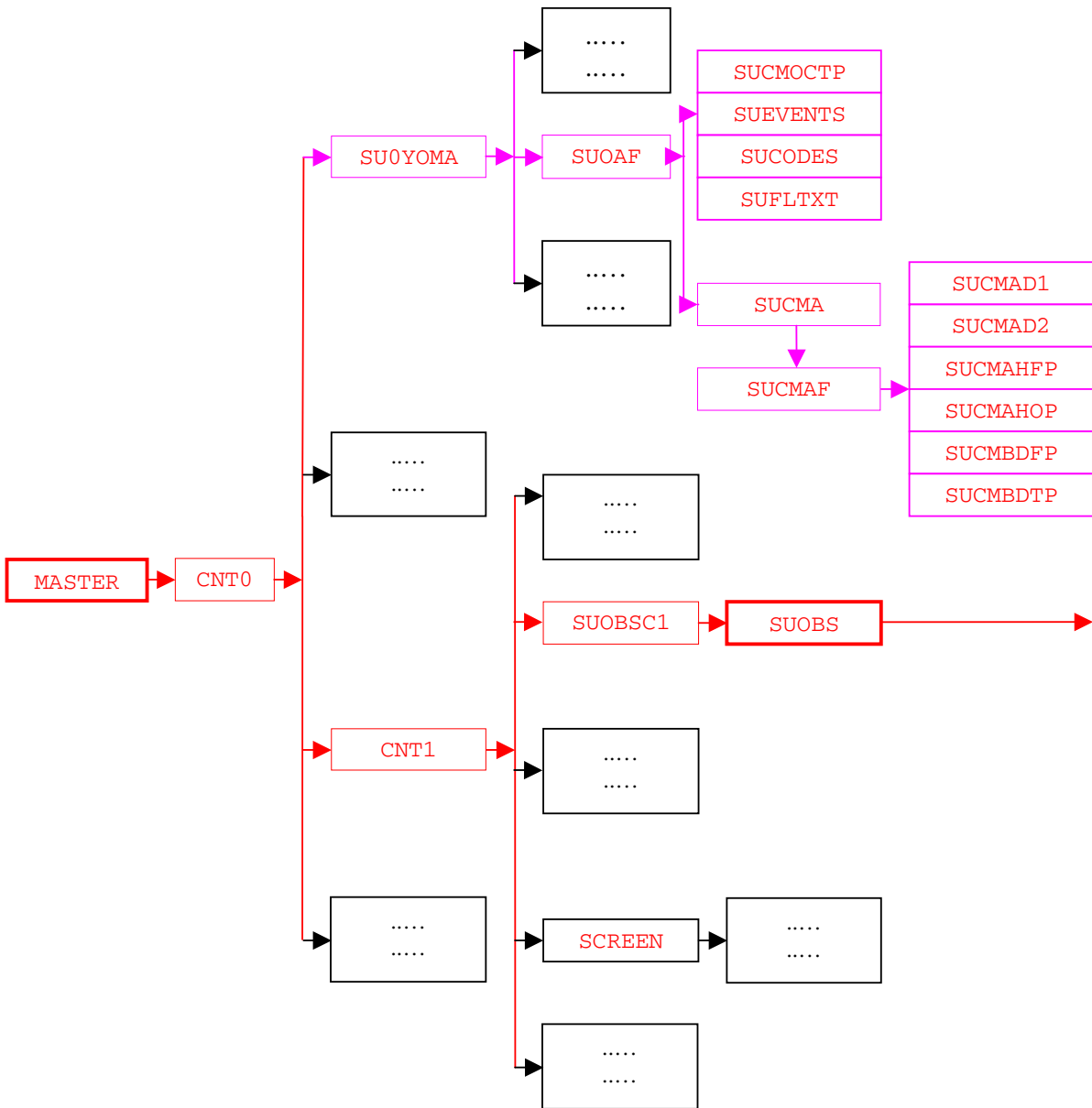


**Figure 9.1** Simplified IFS observation pre-processing flow diagram (*MASTER*). Colour coding scheme: (a) routines in red boxes perform observation pre-processing, (b) routines in pink boxes carry out observation pre-processing set up, and (c) routines in black boxes are not directly involved in observation pre-processing. *Fig. 9.2* continues the flow diagram from *SUOBS*.

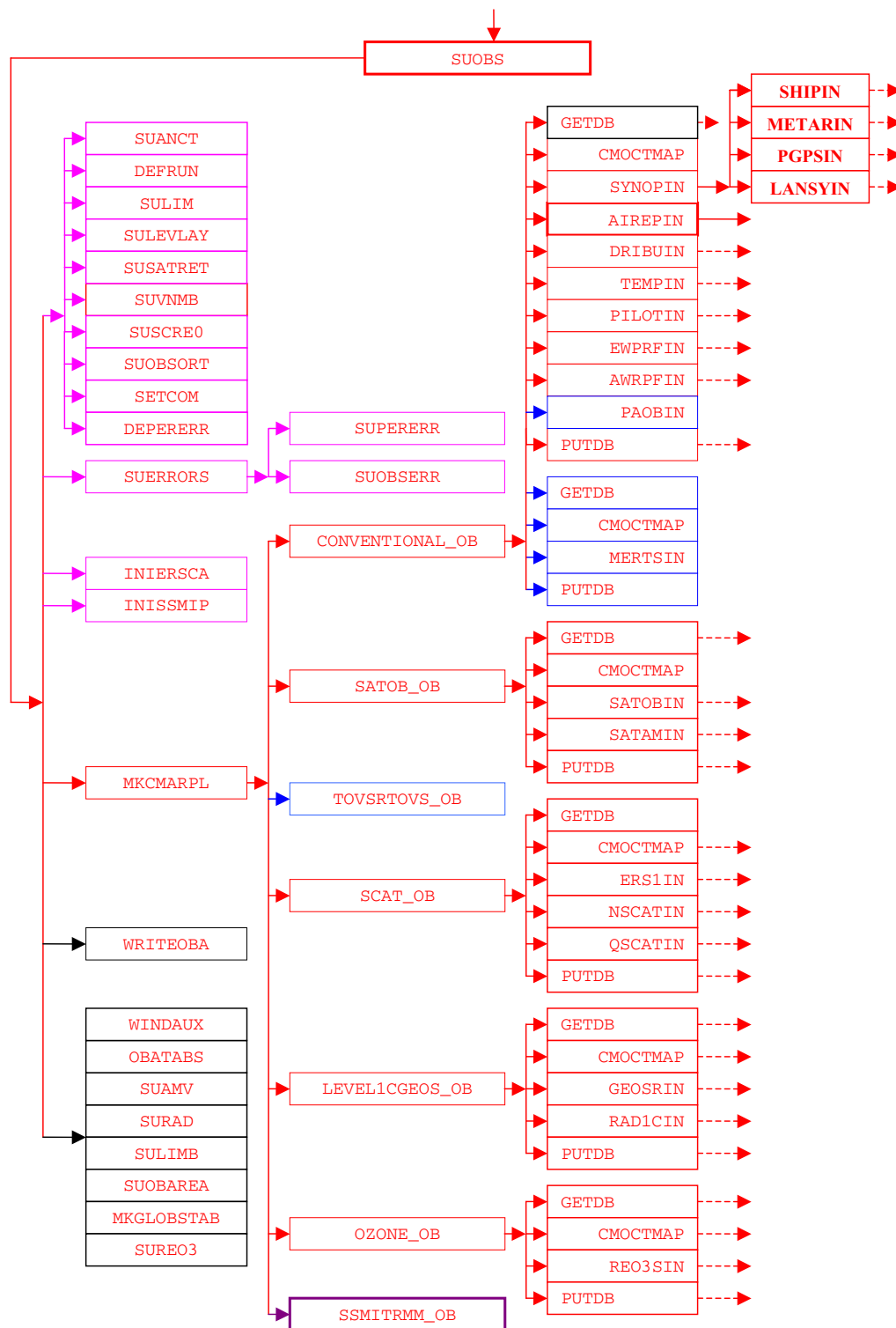


Figure 9.2 (Continued from Fig. 9.1) Simplified IFS observation pre-processing flow diagram (*SUOBS*). Colour coding scheme: (a) routines in red boxes perform observation pre-processing, (b) routines in pink boxes carry out observation pre-processing set up, (c) routines in black boxes are not directly involved in observation pre-processing, (d) routines in blue boxes are obsolete and (e) routines in plum boxes are awaiting revision. Fig. 9.3 continues the flow diagram from *AIREPIN*.

CONVENTIONAL, SATOB, TOVS/RTOVS, SCATT, LEVEL1C/GEOSS and OZONE observations. For each group a separate subroutine is called: **CONVENTIONAL\_OB**, **SATOB\_OB**, **TOVSRTOVS\_OB**, **SCAT\_OB**, **LEVEL1CGOES\_OB** and **OZONE\_OB**. These routines are just cover or hat routines for the actual work to be carried out underneath. However, **TOVSRTOVS\_OB** is currently not called because it is obsolete.

Each cover routine would call the ODB to get the observations it wants to process. This is done by calling the ODB **GETDB** subroutine. As the observations are brought, in one or more worker routines would be called to perform the observation processing functions. Once the worker routines have finished the control is handed back to the cover routine. The next step in the cover routine is to return observations back to the ODB database. This is done by calling the ODB **PUTDB** routine. In some of these cover routines several calls to **GETDB/PUTDB** might be issued. This is because there may be sufficient differences between similar data to justify a slightly different approach in their pre-processing. For example under the **CONVENTIONAL\_OB** routine there are two calls to a **GETDB** and **PUTDB** pair. The first call deals with all conventional observations except SATEMs; the second call deals with the SATEMs. As indicated earlier, between each **GETDB** and **PUTDB** a number of observations type or code type designed worker routines are called.

- **CONVENTIONAL\_OB** calls the following worker routines: **SYNOPIN**, **AIREPIN**, **DRIBUIN**, **TEMPIN**, **PILOTIN**, **EWPRFIN**, **AWPRFIN**, **PAOBIN** and **MERTSIN**. A worker routine name indicates which observations it is dealing with.
- **SATOB\_OB** calls **SATOBIN** and **SATAMIN**.
- **SCAT\_OB** calls **ERS1IN**, **NSCATIN**, **ASCATIN** and **QSCATIN**.
- **LEVEL1CGEOS\_OB** calls **RAD1CIN** and **GOESRIN**.
- **OZONE\_OB** calls only **REO3SIN**.

#### 9.2.4 Basic observation handling routines

The observation pre-processing worker routines referred to in [Subsection 9.2.3](#), names of which always end with “IN”, are the basic observation handling routines. They all follow more or less the same logic. As an example consider **AIREPIN** which deals with AIREP observations (see [Fig. 9.3](#)).

The first thing which is done is to define the instrument specification (**OBINSTP**) followed by preliminary quality control check both at the report level (**PRLMCHK**) as well as at the data level (**GETSETE** and **AIREPBE**).

- **PRLMCHK** calls **REPSEL** and **TIMDIF** to do report selection according to preset criteria and to find out time difference between analysis time and the actual observation time, respectively.
- **GETSETE** makes a local copy of a given observation variable and its related parameters from an ODB supplied array.
- After updating the local copy, **AIREPBE** is called to return the updated local copy back to the ODB supplied array.

The preliminary quality control at the report level consists of making sure that observation position, date and time are reasonable. Furthermore, as there is a possibility of excluding certain observations via the NAMOBS namelist, a check is made of whether the observation is actually wanted at this stage. Once the report level check is passed attention is turned to the data itself. Each datum is checked against predefined list of expected data. If not in the list, datum is rejected and a warning message issued. At this stage it is also ensured that missing indicators used are unique.

After the preliminary phase attention is turned to getting data in the right form and shape for further usage. Thus, in the case of an AIREP observation, this is done in sections of available variables: wind and temperature.

- **Wind**. There are four wind variables: wind direction (*DDD*), wind force (*FFF*), *u* and *v* components. For each of these variables the first thing which is done is to get a local copy of it together with its related parameters from an ODB supplied array (**GETSETE**). Once a variable is made available

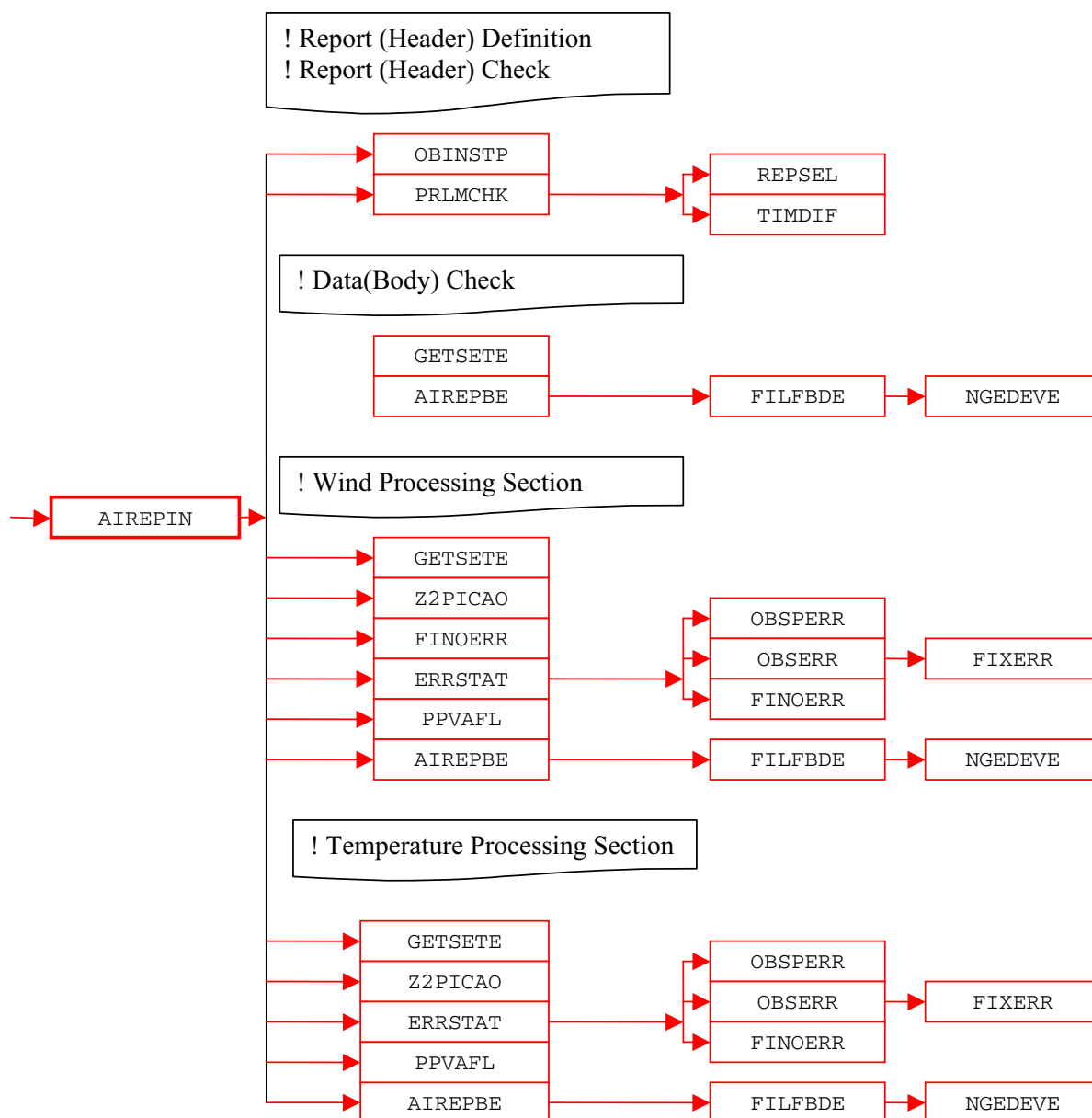


**Figure 9.3** (Continued from Fig. 9.2) *Simplified IFS observation pre-processing flow diagram (AIREPIN). Colour coding scheme: routines in red boxes perform observation pre-processing.*

locally a check is made to ensure that the vertical coordinate is pressure; if instead of pressure a flight level is supplied it is converted into pressure by assuming a standard ICAO atmosphere (**Z2PICAO**). If the variable in question is either  $u$  or  $v$ , then  $DDD$  and  $FFF$  are converted into  $u$  and  $v$  wind components. Furthermore, for each of the four variables appropriate observation error statistics are assigned (**ERRSTAT**, **FINOERR**). Also, if any flags are set at this stage an appropriate word in the local copy is updated (**PPVAFL**). Finally, an updated local copy of an observed quantity and its related parameters are returned back into the ODB (**AIREPBE**).

- (ii) **Temperature.** In the case of temperature only one observed variable is dealt with. The pattern of making a local copy (**GETSETE**), ensuring that pressure is the vertical coordinate (**Z2PICAO**), assigning the observation error statistics (**ERRSTAT**), updating flags (**PPVAFL**) and returning an updated local copy back to the ODB (**AIREPBE**) is repeated.

As just mentioned **ERRSTAT** deals with assigning observation errors for a given observation variable. **ERRSTAT** first calls **OBSPERR** to assign observation persistence error; then it calls **OBSERR** which in turn calls **FIXERR** to assign prescribed observation error. It is worth mentioning that observation errors themselves are already predefined at an earlier stage (**SUERRORS**).

The pattern of activities outlined for **AIREPIN** is repeated more or less in the other worker routines. However, the **SYNOBIN** routine is first split further into **SHIPIN**, **METATRIN**, **PGPSIN** and **LANSYIN**. This is because SHIP, METAR, GPS and SYNOP LAND observations are sufficiently different to justify a separate worker routine. Furthermore, **LANSYIN** is somewhat more complicated than **AIREPIN**. One of the reasons for this is that we have to distinguish between low and high level stations.

## 9.3 OBSERVATION TYPES, SUBTYPES AND CODE TYPES

All observations, both in the BUFR and ODB contexts, are split into a number of observation types. The observation types are then further divided into observation code types (ODB) and observation subtypes (BUFR). Although BUFR observation types and subtypes are not directly used in the IFS they are defined here. BUFR observation types and subtypes are mapped into ODB observation types and code types before the IFS (i.e. the **MERGEODB** step).

### 9.3.1 BUFR observation types and subtypes

There are eight BUFR observation types. However, the number of subtypes differs between observation types; they are listed in [Table 9.1](#).

### 9.3.2 ODB observation and code types

There are ten ODB observation types and, as with BUFR, there are a different number of code types for each of them. It is a reasonable to question why the BUFR and ODB observation types and sub or code types are different. The answer is a historic one. The ODB observation types and code types have been used before BUFR came in to existence and as an international code it was difficult to impose our practice on the others. Also, there was not enough enthusiasm on our side to switch to the BUFR ones. The ODB observation types and code types are listed in [Table 9.2](#).

### 9.3.3 Mapping between ODB and BUFR observation types, code types and subtypes

As indicated in [Subsection 9.3.2](#) the coexistence of different codes used for BUFR and ODB observation types and the subtype and code type requires a mapping from one to another. This is given in [Table 9.3](#).

## 9.4 VARIABLES

Different quantities are observed by different observing systems. It is only a subset of observed quantities that are used in the analysis and most of them are used in their original form. However, some of them are transformed into the ones actually used by the analysis. This transformation, or a change of variable, may also include retrieval from satellite data if they are independent from the background model fields. The original variables may be kept with the derived ones so that first guess departures can be assigned for both. Furthermore, if an observed variable is transformed then, if necessary, so is its observation error statistics. Also, in the case of an off-time SYNOP observation, the observed surface pressure may be adjusted.

### 9.4.1 Observed variables

The exact list of what is observed or present in the list of BUFR observation types and sub types ([Table 9.3](#)) is long. Therefore [Table 9.4](#) just lists (per observation types) those variables which are of interest at present.

### 9.4.2 Derived variables

Variables which are transformed for further use by the analysis are as follows.



Table 9.1 *BUFR observation types and subtypes.*

Observation Type		Subtype	
Code	Name	Code	Name
0	Land Surface	1	Land SYNOP
		3	Automatic Land SYNOP
		9	Abbreviated Land SYNOP
		110	GPS
		140	METAR
1	Sea Surface	9	SHIP
		11	SHIP
		13	Automatic SHIP
		19	Reduced SHIP
		21	DRIBU
		22	BATHY
2	Upper Air Sounding	91	Land PILOT
		92	SHIP PILOT
		95	Wind Profiler (American)
		96	Wind Profiler (European/Japanese)
		101	Land TEMP
		102	SHIP TEMPS
		103	DROP TEMP
		104	ROCOB
		105	SHIP ROCOB
		106	Mobile TEMP
		3	Satellite Sounding
51	High Resolution TOVS		
53	RTOVS		
54	ATOVS		
55	ATOVS		
57	ATOVS		
61	Low Level Temperature SATEM		
62	High Level SATEM		
63	PWC SATEM		
65	Merged SATEM		
71	Low Level TOVS		
72	High Level TOVS		
73	PWC TOVS		
75	Merged TOVS		
129	TRMM		
130	TMI		
161	PAOB		
206	OZONE Retrieved Layers		
4	AIREP	142	AIREP
		143	COLBA
		144	AMDAR
		145	ACARS
5	SATOB	82	Temperature and Wind
		83	Wind Only
		84	Temperature only
		85	Temperature only
		86	High Resolution VIS Wind

Table 9.1 *Continued.*

Observation Type		Subtype	
Code	Name	Code	Name
		87	AMV
		89	Geostationary Clear Sky Radiances (GRAD)
		189	Geostationary Clear Sky Radiances (GRAD)
12	SCATT/SSMI	122	ERS-1, ERS-2
		127	SSMI
		136	NSCAT
		137	QSCAT
		139	ASCAT
253	PAOB	161	PAOB

- (i) Wind direction ( $DDD$ ) and force ( $FFF$ ) are transformed into wind components ( $u$  and  $v$ ) for SYNOP, AIREP, SATOB, DRIBU, TEMP and PILOT observations.
- (ii) Temperature ( $T$ ) and dew point ( $Td$ ) are transformed into relative humidity ( $RH$ ) for SYNOP and TEMP observations, with a further transformation of the  $RH$  into specific humidity ( $Q$ ) for TEMP observations.
- (iii) SCATTEROMETER backscatters ( $\sigma^0$ 's) are transformed into several pairs of ambiguous wind components ( $u$  and  $v$ ); this actually involves a retrieval according to some model function describing the relationship between winds and  $\sigma^0$ 's and requires a fair bit of computational work. Details of this procedure are given in [Section 10.5](#).
- (iv) Mean layer temperature is transformed into thickness ( $DZ$ ) for SATEM and TOVS observations.

All these variable transformations, except for the  $\sigma^0$ 's transformation, are more or less trivial ones. The wind components are worked out as

$$u = -FFF \sin\left(DDD \frac{\pi}{180}\right)$$

$$v = -FFF \cos\left(DDD \frac{\pi}{180}\right)$$

The  $RH$  is derived using

$$RH = \frac{F(Td)}{F(T)}$$

where function  $F$  of either  $T$  or  $Td$  is expressed as

$$F(T) = a \frac{R_{\text{dry}}}{R_{\text{vap}}} e^{b \frac{T-T_0}{T-c}}$$

where  $T_0 = 273.16$  K,  $a = 611.21$ ,  $b = 17.502$ ,  $c = 32.19$ ,  $R_{\text{dry}} = 287.0597$  and  $R_{\text{vap}} = 461.5250$  are constants.

The specific humidity  $Q$  is worked out by using

$$Q = RH \frac{A}{1 - RH \left( \frac{R_{\text{vap}}}{R_{\text{dry}}} - 1 \right) A}$$

with function  $A$  is expressed as

$$A = \min \left[ 0.5, \frac{F(T)}{P} \right]$$

where  $P$  is pressure.  $Q$  is assigned in the [RH2Q](#) subroutine.

Table 9.2 ODB observation types and code types.

Observation Type		Code Type	
Code	Name	Code	Name
1	SYNOP	11	Land SYNOP
		14	Automatic Land SYNOP
		16	French RADOME
		21	SHIP
		22	Abbreviated SHIP
		23	SHRED
		24	Automatic SHIP
		140	METAR
		110	GPS
		2	AIREP
141	AIREP		
142	Simulated AIREP		
144	AMDAR		
145	ACARS		
241	COLBA		
3	SATOBS		
		89	High Resolution VIS wind
		90	AMV
		188	SST
4	DRIBU	63	BATHY
		64	TESAC
		160	ERS as DRIBU
		165	DRIBU
5	TEMP	35	Land TEMP
		36	SHIP TEMP
		37	Mobile TEMP
		39	ROCOB
		40	SHIP ROCOB
		135	DROP TEMP
		137	Simulated TEMP
6	PILOT	32	Land PILOT
		33	SHIP PILOT
		34	American Wind Profiler
		131	Japanese Wind Profiler
		132	Mobile Wind Profiler
		134	European Wind Profiler
7	SATEM	86	GTS SATEM
		184	High Resolution Simulated TOVS
		185	High Resolution Simulated DWL SATEM
		186	High Resolution SATEM
		200	GTS BUFR SATEM 250km
		201	GTS BUFR Clear Radiances
		202	GTS BUFR Retrieved Profiles/Clear Radiances
		210	ATOVS/GRAD
		211	RTOVS
		212	TOVS
		215	SSMI

Table 9.2 *Continued.*

Observation Type		Code Type	
Code	Name	Code	Name
8	PAOB	164	PAOB
9	SCATTEROMETER	122	ERS-1, ERS-2
		210	NSCAT
		301	QuikSCAT
		139	ASCAT
10	RAW RADIANCE		

### 9.4.3 Adjusted variables

The only observed quantity which is adjusted is the SYNOP's surface pressure ( $P_s$ ). This is done by using pressure tendency ( $P_t$ ) information, which in turn may be first adjusted.  $P_t$  is adjusted only in the case of SYNOP SHIP data for the ship movement.

The ship movement information is available from input data in terms of ship speed and direction, which are first converted into ship movement components  $U_s$  and  $V_s$ . The next step is to find pressure gradient ( $\partial p/\partial x$  and  $\partial p/\partial y$ ) given by

$$\frac{\partial p}{\partial x} = C(A_1 u - A_2 v) \frac{1}{2}$$

$$\frac{\partial p}{\partial y} = -C(A_1 u + A_2 v)$$

where  $u$  and  $v$  are observed wind components, and  $A_1 = 0.94$  and  $A_2 = 0.34$  are the sine and cosine of the angle between the actual and geostrophic winds.  $C$  is the Coriolis term multiplied by a drag coefficient ( $D$ ) so that

$$C = 2\Omega D \sin \theta$$

where,  $\theta$  is the latitude and  $\Omega = 0.7292 \times 10^{-4} s^{-1}$  is the angular velocity of the earth and  $D$  is expressed as

$$D = GZ$$

$G = 1.25$  is an assumed ratio between geostrophic and surface wind over sea and  $Z = 0.11 \text{ kgm}^{-3}$  is an assumed air density. Now the adjusted pressure tendency ( $P_t^a$ ) is found as

$$P_t^a = P_t - \left( U_s \frac{\partial p}{\partial x} + V_s \frac{\partial p}{\partial y} \right)$$

Finally, the adjusted surface pressure ( $P_s^a$ ) is found as

$$P_s^a = P_s - P_t^a \Delta t$$

where,  $\Delta t$  is a time difference between analysis and observation time. Of course in the case of non-SHIP data  $P_t^a \equiv P_t$ . Subroutine **PTENDCOR** is used for this adjustment.

### 9.4.4 Codes for variables

To provide easy recognition of 'observed' variables each of them is assigned a numerical code. These codes are then embedded in ODB reports. There are 93 codes used so far. These codes are defined in subroutine **SUVNMB**. For the sake of completeness these codes are listed in [Table 9.5](#).

## 9.5 OBSERVATION ERROR STATISTICS

Three types of observation errors are dealt with at the observation pre-processing level.

**Table 9.3** Mapping between ODB and BUFR observation types, code types and subtypes.

ODB (Observation Type, Code Type)	BUFR (Observation Type, Subtype)
ODB(1, 11)	↔ BUFR[(0,1):(0,9)]
ODB(1, 14)	↔ BUFR(0,3)
ODB(1, 21)	↔ BUFR(1,9)
ODB(1, 22)	↔ BUFR(?,?)
ODB(1, 23)	↔ BUFR(1,19)
ODB(1, 24)	↔ BUFR(1,13)
ODB(1,110)	↔ BUFR(0,110)
ODB(1,140)	↔ BUFR(0,140)
ODB(2,41)	↔ BUFR(?,?)
ODB(2,141)	↔ BUFR(4,142)
ODB(2,142)	↔ BUFR(?,?)
ODB(2,144)	↔ BUFR(4,144)
ODB(2,145)	↔ BUFR(4,145)
ODB(2,241)	↔ BUFR(4,143)
ODB(3,88)	↔ BUFR[(5,82):(5,83):(5,84):(5,85)]
ODB(3,89)	↔ BUFR(5,86)
ODB(3,90)	↔ BUFR(5,87)
ODB(3,188)	↔ BUFR(?,?)
ODB(4,63)	↔ BUFR(1,23)
ODB(4,64)	↔ BUFR(1,22)
ODB(4,160)	↔ BUFR(?,?)
ODB(4,165)	↔ BUFR(1,21)
ODB(5,35)	↔ BUFR(2,101)
ODB(5,36)	↔ BUFR(2,102)
ODB(5,37)	↔ BUFR(2,106)
ODB(5,39)	↔ BUFR(2,104)
ODB(5,40)	↔ BUFR(2,105)
ODB(5,135)	↔ BUFR(2,103)
ODB(5,137)	↔ BUFR(?,?)
ODB(6,32)	↔ BUFR(2,91)
ODB(6,33)	↔ BUFR(2,92)
ODB(6,34)	↔ BUFR(2,94)
ODB(6,131)	↔ BUFR(2,95)
ODB(6,134)	↔ BUFR(2,95)
ODB(7,86)	↔ BUFR[(3,61):(3,62):(3,63):(3,65)]
ODB(7,184)	↔ BUFR(?,?)
ODB(7,185)	↔ BUFR(?,?)
ODB(7,186)	↔ BUFR[(3,71):(3,72):(3,73):(3,75)]
ODB(7,200)	↔ BUFR(?,?)
ODB(7,201)	↔ BUFR(?,?)
ODB(7,202)	↔ BUFR(?,?)
ODB(7,206)	↔ BUFR(?,?)
ODB(7,210)	↔ BUFR[(3,54):(5,89)]
ODB(7,211)	↔ BUFR(3,53)
ODB(7,212)	↔ BUFR[(3,0):(3,51)]
ODB(7,215)	↔ BUFR(12,127)
ODB(8,180)	↔ BUFR(253,154)
ODB(9,8)	↔ BUFR(12,8)
ODB(9,122)	↔ BUFR(12,122)
ODB(9,139)	↔ BUFR(12,139)
ODB(9,210)	↔ BUFR(12,136)
ODB(9,301)	↔ BUFR(12,137)
ODB(9,511)	↔ BUFR(?,?)
ODB(10,1)	↔ BUFR(?,?)

**Table 9.4** *Observed variables.*

Observation Type		Observed Variable
BUFR	ODB	
Land Surface	Land SYNOP	Surface Pressure ( $P_s$ ) 10 m Wind Direction/Force ( $DDD/FFF$ ) 2 m Temperature ( $T_{2m}$ ) 2 m Dew Point ( $Td_{2m}$ ) Pressure Tendency ( $P_t$ ) Cloud Information Precipitation Information Snow Depth ( $Sd$ ) Etc.
Sea Surface	SHIP SYNOP, DRIBU	Surface Pressure ( $P_s$ ) 10 m Wind Direction/Force ( $DDD/FFF$ ) 2 m Temperature ( $T_{2m}$ ) 2 m Dew Point ( $Td_{2m}$ ) Etc.
Upper Air Sounding	TEMP, PILOT	10m/Upper Air Wind Direction/Force ( $DDD/FFF$ ) 2m/Upper Air Temperature ( $T_{2m}/T$ ) 2m/Upper Air Dew Point ( $Td_{2m}/Td$ ) Geopotential Height ( $Z$ ) Etc.
Satellite Sounding	SATEM	Mean Layer Temperature Precipitable Water Content ( $PWC$ ) Brightness Temperature ( $Tb$ )
AIREP	AIREP	Upper Air Wind Direction/Force ( $DDD/FFF$ ) Temperature ( $T$ )
SATOB	SATOB	Upper Air Wind Direction/Force ( $DDD/FFF$ ) Brightness Temperature ( $Tb$ )
SCATTEROMETER SSMI	SCATTEROMETER SSMI	Backscatter ( $\sigma^0$ ) Brightness Temperature ( $Tb$ )

- (i) Persistence observation error.
- (ii) Prescribed observation error.
- (iii) Combination of the two above called the final observation error.

### 9.5.1 Persistence observation error

The persistence error is formulated in such a way to reflect its dependence on the following.

- (i) Season.
- (ii) Actual geographical position of an observation.

Seasonal dependency is introduced by identifying three regimes.

- (i) Winter hemisphere.
- (ii) Summer hemisphere.
- (iii) Tropics.

The positional dependency is then introduced to reflect the dependence on the precise latitude within these three regimes.

Table 9.5 Numbering of variables in the ODB.

No.	Code	Name	Unit
1	3	Wind Component ( $u$ )	$\text{ms}^{-1}$
2	4	Wind Component ( $v$ )	$\text{ms}^{-1}$
3	1	Geopotential ( $Z$ )	$\text{m}^2\text{s}^{-2}$
4	57	Thickness ( $DZ$ )	$\text{m}^2\text{s}^{-2}$
5	29	Relative Humidity ( $RH$ )	numeric
6	9	Precipitable Water Content ( $PWC$ )	$\text{kgm}^{-2}$
7	58	2 m Relative Humidity ( $RH_{2\text{m}}$ )	numeric
8	2	Temperature	K
9	59	Dew Point	K
10	39	2 m Temperature ( $T_{2\text{m}}$ )	K
11	40	2 m Dew Point ( $Td_{2\text{m}}$ )	K
12	11	Surface Temperature ( $T_s$ )	K
13	30	Pressure Tendency ( $P_t$ )	Pa/3h
14	60	Past Weather ( $W$ )	WMO Code 4561
15	61	Present Weather ( $WW$ )	WMO Code 4677
16	62	Visibility ( $V$ )	WMO Code 4300
17	63	Type of High Clouds ( $C_H$ )	WMO Code 0509
18	64	Type of Middle Clouds ( $C_M$ )	WMO Code 0515
19	65	Type of Low Clouds ( $C_L$ )	WMO Code 0513
20	66	Cloud Base Height ( $N_h$ )	m
21	67	Low Cloud Amount ( $N$ )	WMO Code 2700
22	68	Additional Cloud Group Height ( $h_s h_s$ )	m
23	69	Additional Cloud Group Type ( $C$ )	WMO Code 0500
24	70	Additional Cloud Group Amount ( $N_s$ )	WMO Code 2700
25	71	Snow Depth ( $Sd$ )	m
26	72	State of Ground ( $E$ )	WMO Code 0901
27	73	Ground Temperature ( $T_g T_g$ )	K
28	74	Special Phenomena ( $S_p S_p$ )	WMO Code 3778
29	75	Special Phenomena ( $s_p s_p$ )	WMO Code 3778
30	76	Ice Code Type ( $R_s$ )	WMO Code 3551
31	77	Ice Thickness ( $E_s E_s$ )	WMO Code 1751
32	78	Ice ( $I_s$ )	WMO Code 1751
33	79	Time Period of Rain Information ( $t_r t_r$ )	hour
34	80	6 Hour Rain Amount	$\text{kgm}^{-2}$
35	81	Maximum Temperature ( $JJ$ )	K
36	82	Ship Speed ( $V_s$ )	$\text{ms}^{-1}$
37	83	Ship Direction ( $D_s$ )	degree
38	84	Wave Height ( $H_w H_w$ )	m
39	85	Wave Period ( $P_w P_w$ )	s
40	86	Wave Direction ( $D_w D_w$ )	degree
41	87	General Cloud Group	WMO Code
42	88	Relative Humidity from Low Clouds	numeric
43	89	Relative Humidity from Middle Clouds	numeric
44	90	Relative Humidity from High Clouds	numeric
45	91	Total Amount of Clouds	WMO Code 20011
46	92	6 Hour Snowfall	m
47	110	Surface Pressure ( $P_s$ )	Pa
48	111	Wind Direction	degree
49	112	Wind Force	$\text{ms}^{-1}$
50	119	Brightness Temperature ( $Tb$ )	K
51	120	Raw Radiance	K

Table 9.5 *Continued.*

No.	Code	Name	Unit
52	121	Cloud Amount from Satellite	%
53	122	Backscatter ( $\sigma^0$ )	dB
54	5	Wind Shear ( $\partial u/\partial z$ )	$s^{-1}$
55	6	Wind Shear ( $\partial v/\partial z$ )	$s^{-1}$
56	41	$u_{10m}$	$ms^{-1}$
57	42	$v_{10m}$	$ms^{-1}$
58	19	Layer Relative Humidity	numeric
59	200	Auxiliary Variable	numeric
60	123	Cloud Liquid Water ( $Q_l$ )	$kgkg^{-1}$
61	124	Ambiguous v	$ms^{-1}$
62	125	Ambiguous u	$ms^{-1}$
63	7	Specific Humidity ( $Q$ )	$kgkg^{-1}$
64	126	Ambiguous Wind Direction	degree
65	127	Ambiguous Wind Speed	$ms^{-1}$
66	8	Vertical Speed	$ms^{-1}$
67	56	Virtual Temperature ( $Tv$ )	K
68	206	Ozone	Dobson
69	156	Height	m
70	215	SSM/I Pseudo Variable	$kgm^{-2}$
71	160	Past Weather	numeric
72	130	Pressure Tendency Characteristics	numeric
73	12	Sea Water Temperature	K
74	192	Radar Reflectivity	Db
75	128	Atmospheric Path Delay in Satellite Signal	m
76	162	Radio Occultation Bending Angle	Rad
77	187	Horizontal line-of-sight wind component	$ms^{-1}$
78	174	Aerosol optical depth at 0.55 microns (AOD)	
79	163	Limb Radiances	
80	181	GEMS reactive gases, N02	
81	182	GEMS reactive gases, S02	
82	183	GEMS reactive gases, CO	
83	184	GEMS reactive gases	
84	185	GEMS reactive gases, G03	
85	175	Cloud optical depth (COD)	
86	176	Ratio of fine mode to total aerosol optical depth at 0.55 microns (RAO)	
87	177	Aerosol reflectance multi-channel (RFA)	
88	178	Aerosol optical depth multi-channel (ODA)	
89	179	Normalized Soil Moisture	0-100%
90	180	Soil Moisture	$kg^3kg^{-3}$
91	186	GHG	
92	187	GHG	
93	195	Radar doppler wind	



**Table 9.6** Observation persistence errors of maximum 24-hour wind ( $u, v$ ), height ( $Z$ ) and temperature ( $T$ ).

Variable (unit)	1000–700 hPa	699–250 hPa	249–0 hPa
$u, v$ ( $\text{ms}^{-1}$ )	6.4	12.7	19.1
$Z$ (m)	48	60	72
$T$ (K)	6	7	8

The persistence error calculation is split into two parts. In the first part the above dependencies are expressed in terms of factors  $a$  and  $b$  which are defined as

$$a = \sin\left(2\pi\frac{d}{365.25} + \frac{\pi}{2}\right)$$

and

$$b = 1.5 + a\left\{0.5 \min\left[\frac{\max(\theta, 20)}{20}\right]\right\}$$

where  $d$  is a day of year and  $\theta$  is latitude.

The persistence error for time difference between analysis and observation  $\Delta t$  is then expressed as a function of  $b$  with a further dependence on latitude and a maximum persistence error  $E_{\text{maxpers}}$  for 24 hour given by

$$E_{\text{pers}} = \frac{E_{\text{maxpers}}}{6} [1 + 2 \sin(|2\theta|b\Delta t)]$$

where  $\Delta t$  is expressed as a fraction of a day. The  $E_{\text{maxpers}}$  have the values shown in [Table 9.6](#).

Subroutine **SUPERERR** is used to define all relevant points in order to carry out this calculation, and is called only once during the general system initialization. The calculation of the actual persistence error is dealt with by **OBSPERR**.

### 9.5.2 Prescribed observation errors

Prescribed observational errors have been derived by statistical evaluation of the performance of the observing systems, as components of the assimilation system, over a long period of operational use. The prescribed observational errors are given in the [Tables 9.7, 9.8](#) and [9.9](#). Currently, observational errors are defined for each observation type that carries the following quantities.

- (i) Wind components.
- (ii) Height.
- (iii) Temperature.
- (iv) Humidity.

As can be seen from the tables of prescribed observation errors, they are defined at standard pressure levels but the ones used are interpolated to the observed pressures. The interpolation is such that the observation error is kept constant below the lowest and above the highest levels, whereas in between it is interpolated linearly in  $\ln p$ . Several subroutines are used for working out the prescribed observation error: **SUOBSERR**, **OBSERR**, **FIXERR**, **THIOERR** and **PWCOERR**.

- **SUOBSERR** defines observation errors for standard pressure levels.
- **OBSERR** and **FIXERR** calculate the actual values.
- **THIOERR** and **PWCOERR** are two specialised subroutines to deal with thickness and PWC errors.

Relative humidity observation error  $RH_{\text{err}}$  is either prescribed or modelled. More will be said about the modelled  $RH_{\text{err}}$  in [Subsection 9.5.3](#).  $RH_{\text{err}}$  is prescribed only for TEMP and SYNOP data.  $RH_{\text{err}}$  is preset to 0.17 for TEMP and 0.13 for SYNOP. However, if  $RH < 0.2$  it is increased to 0.23 and to 0.28 if  $T < 233$  K for both TEMP and SYNOP.

Table 9.7 Prescribed RMS observation errors for the  $u$  and  $v$  wind components ( $\text{ms}^{-1}$ ).

R RAD	SCATT		PAOB		SATEM		PILOT		TEMP		DRIBU		SATOB		AIREP		SYNOP		Obs Type		
	All	Default	All	ASCAT	All	ASCAT	All	ASCAT	All	ASCAT	All	ASCAT	All	ASCAT	All	ASCAT	All	ASCAT	All	ASCAT	Code Type
n/a	2.00	1.50	n/a	n/a	n/a	n/a	1.80	1.80	1.80	1.80	1.80	1.80	2.00	2.00	2.86	2.46	3.00	1000	1000	Code Type	Levels (hPa)
n/a	2.00	1.50	n/a	n/a	n/a	n/a	1.80	1.80	1.80	1.80	1.80	1.80	2.00	2.00	2.91	2.51	3.00	850	850	Code Type	Levels (hPa)
n/a	2.00	1.50	n/a	n/a	n/a	n/a	1.90	1.90	1.90	1.90	1.80	1.80	2.00	2.00	2.96	2.56	3.00	700	700	Code Type	Levels (hPa)
n/a	2.00	1.50	n/a	n/a	n/a	n/a	2.10	2.10	2.10	2.10	1.80	1.80	3.50	3.50	3.11	2.71	3.40	500	500	Code Type	Levels (hPa)
n/a	2.00	1.50	n/a	n/a	n/a	n/a	2.50	2.50	2.50	2.50	1.80	1.80	4.30	4.30	3.21	2.81	3.60	400	400	Code Type	Levels (hPa)
n/a	2.00	1.50	n/a	n/a	n/a	n/a	2.60	2.60	2.60	2.60	1.80	1.80	5.00	5.00	3.26	2.86	3.80	300	300	Code Type	Levels (hPa)
n/a	2.00	1.50	n/a	n/a	n/a	n/a	2.50	2.50	2.50	2.50	1.80	1.80	5.00	5.00	3.31	2.91	3.20	250	250	Code Type	Levels (hPa)
n/a	2.00	1.50	n/a	n/a	n/a	n/a	2.50	2.50	2.50	2.50	1.80	1.80	5.00	5.00	3.36	2.96	3.20	200	200	Code Type	Levels (hPa)
n/a	2.00	1.50	n/a	n/a	n/a	n/a	2.40	2.40	2.40	2.40	1.80	1.80	5.00	5.00	3.31	2.91	2.40	150	150	Code Type	Levels (hPa)
n/a	2.00	1.50	n/a	n/a	n/a	n/a	2.20	2.20	2.20	2.20	1.80	1.80	5.00	5.00	3.16	2.76	2.20	100	100	Code Type	Levels (hPa)
n/a	2.00	1.50	n/a	n/a	n/a	n/a	2.10	2.10	2.10	2.10	1.80	1.80	5.00	5.00	3.06	2.66	2.00	70	70	Code Type	Levels (hPa)
n/a	2.00	1.50	n/a	n/a	n/a	n/a	2.00	2.00	2.00	2.00	1.80	1.80	5.00	5.00	3.06	2.66	2.00	50	50	Code Type	Levels (hPa)
n/a	2.00	1.50	n/a	n/a	n/a	n/a	2.10	2.10	2.10	2.10	1.80	1.80	5.00	5.00	3.26	2.86	2.00	30	30	Code Type	Levels (hPa)
n/a	2.00	1.50	n/a	n/a	n/a	n/a	2.30	2.30	2.30	2.30	1.80	1.80	5.00	5.00	3.46	3.06	2.50	20	20	Code Type	Levels (hPa)
n/a	2.00	1.50	n/a	n/a	n/a	n/a	3.00	3.00	3.00	3.00	1.80	1.80	5.70	5.70	3.76	3.36	3.00	10	10	Code Type	Levels (hPa)

Table 9.8 Prescribed RMS height observation errors ( $m$ ).

		SYNOP												Observation Type			
		AIREP				Manual SHIP				Automatic SHIP				Manual Land		Code Type	
R	AD	PAOB	SATEM	PILOT	TEMP	DRIBU	SATOB	AI	AI	SHIP	SHIP	SHIP	SHIP	Land	Land	Levels (hPa)	
All	All	All	All	All	All	All	All	All	All	All	All	All	All	All	All	All	
n/a	n/a	24.0	n/a	4.3	4.3	4.97	n/a	n/a	n/a	4.2	4.2	7.1	7.1	4.2	5.6	1000	
n/a	n/a	24.0	n/a	4.4	4.4	4.97	n/a	n/a	n/a	4.2	4.2	7.1	7.1	5.4	7.2	850	
n/a	n/a	24.0	n/a	5.2	5.2	4.97	n/a	n/a	n/a	4.2	4.2	7.1	7.1	6.45	8.6	700	
n/a	n/a	24.0	n/a	8.4	8.4	4.97	n/a	n/a	n/a	4.2	4.2	7.1	7.1	9.07	12.1	500	
n/a	n/a	24.0	n/a	9.8	9.8	4.97	n/a	n/a	n/a	4.2	4.2	7.1	7.1	11.17	14.9	400	
n/a	n/a	24.0	n/a	10.7	10.7	4.97	n/a	n/a	n/a	4.2	4.2	7.1	7.1	14.1	18.8	300	
n/a	n/a	24.0	n/a	11.8	11.8	4.97	n/a	n/a	n/a	4.2	4.2	7.1	7.1	19.05	25.4	250	
n/a	n/a	24.0	n/a	13.2	13.2	4.97	n/a	n/a	n/a	4.2	4.2	7.1	7.1	20.77	27.7	200	
n/a	n/a	24.0	n/a	15.2	15.2	4.97	n/a	n/a	n/a	4.2	4.2	7.1	7.1	24.3	32.4	150	
n/a	n/a	24.0	n/a	18.1	18.1	4.97	n/a	n/a	n/a	4.2	4.2	7.1	7.1	29.55	39.4	100	
n/a	n/a	24.0	n/a	19.5	19.5	4.97	n/a	n/a	n/a	4.2	4.2	7.1	7.1	37.72	50.3	70	
n/a	n/a	24.0	n/a	22.5	22.5	4.97	n/a	n/a	n/a	4.2	4.2	7.1	7.1	44.47	59.3	50	
n/a	n/a	24.0	n/a	25.0	25.0	4.97	n/a	n/a	n/a	4.2	4.2	7.1	7.1	52.35	69.8	30	
n/a	n/a	24.0	n/a	32.0	32.0	4.97	n/a	n/a	n/a	4.2	4.2	7.1	7.1	72.0	96.0	20	
n/a	n/a	24.0	n/a	40.0	40.0	4.97	n/a	n/a	n/a	4.2	4.2	7.1	7.1	85.65	114.2	10	

Table 9.9 Prescribed RMS temperature observations error (K).

R RAD SCATT		PAOB		SATEM		PILOT		TEMP		DRIBU		SATOB		AIREP				SYNOP		Observation Type	
		All		All		All		All		All		All		All but		SHIP	Land	Code Type	Code Type		
		All	All	All	All	All	All	All	All	All	All	All	All	All	All					SHIP	Land
n/a	n/a	n/a	n/a	n/a	n/a	n/a	n/a	1.40	1.40	1.8	n/a	n/a	n/a	1.40	1.65	1.8	2.0	1000	Levels (hPa)		
n/a	n/a	n/a	n/a	n/a	n/a	n/a	n/a	1.25	1.25	1.5	n/a	n/a	n/a	1.18	1.43	1.8	1.5	850			
n/a	n/a	n/a	n/a	n/a	n/a	n/a	n/a	1.10	1.10	1.3	n/a	n/a	n/a	1.00	1.25	1.8	1.3	700			
n/a	n/a	n/a	n/a	n/a	n/a	n/a	n/a	0.95	0.95	1.2	n/a	n/a	n/a	0.98	1.23	1.8	1.2	500			
n/a	n/a	n/a	n/a	n/a	n/a	n/a	n/a	0.90	0.90	1.3	n/a	n/a	n/a	0.96	1.21	1.8	1.3	400			
n/a	n/a	n/a	n/a	n/a	n/a	n/a	n/a	1.00	1.00	1.5	n/a	n/a	n/a	0.05	1.20	1.8	1.5	300			
n/a	n/a	n/a	n/a	n/a	n/a	n/a	n/a	1.15	1.15	1.8	n/a	n/a	n/a	0.95	1.20	1.8	1.8	250			
n/a	n/a	n/a	n/a	n/a	n/a	n/a	n/a	1.20	1.20	1.8	n/a	n/a	n/a	1.06	1.31	1.8	1.8	200			
n/a	n/a	n/a	n/a	n/a	n/a	n/a	n/a	1.25	1.25	1.9	n/a	n/a	n/a	1.18	1.43	1.8	1.9	150			
n/a	n/a	n/a	n/a	n/a	n/a	n/a	n/a	1.30	1.30	2.0	n/a	n/a	n/a	1.30	1.55	1.8	2.0	100			
n/a	n/a	n/a	n/a	n/a	n/a	n/a	n/a	1.40	1.40	2.2	n/a	n/a	n/a	1.40	1.65	1.8	2.2	70			
n/a	n/a	n/a	n/a	n/a	n/a	n/a	n/a	1.40	1.40	2.4	n/a	n/a	n/a	1.50	1.75	1.8	2.4	50			
n/a	n/a	n/a	n/a	n/a	n/a	n/a	n/a	1.40	1.40	2.5	n/a	n/a	n/a	1.60	1.85	1.8	2.5	30			
n/a	n/a	n/a	n/a	n/a	n/a	n/a	n/a	1.50	1.50	2.5	n/a	n/a	n/a	1.80	2.05	1.8	2.5	20			
n/a	n/a	n/a	n/a	n/a	n/a	n/a	n/a	2.10	2.10	2.5	n/a	n/a	n/a	2.10	2.35	1.8	2.5	10			

### 9.5.3 Derived observation errors

Relative humidity observation error,  $RH_{\text{err}}$ , can also be expressed as function of temperature  $T$  so that

$$RH_{\text{err}} = \min[0.18, \min(0.06, -0.0015T + 0.54)]$$

This option is currently used for assigning  $RH_{\text{err}}$ .

Specific humidity observation error,  $Q_{\text{err}}$ , is a function of  $RH$ ,  $RH_{\text{err}}$ ,  $P$ ,  $P_{\text{err}}$ ,  $T$  and  $T_{\text{err}}$ , and formally can be expressed as

$$Q_{\text{err}} = Q_{\text{err}}(RH, RH_{\text{err}}, P, P_{\text{err}}, T, T_{\text{err}})$$

or

$$Q_{\text{err}} = RH_{\text{err}} F_1(RH, P, T) + \frac{RH P_{\text{err}}}{P} F_2(RH, P, T) + RH T_{\text{err}}(RH, P, T)$$

where functions  $F_1$ ,  $F_2$  and  $F_3$  are given by

$$F_1(RH, T, P) = \frac{A}{\left[1 - RH \left(\frac{R_{\text{vap}}}{R_{\text{dry}}} - 1\right) A\right]^2}$$

$$F_2(RH, T, P) = \frac{\left\{ \left[1 - RH \left(\frac{R_{\text{vap}}}{R_{\text{dry}}} - 1\right) A\right] + \left(\frac{R_{\text{vap}}}{R_{\text{dry}}} - 1\right) A \right\}}{\left[1 - RH \left(\frac{R_{\text{vap}}}{R_{\text{dry}}} - 1\right) A\right]^2}$$

$$F_3(RH, T, P) = \frac{Ab(T_0 - c)}{(T - c)^2} \left\{ \left[1 - \left(\frac{R_{\text{vap}}}{R_{\text{dry}}} - 1\right) A\right] RH A \left(\frac{R_{\text{vap}}}{R_{\text{dry}}} - 1\right) \right\}$$

At present only the first term of the above expression for  $Q_{\text{err}}$  is taken into account (dependency on relative humidity). Subroutine **RH2Q** is used to evaluate  $Q_{\text{err}}$ .

Surface pressure observation error  $Ps_{\text{err}}$  is derived by multiplying the height observation error  $Z_{\text{err}}$  by a constant:

$$Ps_{\text{err}} = 1.225 Z_{\text{err}}$$

However, the  $Ps_{\text{err}}$  may be reduced if the pressure tendency correction is applied. For non-SHIP data the reduction factor is 4, whereas for SHIP data the reduction factor is either 2 or 4, depending on if the  $P_t$  is adjusted for SHIP movement or not.

The thickness observation error ( $DZ_{\text{err}}$ ) is derived from  $Z_{\text{err}}$ .

### 9.5.4 Final (combined) observation error

In addition to the prescribed observation and persistence errors, the so called final observation error is assigned at this stage too. This is simply a combination of observation and persistence errors given by

$$F_{\text{OE}} = \sqrt{O_{\text{E}}^2 + P_{\text{E}}^2}$$

where  $F_{\text{OE}}$ ,  $O_{\text{E}}$  and  $P_{\text{E}}$  are final, prescribed and persistence observation errors, respectively. The subroutine used for this purpose is **FINOERR**.

### 9.5.5 Overview over METEOSAT and GEOS imager CSR in the ECMWF archives

[Table 9.10](#) gives a short summary of the CSR data stored at ECMWF either in MARS or in ECFS, including the BUFR subtype of the data. For more information on the actual content of the data see BUFR templates, bearing in mind that not all data items which can be encoded according to the CSR BUFR template are actually always provided (i.e. missing values). Incoming data from Meteosat and GOES are currently recoded into one BUFR format being the interface to observation processing and assimilation in IFS. This BUFR was originally designed for the Meteosat CSR. For the GOES data, not all information from the original BUFR can be retained in this BUFR and a change may be therefore useful once the incoming GOES data are encoded in the agreed common BUFR format, using descriptor 301023.

**Table 9.10** *ECMWF METEOSAT and GEOS CSR archives.*

Satellite	Time Period	Data Type	BUFR Subtype	Location
METEOSAT-5 METEOSAT-6 METEOSAT-7	15/05/1996 To ??/05/1997	Geostationary radiances, 32 × 32 pixel segments, 4 times daily	88	MARS
METEOSAT-5 METEOSAT-6 METEOSAT-7	02/05/1997 To 14/01/2002	Geostationary radiances, 32 × 32 pixel segments, Hourly	88	MARS
METEOSAT-5 METEOSAT-6 METEOSAT-7	Since 25/01/1999	Geostationary clear-sky radiances, 16 × 16 pixel segments, hourly Including clear and cloudy sky fractions	89	MARS
METEOSAT-2 METEOSAT-3	Periods for ERA	Geostationary clear-sky radiances (as above)	89	ECFS <sup>(1)</sup>
GEOS-8 GEOS-10	Since 24/10/2001	Clear sky brightness temperatures, 11 × 17 pixel segments, hourly, Including clear and cloudy sky fractions	89 and original BUFR formats Several changes	ECFS <sup>(2)</sup>
GOES-8 GOES-10	Since 09/04/2002	Clear sky brightness temperatures, 11 × 17 pixel segments, hourly, Including clear and cloudy sky fractions	89 And original BUFR formats Several changes	MARS original data on ECFS <sup>(2)</sup>

ECFS<sup>(1)</sup>: ec:/ERA/era40/obs/bufr/EUM\_reproc/\$yyyy/\$mm/CSR\${yyyymmddhh}  
 ECFS<sup>(2)</sup>: ec:/oparch/gicsbt/\$yyyymm/\$dd/gicsbt..

### 9.5.6 Thinning and screening prior to insertion into the assimilation

In order to reduce the data load of the hourly CSR data, the data are screened in a separate task before insertion into assimilation (IFS). This is done by the program **GEOS.PRESCREEN** (**SATRAD** library). It decodes the BUFR and applies basic checks on latitude, longitude, time values, and on brightness temperatures being within a physical range. Also, data points are rejected where the value for the water vapour channel brightness temperature is missing. Based on specifications given through namelist input, a geographical thinning may (or may not) be applied for each individual satellite. If switched on, the thinning is performed separately for data falling into hourly timeslots. An overview of the number of remaining valid data points per hour and satellite is printed and the remaining data are encoded into BUFR using the same format as the input file.

## 9.6 DEFINITIONS

### 9.6.1 Observation characteristics: instrument specification and retrieval type

Tables 9.11 to 9.19 describe in details how the ODB's instrument specification word is structured. Tables provided are for different observation types.

In Table 9.20 the ODB's header retrieval word codes are described.

### 9.6.2 Vertical coordinate: pressure, satellite ID and level ID codes

In the ODB the vertical coordinate is expressed by various codes, and Table 9.21 describes those codes.

**Table 9.11** *SYNOP instrument specification.*

Type	Bit Position	No. of Bits	Value – Description
Instrument Specification	0	10	32 – SYNOP Instrument Code Type
Not Defined	10–30	21	Reserved

**Table 9.12** *AIREP instrument specification.*

Type	Bit Position	No. of Bits	Value – Description
Instrument Specification	0	10	23 – AIREP Instrument Code Type
Flight Information	10	4	BUFR Code Table 8004 – Flight Phase
Not Defined	10–30	21	Reserved

**Table 9.13** *SATOB instrument specification.*

Type	Bit Position	No. of Bits	Value – Description
Instrument Specification	0	10	60 – GOES 62 – METEOSAT 63 – Indian SATOB 68 – Japan
I1 (Country Name)	10	4	0 – Europe 1 – Japan 2 – USA 3 – USSR 4 – India
I2I2 (Satellite Indicator Figure)	14	8	4 – METEOSAT 177 – Pretoria 0 – GEOS 3 – Japan 20 – India
Not Defined	22–30	8	Reserved

**Table 9.14** *DRIBU instrument specification.*

Type	Bit Position	No. of Bits	Value – Description
Instrument Specification	0	10	Not Defined
K1	10	4	Not Defined
K2	14	4	Not Defined
K3	18	4	Not Defined
Not Defined	22–30	8	Reserved

**Table 9.15** *TEMP instrument specification.*

Type	Bit Position	No. of Bits	Value – Description
Instrument Specification	0	10	Not Defined
Not Defined	10–30	21	Reserved

**Table 9.16** *PILOT instrument specification.*

Type	Bit Position	No. of Bits	Value – Description
Instrument Specification	0	10	Not Defined
A4	10	4	Not Defined
Not Defined	14–30	17	Reserved

**Table 9.17** *SATEM instrument specification.*

Type	Bit Position	No. of Bits	Value – Description
Instrument Specification	0	23	77 777 777B
I3	24	4	WMO Manual On Codes, vol II, section II-4-E-8
I4	28	4	Data processing technique. WMO Manual On Codes, vol II, section II-4-E-9
I2I2	32	7	Satellite name. WMO Manual on Codes, vol II, section II-4-E-7
I1	39	4	Country operating satellite. WMO code 1761
IS	43	7	Instrument specification code. Research Manual 5, Table 7.5
Not Defined	50	18	Reserved

Also, the ODB pressure code word is expressed in terms of codes which are defined in [Table 9.22](#).

Each satellite used in the assimilation has its identification attached to it. The satellite identification codes used are described in [Table 9.23](#).

Upper air observations (TEMP and PILOT) have the level at which the observation was taken defined in terms of what it is and that information is stored in the ODB. Details are given in [Table 9.24](#).

### 9.6.3 ODB report status: events, flags and codes

The status of each ODB report is described in terms of being active, passive, rejected or blacklisted. The ODB report status word is packed with the 4 bits given in [Table 9.25](#).

There is one, 31 bits packed, word for each ODB report to account for various blacklist events. Details are given in [Table 9.26](#).

Each ODB report has two words to store report events. Each report event word uses 31 bits. These events are set during observation processing to describe in more details what happened with a report.

The first ODB report event word is described in [Table 9.27](#).

The second ODB report event word holds an additional set of events which are now dependent on observation type. Details are given in [Tables 9.28 to 9.37](#).



**Table 9.18** *TOVS instrument specification.*

Type	Bit Position	No. of Bits	Value – Description
Instrument Specification	0	10	
A	10	2	0 – No HIRS/2 Data 1 – Clear Radiances are Derived from Clear Spots 2 – Clear Radiances are Derived from the N* method
B	12	2	0 – No HIRS/2 Data 1 – All HIRS/2 channels were used 2 – Tropospheric HIRS/2 channels were unusable due to clouds and only stratospheric channels were used
C	14	2	0 – Statistical retrieval method used 1 – Minimum information retrieval used 2 – Minimum information retrieval attempted but statistical retrieval used
V	16	3	0 – No retrieval 1 – HIRS+MSU 2 – HIRS
W	19	3	0 – No retrieval 1 – HIRS+MSU 2 – HIRS
X	22	3	0 – No retrieval 1 – HIRS(1, 2, 3, 8, 9, 16, 17)+MSU(4) 2 – HIRS(1, 2, 3, 8, 9, 16, 17) 3 – HIRS(1, 2, 3, 9, 17)+MSU(4) 4 – HIRS(1, 2, 3, 9, 17)
Y	25	3	0 – No retrieval 1 – HIRS+SSU+MSU(3, 4) 2 – HIRS+MSU(3, 4) 3 – SSU+MSU(3, 4)
Z	28	3	Not Defined
Not Defined	31	1	Reserved

**Table 9.19** *SSMI instrument specification.*

Type	Bit Position	No. of Bits	Value – Description
Instrument Specification	0	10	Not defined
Not Defined	10–31	22	Reserved

**Table 9.20** *Satellite retrieval codes.*

Retrieval Codes	Description
1	Clear
2	Partly Clear
3	Cloudy

**Table 9.21** *Vertical coordinate.*

Vertical Coordinate Codes	Description
1	Pressure (Pa)
2	Height (GPM)
3	Satellite Channel (numeric)
4	Scatterometer Channel (numeric)

**Table 9.22** *Pressure codes.*

Pressure Codes	Description
0	Sea Level
1	Station Level
2	850 hPa Geopotential
3	700 hPa Geopotential
4	500 hPa Geopotential
5	1000 GPM Pressure
6	2000 GPM Pressure
7	3000 GPM Pressure
8	4000 GPM Pressure
9	900 hPa Geopotential
10	1000 hPa Geopotential
11	500 hPa Geopotential
12	925 hPa Geopotential

**Table 9.23** *Satellite IDs.*

Satellite ID Codes	Description
208/906	NOAA10 – TOVS
235	NOAA10 – SATEM
201/907	NOAA11 – TOVS
236	NOAA11 – SATEM
202/908	NOAA12 – TOVS
237	NOAA12 – SATEM
??*/909	NOAA13 – TOVS
206/910	NOAA14 – TOVS
239	NOAA14 – SATEM
205/911	NOAA15
207	NOAA16
208	NOAA17
209	NOAA18
210	NOAA19
222	NOAA20
202/241	DMSP8
203/242	DMSP9
204/243	DMSP10
205/244	DMSP11
245	DMSP12
246	DMSP13
247	DMSP14
248	DMSP15
1022	DMSP16

Table 9.24 *Level ID.*

Bit Position	No. of Bits	Value – Description
0	1	1 – Max Wind Level
1	1	1 – Tropopause
2	1	1 – D Part
3	1	1 – C Part
4	1	1 – B Part
5	1	1 – A Part
6	1	1 – Surface Level
7	1	1 – Significant Wind Level
8	1	1 – Significant Temperature Level
9–31	24	Not Defined

Table 9.25 *Report Status.*

Bit Position	No. of Bits	Value – Description
0	1	1 – Report Active
1	1	1 – Passive Report
2	1	1 – Rejected Report
3	1	1 – Blacklisted Report

Table 9.26 *Blacklist Events.*

Bit Position	No. of Bits	Value – Description
0	1	1 – Monthly Monitoring
1	1	1 – Constant Blacklisting
2	1	1 – Experimental Blacklisting
3	1	1 – Whitelisting
4	1	1 – Experimental Whitelisting
5	1	1 – Observation Type Blacklisting
6	1	1 – Station ID Blacklisted
7	1	1 – Code Type Blacklisted
8	1	1 – Instrument Type Blacklisted
9	1	1 – Date Blacklisted
10	1	1 – Time Blacklisted
11	1	1 – Latitude Blacklisted
12	1	1 – Longitude Blacklisted
13	1	1 – Station Altitude Blacklisted
14	1	1 – Blacklisted due to Land/Sea Mask
15	1	1 – Blacklisted due to Model Orography
16	1	1 – Blacklisted due to distance from reference point
17–30	14	Not Used

**Table 9.27** *Global report events.*

Bit Position	No. of Bits	Description (Value)
0	1	1 – No Data in Report
1	1	1 – All Data Rejected
2	1	1 – Bad Reporting Practice
3	1	1 – Rejected due to RDB Flag
4	1	1 – Activated due to RDB Flag
5	1	1 - Activated by Whitelist
6	1	1 – Horizontal Position out of Range
7	1	1 – Vertical Position out of Range
8	1	1 – Time out of Range
9	1	1 – Redundant Report
10	1	1 – Over Land
11	1	1 – Over Sea
12	1	1 – Missing Station Altitude
13	1	1 – Model Surface too far from Station level
14	1	1 – Report Rejected via Namelist
15	1	1 – Failed Q/C
16–30	15	Not Used

**Table 9.28** *SYNOP report events.*

Bit Position	No. of Bits	Value – Description
0–30	31	Not Used

**Table 9.29** *AIREP report events.*

Bit Position	No. of Bits	Value – Description
0–30	31	Not Used

**Table 9.30** *SATOB report events.*

Bit Position	No. of Bits	Value – Description
0–30	31	Not Used

**Table 9.31** *DRIBU report events.*

Bit Position	No. of Bits	Value – Description
0–30	31	Not Used

**Table 9.32** *TEMP report events.*

Bit Position	No. of Bits	Value – Description
0	1	1 - Old Style Z Bias Correction Applied
1	1	1 - New Style T Bias Correction Applied
2	1	1 - RH Bias Correction Applied
3–30	28	Not Used

**Table 9.33** *PILOT* report events.

Bit Position	No. of Bits	Value – Description
0	1	1 - American Wind Profiler
1	1	1 - European Wind Profiler
2–30	29	Not Used

**Table 9.34** *SATEM* report events.

Bit Position	No. of Bits	Value – Description
0	1	1 - Thinned Report
1–30	30	Not Used

**Table 9.35** *PAOB* report events.

Bit Position	No. of Bits	Value – Description
0–30	31	Not Used

**Table 9.36** *SCAT* report events.

Bit Position	No. of Bits	Value – Description
0	1	1 - Report thinned in across-node direction
1	1	1 - Reported Wind Directions too Close
2	1	1 - Report in QuikScat outer swath
3	1	1 - Report Contaminated by Rain
4–30	29	Not Used

**Table 9.37** *Raw radiance* report events.

Bit Position	No. of Bits	Value – Description
0–30	31	Not Used

The ODB report RDB flag word is 30 bits packed which contains flags for five report parameters: latitude, longitude, date, time and altitude. Each parameter occupies 6 bits with further stratification which is identical for every parameter as indicated in [Table 9.38](#).

#### 9.6.4 Datum status: events, RDB and analysis flags

The status of each datum, like report status, is described in terms of being: active, passive, rejected or blacklisted. [Table 9.39](#) shows that the ODB datum status is a packed word with 4 bits used to describe its status.

There are two ODB words reserved for datum events. They both use 31 bits each to store relevant information. The first event word has the same structure for all observation types, whereas the second event word is observation type dependent. [Tables 9.40](#) to [9.50](#) describe the event words structures.

Furthermore, each datum in the ODB has a blacklist event word. This word uses 31 bits to describe various blacklist events as indicated in [Table 9.51](#).

**Table 9.38** *RDB report (latitude, longitude, date, time and altitude) flags.*

Parameter	No. of Bits	Bit Position	Bit Position	No. of Bits	Value – Description		
			0	1	0 – No Human Monitoring Substitution 1 – Human Monitoring Substitution		
Latitude	6	0+	+1	1	0 – No Q/C Substitution 1 – Q/C Substitution		
Longitude	6	6+					
Date	6	12+	+2	1	0 – Override Flag not Set 1 – Override Flag Set		
Time	6	18+					
Altitude	6	24+	+3	2	0 – Parameter Correct 1 – Parameter Probably Correct 2 – Parameter Probably Incorrect 3 – Parameter Incorrect		
					+5	1	0 – Parameter Flag Set by Q/C or not Checked 1 – Parameter Flag Set by Human Monitoring

**Table 9.39** *Datum status.*

Bit Position	No. of Bits	Value – Description
0	1	1 – Report Active
1	1	1 – Passive Report
2	1	1 – Rejected Report
3	1	1 – Blacklisted Report

Table 9.40 *Global datum events.*

Bit Position	No. of Bits	Value – Description
0	1	1 – Missing Vertical Coordinate
1	1	1 – Missing Observed Value
2	1	1 – Missing Background (First Guess) Value
3	1	1 – Rejected due to RDB Flag
4	1	1 – Activated due to RDB Flag
5	1	1 – Activated by Whitelist
6	1	1 – Bad Reporting Practice
7	1	1 – Vertical Position out of Range
8	1	1 – Reference Level Position out of Range
9	1	1 – Too Big First Guess Departure
10	1	1 – Too Big Departure in Assimilation
11	1	1 – Too Big Observation Error
12	1	1 – Redundant Datum
13	1	1 – Redundant Level
14	1	1 – Report Over Land
15	1	1 – Report Over Sea
16	1	1 – Not Analysis Variable
17	1	1 – Duplicate Datum/Level
18	1	1 – Too Many Surface Data
19	1	1 – Multi Level Check
20	1	1 – Level Selection
21	1	1 – Vertical Consistency Check
22	1	1 – Vertical Coordinate Changed from Z to P
23	1	1 – Datum Rejected via Namelist
24	1	1 – Combined Flagging
25	1	1 – Datum Rejected due to Rejected Report
26	1	1 – Variational QC Performed
27	1	1 – Observation Error Increased
28–30	3	Not Used

Table 9.41 *SYNOP datum events.*

Bit Position	No. of Bits	Value – Description
0	1	1 – Bias Corrected Ps
1–30	30	Not Used

Table 9.42 *AIREP datum events.*

Bit Position	No. of Bits	Value – Description
0–30	31	Not Used

Table 9.43 *SATOB datum events.*

Bit Position	No. of Bits	Value – Description
0–30	31	Not Used

**Table 9.44** *DRIBU datum events.*

Bit Position	No. of Bits	Value – Description
0	1	1 – Bias Corrected Ps
1–30	30	Not Used

**Table 9.45** *TEMP datum events.*

Bit Position	No. of Bits	Value – Description
0	1	1 – Bias Corrected Value Used
1–30	30	Not Used

**Table 9.46** *PILOT datum events.*

Bit Position	No. of Bits	Value – Description
0–30	31	Not Used

**Table 9.47** *SATEM datum events.*

Bit Position	No. of Bits	Value – Description
0	1	1 – Not Predefined Layer
1	1	1 – Layer Formed by Thinning
2	1	1 – Layer Formed by Summing Up
3	1	1 – Channel Not Used in Analysis
4	1	1 – Overwritten by ADVAR
5–30	26	Not Used

**Table 9.48** *PAOB datum events.*

Bit Position	No. of Bits	Value – Description
0–30	31	Not Used

**Table 9.49** *SCAT datum events.*

Bit Position	No. of Bits	Value – Description
0–30	31	Not Used

**Table 9.50** *Raw radiances datum events.*

Bit Position	No. of Bits	Value – Description
0–30	31	Not Used



Table 9.51 Datum blacklist events.

Bit Position	No. of Bits	Value – Description
0	1	1 – Pressure Blacklisted
1	1	1 – Variable Blacklisted
2	1	1 – Blacklisted due to Pressure Code
3	1	1 – Blacklisted due to Distance from Reference Point
4	1	1 – Blacklisted due to Type of Vertical Coordinate
5	1	1 – Blacklisted due to Observed Value
6	1	1 – Blacklisted due to First Guess departure
7–30	24	Not Used

Table 9.52 RDB pressure (vertical coordinate) and datum flags.

Parameter	No. of Bits	Bit Position	Bit Position	No. of Bits	Value – Description
Pressure	15	0+	0	1	0 – No Human Monitoring Substitution 1 – Human Monitoring Substitution
			+1	1	0 – No Q/C Substitution 1 – Q/C Substitution
Datum	15	15+	+2	1	0 – Override Flag not Set 1 – Override Flag Set
			+3	2	0 – Correct 1 – Probably Correct 2 – Probably Incorrect 3 – Parameter Incorrect
			+5	1	0 – Flag Set by Q/C or not Checked 1 – Flag Set by Human Monitoring
			+6	2	0 – Previous Analysis judged it correct 1 – Previous Analysis judged it probably correct 2 – Previous Analysis judged it probably incorrect 3 – Previous Analysis judged it incorrect
			+8	1	0 – Not used by previous analysis 1 – Used by previous analysis
			+9	5	Not Used

For each datum in ODB there is an RDB flag word which holds flags for pressure (vertical coordinate) and the datum itself. This is packed word with 30 bits used – see Table 9.52. Pressure and datum RDB flags use 15 bits each. Thus pressure RDB flag starts at bit position 0, whereas the datum flag starts at bit position 15. Each 15 bits structure is further stratified in exactly the same way for both parameters:

**Table 9.53** *Analysis flags.*

Flag Type	Bit Position	No. of Bits	Value – Description
Final	0	4	0 – Correct 1 – Probably correct 2 – Probably incorrect 3 – Incorrect
First Guess	4	4	0 – Correct 1 – Probably correct 2 – Probably incorrect 3 – Incorrect
Departure	8	4	0 – Correct 1 – Probably correct 2 – Probably incorrect 3 – Incorrect
Variational Q/C	12	4	0 – Correct 1 – Probably correct 2 – Probably incorrect 3 – Incorrect
Blacklist	16	4	0 – Correct 1 – Probably correct 2 – Probably incorrect 3 – Incorrect
Not Defined	20	11	Reserved

In addition to RDB datum flags there is a word in ODB to store analysis flags. There are five types of analysis flags: final analysis, first guess, departure, variational q/c and blacklist flags. Each flag occupies 4 bits and the exact description is given in [Table 9.53](#).

# Chapter 10

## Observation screening

### Table of contents

- 10.1 Introduction**
- 10.2 The structure of the observation screening**
  - 10.2.1 The incoming observations
  - 10.2.2 The screening run
  - 10.2.3 General rationale of the observation screening
  - 10.2.4 3D-Var versus 4D-Var screening
- 10.3 The independent observation screening decisions**
  - 10.3.1 Preliminary check of observations
  - 10.3.2 Blacklisting
  - 10.3.3 Background quality control
- 10.4 Screening of satellite radiances**
  - 10.4.1 Pre-screening
  - 10.4.2 Cloud and rain rejection
  - 10.4.3 Blacklisting decisions
- 10.5 Screening of Scatterometer data**
  - 10.5.1 Wind retrieval
  - 10.5.2 Quality control
  - 10.5.3 Rain contamination
  - 10.5.4 Bias corrections
  - 10.5.5 Blacklisting decisions
- 10.6 The dependent observation screening decisions**
  - 10.6.1 Update of the observations
  - 10.6.2 Global time–location arrays
  - 10.6.3 Vertical consistency of multilevel reports
  - 10.6.4 Removal of duplicated reports
  - 10.6.5 Redundancy check
  - 10.6.6 Thinning
  - 10.6.7 A summary of the current use of observations
  - 10.6.8 Compression of the ODB
- 10.7 A massively-parallel computing environment**
- Appendix A**
  - A.1 Bad reporting practice of synop and temp reports
  - A.2 Revised background quality control for selected observations
  - A.3 Use of atmospheric motion winds

### 10.1 INTRODUCTION

This chapter describes the observation screening in the ECMWF 3D/4D-Var data assimilation. A more general description can be found in [Järvinen and Undén \(1997\)](#). The purpose of the observation screening is to select a clean array of observations to be used in the data assimilation. This selection involves quality checks, removal of duplicated observations, thinning of their resolution etc.. The current selection

algorithm has been operational since September 1996 and was to a large extent designed to reproduce the functionalities of the corresponding codes in the ECMWF OI analysis (Lönnberg and Shaw, 1985, 1987; Lönnberg, 1989).

This chapter was prepared in September 1997 by Heikki Järvinen, Roger Saunders and Didier Lemeur. It was updated in February 1999 by Roger Saunders for TOVS processing, by Elias Holm and Francois Bouttier for the remainder, with further updates in October 2004 (to Cy28r1) by Erik Andersson, Drasko Vasiljevic, Tony McNally (generalised radiance data processing) and Hans Hersbach (scatterometer).

## 10.2 THE STRUCTURE OF THE OBSERVATION SCREENING

### 10.2.1 The incoming observations

Before the first trajectory integration of the assimilation various observation processing steps take place. The observations for the current assimilation period are extracted from the Reports Data Base (RDB) of observations, coded in BUFR. The extracted data reside in separate BUFR files for each main observing systems e.g. conventional (that also contains AMVs), ATOVS (that also contains AIRS radiances), geostationary radiances and IASI). These data have already undergone some rudimentary quality control, e.g. a check for the observation format and position, for the climatological and hydrostatic limits, as well as for the internal and temporal consistency. The so-called RDB flag has been assigned according to the outcome of such checks.

The Observation Data Base (ODB, see separate documentation) is filled from the BUFR files in a sequence of jobs called BUFR2ODB. These jobs are multi-tasked running on parallel servers. Several or all observation types can run synchronously. The resulting ‘raw’ ODB is processed further by the IFS, in preparation for the main analysis tasks. These ODB and data manipulation tasks are referred to as ‘the make CMA replacement’ (for historical reasons), and are activated by the switch LMKCMARPL. **MKCMARPL** entails format conversions, changes of some observed variables, such as calculation of relative humidity from dry and wet bulb temperatures and wind components from speed and direction. The assignment of observation error statistics is also done at this stage, at least for conventional data.

The resulting ‘extended’ ODB data base (the ECMA) contains all the observational information for the data window as required for 3D/4D-Var as well as all data that are going to be monitored. The next step is that the observations are compared to the model as it is integrated for the length of the assimilation window (Chapter 2). The observation minus model differences (the departures) are computed as described in Chapter 5 and stored in the ODB. These departures are an important input to the data selection procedures as many quality-control decisions depend on the magnitude of the departure. The collection of routines that perform data selection are jointly referred to as ‘the screening’. The purpose of the observation screening is to select the best quality observations, to detect duplicates, and reduce data redundancy through thinning.

### 10.2.2 The screening run

The ECMWF 3D/4D-Var data assimilation system makes use of an incremental minimization scheme, as described in Chapter 2. The sequence of jobs starts with the first (high resolution) trajectory run. During this run the model counterparts for all the observations are calculated through the non-linear observation operators, and the observation minus model difference (the departures) are calculated. As soon as these background departures are available for all observations, the screening can be performed. Prior to the screening the model fields are deallocated (dealmod) as most of the information necessary in the screening is stored in the observation data base (ODB). For the observation screening, the background errors (available as grid data in the ‘errgrib’ file, see Chapter 13) are interpolated to the observation locations for the observed variables (**INIFGER**, **SUFGER** and **GEFGER**).

Technically, the final result of the observation screening is a pair of ODBs. The original ‘extended’ observation data base now contains observations complemented by the background departures, together with quality control information for most of the observations. This ECMA ODB remains on disc for later use in feedback creation. The compressed ODB, the CCMA, is a subset of the original observations, and

is passed for the subsequent minimization job. The CCMA contains only those observations that are to be used in the minimization.

### 10.2.3 General rationale of the observation screening

The general logic in the 3D/4D-Var observation screening algorithm is to make the *independent* decisions first, i.e. the ones that do not depend on any other observations or decisions (**DECIS**). One example is the background quality control for one observed variable. These can be carried out in any order without affecting the result of any other independent decision. The rest of the decisions are considered as mutually *dependent* on other observations or decisions, and they are taken next, following a certain logical order. For instance, the horizontal thinning of radiance reports is only performed for the subset of reports that passed the background quality control. Finally, the CCM data base is created for the minimization in such a way that it only contains the data that will be used.

### 10.2.4 3D-Var versus 4D-Var screening

In the original 3D-Var assimilation system the screening rules were applied once, for the complete set of observations spanning a six-hour period. In the early implementation of the 4D-Var assimilation system, the same data selection approach called ‘3D-screening’ was applied over the 6-hour long 4D-Var time window, which resulted in essentially the same screening decisions as in 3D-Var.

In summer 1997, a new screening procedure called 4D-screening was implemented that took into account the temporal distribution of the observations. The time window is divided into time-slots of typically half-hour length (15 minutes for the first and the last time slots). The 3D-screening algorithm was then applied separately to observations within each time-slot. This allowed more data to be used by 4D-Var, for instance, all messages from an hourly reporting station can now be used, whereas only one (closest to central time) would have been allowed by the redundancy check in the 3D-screening. The 4D-screening behaviour is activated by switch **LSCRE4D**; it is meant to be used in conjunction with time correlation of observation errors where appropriate, as explained in [Järvinen \*et al.\* \(1999\)](#) and in [Chapter 5](#). Also the current 3D-FGAT configuration ([Chapter 3](#)) relies on 4D-screening (**LSCRE4D** = .TRUE.).

## 10.3 THE INDEPENDENT OBSERVATION SCREENING DECISIONS

### 10.3.1 Preliminary check of observations

The observation screening begins with a preliminary check of the completeness of the reports (**PRECH**). None of the following values should be missing from a report: observed value, background departure, observation error and vertical coordinate of observation. Also a check for a missing station altitude is performed for synop, temp and pilot reports. The reporting practice for synop and temp mass observations (surface pressure and geopotential height) is checked (**REPRE**), as explained in [Appendix A](#). At this stage also, the observation error for synop geopotential observations is inflated if the reported level is far from the true station level (**ADDOER**). The inflation is defined as a proportion of the difference between the reported level and the true station altitude by adding 2% of the height difference to the observation error.

### 10.3.2 Blacklisting

Next, the observations are scanned through for blacklisting (subroutine **BLACK**). At the set-up stage the blacklist interface is initialized (**BLINIT**) to the external blacklist library. The interface between the IFS and the blacklist described in further detail in [Chapter 5](#), and in the full Blacklist documentation available elsewhere. The blacklist files ([Chapter 13](#)) consist formally of two parts. Firstly, the selection of variables for assimilation is specified in the ‘data selection’ part of the blacklist file. This controls which observation types, variables, vertical ranges etc. will be selected for the assimilation. Some more complicated decisions are also performed through the data selection file; for instance, an orographic rejection limit is applied in the case of the observation being too deep inside the model orography. This part of the blacklist also provides a handy tool for experimentation with the observing system, as well as with the assimilation system itself. Secondly, a ‘monthly monitoring’ blacklist file is provided for discarding the stations that

**Table 10.1** *The predefined limits for the background quality control, given in terms of multiples of the expected variance of the normalized background departure.*

Variable	Flag 1	Flag 2	Flag 3
u, v	9.00	16.00	25.00
z, ps	12.25	25.00	36.00
dz	x	x	x
T	9.00	16.00	25.00
rh, q	9.00	16.00	25.00

Flag values are denoted by 1 for a probably correct, 2 for a probably incorrect and 3 for an incorrect observation. The variables are denoted by u and v for wind components, z for geopotential height, ps for surface pressure, dz for thickness, T for temperature, rh for relative humidity and q for specific humidity, respectively.

have recently been reporting in an excessively noisy or biased manner compared with the ECMWF background field.

### 10.3.3 Background quality control

The background quality control (FIRST) is performed for all the variables that are intended to be used in the assimilation. The procedure is as follows. The variance of the background departure  $y - H(\chi_b)$  can be estimated as a sum of observation and background-error variances  $\sigma_o^2 + \sigma_b^2$ , assuming that the observation and the background errors are uncorrelated. After normalizing with  $\sigma_b$ , the estimate of variance for the normalized departure is given by  $1 + \sigma_o^2/\sigma_b^2$ . In the background quality control, the square of the normalized background departure is considered as suspect when it exceeds its expected variance more than by a predefined multiple (**FGCHK**, **SUFGLIM**). For the wind observations, the background quality control is performed simultaneously for both wind components (**FGWND**). In practice, there is an associated background quality-control flag with four possible values, namely 0 for a correct, 1 for a probably correct, 2 for a probably incorrect and 3 for an incorrect observation, respectively (**SUSCRE0**). [Table 10.1](#) gives the predefined limits for the background quality control in terms of multiples of the expected variance of the normalized background departure. These values are set in DEFRUN and can be changed in namelist **NAMJO**. For SATOB winds the background error limits are modified as explained in [Appendix A](#).

There is also a background quality control for the observed wind direction (**FGWND**). The predefined error limits of  $60^\circ$ ,  $90^\circ$  and  $120^\circ$  apply for flag values 1, 2 and 3, respectively. The background quality control for the wind direction is applied only above 700 hPa for upper-air observations for wind speeds larger than  $15 \text{ ms}^{-1}$ . If the wind-direction background quality-control flag has been set to a value that is greater than or equal to 2, the background quality-control flag for the wind observations is increased by 1.

There is no first-guess check for scatterometer data. It is demanded, though, that neither scatterometer nor model wind speed should exceed  $35 \text{ ms}^{-1}$ , since that marks the range of validity for scatterometer wind inversion.

## 10.4 SCREENING OF SATELLITE RADIANCES

### 10.4.1 Pre-screening

Radiance observations undergo a pre-screening process before being loaded into the OBD for input to the main IFS screening. Firstly, this is used to reduce the data volume and thus the computational burden of the main screening. Secondly, this rejects observations that fail to contain crucial header information and/or the correct number of channels that could potentially cause a computational run-time failure in the

main screening. Observations in BUFR are decoded and checked inside `SCREEN_1C` where, additionally, data measured at particular scan lines and or scan positions may be removed to reduce the data volume (by setting `LINE_THIN`, `FOV_THIN` in the calling script `PRE_1CRAD`). Observations which survive the checking and thinning process are then re-encoded in BUFR and supplied to the ODB loader. A key consideration for rejecting data in the pre-screening is that removed observations will NOT be passed through the IFS screening and thus will NOT accrue feedback quality information. Currently all pre-screening tasks are scalar (i.e. not parallel). However, for IASI (by far the largest data volume) the process is effectively parallelized by splitting the input BUFR file and launching multiple scalar tasks simultaneously.

#### 10.4.2 Cloud and rain rejection

After the pre-screening, surviving observations are passed into the main IFS screening process. Here, data contaminated by significant cloud or rain signals must be removed before being supplied to the 4D-Var minimization in the clear-sky assimilation scheme. Microwave imager radiances from the SSM/I(S), TMI and similar are assimilated in all-sky conditions, so no cloud or rain rejection is done. For other microwave radiances (AMSU-A/B) rain contamination is detected by scene classification based on observed window channel values inside `AMSU_SFC`. For infrared radiances the test for clouds is done in routine `CLOUD_DETECT` for AIRS/IASI and routine `HIRS_CLD` for HIRS. The former is based on the algorithm described in McNally and Watts (2003). The latter is described in Kelly (2007). In both cases the aim is to identify which infrared channels can be used in a particular scene and which must be rejected. For both the microwave and infrared data, if cloud or rain is detected and the rejection flag is set - these observations will not influence any aspects of the analysis including bias parameter evolution in the VARBC.

There is a special case of infrared cloud contamination that does not lead to channels being rejected. In parallel to the setting of clear and cloudy flags, simplified cloud parameters (cloud top pressure and effective cloud fraction) are estimated from the infrared data (HIRS, AIRS and IASI) in routine `CLOUD_ESTIMATE`. In the case that a pixel is diagnosed as completely overcast and subject to some additional restrictions placed upon the altitude of the diagnosed cloud (e.g. that it is not within 100hPa of the surface), the rejection flags are NOT set. All channels in that pixel are then assimilated with the estimated cloud parameters passed to the forward operator and further evolved as local extensions to the control vector in the minimization. The additional use of overcast infrared radiances can be disabled by setting the logical variable `LCLDSINK` to false.

#### 10.4.3 Blacklisting decisions

Like any other observations decisions are made to use or not use a particular radiance observation in the blacklist. These fall into two distinct types: The first is the usual a priori type decision which takes no account of the actual value of the observation. Examples for radiances include the exclusion of data measured by new instruments which we do not yet wish to use, data measured by bad/failed instruments, data measured at extreme scan positions, exclusion of data measured over land or high orography and the exclusion of data at certain times of year when solar intrusions may cause problems (there are others). The second type of test is particular to radiances and is a run-time decision based on the observed values (or more correctly the radiance departure from the background).

Depending on the magnitude of the radiance departure in key window channels, individual or combinations of microwave and infrared channels may be rejected. In some respects this may be considered an additional first-guess check that takes place in the blacklists. It can equally well be considered as an additional cloud/rain detection check that takes place in the blacklist as it exclusively involves window channels. No attempt is made here to document the particular test and threshold which are applied to each channel on every instrument and the user is referred to the data selection blacklists files for details. For both types of test applied in the blacklists environment, if it is failed there are two options for what then results. The setting of a `FAIL(CONSTANT)` flag means that the observations will effectively be rejected and take no further part in the analysis. The setting of a `FAIL(EXPERIMENTAL)` flag means that the observation will enter the main analysis in such a way that it cannot force increments of e.g. temperature or humidity, but it can influence the calculation and evolution of bias correction coefficients

inside VARBC. An example of when the latter is used would be for new a satellite for which we do not wish to actively assimilate the data, but wish to establish an accurate bias correction. Another application of the FAIL(EXPERIMENTAL) facility is its use for window channels used in the quality control of other data.

## 10.5 SCREENING OF SCATTEROMETER DATA

The screening of scatterometer data involves the conversion of the backscatter measurements acquired by the instrument (triplets for ERS and ASCAT and quadruplets for NSCAT and QuikSCAT) into ambiguous  $u$  and  $v$  wind components that will actually be assimilated into the IFS (see [Section 5.8.4](#)). The (empirical) relation between wind and backscatter is described by a geophysical model function (GMF). Although in principle inverted wind components are provided as a level 2 product, at ECMWF the wind inversion is performed in house. In this way any drifts in backscatter levels can be corrected in a direct manner.

Data from the AMI instrument on ERS-2 have been used from June 1996 (with an interruption from January 2001 till March 2004), data from the SeaWinds instrument on-board QuikSCAT was used from January 2002 until November 2009 (when QuikSCAT failed), and data from ASCAT on MetOp have been assimilated from June 2007 onwards. Data from NSCAT have never been used in an operational setup, although offline assimilation experiments have been performed. From November 2010 onwards scatterometer data is assimilated as equivalent-neutral 10-metre wind, rather than (real) 10-metre wind, since the former model winds are closer related to scatterometer observations.

### 10.5.1 Wind retrieval

Since geometry and measurement principle of ERS and ASCAT are alike, data from these instruments is processed in a similar way. The procedure for wind inversion closely follows the wind retrieval and ambiguity removal scheme originally developed for the ERS-1 scatterometer ([Stoffelen and Anderson, 1997](#)), though the original geophysical model function CMOD4 has been replaced by CMOD5 ([Hersbach \*et al.\*, 2007](#)) in March 2004, by CMOD5.4 in June 2007, and by CMOD5.n ([Hersbach, 2010b](#)) in November 2010, after which scatterometer winds are assimilated as equivalent-neutral wind ([Hersbach, 2010a](#)).

For QuikSCAT the task of wind inversion is performed in the pre-screening ([PRESCAT](#)). Data are like ERS and ASCAT, provided at a resolution of 25 km. Rather than data thinning (see [Subsection 10.6.6](#)), for QuikSCAT a 50 km product is created which contains information about backscatter from the four underlying original sub-cells. The weight of the scatterometer cost function (defined in routine [HJO](#)) of each 50 km wind vector cell is reduced by a factor four, which effectively mimics the assimilation of a 100 km product. It is the re-sampled 50 km product that is stored in ODB. Original backscatter observations at 25 km are not available within the assimilation.

In general, the wind retrieval is performed by minimizing the distance between observed backscatter values  $\sigma_{oi}^0$  and modelled backscatter values  $\sigma_{mi}^0$  given by

$$D(u) = \sum_i^n \frac{[(\sigma_{oi}^0)^p - \sigma_{mi}^0(u)^p]^2}{k_p \left[ \sum_j^n \sigma_{mj}^0(u)^p \right]^2} \quad (10.1)$$

For ERS and ASCAT data, the sum is over triplets, while for QuikSCAT the sum may extend to 16 values (four 25 km sub-cells with each four observations). The quantity  $p$  is equal to unity for NSCAT and QuikSCAT. For ERS and ASCAT data, a value of  $p = 0.625$  was introduced because it makes the underlying GMF more harmonic, which helps to avoid direction-trapping effects ([Stoffelen and Anderson, 1997](#)). The noise to signal ratio  $k_p$  provides an estimate for the relative accuracy of the observations.

The simulation of  $\sigma_m^0$  is for ERS and ASCAT data based on the CMOD5.4 model function. For NSCAT data the NSCAT-2 GMF has been utilized. For QuikSCAT data, the choice of GMF is handled by a logical switch LQTABLE. By default LQTABLE = .TRUE. and the QSCAT-1 model function is used, otherwise, modelled backscatter values are based on the NSCAT-2 GMF. The minimization is achieved using a tabular form of the GMF, giving the value of the backscatter coefficient for wind speeds, direction



and incidence angles discretized with, for ERS and ASCAT data, steps of  $0.5 \text{ ms}^{-1}$ ,  $5^\circ$  and  $1^\circ$ , respectively. For NSCAT and QuikSCAT data the corresponding values are  $0.2 \text{ ms}^{-1}$ ,  $2.5^\circ$  and  $1^\circ$ . ERS and ASCAT use the same table, which is read in the initialisation subroutine **INIERSCA**. For QuikSCAT, inversion takes place in the **QSCAT25TO50KM** program in the **PRESCAT** task.

### 10.5.2 Quality control

The wind inversion involves some quality control. For ERS (**ERS1IF**),  $k_p$  must for each antenna be below 10%, and a missing packet number must be less than 10 to ensure that enough individual backscatter measurements have been averaged for estimating the value.

For ASCAT (**ASCATIF**)  $a$  in the product provided land fraction must be zero for each backscatter measurement. No restriction on  $k_p$  is imposed, other than that values should be non missing. It is checked whether two other provided quality flags ('sigma0 usability' and 'kp quality') have acceptable values. However, no quality control decisions are made on these two indicators for the moment, since so far, they have not been fully calibrated and validated by EUMETSAT.

For QuikSCAT, from 38 across-track 50 km cells, the outer 4 at either side of the swath are, due to their known reduced quality rejected. In addition, for QuikSCAT, it is verified whether inverted winds are well-defined, i.e. whether minima  $D(u)$  are sufficiently sharp. In practise this is mainly an issue for cells in the central part of the swath. Data is rejected when the angle between the most likely solution and its most anti-parallel one is less than  $135^\circ$  (routine **SCAQC**).

After wind inversion, a further check is done on the backscatter residual associated to the rank-1 solution (also called 'distance to the cone'). This misfit contains both the effects of instrumental noise and of GMF errors. Locally, these errors can become large when the measurements are affected by geophysical parameters not taken into account by the GMF, such as sea-state or intense rainfall. For ERS, a triplet is rejected when the cone distance exceeds a threshold of three times its expected value. For QuikSCAT and ASCAT data such a test is not performed.

In addition to a distance-to-cone test on single observations, a similar test is performed for averages for data within certain time slots. If these averages exceed certain values, all data within the considered time slot is suspected to be affected by an instrument anomaly, since geophysical fluctuations are expected to be averaged out when grouping together large numbers of data points. For ERS and ASCAT, cell-wise averages are calculated for the default 4D-Var observation time slot (30 minutes) in the IFS routine **SCAQC**, and its rejection threshold (1.5 times average values) are defined in the IFS routine **SUFGLIM**. For QuikSCAT averages are considered over six-hourly data files and are evaluated in the pre-screening (**DCONE\_OC**), using a threshold of 1.45 for any of cells between 5 and 34.

### 10.5.3 Rain contamination

Thanks to the usage of C-band frequency, rain contamination is mild for ERS and ASCAT. For QuikSCAT and NSCAT, which operate in Ku band, rain contamination is a serious issue.

For QuikSCAT the check on rain contamination occurs in the pre-screening and is imposed on the original 25 km observations. Any 25 km rejected cell is not used in the determination of the 50 km wind product. When more than one 25 km sub-cell is rejected, the entire 50 km product is rejected (decision made in **SCAQC**).

Since February 2000, the BUFR product provides a rain flag. This flag, which was developed by NASA/JPL, is based on a multidimensional histogram (MUDH) incorporating various quantities that may be used for the detection of rain ([Huddleston and Stiles, 2000](#)). Examples of such parameters are *mp\_rain\_probability* (an empirically determined estimate for the probability of a columnar rain rate larger than  $2 \text{ m}^2 \text{ hr}^{-1}$ ; typically values larger than 0.1 indicate rain contamination) and *nof\_rain\_index* (a rescaled normalized objective function – values larger than 20 give a proxy for rain). Since at the time of implementation, the quality of the JPL rain flag had not been fully confirmed, an alternative (more aggressive) flag was established in house. Based on a study in which QuikSCAT winds were compared to collocated ECMWF first guess winds, a quality flag was introduced. It is given by

$$L_{\text{rain}} = \{ \text{nof\_rain\_index} + 200 \text{ mp\_rain\_probability} > 30 \}.$$

Both *mp\_rain\_probability* and *nof\_rain\_index* are provided in the original 25 km BUFR product (for details see [Leidner et al., 2000](#)). When one of these quantities is missing, the above mentioned condition for the remaining quantity is used.

#### 10.5.4 Bias corrections

For ASCAT and ERS, bias corrections are applied, both in terms of backscatter (before wind inversion) and wind speed (after inversion), particularly to compensate for any change in the instrumental calibration and to ensure consistency between the retrieved and model winds. The backscatter and wind-speed bias corrections are defined by dedicated files read in the initialization subroutine **INIERSCA**. Files are in principle model-cycle and date dependent. Currently for ERS-2, the appropriate files have no effect (i.e. containing only unity correction factors and zeros), since the CMOD5.4 GMF was tuned on ERS-2. For ASCAT, though, the usage of bias corrections is essential, since the backscatter product for this instrument has been calibrated differently from ERS. The bias correction file for backscatter has been updated every time a change in the calibration of ASCAT was imposed by EUMETSAT.

For QuikSCAT data no bias corrections in  $\sigma^0$  space is applied, though, wind-bias corrections are made. This also takes place in the pre-screening. Corrections are performed in three steps. First of all, wind speeds are slightly reduced according to:

$$v' = 0.2 + 0.96 v.$$

Where  $v$  is the wind speed as obtained from inversion (10.1) The addition of  $0.2 \text{ ms}^{-1}$  is used in the operational configuration, where scatterometer data is assimilated as equivalent neutral wind. In case this is not desired (expressed by `LSCATT_NEUTRAL=false`) only the rescaling factor of 0.96 is used. It was observed that the residual bias between QuikSCAT winds and ECMWF first guess winds depends on the value of *mp\_rain\_probability*. The motivation is that, for higher amounts of precipitation, a larger part of the total backscatter is induced by rain, leaving a smaller part for the wind signal. The correction applied is

$$v'' = v' - 20 \langle mp\_rain\_probability \rangle,$$

where  $\langle \rangle$  denotes the average value over the 25 km sub-cells that were taken into account in the inversion (i.e. over rain-free sub-cells). The maximum allowed correction is  $2.5 \text{ ms}^{-1}$ , which is seldom reached. Finally, for strong winds, QuikSCAT winds were found to be quite higher than their ECMWF first guess counterparts. In order to accommodate this, for winds stronger than  $19 \text{ ms}^{-1}$  the following correction is applied:

$$v''' = v'' - 0.2(v'' - 19.0).$$

#### 10.5.5 Blacklisting decisions

In order to screen on sea-ice contamination, scatterometer data are removed (within the blacklist mechanism) whenever the model sea-ice fraction exceeds 1% or the model sea-surface-temperature analysis is below 273.15 K. Land is removed by imposing that the model land-sea mask should not exceed 10%.

## 10.6 THE DEPENDENT OBSERVATION SCREENING DECISIONS

### 10.6.1 Update of the observations

Just before performing the dependent screening decisions, the flag information gathered so far is converted into a status of the reports, namely: **active**, **passive**, **rejected** or **blacklisted**, and also into a status of the data in the reports (**FLGTST**). The reports with a RDB report flag value 2 (probably incorrect) or higher for latitude, longitude, date and time are rejected. For the observed data there are RDB datum flags for the variable and for the pressure, i.e. the pressure level of the observation. The rejection limits for these are as follows: all data are rejected for the maximum RDB datum flag value 3 (incorrect), non-standard-level data are rejected for the maximum RDB datum flag value 2, and for the pressure RDB datum flag the rejection limit is 1 (probably correct). The background quality control rejection limits are flag value 3 for all the data, and flag value 2 for the non-standard-level data.

### 10.6.2 Global time–location arrays

Some of the dependent decisions require a global view to the data which is not available as the memory is distributed. Therefore *ad hoc* global time–location arrays are formed and broadcast in order to provide this view (GLOBA, DISTR).

### 10.6.3 Vertical consistency of multilevel reports

The first dependent decisions are the vertical-consistency check of multilevel reports (**VERCO**), and the removal of duplicated levels from the reports. The vertical-consistency check of multilevel reports is applied in such a way that if four consecutive layers are found to be of suspicious quality, even having a flag value one, then these layers are rejected, and also all the layers above these four are rejected in the case of geopotential observations. These decisions clearly require the quality-control information, and they are therefore ‘dependent’ on the preceding decisions.

### 10.6.4 Removal of duplicated reports

The duplicated reports will be removed next. That is performed (**MISCE**, **DUPLI**, **REDSL**) by searching pairs of collocated reports of the same observation types, and then checking the content of these reports. It may, for instance, happen that an airep report is formally duplicated by having a slightly different station identifier but with the observed variables inside these reports being exactly the same, or partially duplicated. The pair-wise checking of duplicates results in a rejection of some or all of the content of one of the reports.

### 10.6.5 Redundancy check

The redundancy check of the reports, together with the level selection of multi-level reports, is performed next for the active reports that are collocated and that originate from the same station (**REDUN**). In 3D-screening, this check applies to the whole observation time window. In 4D-screening (**LSCRE4D** = **.TRUE.**), this check applies separately in each timeslot.

For **land synop and paob** reports, the report closest to the analysis time with most active data is retained, whereas the other reports from that station are considered as redundant and are therefore rejected from the assimilation (**REDRP**, **REDMO**). For **ship synop and dribu** observations the redundancy check is done in a slightly modified fashion (**REDGL**). These observations are considered as potentially redundant if the moving platforms are within a circle with a radius of 1° latitude. Also in this case only the report closest to the analysis time with most active data is retained. All the data from the multilevel **temp and pilot** reports from same station are considered at the same time in the redundancy check (**REDOR**, **SELEC**). The principle is to retain the best quality data in the vicinity of standard levels and closest to the analysis time. One such datum will, however, only be retained in one of the reports. A wind observation, for instance, from a sounding station may therefore be retained either in a temp or in a pilot report, depending on which one happens to be of a better quality. A **synop mass** observation, if made at the same time and at the same station as the temp report, is redundant if there are any temp geopotential height observations that are no more than 50 hPa above the synop mass observation (**REDSM**).

### 10.6.6 Thinning

Finally, a horizontal thinning is performed for the AIREP, radiances (ATOVS,AIRS,IASI), GEOS, SATOB, ERS and SCAT SCAT reports. The horizontal thinning of reports means that a predefined minimum horizontal distance between the nearby reports from the same platform is enforced. For AIREP reports the free distance between reports is currently enforced to about 60 km (*Cardinali et al., 2003*). The thinning of the AIREP data is performed with respect to one aircraft at a time (**MOVPL**, **THIAIR**). Reports from different aircraft may however be very close to each other. In this removal of redundant reports the best quality data is retained as the preceding quality controls are taken into account. In vertical, the thinning is performed for layers around model levels, thus allowing more reports for ascending and descending flight paths.

Thinning of radiances, GRAD, SATOB, ERS and ASCAT SCAT reports are each done in two stages controlled by THINN. For radiances (**THINNER**), a minimum distance of about 70 km is enforced and, thereafter, a repeat scan is performed to achieve the final separation of roughly 250 km or 120 km between reports from one platform. This is controlled through settings in **DEFRUN**, that can also be modified through namelist (**NAMSCC**). The thinning algorithm is the same as used for AIREPs except that for radiances a different preference order is applied: a sea sounding is preferred over a land one, a clear sounding is preferred over a cloudy one and, finally, the closest observation time to the analysis time is preferred. For geostationary water vapour radiances, a similar thinning in two stages is applied with currently about 70 km minimum distance and about 125 km final separation (**THINNER**). During the thinning, preference is given to data having the largest fraction of clear sky in the clear-sky radiance average, high infrared brightness temperature (for GOES data) and, finally, a small standard deviation of brightness temperatures within the CSR mean. A similar thinning technique is applied to SATOB high-density data (**THINNER**). Note that prior to assimilation a coarser pre-thinning may take place already during observation pre-processing in order to reduce otherwise excessive data volumes.

The screening of SATOB data has been extended for atmospheric motion wind observations, including individual quality estimate. The quality information from the quality control performed by the producer at extraction time is appended to each wind observation. This Quality Indicator (QI) is introduced as an additional criterion in the thinning step; priority is given to the observation with the highest QI value.

For ERS and ASCAT scatterometer data, the above described thinning algorithm is only applied along track. In across-track direction, backscatter data from these platforms are provided into wind-vector cells (WVC) with a spatial resolution of 25 km. In this direction, data is thinned by selecting predefined wind-vector cells (subroutine **SCAQC**). For ERS, from 19 cells, only 3, 7, 11, 15 and 19 are regarded (cells 1 and 2 are of known lower quality). For ASCAT, from 42 cells (two swaths of 21 cells each) only cells 1, 5, 9, 13, 17, 21, 22, 26, 30, 34, 38 and 42 are used. After this across-track thinning, the generic thinning algorithm is applied to the remaining cells in along-track direction. QuikSCAT data (also provided on a 25 km grid) are not thinned. Instead, a 50 km wind product is determined from backscatter data from four underlying 25 km cells, each given a reduced weight of one fourth (see [Subsection 10.5](#)).

Scatterometer winds are besides thinning subject to a high-wind rejection test with an upper-wind speed limit set to  $35 \text{ ms}^{-1}$  to both the scatterometer and background winds (**FGWND**).

### 10.6.7 A summary of the current use of observations

A summary of the current status of use of observations in the 3D-Var data assimilation is given in [Table 10.2](#). For most current information we refer to the data-selection blacklist files themselves. The history of such files as used in ECMWF operations is also available.

### 10.6.8 Compression of the ODB

After the observation screening roughly a fraction of 1/10 of all the observed data are active and so the compressed observation ODB (the CCMA) for the minimization run only contains those data. The large compression rate is mainly driven by the number of radiance data, since after the screening there are only 10–20% of the radiance reports left, whereas for the conventional observations the figure is around 40%. As a part of the compression, the observations are re-sorted amongst the processors for the minimization job in order to achieve a more optimal load balancing of the parallel computer.

## 10.7 A MASSIVELY-PARALLEL COMPUTING ENVIRONMENT

The migration of operational codes at the ECMWF to support a massively-parallel computing environment has set a requirement for reproducibility. The observation screening needs to result in exactly the same selection of observations when different numbers of processors are used for the computations. As mentioned earlier, in the observation screening there are the two basic types of decision to be made. Independent decisions, on one hand, are those where no information concerning any other observation or decision is needed. In a parallel-computing environment these decisions can be happily made by different processors fully in parallel. For dependent decisions, on the other hand, a global view of the observations is needed which implies that some communication between the processors is required. The observation

**Table 10.2** A summary of the current use of observations in the 3D/4D-Var data assimilation at ECMWF. These usage rules are subject to change. For the most current information we refer to the data-selection blacklist files. These files are archived, so the history is preserved.

Observation type	Variables used	Remarks
SYNOP, SHIP	$u, v, ps$ (or $z$ ), $rh$	$u$ and $v$ used only over sea, in the tropics also over low terrain (<150 m). Orographic rejection limit 6 hPa for $rh$ , 100 hPa for $z$ and 800 m for $ps$ .
AIREP	$u, v, T$	Thinned to approximately 60 km along flight tracks. Ascending and descending aircraft are thinned in the vertical to the model resolution.
SATOB	$u, v$	Selected areas and levels. Thinning of high-density winds. Strict background check to avoid slow wind-speed bias in the data.
DRIBU	$u, v, ps$	Orographic rejection limit 800 m for $ps$ .
TEMP	$u, v, T, q$	Used on all reported levels. $q$ only below 300 hPa. 10 m $u$ and $v$ used over land only in tropics over low terrain (<150 m). Orographic rejection limit 10 hPa for $u, v$ and $T$ , and -4 hPa for $q$ .
PILOT	$u, v$	Used on all reported levels. 10 m $u$ and $v$ used over land only in tropics over low terrain (<150 m). Orographic rejection limit 10 hPa for $u$ and $v$ .
Profilers	$u, v$	Thinned to 5 hPa separation in the vertical. Data from American, European and Japanese networks are used.
Radiance data	$Tb$	Information to be supplied by the Satellite Section.
PAOB	$ps$	Used south of 19°S. Orographic rejection limit 800 m for $ps$ .
Scatterometer	$u, v$	Used if SST is warmer than 273 K and sea ice fraction below 1% and only when both observed and background wind are less than 35 ms <sup>-1</sup> .

The variables are as in [Table 10.1](#), with the addition that  $Tb$  stands for brightness temperature. The observation types are shortened by *SYNOP* for synoptic surface observations, *AIREP* for aircraft reports, *SATOB* for satellite cloud track winds, *DRIBU* for drifting buoy reports, *TEMP* for radiosonde soundings, *PILOT* for wind soundings and *PAOB* for pseudo observations of surface pressure obtained from satellite images.

array is, however, far too large to be copied for each individual processor. Therefore, the implementation of observation screening at the ECMWF is such that only the minimum necessary information concerning the reports is communicated globally.

The global view of the observations is provided in the form of a global ‘time–location’ array for selected observation types. That array contains compact information concerning the reports that are still active at this stage. For instance, the observation time, location and station identifier as well as the owner processor of that report are included. The time–location array is composed at each processor locally and then collected for merging and redistribution to each processor. After the redistribution, the array is sorted locally within the processors according to the unique sequence number. Thus, every processor has exactly the same information to start with, and the dependent decisions can be performed in a reproducible manner independently of the computer configuration.

The time–location array is just large enough for all the dependent decisions, except for the redundancy checking of the multilevel temp and pilot reports. This is a special case, in the sense that the information concerning each and every observed variable from each level is needed. Hence, the whole multilevel report has to be communicated. The alternative to this would be to force the observation clusters of the multilevel reports always into one processor without splitting them. In that case the codes responsible for the creation of the observation arrays for assimilation would need to ensure the geographical integrity

of the observation arrays distributed amongst the processors. This is, however, not possible in all the cases, and the observation screening has to be able to cope with this. Currently, it is coded in such a way that only a limited number of multilevel temp and pilot reports, based on the time–location array, are communicated between the appropriate processors as copies of these common stations.

## APPENDIX A

### A.1 Bad reporting practice of synop and temp reports

The way the synoptic surface stations report mass observations (pressure or geopotential height) is considered as bad if:

- station altitude is above 800 m and station reports mean sea level pressure
- station altitude is above 800 m and station reports 1000 hPa level
- station altitude is above 1700 m and station reports 900 hPa level
- station altitude is below 300 m and station reports 900 hPa level
- station altitude is above 2300 m and station reports 850 hPa level
- station altitude is below 800 m and station reports 850 hPa level
- station altitude is above 3700 m and station reports 700 hPa level
- station altitude is below 2300 m and station reports 700 hPa level
- station altitude is below 3700 m and station reports 500 hpa level

The reporting practice is also considered as bad if the station reports 500 gpm, 1000 gpm, 2000 gpm, 3000 gpm or 4000 gpm level pressure, respectively, and station altitude is more than 800 m different from the reported level.

For temp geopotentials the reporting practice is considered as bad if:

- station altitude is above 800 m and station reports 1000 hPa level
- station altitude is above 2300 m and station reports 850 hPa level
- station altitude is above 3700 m and station reports 700 hPa level

### A.2 Revised background quality control for selected observations

The background quality-control rejection limits are applied more strictly for some observation types than stated in [Table 10.1](#). The special cases are the following ones.

- AIREP wind observations with zero wind speed are rejected if the background wind exceeds  $5 \text{ m s}^{-1}$ .
- For AIREP and DRIBU wind observations the rejection limit is multiplied by 0.5, and for pilot wind by 0.8.
- For SATOB wind observations the rejection limit is multiplied by 0.1, except below 700 hPa level where it is multiplied by 0.2.
- No background quality control is applied for SCAT winds.
- For DRIBU surface pressure observations the rejection limit is multiplied by 0.9, and for paob surface pressure by 0.7.
- For AIREP temperature observations the rejection limit is multiplied by 1.6.

### A.3 Use of atmospheric motion winds

This appendix describes those parts of the ECMWF assimilation system which involves some special code for the AMW case, i.e. the data selection and the FG quality check. It refers to the operational status as from December 1996. A thinning procedure was introduced for high-density winds in Spring 1998.

#### A.3.1 Data selection

There are several model independent checks which AMW data have to pass in order to be considered for the assimilation process:

Check on longitude/latitude

- AMW must be within a circle of  $55^\circ$  from the sub-satellite point

Check on levels depending on the computational method

- WW CMW and WVMW must be above 400 hPa
- VIS CMW must be below 700 hPa
- IR CMW can be used at all levels.

Check on land/sea

- All AMW over sea are used.
- AMW over land is not used north of  $20^\circ\text{N}$ .
- For Meteosat ( $0^\circ$  mission) instead of  $20^\circ\text{N}$  this threshold is  $35^\circ\text{N}$  to allow usage of AMW over north Africa.
- For Meteost ( $63^\circ$  mission) the use of AMW has been extended over Asia if above 500 hPa. This is restricted for longitudes east of  $30^\circ\text{E}$ .
- AMW are blacklisted over the Himalayas as a precautionary measure.
- AMW over land south of  $20^\circ\text{N}$  ( $35^\circ\text{N}$  for Meteosat) is used if above 500 hPa.

Check on satellite ( $35^\circ\text{N}$  for Meteosat) is used if above 500 hPa.

This is a temporary selection on certain channels or satellites. At present channels and satellite used are:

- METEOSAT cloud tracked winds with 90 min temporal sampling
- METEOSAT IR (not at medium level), VIS, WV
- METEOSAT HVIS, also at asynoptic times, only if  $QI_2 \equiv 0$  (Automatic Quality Control  $\equiv$  PASSED)
- GOES IR & WV (NOT at asynoptic times)
- GMS IR & VIS

### A.3.2 Background quality check

The background quality check is based on a comparison of the AMW deviation from the background. Observed wind components are checked together. The AMW is flagged with  $j = 1$  or 2 or 3 if this deviation squared is greater than a predetermined multiple  $\text{ERRLIM} * \text{ZREJMOD}$  of its estimated variance, as given by the following expression:

if  $[D2 > (\text{sfg}^2 + \text{sobs}^2) * \text{ERRLIM}_j * \text{ZREJMOD}]$  then  $\text{flag} = j$  where  $D2 = 1/2 (D_u^2 + D_v^2)$  with  $D_u$ ,  $D_v$  wind component deviations from background;  $\text{sfg}$  std of the background wind component error (mean for  $u$  and  $v$ );  $\text{sobs}$  std of the observation wind component error,  $2 \text{ m s}^{-1}$  for levels below 700 hPa included,  $3.5 \text{ m s}^{-1}$  at 500 hPa,  $4.3 \text{ m s}^{-1}$  at 400 hPa and  $5 \text{ m s}^{-1}$  for all levels above;  $\text{ERRLIM}_j$  is 8 for  $j = 1$ , 18 for  $j = 2$  and 20 for  $j = 3$ . The value of  $\text{ZREJMOD}$  depends on the level of AMW and normally its value is:

- $\text{ZREJMOD} = 0.2$  for low level
- $\text{ZREJMOD} = 0.1$  for all others levels

A special check or asymmetric check is applied when the observed speed is more than  $4 \text{ m s}^{-1}$  slower than the background speed  $\text{SPD}_{\text{fg}}$ . This check has a more restrictive rejection limit:

- $\text{ZREJMOD} = 0.15$  at low level
- $\text{ZREJMOD} = 0.07$  in the tropics
- $\text{ZREJMOD} = 0.075 - 0.00125 * \text{SPD}_{\text{fg}}$  all others
- $\text{ZREJMOD} = 0.0$  if  $\text{SPD}_{\text{fg}} > 60 \text{ m s}^{-1}$  (observation gets always flag  $j = 3$ )

When the data is passed to the following variational quality control its probability of being used depend on the flag  $j$ . With flag  $j = 1$  the data will be assimilated, with flag  $j = 2$  it will be given an intermediate probability and might be used or not and finally the analysis will reject all data with  $j = 3$ .



# Chapter 11

## Land-surface analysis

### Table of contents

- 11.1 Introduction**
- 11.2 2D Optimum Interpolation screen-level analysis**
  - 11.2.1 Methodology
  - 11.2.2 Quality controls
  - 11.2.3 Technical aspects
- 11.3 2D Optimum Interpolation snow analysis**
  - 11.3.1 Organisation
  - 11.3.2 Methodology
  - 11.3.3 Quality controls
  - 11.3.4 Technical aspects
- 11.4 Simplified Extended Kalman Filter Soil moisture analysis**
  - 11.4.1 Methodology
  - 11.4.2 Quality controls
  - 11.4.3 Technical aspects
- 11.5 1D OI soil and snow temperature analysis**

### 11.1 INTRODUCTION

The land-surface analysis includes the screen-level parameters analysis, the snow depth analysis, the soil moisture analysis, the soil temperature and snow temperature analysis. The screen level parameters analysis and the snow analysis rely on a 2-dimensional Optimum Interpolation (2D OI). The soil moisture analysis is based on a simplified Extended Kalman Filter (EKF). The soil and snow temperature analysis uses a 1-dimensional OI (1D OI).

The surface-analysis module includes also the sea-surface temperature, sea-ice fraction and screen-level temperature analysis described separately in [Chapter 12](#).

Snow water equivalent, soil temperature, snow temperature and soil water content are prognostic variables of the forecasting system and, as a consequence, they need to be initialised at each analysis cycle. The ECMWF soil moisture, soil temperature and snow temperature analyses rely on SYNOP relative humidity and temperature at screen-level (2 metres) available on the GTS (around 12,000 reports over the globe are provided every 6 hours). The snow analysis relies on SYNOP and national ground observations of snow depth available on the GTS, as well as on the NOAA/NESDIS (National Oceanic and Atmospheric Administration - National Environmental Satellite, Data, and Information Service) Interactive Multi-sensor Snow and Ice Mapping System (IMS) snow cover information.

The structure of the land surface analysis components and their dependencies are shown in [Fig. 11.1](#). Firstly, a screen-level analysis is performed for temperature and humidity. Secondly, the snow analysis and the soil moisture analysis are conducted. Then the soil temperature and snow temperature analysis is performed. Analysed screen-level temperature and relative humidity are used as input of the simplified EKF soil moisture analysis. while screen-level analysis temperature increments are used as inputs of the 1D OI soil and snow temperature analysis.

Land analysis is run separately from the upper-air analysis. It feedbacks to the upper-air analysis of the next cycle through its influence on the short forecast that propagates information from one cycle to the

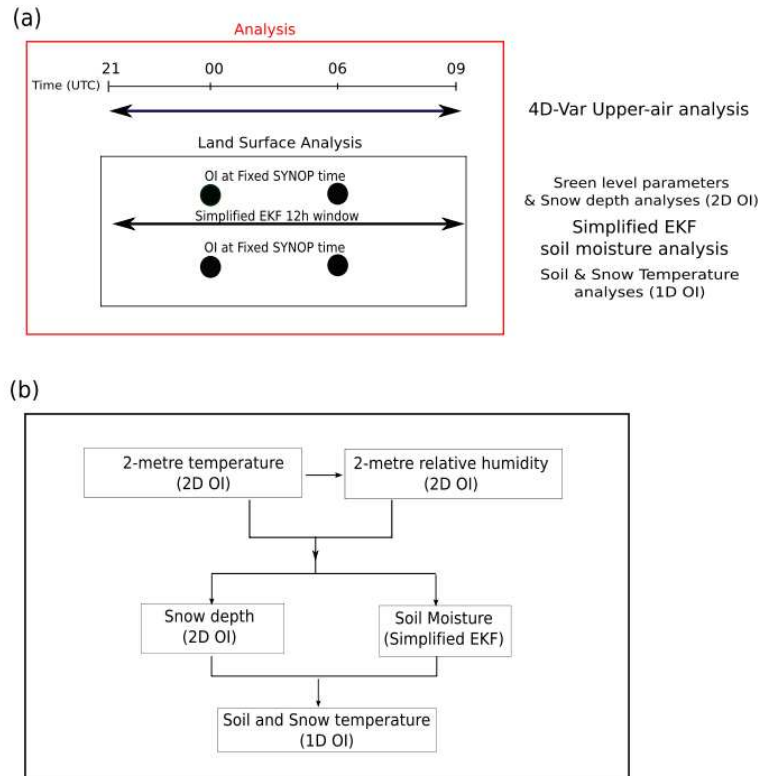


**Figure 11.1** Land surface analysis components and tasks organisation, for an example of a 12-hour (21:00 UTC to 09:00 UTC) data assimilation window.

next. Reciprocally, the 4D-Var influences through the short forecasts the land surface analysis from one cycle to the next. The OI analyses of screen level parameters, snow depth, snow and soil temperature are performed at fixed times at 0000, 0600, 1200, and 1800 UTC. The simplified EKF analysis runs at the same time as the 4D-Var windows for both the delayed cut-off and the early delivery analyses.

## 11.2 2D OPTIMUM INTERPOLATION SCREEN-LEVEL ANALYSIS

### 11.2.1 Methodology

Two independent analyses are performed for 2-metre temperature and 2-metre relative humidity. The method used is a two-dimensional univariate Optimum Interpolation (2D OI). In a first step, the background field (6-hour or 12-hour forecast) is interpolated horizontally to the observation locations using a bilinear interpolation scheme and background increments  $\Delta X_i$  are estimated at each observation location  $i$ .

The analysis increments  $\Delta X_p^a$  at each model grid-point  $p$  are then expressed as a linear combination of the first-guess increments (up to  $N$  values) given by

$$\Delta X_p^a = \sum_{i=1}^N W_i \times \Delta X_i \tag{11.1}$$

where  $W_i$  are optimum weights given (in matrix form) by

$$(\mathbf{B} + \mathbf{O})\mathbf{W} = \mathbf{b} \tag{11.2}$$

The column vector  $\mathbf{b}$  (dimension  $N$ ) represents the background error covariance between the observation  $i$  and the model grid-point  $p$ . The  $(N \times N)$  matrix  $\mathbf{B}$  describes the error covariances of background fields

between pairs of observations. The horizontal correlation coefficients (structure functions) of  $\mathbf{b}$  and  $\mathbf{B}$  are assumed to have the form

$$\mu(i, j) = \exp\left(-\frac{1}{2}\left[\frac{r_{ij}}{d}\right]^2\right) \quad (11.3)$$

where  $r_{ij}$  is the horizontal separation between points  $i$  and  $j$ , and  $d$  is a parameter defined to be 300 km, corresponding to the e-folding distance taken of 420 km.

Therefore

$$B(i, j) = \sigma_b^2 \times \mu(i, j) \quad (11.4)$$

with  $\sigma_b$  the standard deviation of background errors.

The covariance matrix of observation errors  $\mathbf{O}$  is set to  $\sigma_o^2 \times \mathbf{I}$  where  $\sigma_o$  is the standard deviation of observation errors and  $\mathbf{I}$  the identity matrix.

The standard deviations of background and observation errors are set respectively to 1.5 K and 2 K for temperature and 5% and 10% for relative humidity. The number of observations closest to a given grid point that are considered for solving (11.1) is  $N = 50$  (scanned within a radius of 1000 km). The analysis is performed over land and ocean but only land (ocean) observations are used for model land (ocean) grid points.

### 11.2.2 Quality controls

Gross quality checks are first applied to the observations such as  $RH \in [2, 100]$  and  $T > T^d$  where  $T^d$  is the dew point temperature. Redundant observations are also removed by keeping only the closest (and more recent) to the analysis time.

Observation points that differ by more than 300 m from the model orography are rejected.

For each datum a check is applied based on statistical interpolation methodology. An observation is rejected if it satisfies

$$|\Delta X_i| > \gamma \sqrt{\sigma_o^2 + \sigma_b^2} \quad (11.5)$$

where  $\gamma$  has been set to 3, both for temperature and humidity analyses.

The number of used observations every 6 hours varies between 4,000 and 6,000 corresponding to around 40% of the available observations.

The final relative humidity analysis is bounded between 2% and 100%. The final MARS archived product is dew-point temperature that uses the 2-metre temperature analysis  $T_a$  to perform the conversion so that

$$T^d = \frac{17.502 \times 273.16 - 32.19 \times \Psi}{17.05 - \Psi} \quad (11.6)$$

with

$$\Psi = \log(RH_a) + 17.502 \times \frac{T_a - 273.16}{T_a - 32.19} \quad (11.7)$$

### 11.2.3 Technical aspects

The screen-level analysis software is implemented as a branch of the more comprehensive surface and screen-level analysis (SSA) package. The other branches currently include snow analysis and sea surface temperature and sea-ice fraction analyses. The program organisation when performing screen-level parameters analysis is roughly as shown in [Fig. 11.2](#).

The main program SSA calls CONTROL\_SSA where most of the setup and namelist handling are done. Routine INIT2M performs initialisation of the analysis of the actual screen-level parameters by sensing the size of the observation array file (CMA-file) in SCAN\_DDR and generating latitudinal coordinates that stem from the model resolution and zeros of the Bessel function.

After this, all input fields are read into memory in GETFIELDS. They consist of the 2-metre temperature, 2-metre dew point temperature, 2-metre relative humidity from the first-guess (6-hour forecast), land/sea mask and the orography in a form of the geopotential.

- SSA
  - CONTROL\_SSA
    - **INIT2M**
      - SCAN\_DDR
      - COORDINATES
      - GETFIELDS
      - SCAN\_CMA\_ODB
        - SCAN\_OBS
          - LAND\_OBS
          - INITIAL\_REJECTION
          - REDUNDANT\_OBS
    - **T2M\_ANALYSIS**
      - SCAN\_OBS
        - FG2OBS
      - OIUPD
        - CALC\_DISTANCE
        - OISET
        - OIINC
          - EQU SOLVE
          - DOT\_PRODUCT
  - FDB\_OUTPUT
  - PRINT\_SUMMARY
  - PLOTDATA
  - FEEDBACK

**Figure 11.2** Program organisation when performing the 2D OI screen-level parameters analysis. Red colour highlights differences with the snow analysis program organisation shown in Fig. 11.4

In SCAN\_CMA\_ODB observations are read into memory and a quick validity check of the non-applicable observations for this analysis is performed.

Additional screening is done in INITIAL\_REJECTION and in REDUNDANT\_OBS. The first of these sets up an internal table where all the observations which survived from the quick screening are placed with a minimum amount of context information. This routine rejects some of the observations entered into the table due to inconsistencies.

The routine REDUNDANT\_OBS removes time duplicates and retains the observations of the considered station with the closest (and the most recent) to the analysis time. Slowly moving platform handling is present in the REDUNDANT\_OBS for the 2-metre temperature and 2-metre relative humidity analyses.

The actual 2-metre temperature and 2-metre relative humidity analyses are performed under T2M\_ANALYSIS. The analysis increments are computed in the subroutine OIUPD. Subroutines CALC\_DISTANCE and OISET select and sort the  $N$  closest observations from a given grid-point. Subroutine OIINC provides the analysis increments from (11.1) and (11.2), by first computing  $\mathbf{q} = (\mathbf{B} + \mathbf{O})^{-1} \Delta \mathbf{X}$  (in subroutine EQU SOLVE – inversion of a linear system), which does not depend upon the position of the analysis grid point, and then estimating  $\mathbf{b}^T \mathbf{q}$  (in subroutine DOT\_PRODUCT).

Most of the control parameters of the screen-level analysis are defined in the namelist NAMSSA.

- (i) C\_SSA\_TYPE: ‘t2m’ for temperature analysis and ‘rh2m’ for relative humidity analysis.
- (ii) L\_OI : .TRUE. for statistical interpolation and .FALSE. for Cressman interpolation.
- (iii) N\_OISET: number of observations (parameter  $N$ ).
- (iv) SIGMAB: standard deviation of background error (parameter  $\sigma_b$ ).
- (v) SIGMAO: standard deviation of observation error (parameter  $\sigma_o$ ).
- (vi) TOL\_RH: Tolerance criteria for RH observations (parameter  $\gamma$  in (11.5)).
- (vii) TOL\_T: Tolerance criteria for T observations (parameter  $\gamma$  in (11.5)).

(viii) SCAN\_RAD\_2M(1): Scanning radius for available observations (set to 1000 km).

## 11.3 2D OPTIMUM INTERPOLATION SNOW ANALYSIS

### 11.3.1 Organisation

The snow analysis is a 2 Dimensional Optimum Interpolation performed every 6 hours, at 00 UTC, 06 UTC, 12 UTC and 18 UTC. The snow-depth background  $S^b$  (units: m) is estimated from the short-range forecast of snow water equivalent  $SW E_s^b$  (units: m of water equivalent) and snow density  $\rho_s^b$  (units:  $\text{kg m}^{-3}$ ). It is given by

$$S^b = \frac{1000 \times SW E_s^b}{\rho_s^b} \quad (11.8)$$

The snow analysis is performed using snow-depth observations, the snow-depth background field, and the high resolution (4km) NOAA/NESDIS snow extent. Snow depth observations include conventional snow depth reports from SYNOP stations as well as additional national snow depth observations reported by several member states and available on the GTS (de Rosnay *et al.*, 2011a). If snow-depth observations are not available, the snow accumulation/melting is simulated from the model 6-hour forecast. The use of the satellite derived snow extent is optional. In the current default configuration, it is used once per day, for the 12 UTC analysis. As an alternative, snow climate can be used to ensure the stability of the scheme and to give a seasonal snow trend in areas without any observations.

### 11.3.2 Methodology

The snow analysis is a two-step algorithm. In the first step, the background field  $S^b$  (as defined above) is compared with the NOAA/NESDIS snow extent product (Drusch *et al.*, 2004). Grid boxes, which are “snow free” in the first guess but snow covered in the satellite derived product, are updated with a constant snow depth of 100mm of density  $100 \text{kgm}^{-2}$ . A relaxation threshold has been introduced so that grid point are considered “snow free” when they have less than 1 cm of snow depth. In the second step, the actual OI snow analysis is performed based on  $N$  observations from ground stations reports and snow free satellite observations, which enter the analysis with a snow depth of 0 cm. Following the same 2D OI method than for the screen level parameters analysis, the snow depth analysis increment is computed at each model grid point  $p$ :

$$\Delta S_p^a = \sum_{i=1}^N W_i \times \Delta S_i \quad (11.9)$$

where  $\Delta S_i$  is the background increment at each observation  $i$  location,  $W_i$  are optimum weights given (in matrix form) by:

$$(\mathbf{B} + \mathbf{O})\mathbf{W} = \mathbf{b} \quad (11.10)$$

The column vector  $\mathbf{b}$  (dimension  $N$ ) represents the background error covariance between the observation  $i$  and the model grid-point  $p$ . The  $(N \times N)$  matrix  $\mathbf{B}$  describes the error covariances of background fields between pairs of observations  $(i, j)$ .

For the snow analysis the horizontal correlation coefficients (structure functions) of  $\mathbf{b}$  and  $\mathbf{B}$  follow the formulation proposed by Brasnett (1999):

$$\mu_{ij} = \alpha(r_{ij})\beta(\Delta z_{ij}) \quad (11.11)$$

where  $r_{ij}$  and  $z_{ij}$  are the horizontal and the vertical separation between points  $i$  and  $j$ , respectively.  $\alpha(r_{ij})$  and  $\beta(\Delta z_{ij})$  are the horizontal and vertical structure functions respectively:

$$\alpha(r_{ij}) = \left(1 + \frac{r_{ij}}{L}\right) \exp\left(-\frac{r_{ij}}{L}\right) \quad (11.12)$$

$L$  is the horizontal length parameter taken to 55000m, corresponding to an e-folding distance taken to 120 km.

$$\beta(\Delta z_{ij}) = \exp\left(-\left[\frac{\Delta z_{ij}}{h}\right]^2\right) \quad (11.13)$$

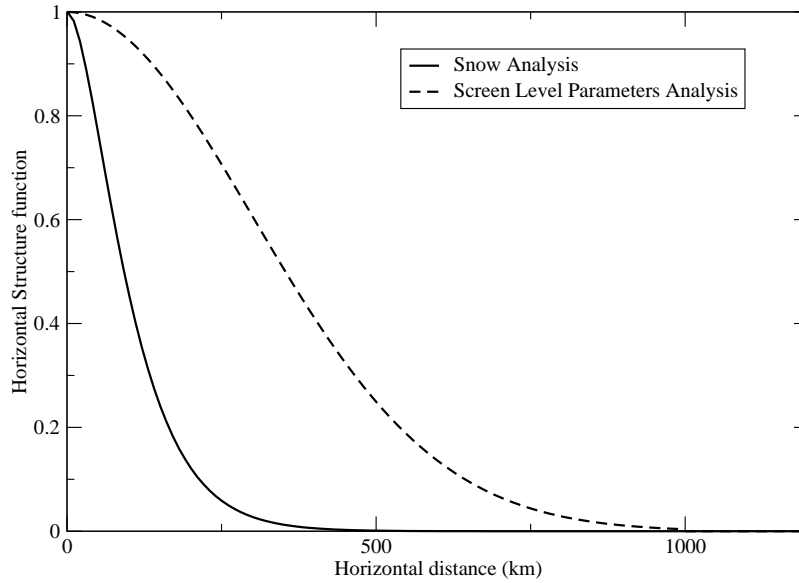


**Figure 11.3** Horizontal structure functions used in the Optimum Interpolation scheme for the screen level parameters and snow depth analyses.

$h$  is the vertical length scale taken to 800 m. The two parameters  $L$  and  $h$  are controlled in the namelist NAMSSA and in the current version their value is defined in the script SSAANA. The horizontal structure functions used in the snow analysis and in the screen level parameters analysis is represented in Fig. 11.3.

The correlation matrix  $B$  is expressed as:

$$B(i, j) = \sigma_b^2 \times \mu(i, j) \quad (11.14)$$

with  $\sigma_b$  the standard deviation of background errors.

The covariance matrix of observation errors  $\mathbf{O}$  is set to  $\sigma_o^2 \times \mathbf{I}$  where  $\sigma_o$  is the standard deviation of observation errors and  $\mathbf{I}$  the identity matrix.

The standard deviations of background and observation errors are set respectively to 3 cm and 4 cm. The number of observations closest to a given grid point that are considered is  $N = 50$  (scanned within a radius of 250 km).

The final snow water equivalent product  $SWE_s^a$  is then calculated using the analysed snow depth  $S^a$ :

$$SWE_s^a = \frac{\rho_s^b \times S^a}{1000} \quad (11.15)$$

The snow density is updated to ensure the consistency between the analysis and the physical parameterisation:

- In the case of positive analysis increments on snow free areas in the first guess, the snow density of fresh snow is applied. It accounts for compaction effects of fresh snow due to meteorological conditions, following a function of near surface air temperature and wind speed as described in the IFS documentation Part IV: Physical processes Chapter 8.4.2.
- In the other cases, the snow density remains unchanged.

Areas with permanent snow and ice (defined using the Global Land Cover Characterisation product) are set to an arbitrary high value at each analysis cycle ( $SWE_s^a = 10$  m).

The snow temperature analysis is performed within the soil and snow temperature analysis as described in Section 11.5.

### 11.3.3 Quality controls

For each datum a check is applied based on statistical interpolation methodology. An observation is rejected if it satisfies

$$|\Delta S_i| > \gamma \sqrt{\sigma_o^2 + \sigma_b^2} \quad (11.16)$$

where  $\gamma$  is the tolerance, controlled in the namelist NAMSSA and set to 5 for the snow analysis in the SSAANA script.

Use of satellite data in mountainous area is switched off in the subroutine CALC\_DISTANCE. This prevents from using relatively large scale information (4 km resolution of the NOAA/NESDIS product), in areas where very local scale conditions apply.

In addition to the preliminary quality control, the following checks are applied for each grid point when using SYNOP snow depth report.

- (i) If  $T_{2m}^b < 8^\circ\text{C}$  only snow-depth observations below 140 cm are accepted.
- (ii) This limit is reduced to 70 cm if  $T_{2m}^b > 8^\circ\text{C}$ .
- (v) Snow-depth analysis is limited to 140 cm.
- (vi) Snow-depth increments are set to zero when larger than  $(160 - 16T_{2m}^b)$  mm (where  $T_{2m}^b$  is expressed in Celsius).

Satellite-derived snow extent is used in the analysis to replace the role of snow depth climatology in correcting for the model bias. However, there is the option to weight the analysis of snow depth with the climatological value  $S^{\text{clim}}$  so that the final analysis is provided by

$$S^a = (1 - \alpha)S^o + \alpha S^{\text{clim}} \quad (11.17)$$

The relaxation coefficient  $\alpha$  can be changed through the namelist. Its default value is set to 0.02, which corresponds to a time scale of 12.5 days at six-hourly cycling.

### 11.3.4 Technical aspects

The technical aspects are very similar to those of the screen-level parameters analysis (see [Section 11.2.3](#)). So, the program organisation when performing snow analysis is roughly as shown in [Fig. 11.4](#).

The routine INISNW performs initialisation of the actual snow analysis (instead of INIT2M for the screen-level parameters analysis). Input fields read into memory in GETFIELDS consist of the snow water equivalent and snow density from the first-guess (6-hour forecast), 2-metre temperature first guess, snow-depth climate (varies monthly with a linear temporal interpolation), land/sea mask and finally the orography in a form of the geopotential.

In SUB\_PREP\_NES the satellite data are retrieved from BUFR. The actual snow analysis is performed under SNOW\_ANALYSIS. In a first step, the first guess field is updated with the satellite observations (routine NESDIS\_FILL). The satellite observations that contain snow are retrieved from BUFR (routine SUB\_PREP\_NES).

The analysis increments are computed in the subroutine OIUPD. Subroutines CALC\_DISTANCE and OISET select and sort the  $N$  closest observations from a given grid-point. Subroutine OIINC provides the analysis increments computed from equations (11.9) and (11.14). This increment is finally added to the snow-depth fields at grid points producing the final snow-depth output field, which is output in routine FDB\_OUTPUT. Statistics are summarised in PRINT\_SUMMARY.

The main logicals of the namelist NAMSSA are as follows.

- (i) L\_SNOW\_ANALYSIS: When set to .TRUE., the snow analysis is performed.
- (ii) L\_SNOW\_DEPTH\_ANA: When set to .TRUE., the snow analysis is performed in snow depth (in opposition to snow water equivalent assuming a constant value of  $250 \text{ kg m}^{-2}$  for observed snow density).

- SSA
  - CONTROL\_SSA
    - **INISNW**
      - SCAN\_DDR
      - COORDINATES
      - GETFIELDS
      - **SUB\_PREP\_NES**
      - SCAN\_CMA\_ODB
        - SCAN\_OBS
          - LAND\_OBS
          - INITIAL\_REJECTION
          - REDUNDANT\_OBS
    - **SNOW\_ANALYSIS**
      - **NESDIS\_FILL**
        - **SUB\_PREP\_NES**
      - SCAN\_OBS
        - FG2OBS
      - OIUPD
        - CALC\_DISTANCE
        - OISET
        - OIINC
          - EQU SOLVE
          - DOT\_PRODUCT
    - FDB\_OUTPUT
    - PRINT\_SUMMARY
    - PLOTDATA
    - FEEDBACK

**Figure 11.4** Program organisation when performing snow analysis. Red colour highlights differences with the snow analysis program organisation shown in [Fig. 11.2](#)

- (iii) L\_USE\_SNOW\_CLIMATE: When set to `.TRUE.`, a relaxation of the snow analysis towards a monthly climatology is performed with a time scale of 12.5 days (the relaxation coefficient is passed through NAMSSA).
- (iv) L\_USE\_FG\_FIELD: When set to `.TRUE.` the snow analysis is set to the first-guess value (no use of observations) and there is no relaxation to climatology.
- (v) L\_USE\_SCOVER\_NESDIS: When set to `.TRUE.`, the NOAA/NESDIS satellite product is used.

Most of the control parameters of the screen-level analysis are defined in the namelist NAMSSA. In addition to those defined in [Section 11.2.3](#)

- (vi) TOL\_SN: Tolerance criteria for snow depth observations (parameter  $\gamma$  in [11.16](#)).
- (viii) RSCALE\_X: horizontal distance  $L$  used in the horizontal structure function in [\(11.12\)](#), set to 55000 m.
- (ix) RSCALE\_Z: vertical distance  $h$  used in the vertical structure function in [\(11.13\)](#), set to 800 m.

## 11.4 SIMPLIFIED EXTENDED KALMAN FILTER SOIL MOISTURE ANALYSIS

### 11.4.1 Methodology

The simplified EKF soil moisture analysis used at ECMWF is a point wise data assimilation scheme, as described in [Drusch \*et al.\* \(2009\)](#); [de Rosnay \*et al.\* \(2011b\)](#). The analysed soil moisture state vector  $\mathbf{x}^a$  is computed at time  $t_i$  for each grid point as:

$$\mathbf{x}^a(t_i) = \mathbf{x}^b(t_i) + \mathbf{K}_i [\mathbf{y}^o(t_i) - \mathcal{H}_i(\mathbf{x}^b)] \quad (11.18)$$



with superscripts  $a$ ,  $b$ ,  $o$  standing for background, analysis and observations, respectively,  $\mathbf{x}$  the model state vector,  $\mathbf{y}$  the observation vector and  $\mathcal{H}$  the non-linear observation operator. The Kalman gain matrix  $\mathbf{K}_i$  is computed at time  $t_i$  as:

$$\mathbf{K}_i = \left[ \mathbf{P}^{-1} + \mathbf{H}_i^T \mathbf{R}^{-1} \mathbf{H}_i \right]^{-1} \mathbf{H}_i^T \mathbf{R}^{-1} \quad (11.19)$$

where  $\mathbf{H}_i$  is the linearised observation operator,  $\mathbf{P}$  is the error covariance matrix associated with  $\mathbf{x}$  and  $\mathbf{R}$  is the observation errors covariance matrix.

The background error covariance matrix  $\mathbf{P}$  and the observation error matrix  $\mathbf{R}$  are static, with diagonal terms composed of error variances. These terms are based on soil moisture standard deviation  $\sigma_b = 0.01 m^3 m^{-3}$  and screen levels parameters standard deviations of  $\sigma_T = 2K$  for the 2-metre temperature and  $\sigma_{RH} = 10\%$  for the relative humidity.

The linearisation of the observation operator is computed in finite differences, by using individual perturbations of the model state vector by a small amount  $\delta x_n$  of the  $n^{th}$  component of the model state vector. One perturbed simulation is required for each element of the control state vector. For each perturbed simulation, initial background state vector is perturbed by a vector  $\delta \mathbf{x}_n^b$  that contains  $\delta x_n$  for the perturbed  $n^{th}$  element and zero for all the others elements. Using index  $m$  to represent the  $m^{th}$  element of the observations vector, the Jacobian elements  $\mathbf{H}_{mn,i}$  of the observation operator at time  $t_i$  is written as:

$$\mathbf{H}_{mn,i} = \frac{\mathcal{H}_{m,i}(\mathbf{x}^b + \delta \mathbf{x}_n^b) - \mathcal{H}_{m,i}(\mathbf{x}^b)}{\delta x_n} \quad (11.20)$$

The model state vector evolution from time  $t_i$  to time  $t_{i+1}$  is then controlled by the equation:

$$\mathbf{x}^b(t_{i+1}) = \mathcal{M}_i[\mathbf{x}^a(t_i)] \quad (11.21)$$

with  $\mathcal{M}$  the non-linear state forecast model.

In the current implementation, the state vector is soil moisture. It has dimension  $n_{max} = 3$  since the first three layers of the HTESSEL LSM are analysed. The observations vector  $\mathbf{y}$  includes 2-metre temperature and relative humidity analyses. When 12-hour assimilation windows are used,  $\mathbf{y}$  has dimension  $m_{max} = 4$  since 2-metre temperature and relative humidity analyses are available twice per assimilation window, at synoptic times.

#### 11.4.2 Quality controls

To avoid spurious corrections the soil moisture analysis is locally switched off if the Jacobians become larger than  $50K/m^3 m^{-3}$  or  $5/m^3 m^{-3}$  for the  $T_{2m}$  or  $RH_{2m}$  component respectively. In addition, the analysis is switched off if the soil moisture increment for any layer is larger than  $0.1 m^3 m^{-3}$ .

#### 11.4.3 Technical aspects

The simplified EKF soil moisture analysis is a configuration of the IFS (NCONF=302). It is controlled by the namelist NAMSEKF. In the current IFS cycle, a number of control parameters of this namelist are defined in the SEKF\_SM script:

- Number of control variables, N\_SEKF\_CV=3, (ie number of analysed soil layers)
- Soil moisture perturbation  $\delta x_n$  for each layer, VSM\_PERT\_INC, set to  $0.01 m^3 m^{-3}$  in the current configuration,
- Background soil moisture error, BACK\_ERR=0.0001  $m^6 m^{-6}$ , corresponds to  $\sigma_b = 0.01 m^3 m^{-3}$
- Screen level analysis errors, T2M\_ERR=4, RH2M\_ERR=100, correspond to  $\sigma_T = 2K$  for the 2-metre temperature and  $\sigma_{RH} = 10\%$ .
- A switch is present to activate the use of the ASCAT (Advanced SCATterometer) soil moisture data (LUSE\_ASCAT). It is set to false by default.

- CNT0
  - SEKF1
    - SEKF2
      - SUSEKF
      - CNT3
        - PERTSEKF\_V2
        - CNT4
        - OBSGEN
        - SEKF\_PREP\_ASCAT
        - SM\_EKF\_MAIN
          - SEKF\_MAGN\_RH
          - SEKF\_GAIN
          - SEKF\_COSTF
      - SM\_WRITE

**Figure 11.5** Program organisation for the simplified EKF soil moisture analysis ( $NCONF=302$ ).

Fig. 11.5 shows the main steps of the simplified EKF soil moisture analysis. CNT0, SEKF1 and SEKF2 are the control programs. From CSEKF2, SUSEKF does the setup of the EKF analysis. CNT3 is the main control program of the simplified EKF analysis. It defines the perturbed soil moisture initial conditions, by calling PERTSEKF\_V2. Then it does a loop on the control and the perturbed runs with one CNT4 call for each of the control and perturbed cases. Resulting soil moisture and screen level parameters fields are stored from the routine STORE\_SEKF\_CV which is called at lower level from CALLPAR and EC\_PHYS. After this loop on CNT4 call, all the model soil moisture and screen level conditions that will enter the equation 11.18 are stored.

OBSGEN and SEKF\_PREP\_ASCAT are the routine that prepare the observations to be used in the simplified EKF analysis. Then CNT4 calls the simplified EKF programme SM\_EKF\_MAIN which runs the EKF on each grid point of the model. Here the simplified EKF vectors and matrices defined in Equations 11.18 to 11.21 are filled with model and observation values stored in the previous routines. SEKF\_MAGN\_RH computes the relative humidity from the dew point and air temperatures. SEKF\_GAIN computes the Kalman Gain.

## 11.5 1D OI SOIL AND SNOW TEMPERATURE ANALYSIS

The temperature of the first layer of soil (0-7cm) and the snow layer are analysed using a “local” 1-dimensional optimum interpolation (1D OI) technique as described in Mahfouf (1991) and Douville *et al.* (2001). The analysis increments from the screen-level temperature analysis are used to produce increments for the first layer soil temperature and snow temperature:

$$\Delta T = c \times (T_a - T_b) \quad (11.22)$$

with  $T_a$  and  $T_b$  the analysed and model first-guess temperatures, respectively. The coefficient  $c$  providing the analysis increments is:

$$c = (1 - F_1)F_3 \quad (11.23)$$

$F_1$  and  $F_3$  are empirical functions.  $F_1$  is function of the cosine of the mean solar zenith angle  $\mu_M$ , averaged over the 6-hours before the analysis time given by:

$$F_1 = \frac{1}{2} \{1 + \tanh[\lambda(\mu_M - 0.5)]\} \quad \lambda = 7 \quad (11.24)$$

The empirical function  $F_3$  reduces increments over mountainous areas so that

$$F_3 = \begin{cases} 0 & Z > Z_{\max} \\ \left( \frac{Z - Z_{\max}}{Z_{\min} - Z_{\max}} \right)^2 & Z_{\min} < Z < Z_{\max} \\ 1 & Z < Z_{\min} \end{cases} \quad (11.25)$$

where  $Z$  is the model orography,  $Z_{\min} = 500$  m and  $Z_{\max} = 3000$  m.

The coefficient  $c$  is such that soil and snow temperatures are more effective during night and in winter, when the temperature errors are less likely to be related to soil moisture. In the 12-hour 4D-Var configuration, the snow and soil temperature analysis is performed twice during the assimilation window and the sum of the increments is added to the background values at analysis time.



## Chapter 12

# Analysis of sea-ice concentration and sea surface temperature

### 12.1 INTRODUCTION

The analyses of sea-ice concentration (CI) and sea surface temperature (SST) are interpolations to the model grid of daily global datasets provided by The Metoffice, with backup from NCEP in case OSTIA is not available. The Metoffice OSTIA product is described by [Stark \*et al.\* \(2007\)](#) and is available in the ECMWF archives from 20071020 onwards. Its sea ice component is taken from the Satellite Application Facility on Ocean and Sea Ice (OSI-SAF) product. The NCEP RTG real-time global SST product is described by <http://polar.wwb.noaa.gov.sst> and is available in the ECMWF archives from 20010130. The only lake information in these two products is for the Caspian Sea, with the addition of the Great Lakes in NCEP RTG. For other lakes, climatological values are used.

### 12.2 CHOICE OF PRODUCT

Both the OSTIA and the NCEP products are read in if available. If both are available, OSTIA is used for the oceans and the Caspian Sea and the Great Lakes are taken from NCEP. If NCEP is missing, no new information is used for the Great Lakes. If OSTIA is missing, NCEP data are used everywhere. If both are missing, yesterdays fields will be used.

Since the OSI-SAF sea-ice product does not include ice coverage over the Caspian Sea and Sea of Azov, the NCEP sea-ice product is used over these areas between 15 September and 1 May (from 2011).

### 12.3 ECMWF RE-SAMPLING TO MODEL GRID

The OSTIA product comes oversampled (i. e. at higher resolution than there is real information) at 0.05 degree resolution, which is then area averaged over the boxes of the models reduced Gaussian grid. The NCEP RTG product comes at 0.5 degree resolution and is bi-linearly interpolated to to the models reduced Gaussian grid. For both products checks are made that the values lie within realistic values. The temperature can not be lower than 271.46K when sea ice is below 20%, and the temperature is set to 273.16K when sea ice is above 20%. For temperatures above 274.26K, the sea ice concentration is set to zero.



## Chapter 13

# Data flow

### Table of contents

- 13.1 Notation**
- 13.2 Data assimilation cycling**
- 13.3 Overview of 4D-Var data flow**
- 13.4 Input GRIB fields**
  - 13.4.1 reftrajshml
  - 13.4.2 reftrajggml
  - 13.4.3 reftrajggsfc
  - 13.4.4 errgrib
  - 13.4.5 spmoderr\_bg\_01
  - 13.4.6 wam\_specwavein
  - 13.4.7 wam\_cdwavein
  - 13.4.8 wam\_uwavein
  - 13.4.9 wam\_sfcwindin
- 13.5 Input observation data**
- 13.6 Input data files**
  - 13.6.1 Invariant data files
  - 13.6.2 Date-dependent data files
- 13.7 Output GRIB fields**
  - 13.7.1 Output type ‘an’ model level spectral fields
  - 13.7.2 Output type ‘an’ model level Gaussian grid-point fields
  - 13.7.3 Output type ‘an’ surface Gaussian grid-point fields
  - 13.7.4 Output type ‘an’ wave model fields
  - 13.7.5 Output error fields
  - 13.7.6 Output model error fields
- 13.8 Output observation data**
- 13.9 Output data files**
- 13.10 Sea surface temperature analysis**
  - 13.10.1 Input GRIB fields on model grid
  - 13.10.2 Input OSTIA and NCEP fields
  - 13.10.3 Input data files
  - 13.10.4 Output GRIB fields on model grid
- 13.11 2 metre temperature analysis**
  - 13.11.1 Input GRIB fields on model grid
  - 13.11.2 Input observation data
  - 13.11.3 Output GRIB field on model grid
- 13.12 2 metre relative humidity analysis**
  - 13.12.1 Input GRIB fields on model grid
  - 13.12.2 Input observation data
  - 13.12.3 Output GRIB field on model grid
- 13.13 Snow analysis**
  - 13.13.1 Input GRIB fields on model grid
  - 13.13.2 Input data files

- 13.13.3 Input observation data
- 13.13.4 Output GRIB fields on model grid
- 13.14 Soil moisture analysis**
  - 13.14.1 Input GRIB fields on model grid
  - 13.14.2 Output GRIB fields on model grid
  - 13.14.3 Invariant climatological fields

## 13.1 NOTATION

The following environment variables, which are used in the same way in the data assimilation scripts, are referred to in this chapter.

**Table 13.1** *Definition of environment variables.*

Variable	Meaning	Default value
<code>DATA</code>	Data directory for invariant files	
<code>GTYPE</code>	Gaussian grid type	l.2 (ie linear reduced Gaussian grid)
<code>IFS_CYCLE</code>	IFS cycle name	CY36R1
<code>LEVELS</code>	Number of vertical model levels	91
<code>MM</code>	Month	
<code>RESOL</code>	Spectral truncation	1279
<code>starttime</code>	Start of 4D-Var window as yyymmddhh	
<code>WDIR</code>	Work directory (1 for each cycle)	

In this chapter, the notation illustrated in Fig. 13.1 is used in diagrams to distinguish between computation steps and data sets.

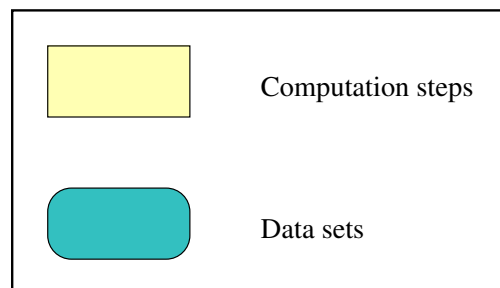


**Figure 13.1** *Notation.*

## 13.2 DATA ASSIMILATION CYCLING

Fig. 13.2 gives an overview of the data flow through the data assimilation system with the operational early-delivery configuration. The 12-hour 4D-Var analyses are run with a delayed cut-off time, in order to use the maximum possible number of observations. The 0000 UTC analysis uses observations from the time window 2101–0900 UTC, while the 1200 UTC analysis uses observations in the window 0901–2100 UTC. The extraction tasks for observations in the periods 2101–0300 UTC and 0301–0900 UTC are run at 1345 and 1400 UTC respectively, while the extraction tasks for the observations in the periods 0901–1500 UTC and 1501–2100 UTC are run at 0145 and 0200 UTC. The 0000 UTC 12-hour 4D-Var analysis generates two sets of analysed fields, at 0000 and 0600 UTC. A separate surface analysis is run every 6 hours. The final analysis is a combination of the fields from 4D-Var and from the surface analysis. The first guess for the 0000 UTC 12-hour 4D-Var analysis is the three-hour forecast from the previous day’s 1800 UTC delayed cut-off analysis. The first guess for the 1200 UTC 12-hour 4D-Var delayed cut-off



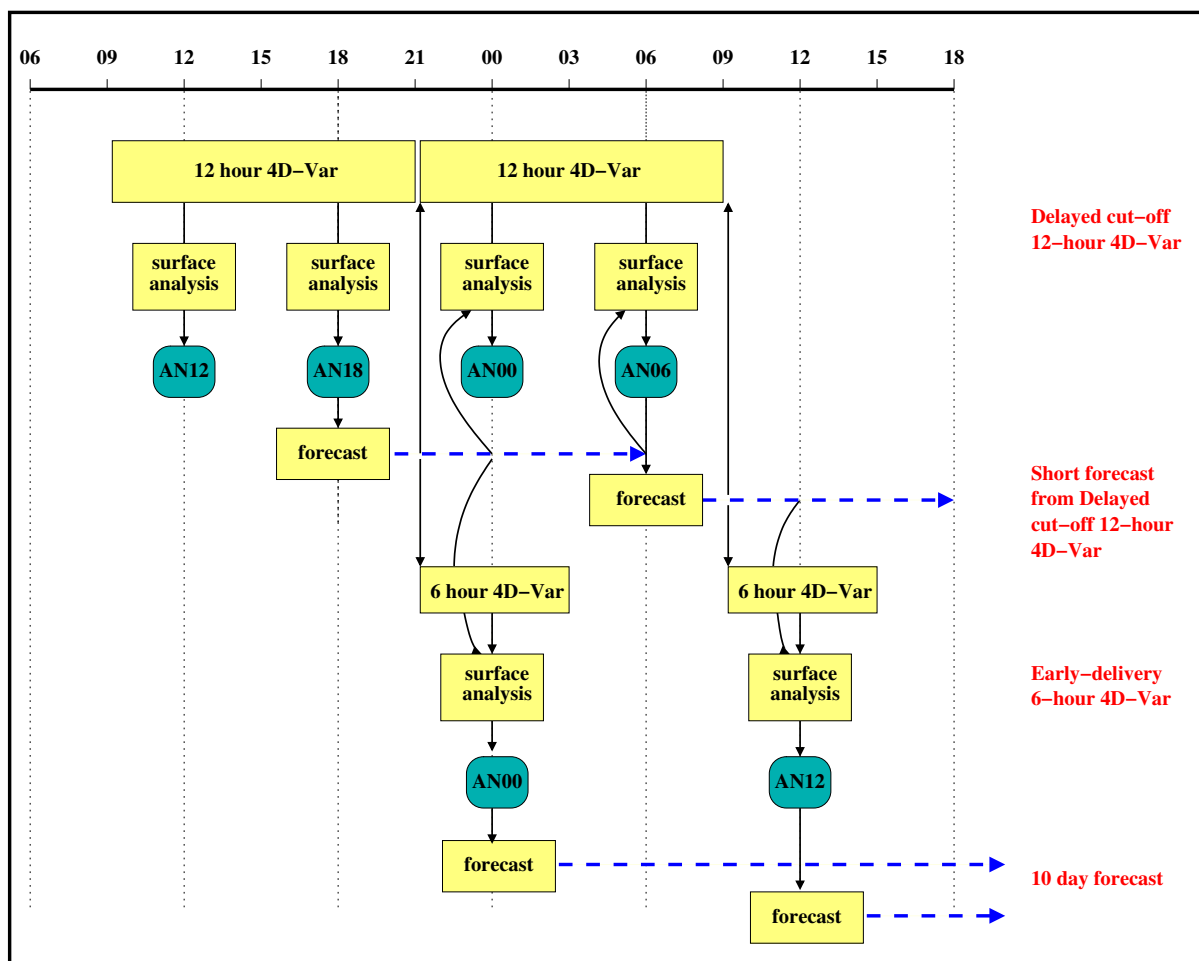


Figure 13.2 Data assimilation cycling with the Early Delivery configuration.

analysis is the three-hour forecast from the 0600 UTC analysis. It is these 12-hour 4D-Var delayed cut-off analyses that propagate information forwards from day to day.

The early-delivery analyses do not propagate information from cycle to cycle. Each analysis is reinitialized with the best available model fields from the delayed cut-off assimilation. The 0000 UTC early-delivery analysis is a 6-hour 4D-Var analysis that uses observations in the time window 2101–0300 UTC. The cut-off time is 0400 UTC, and any observations which arrive after this time are not used by the early-delivery analysis. However, if they arrive by 1400 UTC, they can still be used by the delayed cut-off 12-hour 4D-Var 0000 UTC analysis. The first guess for the 0000 UTC early-delivery analysis is the three-hour forecast from the previous day's 1800 UTC delayed cut-off analysis.

The early-delivery 1200 UTC analysis is a 6-hour 4D-Var analysis that uses observations in the time window 0901–1500 UTC, with a cut-off time of 1600 UTC. Its first guess is the three-hour forecast from the 0600 UTC delayed cut-off analysis.

### 13.3 OVERVIEW OF 4D-VAR DATA FLOW

Fig. 13.3 gives an overview of the data input to and output from 4D-Var. There are three types of input data.

- (i) GRIB fields from the Fields Data Base (FDB). GRIB is a World Meteorological Organisation (WMO) standard format for the representation of General Regularly-distributed Information in

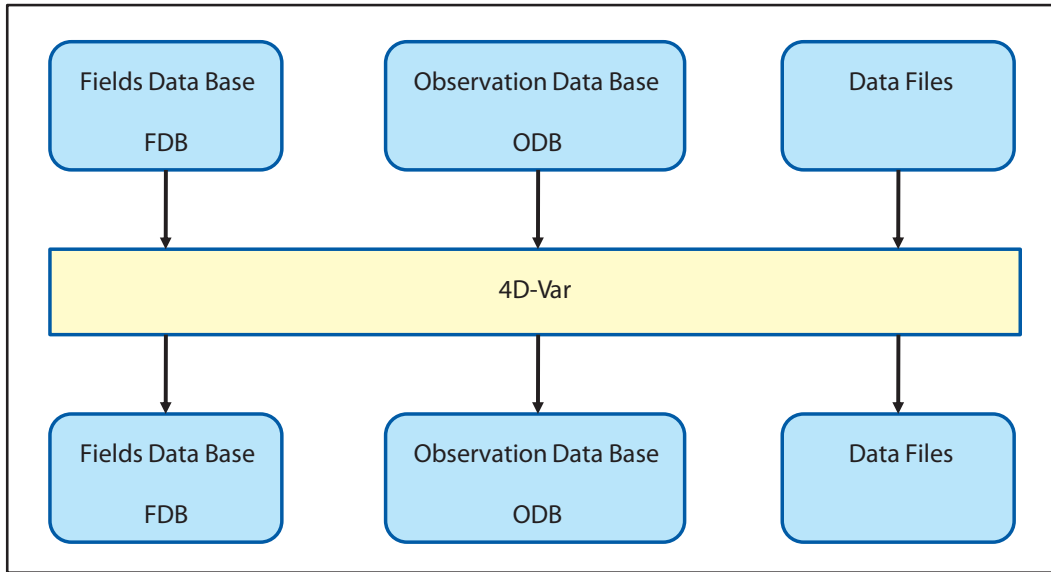


**Figure 13.3** *4D-Var data flow.*

Binary. The GRIB code is described at <http://www.ecmwf.int/products/data/software/grib.html>. The background fields, forecast errors and model errors are read from the Fields Data Base.

- (ii) Observations from the Observation Data Base (ODB).
- (iii) Cycling variational bias correction and emissivity files, plus other data files.

Output data from 4D-Var is in three forms.

- (i) GRIB fields in the Fields Data Base, eg analysis fields, error fields.
- (ii) updates to the ODB, including departures of observations from the background and the analysis and quality control information.
- (iii) updated variational bias correction and emissivity files.

### 13.4 INPUT GRIB FIELDS

The following files in the work directory, \$WDIR, contain GRIB format fields which have been extracted from the Fields Data Base. Fields of type 'fc' are taken from the forecast from the previous cycle's analysis, and are valid at the start of the 4D-Var window. Fields of type 'an' are taken from the previous analysis. The spectral orography is taken from the climatology file of the appropriate resolution, to ensure that the orography is not changed by encoding into and decoding from GRIB. Fields of type 'ef', forecast error in radiance space, and 'me', model error, were output from the previous cycle's 4D-Var analysis. Fields of type 'ses', ensemble based filtered upper air forecast errors, are output from the attached ensemble data assimilation run.

Files which are needed as input to the coupled wave model also have the stream defined. If stream = DA, then the fields were output from the atmospheric model, and the GRIB codes are defined in (ECMWF local table 2, Version 128). If stream = WAVE, then the fields were output from the wave model and the GRIB codes are defined in (ECMWF local table 2, Version 140).

## 13.4.1 reftrajshml

Table 13.2 Background, spherical harmonics, model levels.

Code	Name	Description	Units	Levels	Type
129	Z	Orography (geopotential)	$\text{m}^2 \text{s}^{-2}$	1	climate
130	T	Temperature	K	1-\$LEVELS	fc
138	VO	Vorticity	$\text{s}^{-1}$	1-\$LEVELS	fc
152	LNSP	Logarithm of surface pressure		1	fc
155	D	Divergence	$\text{s}^{-1}$	1-\$LEVELS	fc

## 13.4.2 reftrajggml

Table 13.3 Background, Gaussian grid, model levels.

Code	Name	Description	Units	Levels	Type
133	Q	Specific humidity	$\text{kg kg}^{-1}$	1-\$LEVELS	fc
203	O3	Ozone mass mixing ratio	$\text{kg kg}^{-1}$	1-\$LEVELS	fc
75	CRWC	Cloud rain water content	$\text{kg kg}^{-1}$	1-\$LEVELS	fc
76	CSWC	Cloud snow water content	$\text{kg kg}^{-1}$	1-\$LEVELS	fc
246	CLWC	Cloud liquid water content	$\text{kg kg}^{-1}$	1-\$LEVELS	fc
247	CIWC	Cloud ice water content	$\text{kg kg}^{-1}$	1-\$LEVELS	fc
248	CC	Cloud cover	(0-1)	1-\$LEVELS	fc

## 13.4.3 reftrajggsfc

**Table 13.4** *Surface fields, Gaussian grid, background (variable fields) and analysis (invariant fields).*

Code	Name	Description	Units	Type
031	CI	Sea-ice cover	(0-1)	fc
032	ASN	Snow albedo	(0-1)	fc
033	RSN	Snow density	kg m <sup>-3</sup>	fc
034	SST	Sea surface temperature	K	fc
035	ISTL1	Ice surface temperature, layer 1	K	fc
036	ISTL2	Ice surface temperature, layer 2	K	fc
037	ISTL3	Ice surface temperature, layer 3	K	fc
038	ISTL4	Ice surface temperature, layer 4	K	fc
039	SWVL1	Volumetric soil water, layer 1	m <sup>3</sup> m <sup>-3</sup>	fc
040	SWVL2	Volumetric soil water, layer 2	m <sup>3</sup> m <sup>-3</sup>	fc
041	SWVL3	Volumetric soil water, layer 3	m <sup>3</sup> m <sup>-3</sup>	fc
042	SWVL4	Volumetric soil water, layer 4	m <sup>3</sup> m <sup>-3</sup>	fc
139	STL1	Soil temperature level 1	K	fc
141	SD	Snow depth	m of water equivalent	fc
148	CHNK	Charnock parameter		fc
170	STL2	Soil temperature level 2	K	fc
183	STL3	Soil temperature level 3	K	fc
198	SRC	Skin reservoir content	m of water	fc
235	SKT	Skin temperature	K	fc
236	STL4	Soil temperature level 4	K	fc
238	TSN	Temperature of snow layer	K	fc
228131	U10N	Neutral wind u component at 10m	m s <sup>-1</sup>	fc
228132	V10N	Neutral wind v component at 10m	m s <sup>-1</sup>	fc
244	FSR	Surface roughness	m	fc
245	FLSR	Logarithm of surface roughness	m	fc
015	ALUVP	UV visible albedo for direct radiation	(0-1)	an
016	ALUVD	UV visible albedo for diffuse radiation	(0-1)	an
017	ALNIP	Near IR albedo for direct radiation	(0-1)	an
018	ALNIP	Near IR albedo for diffuse radiation	(0-1)	an
027	CVL	Low vegetation cover	(0-1)	an
028	CVH	High vegetation cover	(0-1)	an
029	TVL	Type of low vegetation	Table index	an
030	TVH	Type of high vegetation	Table index	an
043	SLT	Soil type		an
066	LAI_LV	Leaf area index, low vegetation	m <sup>2</sup> m <sup>-2</sup>	an
067	LAI_HV	Leaf area index, high vegetation	m <sup>2</sup> m <sup>-2</sup>	an
074	SDFOR	Standard deviation of filtered sub-gridscale orography		an
160	SDOR	Standard deviation of orography		an
161	ISOR	Anisotropy of sub-gridscale orography		an
162	ANOR	Angle of sub-gridscale orography	rad	an
163	SLOR	Slope of sub-gridscale orography		an
172	LSM	Land-sea mask	(0, 1)	an
173	SR	Surface roughness	m	an
174	ALB	Albedo	(0-1)	an
234	LSRH	Logarithm of surface roughness		an

13.4.4 `errgrib`Table 13.5 *Background errors, model levels, Gaussian grid.*

Code	Name	Description	Units	Levels	Type
130	T	Temperature	K	1-\$LEVELS	ses
131	U	$u$ velocity	$\text{m s}^{-1}$	1-\$LEVELS	ses
132	V	$v$ velocity	$\text{m s}^{-1}$	1-\$LEVELS	ses
133	Q	Specific humidity	$\text{kg kg}^{-1}$	1-\$LEVELS	ses
138	VO	Vorticity	$\text{s}^{-1}$	1-\$LEVELS	ses
152	LNSP	Logarithm of surface pressure		1	ses
156	GH	Geopotential height	m	1-\$LEVELS	ses
157	R	Relative humidity	%	1-\$LEVELS	ses
194	BTMP	Brightness temperature	K	channels 1-54	ef
203	O3	Ozone mass mixing ratio	$\text{kg kg}^{-1}$	1-\$LEVELS	ses

13.4.5 `smoderr_bg_01`Table 13.6 *Model error, spherical harmonics, model levels.*

Code	Name	Description	Units	Levels	Type
130	T	Temperature	K	1-\$LEVELS	me
138	VO	Vorticity	$\text{s}^{-1}$	1-\$LEVELS	me
152	LNSP	Logarithm of surface pressure		1	me
155	D	Divergence	$\text{s}^{-1}$	1-\$LEVELS	me

13.4.6 `wam_specwavein`Table 13.7 *Background, surface, regular latitude/longitude grid, input for wave model.*

Code	Name	Description	Units	Type	Stream
251	2DFD	2D wave spectra	$\text{m}^2 \text{s radian}^{-1}$	fc	WAVE

13.4.7 `wam_cdwavein`Table 13.8 *Background, surface, regular latitude/longitude grid, input for wave model.*

Code	Name	Description	Units	Type	Stream
233	CDWW	Coefficient of drag with waves		fc	WAVE

13.4.8 `wam_uwavein`Table 13.9 *Background, surface, regular latitude/longitude grid, input for wave model.*

Code	Name	Description	Units	Type	Stream
245	WIND	10 metre wind speed	$\text{m s}^{-1}$	fc	WAVE

### 13.4.9 wam\_sfcwindin

**Table 13.10** *Background, surface, Gaussian grid, input for wave model.*

Code	Name	Description	Units	Type	Stream
031	CI	Sea-ice cover	(0-1)	fc	DA
165	10U	10 metre U wind component	m s <sup>-1</sup>	fc	DA
166	10V	10 metre U wind component	m s <sup>-1</sup>	fc	DA

## 13.5 INPUT OBSERVATION DATA

Observations are read into 4D-Var from the Observation Data Base (ODB). The observation processing is described in more detail in the ODB documentation (file:///home/rd/mps/public/ugodb.pdf).

## 13.6 INPUT DATA FILES

Input data files can be split into two categories, invariant and date-dependent. For the invariant files, a single copy is used for the lifetime of the experiment or the operational suite. The file is copied or linked into the experiment's `DATA` directory at start-up time in task datalinks.

Some files, such as blacklists and bias files, are date-dependent. In the operational suite, the blacklist can be changed at short notice if, for example, a satellite channel fails or a new data source arrives which has to be passively monitored to assess its quality before it can be used actively. Date-dependent files are copied to the `WDIR` directory in task vardata at the beginning of each data assimilation cycle.

### 13.6.1 Invariant data files

- `DATA/an/cmod.table.ieee` – scatterometer coefficients
- `DATA/an/external_bl_mon_monit.b` – external blacklist file
- `DATA/an/moderr.cov` – model error covariances for weak-constraint 4D-Var
- `DATA/an/neuroflux_LLEVELS` – extended linearized longwave radiation
- `DATA/an/radjacobian_LLEVELS` – extended linearized longwave radiation
- `DATA/an/rs.bias_T_table1` – radiosonde temperature bias correction coefficients
- `DATA/an/rs.bias_T_table2` – radiosonde temperature bias correction coefficients
- `DATA/an/rs.bias_T_table3` – radiosonde temperature bias correction coefficients
- `DATA/an/rszcoef_fmt` – radiosonde height observation error correlation coefficients
- `DATA/an/ship_anemometer_heights` – ship anemometer heights
- `DATA/an/stabal96.bal` – background error balance parameters
- `DATA/an/stabal96.cv` – background error correlations
- `DATA/an/stdev_of_climate/mMM` – climatological standard deviations for use in error growth model
- `DATA/an/wavelet_TRESOLINC_n_LLEVELS.cv` – wavelet Jb background error covariances
- `DATA/climate/RESOL/GTYPE/O3CHEMMM` – monthly ozone chemistry climate files
- `DATA/ifs/namelist_IFS_CYCLE` – an empty copy of all the IFS namelists
- `DATA/ifs/rtableGTYPERESOL` – namelist NAMRGRI, defining the number of points on each row of the Gaussian grid
- `DATA/ifs/vtable_LLEVELS` – namelist NAMVV1, defining the hybrid vertical coordinate level coefficients
- `DATA/sat/mwave_error_platform_instrument.dat` – microwave error files
- `DATA/sat/AIRS_CLDDET.NL` – list of channels to be used for AIRS with cloud detection
- `DATA/sat/amv_bias_info` – atmospheric motion vector information
- `DATA/sat/bcor_reo3` – ozone bias correction file
- `DATA/sat/chanspec_noaa` – noaa channel specification file

- `/${DATA}/sat/cstlim_noaa` – noaa cost limit file
- `/${DATA}/sat/filbiaso_[ssmi|tmi]` – SSMI/TMI 1D-Var bias file
- `/${DATA}/sat/filcmix_[ssmi|tmi]` – SSMI/TMI 1D-Var coefficient file
- `/${DATA}/sat/filcovb` – SSMI 1D-Var coefficient file
- `/${DATA}/sat/filcovo_[ssmi|tmi]` – SSMI/TMI 1D-Var coefficient file
- `/${DATA}/sat/filcwat_[ssmi|tmi]` – SSMI/TMI 1D-Var coefficient file
- `/${DATA}/sat/iasichannels` – list of channels to be used for IASI
- `/${DATA}/sat/IASI_CLDDET.NL` – list of channels to be used for IASI with cloud detection
- `/${DATA}/sat/mask_asc` – radiosonde mask
- `/${DATA}/sat/mietable_dmsp_ssmi` – optical properties of hydrometeors used in the scattering calculations for 1D-Var rain
- `/${DATA}/sat/rmtberr_[noaa|airs|iasi]` – measurement error files
- `/${DATA}/sat/rttov/rtcoef_${platform}_${instrument}.dat` – RTTOV radiative transfer coefficient files, for all current and historic satellite platforms and instruments
- `/${DATA}/sat/scanbias.ssmi` – SSMI scan bias coefficients
- `/${DATA}/sat/[sigmab|correl]` – background error files
- `/${DATA}/sat/ssmi_tovs1c_buf` – ATOVS BUFR template for conversion of SSMI data to 1c-radiances
- `/${DATA}/sat/thin_reo3` – ozone thinning file
- `/${DATA}/scat/mle_norm.dat` – QuikSCAT look-up tables
- `/${DATA}/scat/nscat2.noise` – QuikSCAT noise look-up tables
- `/${DATA}/scat/nscat2.table` – QuikSCAT GMF look-up tables
- `/${DATA}/scat/qscat1.table` – QuikSCAT GMF look-up tables

### 13.6.2 Date-dependent data files

- `/${WDIR}/bl_data_sel` – data selection blacklist
- `/${WDIR}/monthly_bl_mon_monit.b` – monthly monitoring blacklist
- `/${WDIR}/VARBC.cycle.prev` – variational bias correction file from previous cycle
- `/${WDIR}/emiskf.cycle.prev.tar` – emissivity file from previous cycle
- `/${WDIR}/vardir/erss0` – ERS1 scatterometer sigma0 bias correction
- `/${WDIR}/vardir/erssp` – ERS1 scatterometer speed bias correction
- `/${WDIR}/vardir/ascats0` – ASCAT scatterometer sigma0 bias correction
- `/${WDIR}/vardir/ascatsp` – ASCAT scatterometer speed bias correction

## 13.7 OUTPUT GRIB FIELDS

Fields of type ‘4v’ (4D-Var analysis), ‘an’ (analysis), ‘ea’ (analysis errors), ‘ef’ (forecast errors) and ‘me’ (model error) are written in GRIB code to the Fields Data Base from 4D-Var. Fig. 13.4 illustrates the difference between type ‘4v’ and type ‘an’ analysis fields. For type ‘4v’ fields, the analysis increment from the final minimization is interpolated back to high resolution and added to the penultimate high resolution trajectory at its starting point. Analysis fields output from the final high resolution non-linear trajectory are of type ‘4v’, with a base time at the start of the trajectory and a step corresponding to the number of hours into the trajectory. So, for example, for the 1200 UTC 12-hour 4D-Var for date `yyyymmdd`, with an observation window from 0300 to 1500 UTC, the 4D-Var analysis at 1200 UTC is stored in the Fields Data Base and MARS with parameters:

```
date = yyyymmdd, hour = 03, step = 9, type = 4v
```

For type ‘an’ fields, the increment from the final minimization is added to the penultimate high resolution trajectory at the actual analysis time. Fields from the surface analysis are combined with fields from 4D-Var to give the full analysis. For the 1200 UTC 12-hour 4D-Var for date `yyyymmdd`, with an observation window from 0300 to 1500 UTC, the type ‘an’ analysis at 1200 UTC is stored in the Fields Data Base and MARS with parameters:

```
date = yyyymmdd, hour = 12, step = 0, type = an
```

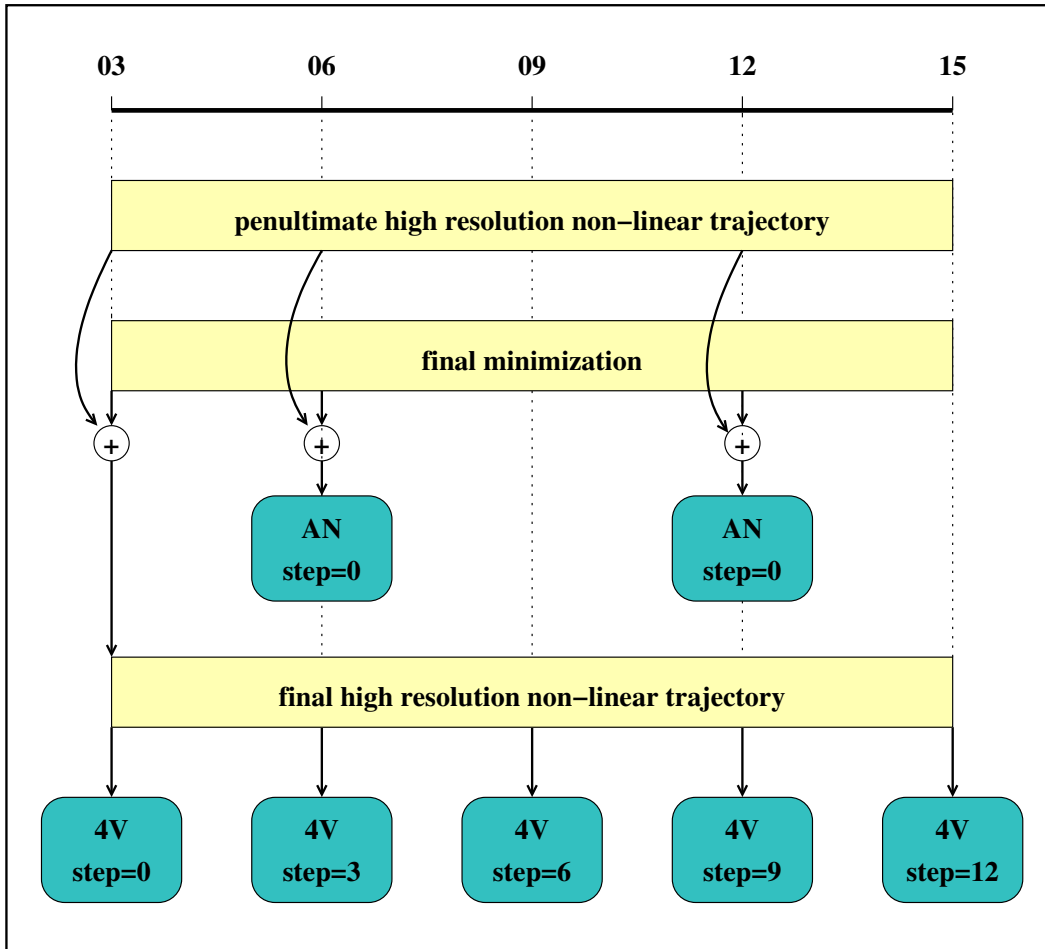


Figure 13.4 Type ‘an’ and type ‘4v’ fields written from 4D-Var to the Fields Data Base.

Output analysis fields, of type ‘4v’ and ‘an’, can be generated on model levels, pressure levels and isentropic surfaces. Namelist NAMFPC controls the content of the post-processing, and there is a wide selection of fields that can be produced. The IFS determines internally whether fields should be generated in spectral or grid-point form. Described below is only the list of fields that are needed as input for the next forecast in order to cycle the data assimilation forward in time. The forecast starts from fields of type ‘an’. Some of the surface fields are generated by the surface analysis jobs, which run at the same time as 4D-Var. It is important that these fields are excluded from the type ‘an’ post-processing of 4D-Var, so that they cannot overwrite the surface analysis fields.

### 13.7.1 Output type ‘an’ model level spectral fields

Table 13.11 Output type ‘an’ model level spectral fields.

Code	Name	Description	Units	Levels
130	T	Temperature	K	1-\$LEVELS
135	W	Vertical velocity	m s <sup>-1</sup>	1-\$LEVELS
138	VO	Vorticity	s <sup>-1</sup>	1-\$LEVELS
152	LNSP	Logarithm of surface pressure		1
155	D	Divergence	s <sup>-1</sup>	1-\$LEVELS



### 13.7.2 Output type ‘an’ model level Gaussian grid-point fields

**Table 13.12** *Output type ‘an’ model level Gaussian grid-point fields.*

Code	Name	Description	Units	Levels
75	CRWC	Cloud rain water content	kg kg <sup>-1</sup>	1-\$LEVELS
76	CSWC	Cloud snow water content	kg kg <sup>-1</sup>	1-\$LEVELS
133	Q	Specific humidity	kg kg <sup>-1</sup>	1-\$LEVELS
203	O3	Ozone mass mixing ratio	kg kg <sup>-1</sup>	1-\$LEVELS
246	CLWC	Cloud liquid water content	kg kg <sup>-1</sup>	1-\$LEVELS
247	CIWC	Cloud ice water content	kg kg <sup>-1</sup>	1-\$LEVELS
248	CC	Cloud cover	(0-1)	1-\$LEVELS

## 13.7.3 Output type ‘an’ surface Gaussian grid-point fields

Table 13.13 Output type ‘an’ surface Gaussian grid-point fields.

Code	Name	Description	Units
015	ALUVP	UV visible albedo for direct radiation	(0-1)
016	ALUVD	UV visible albedo for diffuse radiation	(0-1)
017	ALNIP	Near IR albedo for direct radiation	(0-1)
018	ALNIP	Near IR albedo for diffuse radiation	(0-1)
027	CVL	Low vegetation cover	(0-1)
028	CVH	High vegetation cover	(0-1)
029	TVL	Type of low vegetation	Table index
030	TVH	Type of high vegetation	Table index
032	ASN	Snow albedo	(0-1)
035	ISTL1	Ice surface temperature, layer 1	K
036	ISTL2	Ice surface temperature, layer 2	K
037	ISTL3	Ice surface temperature, layer 3	K
038	ISTL4	Ice surface temperature, layer 4	K
042	SWVL4	Volumetric soil water, layer 4	$\text{m}^3 \text{m}^{-3}$
043	SLT	Soil type	
066	LAI-LV	Leaf area index, low vegetation	$\text{m}^2 \text{m}^{-2}$
067	LAI-HV	Leaf area index, high vegetation	$\text{m}^2 \text{m}^{-2}$
074	SDFOR	Standard deviation of filtered subgrid orography	
128	BV	Budget values	-
129	Z	Orography (geopotential)	$\text{m}^2 \text{s}^{-2}$
134	SP	Surface pressure	Pa
136	TCW	Total column water	$\text{kg m}^{-2}$
137	TCWV	Total column water vapor	$\text{kg m}^{-2}$
148	CHNK	Charnock parameter	
151	MSL	Mean sea level pressure	Pa
160	SDOR	Standard deviation of orography	
161	ISOR	Anisotropy of sub-gridscale orography	
162	ANOR	Angle of sub-gridscale orography	rad
163	SLOR	Slope of sub-gridscale orography	
164	TCC	Total cloud cover	(0-1)
165	10U	10 metre U wind component	$\text{m s}^{-1}$
166	10V	10 metre V wind component	$\text{m s}^{-1}$
172	LSM	Land-sea mask	(0,1)
173	SR	Surface roughness	m
174	ALB	Albedo	(0-1)
186	LCC	Low cloud cover	(0-1)
187	MCC	Medium cloud cover	(0-1)
188	HCC	High cloud cover	(0-1)
198	SRC	Skin reservoir content	m of water
206	TCO3	Total column ozone content	$\text{kg m}^{-2}$
234	LSRH	Logarithm of surface roughness	
235	SKT	Skin temperature	K
236	STL4	Soil temperature level 4	K
228021	FDIR	Total-sky direct solar radiation at surface	$\text{J m}^{-2}$
228022	CDIR	Clear-sky direct solar radiation at surface	$\text{J m}^{-2}$
228246	100U	Wind u component at 100 m	$\text{m s}^{-1}$
228247	100V	Wind v component at 100 m	$\text{m s}^{-1}$

### 13.7.4 Output type ‘an’ wave model fields

The output wave model fields are on a regular latitude/longitude grid. They are identified by stream ‘WAVE’ and are encoded with GRIB codes defined in ECMWF local table 2, Version 140.

**Table 13.14** *Output type ‘an’ wave model fields.*

Code	Name	Description	Units
251	2DFD	2D wave spectra	$\text{m}^2 \text{s} \text{radian}^{-1}$
233	CDWW	Coefficient of drag with waves	
245	WIND	10 metre wind speed	$\text{m s}^{-1}$

### 13.7.5 Output error fields

The forecast errors output from one cycle are used as the background errors input to the next cycle, and their content is described in [Section 13.4.4](#) above. The analysis errors contain similar fields, but are of type ‘ea’. The analysis errors are used to calculate the perturbations for the Ensemble Prediction System.

### 13.7.6 Output model error fields

The model error fields which are output from the analysis are input to the next forecast. Their content is described in [Section 13.4.5](#) above.

## 13.8 OUTPUT OBSERVATION DATA

Departures of observations from the background and the analysis, and quality information are written to the Observation Data Base (ODB). The observation processing is described in more detail in Part I.

## 13.9 OUTPUT DATA FILES

- $\{\text{WDIR}\}/\text{VARBC.cycle}$  – updated variational bias correction file
- $\{\text{WDIR}\}/\text{emiskf.cycle.tar}$  – updated emissivity file

## 13.10 SEA SURFACE TEMPERATURE ANALYSIS

The sea surface temperature analysis is done every 6 hours.

### 13.10.1 Input GRIB fields on model grid

These are extracted from the Fields Data Base. The background fields, of type ‘fc’, are taken from the forecast from the previous 4D-Var analysis time. The persistence analysis, of type ‘an’, is taken from the previous sea surface temperature analysis time, 6 hours earlier (which is not necessarily a 4D-Var analysis time). In the table below, ‘T’ is used to denote the analysis time, and ‘T-6’ is used to denote the persistence analysis time.

**Table 13.15** *Input GRIB fields on model grid.*

Code	Name	Description	Units	Type	Time
031	CI	Sea-ice cover	(0-1)	fc	T
034	SST	Sea surface temperature	K	fc	T
034	SST	Sea surface temperature	K	an	T-6

### 13.10.2 Input OSTIA and NCEP fields

- \$WDIR/surf\_anal/ostia – OSTIA sea surface temperature and sea ice concentration fields, encoded as BUFR data
- \$WDIR/surf\_anal/cfnmc – NCEP sea surface temperature analysis
- \$WDIR/surf\_anal/icenmc – NCEP sea ice analysis

The sea surface temperature analysis and sea ice analysis from NCEP (National Center for Environmental Prediction, Washington) are input on a  $0.5 \times 0.5$  degree regular latitude/longitude grid. These fields are extracted from MARS with parameters:

expver = 1, origin = kwbc

### 13.10.3 Input data files

- \$DATA/sst/lstfil – land/sea mask for NCEP data,  $0.5 \times 0.5$  degree regular latitude/longitude grid,  $720 \times 360$  points
- \$DATA/sst/sst\_clim – surface air temperature monthly climatology, reduced to mean-sea level ( $0.5 \times 0.5$  degree regular latitude/longitude grid,  $720 \times 361$  points)
- \$DATA/sst/ice\_clim – ice monthly climatology
- \${DATA}/climate/\${RESOL}/\${GTYPE}/lsmoro – land/sea mask and orography on model Gaussian grid
- \${DATA}/climate/\${RESOL}/\${GTYPE}/clake – lake mask

### 13.10.4 Output GRIB fields on model grid

The following fields are written to the Fields Data Base:

**Table 13.16** *Output GRIB fields on model grid.*

Code	Name	Description	Units	Type
031	CI	Sea-ice cover	(0-1)	an
034	SST	Sea surface temperature	K	an

## 13.11 2 METRE TEMPERATURE ANALYSIS

The 2 metre temperature analysis is done every 6 hours.

### 13.11.1 Input GRIB fields on model grid

These are extracted from the Fields Data Base. The background fields, of type ‘fc’, are taken from the forecast from the previous 4D-Var analysis time. The invariant fields, of type ‘an’, are taken from the previous 4D-Var analysis.

**Table 13.17** *Input GRIB fields on model grid.*

Code	Name	Description	Units	Type
129	Z	Orography	$m^2 s^{-2}$	an
172	LSM	Land/sea mask	(0-1)	an
139	STL1	Soil temperature level 1	K	fc
167	2T	2 metre temperature	K	fc
168	2D	2 metre dewpoint temperature	K	fc

### 13.11.2 Input observation data

Observations are read from the Observation Data Base.

### 13.11.3 Output GRIB field on model grid

The analysed 2 metre temperature field is written to the Fields Data Base.

**Table 13.18** *Output GRIB field on model grid.*

Code	Name	Description	Units	Type
167	2T	2 metre temperature	K	an

## 13.12 2 METRE RELATIVE HUMIDITY ANALYSIS

The 2 metre relative humidity analysis is done every 6 hours. Although the analysed field is 2 metre relative humidity, the final output product is 2 metre dewpoint temperature. The 2 metre relative humidity analysis cannot start until the 2 metre temperature analysis has completed, since the output from the 2 metre temperature analysis is needed in the computation of the 2 metre dewpoint temperature.

### 13.12.1 Input GRIB fields on model grid

These are extracted from the Fields Data Base. The background fields, of type ‘fc’, are taken from the forecast from the previous 4D-Var analysis time. The invariant fields, of type ‘an’, are taken from the previous 4D-Var analysis.

**Table 13.19** *Input GRIB fields on model grid.*

Code	Name	Description	Units	Type
129	Z	Orography	$\text{m}^2 \text{s}^{-2}$	an
172	LSM	Land/sea mask	(0-1)	an
139	STL1	Soil temperature level 1	K	fc
167	2T	2 metre temperature	K	fc
168	2D	2 metre dewpoint temperature	K	fc

### 13.12.2 Input observation data

Observations are read from the Observation Data Base.

### 13.12.3 Output GRIB field on model grid

The derived 2 metre dewpoint temperature field is written to the Fields Data Base.

**Table 13.20** *Output GRIB field on model grid.*

Code	Name	Description	Units	Type
168	2D	2 metre dewpoint temperature	K	an

## 13.13 SNOW ANALYSIS

The snow analysis is done every 6 hours. It cannot start until the 2 metre temperature analysis has completed, since the 2 metre temperature analysis field is one of the inputs to the snow analysis.

### 13.13.1 Input GRIB fields on model grid

These are extracted from the Fields Data Base. The background fields, of type ‘fc’, are taken from the forecast from the previous 4D-Var analysis time. The invariant fields of type ‘an’, orography and land/sea mask, are taken from the previous 4D-Var analysis. This is denoted T4V in the table below. The persistence snow depth analysis, of type ‘an’, is taken from the previous snow analysis time, 6 hours earlier (which is not necessarily a 4D-Var analysis time). In the table below, ‘T’ is used to denote the snow analysis time, and ‘T-6’ is used to denote the persistence snow analysis time.

**Table 13.21** *Input GRIB fields on model grid.*

Code	Name	Description	Units	Type	Time
129	Z	Orography	$\text{m}^2 \text{s}^{-2}$	an	T4V
172	LSM	Land/sea mask	(0-1)	an	T4V
033	RSN	Snow density	$\text{kg m}^{-3}$	fc	T
141	SD	Snow depth	m of water equivalent	fc	T
141	SD	Snow depth	m of water equivalent	an	T-6
167	2T	2 metre temperature	K	an	T

### 13.13.2 Input data files

- $\{\text{DATA}\}/\text{climate}/\{\text{RESOL}\}\{\text{GTYPE}\}/\text{snow}$  – snow depth climatology (m of water equivalent) on model Gaussian grid
- $\{\text{DATA}\}/\text{climate}/\{\text{RESOL}\}\{\text{GTYPE}\}/\text{cicecap}$  – on model Gaussian grid
- $\$\text{WDIR}/\text{imssnow}$  – NESDIS snow cover field (0,1) on polar stereographic grid of approximately 25 km resolution. The data is in BUFR format, with triplets of latitude/longitude/snow cover. The NESDIS snow cover field is only used once per day, for the 06Z snow analysis.

### 13.13.3 Input observation data

Observations are read from the Observation Data Base.

### 13.13.4 Output GRIB fields on model grid

The following fields are written to the Fields Data Base:

**Table 13.22** *Output GRIB fields on model grid.*

Code	Name	Description	Units	Type
033	RSN	Snow density	$\text{kg m}^{-3}$	an
141	SD	Snow depth	m of water equivalent	an

## 13.14 SOIL MOISTURE ANALYSIS

The soil moisture analysis is done every 6 hours. It cannot start until the sea surface temperature analysis and the snow analysis have completed.

### 13.14.1 Input GRIB fields on model grid

These are extracted from the Fields Data Base. The background fields, of type ‘fc’, are taken from the forecast from the previous 4D-Var analysis time. The analysed fields, of type ‘an’, are output from the current 4D-Var analysis, the sea surface temperature analysis, the 2 metre temperature analysis, the 2 metre relative humidity analysis or the snow analysis.

Table 13.23 Input GRIB fields on model grid.

Code	Name	Description	Units	Type	Origin
039	SWVL1	Volumetric soil water, layer 1	m <sup>3</sup> m <sup>-3</sup>	fc	Forecast
040	SWVL2	Volumetric soil water, layer 2	m <sup>3</sup> m <sup>-3</sup>	fc	Forecast
041	SWVL3	Volumetric soil water, layer 3	m <sup>3</sup> m <sup>-3</sup>	fc	Forecast
133	Q	Specific humidity on lowest model level	kg kg <sup>-1</sup>	fc	Forecast
139	STL1	Soil temperature, level 1	K	fc	Forecast
142	LSP	Large scale precipitation	m	fc	Forecast
143	CP	Convective precipitation	m	fc	Forecast
167	2T	2 metre temperature	K	fc	Forecast
168	2D	2 metre dewpoint temperature	K	fc	Forecast
170	STL2	Soil temperature, level 2	K	fc	Forecast
176	SSR	Surface solar radiation	W m <sup>-2</sup> s	fc	Forecast
183	STL3	Soil temperature level 3	K	fc	Forecast
238	TSN	Temperature of snow layer	K	fc	Forecast
027	CVL	Low vegetation cover	(0-1)	an	4D-Var
028	CVH	High vegetation cover	(0-1)	an	4D-Var
029	TVL	Type of low vegetation	Table index	an	4D-Var
030	TVH	Type of high vegetation	Table index	an	4D-Var
129	Z	Orography	m <sup>2</sup> s <sup>-2</sup>	an	4D-Var
133	Q	Specific humidity on lowest model level	kg kg <sup>-1</sup>	an	4D-Var
141	SD	Snow depth	m of water equivalent	an	Snow analysis
165	10U	10 metre U wind component	m s <sup>-1</sup>	an	4D-Var
166	10V	10 metre V wind component	m s <sup>-1</sup>	an	4D-Var
167	2T	2 metre temperature	K	an	2 metre temp. anal.
168	2D	2 metre dewpoint temperature	K	an	2 metre rel. hum. anal.
172	LSM	Land-sea mask	(0, 1)	an	4D-Var
174	AL	Albedo	(0-1)	an	4D-Var

### 13.14.2 Output GRIB fields on model grid

The following fields are output from the soil moisture analysis and written to the Fields Data Base. Before being written, the *STL1* (soil temperature level 1) field is manipulated as follows:

- (i) land values are unchanged
- (ii) over sea,

$$STL1 = SST \times (1 - CI) + ISTL1 \times CI$$

where

*SST* = analysed sea surface temperature

*CI* = analysed sea ice field, which varies between 0 (open water) and 1 (full ice cover)

*ISTL1* = background soil temperature level 1

**Table 13.24** *Output GRIB fields on model grid.*

Code	Name	Description	Units
039	SWVL1	Volumetric soil water, layer 1	$\text{m}^3 \text{m}^{-3}$
040	SWVL2	Volumetric soil water, layer 2	$\text{m}^3 \text{m}^{-3}$
041	SWVL3	Volumetric soil water, layer 3	$\text{m}^3 \text{m}^{-3}$
042	SWVL4	Volumetric soil water, layer 4	$\text{m}^3 \text{m}^{-3}$
139	STL1	Soil temperature, level 1	K
170	STL2	Soil temperature, level 2	K
183	STL3	Soil temperature, level 3	K
238	TSN	Temperature of snow layer	K

### 13.14.3 Invariant climatological fields

The final step of the soil moisture analysis task is to copy the invariant fields from the climatology files to the analysis, after first manipulating the GRIB headers to give values appropriate for the current data assimilation cycle. In this way, it is ensured that invariant fields remain unchanged, without any loss of precision due to repeatedly encoding and decoding GRIB fields.

**Table 13.25** *Invariant climatological fields.*

Code	Name	Description	Units
015	ALUVP	UV visible albedo for direct radiation	(0-1)
016	ALUVD	UV visible albedo for diffuse radiation	(0-1)
017	ALNIP	Near IR albedo for direct radiation	(0-1)
018	ALNIP	Near IR albedo for diffuse radiation	(0-1)
027	CVL	Low vegetation cover	(0-1)
028	CVH	High vegetation cover	(0-1)
029	TVL	Type of low vegetation	Table index
030	TVH	Type of high vegetation	Table index
043	SLT	Soil type	
129	Z	Orography	$\text{m}^2 \text{s}^{-2}$
160	SDOR	Standard deviation of orography	
161	ISOR	Anisotropy of sub-gridscale orography	
162	ANOR	Angle of sub-gridscale orography	rad
163	SLOR	Slope of sub-gridscale orography	
172	LSM	Land-sea mask	(0,1)
173	SR	Surface roughness	m
174	ALB	Albedo	(0-1)
234	LSRH	Logarithm of surface roughness	



## References

- Alduchov, O. A. and Eskridge, R. E. (1996). Improved Magnus form approximation of saturation vapor pressure. *J. Appl. Meteorol.*, **35**, 601–609.
- Andersson, E., Beljaars, A., Bidlot, J., Miller, M., Simmons, A. and Thépaut, J. N. (2003). A major new cycle of the IFS: Cycle 25r4. *ECMWF Newsletter No. 97*, pp. 12–20.
- Andersson, E., Cardinali, C., Isaksen, L. and Garcia-Mendez, A. (2001). On the impact of frequent data in ECMWF’s 4D-Var scheme: Hourly surface pressure data, European profilers and profiling aircraft data. In *Proc. of the 8th ECMWF Workshop on Meteorological Operational Systems*, pp. 179–183, Reading, 12–16 November, 2001.
- Andersson, E., Fisher, M., Munro, R. and McNally, A. (2000). Diagnosis of background errors for radiances and other observable quantities in a variational data assimilation scheme, and the explanation of a case of poor convergence. *Q. J. R. Meteorol. Soc.*, **126**, 1455–1472.
- Andersson, E. and Garcia-Mendez, A. (2002). Assessment of European wind profiler data, in an NWP context. *ECMWF Tech. Memo. No. 372*.
- Andersson, E., Haseler, J., Undén, P., Courtier, P., Kelly, G., Vasiljevic, D., Brankovic, C., Cardinali, C., Gaffard, C., Hollingsworth, A., Jakob, C., Janssen, P., Klinker, E., Lanzinger, A., Miller, M., Rabier, F., Simmons, A., Strauss, B., Thépaut, J.-N. and Viterbo, P. (1998). The ECMWF implementation of three dimensional variational assimilation (3D-Var). Part III: Experimental results. *Q. J. R. Meteorol. Soc.*, **124**, 1831–1860.
- Andersson, E., Hólm, E. and Thépaut, J. N. (2004). Impact studies of main types of conventional and satellite humidity data. In *Proc. 3<sup>rd</sup> WMO Workshop on The Impact of Various Observing Systems on NWP*, Alpbach, Austria, 9–12 March 2004.
- Andersson, E. and Järvinen, H. (1999). Variational quality control. *Q. J. R. Meteorol. Soc.*, **125**, 697–722.
- Andersson, E., Pailleux, J., Thépaut, J.-N., Eyre, J. R., McNally, A. P., Kelly, G. A. and Courtier, P. (1994). Use of cloud-cleared radiances in three/four-dimensional variational data assimilation. *Q. J. R. Meteorol. Soc.*, **120**, 627–653.
- Bauer, P., Geer, A. J., Lopez, P. and Salmond, D. (2010). Direct 4D-Var assimilation of all-sky radiances: Part I. Implementation. *Q. J. R. Meteorol. Soc.*, **136**, 1868–1885.
- Benedetti, A. and Fisher, M. (2006). Background error statistics for aerosols. *ECMWF Tech. Memo. No. 489*.
- Betts, A. (1997). The parametrization of deep convection: A review. In *Proc. ECMWF Workshop on New Insights and Approaches to Convective Parametrization*, pp. 166–188, Reading, 4–7 November 1996.
- Blackadar, A. K. (1962). The vertical distribution of wind and turbulent exchange in a neutral atmosphere. *J. Geophys. Res.*, **67**, 3095–3102.
- Blondin, C. (1991). Parametrization of land surface processes in numerical weather prediction. In T. J. Schmugge and J.-C. André (Eds), *Land Surface Evaporation: Measurement and Parametrization*, pp. 31–54, Springer-Verlag.

- Bonavita, M., Isaksen, L. and Holm, E. (2012a). On the use of EDA background error variances in the ECMWF 4D-Var. *ECMWF Tech. Memo. No. 664*.
- Bonavita, M., Isaksen, L. and Holm, E. (2012b). On the use of eda background error variances in the ecmwf 4d-var. *Q. J. R. Meteorol. Soc.*, **138**, 1540–1559.
- Bonnell, B., Fouquart, Y., Vanhoutte, J.-C., Fravallo, C. and Rosset, R. (1983). Radiative properties of some african and mid-latitude stratocumulus. *Beitr. Phys. Atmos.*, **56**, 409–428.
- Bormann, N. and Healy, S. (2006). A fast radiative-transfer model for the assimilation of MIPAS limb radiances: Accounting for horizontal gradients. *Q. J. R. Meteorol. Soc.*, **132**, 2357–2376.
- Bormann, N., Healy, S. and Hamrud, M. (2007). Assimilation of MIPAS limb radiances in the ECMWF system. Part II: Experiments with a 2-dimensional observation operator and comparison to retrieval assimilation. *Q. J. R. Meteorol. Soc.*, **133**, in press.
- Bormann, N., Matricardi, M. and Healy, S. (2005). A fast radiative transfer model for the assimilation of infrared limb radiances from MIPAS. *Q. J. R. Meteorol. Soc.*, **131**, 1631–1653.
- Bormann, N., Saarinen, S., Kelly, G. and Thépaut, J.-N. (2003). The spatial structure of observation errors in atmospheric motion vectors from geostationary satellite data. *Mon. Wea. Rev.*, **131**, 706–718.
- Bormann, N. and Thépaut, J.-N. (2007). Assimilation of MIPAS limb radiances in the ECMWF system. Part I: Experiments with a 1-dimensional observation operator. *Q. J. R. Meteorol. Soc.*, **133**, in press.
- Bouttier, F. (2001a). The development of 12-hourly 4D-Var. *ECMWF Tech. Memo. No. 348*.
- Bouttier, F. (2001b). The use of profiler data at ECMWF. *Meteorologische Zeitschrift*, **10**, 497–510.
- Bouttier, F., Derber, J. and Fisher, M. (1997). The 1997 revision of the Jb term in 3D/4D-Var. *ECMWF Tech. Memo. No. 238*.
- Brasnett, B. (1999). A global analysis of snow depth for numerical weather prediction. *J. Appl. Meteorol.*, **38**, 726–740.
- Buck, A. L. (1981). New equations for computing vapor pressure and enhancement factor. *J. Appl. Meteorol.*, **20**, 1527–1532.
- Cardinali, C., Andersson, E., Viterbo, P., Thépaut, J.-N. and Vasiljevic, D. (1994). Use of conventional surface observations in three-dimensional variational data assimilation. *ECMWF Tech. Memo. No. 205*.
- Cardinali, C., Isaksen, L. and Andersson, E. (2003). Use and impact of automated aircraft data in a global 4D-Var data assimilation system. *Mon. Wea. Rev.*, **131**, 1865–1877.
- Courtier, P., Andersson, E., Heckley, W., Pailleux, J., Vasiljevic, D., Hamrud, M., Hollingsworth, A., Rabier, F. and Fisher, M. (1998). The ECMWF implementation of three dimensional variational assimilation (3D-Var). I: Formulation. *Q. J. R. Meteorol. Soc.*, **124**, 1783–1807.
- Courtier, P., Thépaut, J.-N. and Hollingsworth, A. (1994). A strategy for operational implementation of 4D-Var, using an incremental approach. *Q. J. R. Meteorol. Soc.*, **120**, 1367–1388.
- de Rosnay, P., Dragosavac, M., Isaksen, L., Andersson, E. and Haseler, J. (2011a). Use of new snow data from sweden in ifs cycle 36r4. *ECMWF Res. Dept. Memo. No. 1139*.
- de Rosnay, P., drusch, M., Balsamo, G., Albergel, C. and Isaksen, L. (2011b). Extended kalman filter soil-moisture analysis in the ifs. *ECMWF No. 127*, pp. 12–16.
- Deblonde, G. and English, S. (2001). Evaluation of the fastem-2 fast microwave oceanic surface emissivity model. In *Tech. Proc. ITSC-XI*, pp. 67–78, Budapest.
- Dee, D. (2004). Variational bias correction of radiance data in the ECMWF system. In *Proc. of the ECMWF Workshop on Assimilation of High Spectral Resolution Sounders in NWP*, pp. 97–112, Reading, 28 June–1 July, 2004.

- Dee, D. P., Uppala, S. M., Simmons, A. J., Berrisford, P., Poli, P. *et al.* (2011). The ERA-Interim reanalysis: configuration and performance of the data assimilation system. *Q. J. R. Meteorol. Soc.*, **137**, 553–597.
- Dent, D., Hoffmann, G.-R., Janssen, P. A. E. M. and Simmons, A. J. (1997). Use of the Fujitsu VPP700 for weather forecasting at ECMWF. *ECMWF Tech. Memo. No. 235*.
- Derber, J. C. and Bouttier, F. (1999). A reformulation of the background error covariance in the ECMWF global data assimilation system. *Tellus*, **51A**, 195–221.
- Dethof, A. and Holm, E. (2004). Ozone assimilation in the ERA-40 reanalysis project. *Q. J. R. Meteorol. Soc.*, **130**, 2851–2872.
- Douville, H., Viterbo, P., Mahfouf, J.-F. and Beljaars, A. C. M. (2001). Evaluation of the optimum interpolation and nudging techniques for soil moisture analysis using FIFE data. *Mon. Wea. Rev.*, **128**, 1733–1756.
- Drusch, M., Scipal, K., de Rosnay, P., Balsamo, G., Andersson, E., Bougeault, P. and Viterbo, P. (2009). Towards a Kalman Filter based soil moisture analysis system for the operational ECMWF Integrated Forecast System. *G. Res. Lett.*, **36**, L10401, doi:10.1029/2009GL037716.
- Drusch, M., Vasiljevic, D. and Viterbo, P. (2004). ECMWF’s global snow analysis: Assessment and revision based on satellite observations. *J. Appl. Meteorol.*, **43**(9), 1282–1294.
- Dubuisson, P. J., Buriez, J. and Fouquart, Y. (1996). High spectral solar radiative transfer in absorbing and scattering media: Application to the satellite simulation. *J. Quant. Spectrosc. Radiat. Transfer*, **55**, 103–126.
- Ebert, E. E. and Curry, J. A. (1992). A parametrization of ice optical properties for climate models. *J. Geophys. Res.*, **97D**, 3831–3836.
- Engelen, R. J., Andersson, E., Chevallier, F., Hollingsworth, A., Matricardi, M., McNally, A., Thépaut, J.-N. and Watts, P. (2004). Estimating atmospheric CO<sub>2</sub> from advanced infrared satellite radiances within an operational 4D-Var data assimilation system: Methodology and first results. *J. Geophys. Res.*, **109**, D19309.
- Eyre, J. R. (1991). A fast radiative transfer model for satellite sounding systems. *ECMWF Tech. Memo. No. 176*.
- Fisher, M. (1996). The specification of background error variances in the ECMWF variational analysis system. In *Proc. ECMWF Workshop on Non-linear Aspects of Data Assimilation*, pp. 645–652, Reading, 9–11 September 1996.
- Fisher, M. (1998). Minimization algorithms for variational data assimilation. In *Proc. ECMWF Seminar on Recent Developments in Numerical Methods for Atmospheric Modelling*, pp. 364–385, Reading, 7–11 September 1998.
- Fisher, M. (2003). Background error covariance modelling. In *Proc. ECMWF Seminar on Recent Developments in Data Assimilation for Atmosphere and Ocean*, pp. 45–64, Reading, 8–12 Sept 2003.
- Fisher, M. (2004). Generalized frames on the sphere, with application to the background error covariance modelling. In *Proc. ECMWF Seminar on Recent Developments in Numerical Methods for Atmospheric and Ocean Modelling*, pp. 87–102, Reading, 6–10 September 2004.
- Fisher, M. (2006). Wavelet jb - a new way to model the statistics of background errors. *ECMWF Newsletter No. 106*, pp. 23–28.
- Fisher, M. and Andersson, E. (2001). Developments in 4D-Var and Kalman Filtering. *ECMWF Tech. Memo. No. 347*.
- Fisher, M. and Courtier, P. (1995). Estimating the covariance matrices of analysis and forecast error in variational data assimilation. *ECMWF Tech. Memo. No. 220*.

- Fisher, M., Tremolet, Y., Auvinen, H., Tan, D. and Poli, P. (2011). Weak-Constraint and Long-Window 4D-Var. *ECMWF Tech. Memo. No. 655*.
- Fouquart, Y. (1987). Radiative transfer in climate models. In M. E. Schlesinger (Ed.), *Physically Based Modelling and Simulation of Climate and Climate Changes*, pp. 223–284, Kluwer Acad. Publ.
- Fouquart, Y. and Bonnel, B. (1980). Computations of solar heating of the earth’s atmosphere: A new parametrization. *Beitr. Phys. Atmos.*, **53**, 35–62.
- Fritts, D. C. and Nastrom, D. D. (1993). Spectral estimates of gravity wave energy and momentum fluxes. Part I: Energy dissipation, acceleration, and constraints. *J. Atmos. Sci.*, **50**, 3685–3694.
- Gauthier, P. and Thépaut, J.-N. (2001). Impact of the digital filter as a weak constraint in the preoperational 4DVAR assimilation system of Meteo-France. *Mon. Wea. Rev.*, **129**, 2089–2102.
- Geer, A. J. and Bauer, P. (2011a). Assimilating amsu-a radiances sensitive to cloud and temperature using the all-sky approach. *ECMWF technical memorandum, in preparation*.
- Geer, A. J. and Bauer, P. (2011b). Observation errors in all-sky data assimilation. *Q. J. R. Meteorol. Soc.*, DOI: 10.1002/qj.830.
- Geer, A. J., Bauer, P. and Lopez, P. (2008). Lessons learnt from the operational 1D+4D-Var assimilation of rain- and cloud-affected SSM/I observations at ECMWF. *Q. J. R. Meteorol. Soc.*, **134**, 1513–1525.
- Geer, A. J., Bauer, P. and Lopez, P. (2010). Direct 4D-Var assimilation of all-sky radiances: Part II. Assessment. *Q. J. R. Meteorol. Soc.*, **136**, 1886–1905.
- Geleyn, J.-F. (1988). Interpolation of wind, temperature and humidity values from the model levels to the height of measurement. *Tellus*, **40**, 347–351.
- Geleyn, J.-F. and Hollingsworth, A. (1997). An economical and analytical method for the interactions between scattering and line absorption of radiation. *Contrib. to Atmos. Phys.*, **52**, 1–16.
- Gilbert, J. C. and Lemaréchal, C. (1989). Some numerical experiments with variable storage quasi-Newton algorithms. *Math. Prog.*, **B25**, 407–435.
- Gustafsson, N. (1992). Use of a digital filter as a weak constraint in variational data assimilation. In *Proc. ECMWF Workshop on Variational Data Assimilation with Special Emphasis on 3-dimensional Aspects*, pp. 327–338, Reading, 9–12 November, 1992.
- Haseler, J. (2004). Early-delivery suite. *ECMWF Tech. Memo. No. 454*.
- Healy, S. and Thépaut, J.-N. (2006). Assimilation experiments with CHAMP GPS radio occultation measurements. *Q. J. R. Meteorol. Soc.*, **132**, 605–623.
- Hersbach, H. (2010a). Assimilation of scatterometer data as equivalent-neutral wind. *ECMWF Tech. Memo. No. 629*.
- Hersbach, H. (2010b). Comparison of c-band scatterometer cmod5.n equivalent neutral winds with ecmwf. *J. Atmos. Oceanic Technol.*, **27**, 721–736.
- Hersbach, H. (2011). Sea surface roughness and drag coefficient as functions of neutral wind speed. *J. Phys. Oceanogr.*, **41**, 247–251.
- Hersbach, H., Stoffelen, A. and de, S. H. (2007). An improved C-band scatterometer ocean geophysical model function: CMOD5. *J. Geophys. Res.*
- Hólm, E., Andersson, E., Beljaars, A., Lopez, P., Mahfouf, J.-F., Simmons, A. J. and Thépaut, J.-N. (2002). Assimilation and modeling of the hydrological cycle: ECMWF’s status and plans. *ECMWF Tech. Memo. No. 383*.
- Huddleston, J. N. and Stiles, B. W. (2000). Multidimensional histogram (MUDH) rain flag. *Product Description Version 2.1*, URL <http://podaac-www.jpl.nasa.gov/quikscat/>.

- Ingleby, N. B. and Lorenc, A. C. (1993). Bayesian quality control using multivariate normal distributions. *Q. J. R. Meteorol. Soc.*, **119**, 1195–1225.
- Isaksen, L. (1997). Impact of ERS scatterometer data in the ECMWF 4D-Var assimilation system. Preliminary studies. In *Space at the Service of our Environment*, pp. 1829–1851, Florence, Italy, May 1997, ESTEC, European Space Agency [SP-414]. Available from ESA Publications Division, ESTEC Noordwijk, The Netherlands.
- Isaksen, L., Bonavita, M., Buizza, R., Fisher, M., Haseler, J. and Raynaud, L. (2010). Ensemble of data assimilations at ecmwf. *ECMWF Tech. Memo. No. 636*.
- Isaksen, L. and Janssen, P. A. E. M. (2004). Impact of ERS scatterometer winds in ECMWF’s assimilation. *Q. J. R. Meteorol. Soc.*, **130**, 1793–1814.
- Isaksen, L. and Stoffelen, A. C. M. (2000). ERS scatterometer wind data impact on ECMWF’s tropical cyclone forecasts. *IEEE Trans. Geosci. Remote Sens.*, **38**, 1885–1892.
- Jakob, C. and Siebesma, A. P. (2003). A new subcloud model for mass flux convection schemes. influence on triggering, updraught properties and model climate. *Mon. Wea. Rev.*, **131**, 2765–2778.
- Janisková, M., Mahfouf, J.-F., Morcrette, J.-J. and Chevallier, F. (2002). Linearized radiation and cloud schemes in the ECMWF model: Development and evaluation. *Q. J. R. Meteorol. Soc.*, **128**, 1505–1527.
- Järvinen, H., Andersson, E. and Bouttier, F. (1999). Variational assimilation of time sequences of surface observations with serially correlated errors. *ECMWF Tech. Memo. No. 266*.
- Järvinen, H., Saarinen, S. and Undén, P. (1996). *User’s Guide for Blacklisting*. Available on request from ECMWF, Shinfield Park, RG2 9AX, Reading, Berkshire, UK.
- Järvinen, H. and Undén, P. (1997). Observation screening and first guess quality control in the ECMWF 3D-Var data assimilation system. *ECMWF Tech. Memo. No. 236*.
- Karbou, F., Gérard, E. and Rabier, F. (2006). Microwave land emissivity and skin temperature for AMSU-A and -B assimilation over land. *Q. J. R. Meteorol. Soc.*, **132**, 2333–2355.
- Kelly, G. (2007). The evaluation of the hirs/4 instrument on metop 2 by using the ecmwf data assimilation system to provide a reference to compare with other sensors. *ECMWF Tech. Memo. No. 523*.
- Kelly, G., Andersson, E., Hollingsworth, A., Lönnberg, P., Pailleux, J. and Zhang, Z. (1991). Quality control of operational physical retrievals of satellite sounding data. *Mon. Wea. Rev.*, **119**, 1866–1880.
- Kelly, G. and Pailleux, J. (1988). Use of satellite vertical sounder data in the ECMWF analysis system. *ECMWF Tech. Memo. No. 143*.
- Kessler, E. (1969). *On the distribution and continuity of water substance in atmospheric circulation, Meteorological Monographs*, Vol. 10. Am. Meteorol. Soc., Boston, MA.
- Klinker, E., Rabier, F., Kelly, G. and Mahfouf, J. F. (2000). The ECMWF operational implementation of four-dimensional variational assimilation. Part I: Experimental results and diagnostics with operational configuration. *Q. J. R. Meteorol. Soc.*, **126**, 1191–1215.
- Köpken, C., Kelly, G. and Thépaut, J.-N. (2004). Assimilation of Meteosat radiance data within the 4D-Var system at ECMWF: Assimilation experiments and forecast impact. *Q. J. R. Meteorol. Soc.*, **130**, 2277–2292.
- Krzeminski, B., Bormann, N., Karbou, F. and Bauer, P. (2009). Improved use of surface-sensitive microwave radiances at ECMWF. In *Proceedings of 2009 EUMETSAT Meteorological Satellite Conference*, Bath, United Kingdom.
- Leidner, S. M., Hoffman, R. N. and Augenbaum, J. (2000). *SeaWinds Scatterometer Real-Time BUFR Geophysical Data Product, User’s Guide Version 2.3.0*. NOAA/NESDIS.

- Lönnerberg, P. (1989). Developments in the ECMWF analysis system. In *Proc. ECMWF Seminar on Data assimilation and the Use of Satellite Data*, pp. 75–119, Reading, 5–9 September 1988.
- Lönnerberg, P. and Shaw, D. (1985). Data selection and quality control in the ECMWF analysis system. In *ECMWF Workshop on The Use And Quality Control of Meteorological Observations*, pp. 225–254, Reading, 6–9 November 1984.
- Lönnerberg, P. and Shaw, D. (Eds) (1987). *ECMWF Data Assimilation Scientific Documentation, Research Manual 1*.
- Lopez, P. and Moreau, E. (2005). A convection scheme for data assimilation: Description and initial tests. *Q. J. R. Meteorol. Soc.*, **131**, 409–436.
- Lorenc, A. C. (1986). Analysis methods for numerical weather prediction. *Q. J. R. Meteorol. Soc.*, **112**, 1177–1194.
- Lorenc, A. C. (1988). Optimal nonlinear objective analysis. *Q. J. R. Meteorol. Soc.*, **114**, 205–240.
- Lott, F. and Miller, M. J. (1997). A new subgrid-scale orographic drag parametrization: Its formulation and testing. *Q. J. R. Meteorol. Soc.*, **123**, 101–127.
- Louis, J.-F. (1979). A parametric model of vertical eddy fluxes in the atmosphere. *Boundary-Layer Meteorol.*, **17**, 187–202.
- Louis, J.-F., Tiedtke, M. and Geleyn, J.-F. (1982). A short history of the PBL parametrization at ECMWF. In *Proc. ECMWF Workshop on Planetary Boundary Layer Parameterization*, pp. 59–80, Reading, 25–27 November, 1981.
- Lynch, P. (1993). Digital Filters for Numerical Weather Prediction. *HIRLAM Technical Report No. 10*.
- Lynch, P. (1997). The Dolph-Chebyshev Window: A simple optimal filter. *Mon. Wea. Rev.*, **125**, 655–660.
- Machenhauer, B. (1977). On the dynamics of gravity oscillations in a shallow water model, with application to normal mode initialization. *Contrib. Atmos. Phys.*, **50**, 253–271.
- Mahfouf, J.-F. (1991). Analysis of soil moisture from near surface parameters: A feasibility study. *J. Appl. Meteorol.*, **30**, 1534–1547.
- Mahfouf, J.-F. (1999). Influence of physical processes on the tangent-linear approximation. *Tellus*, **51A**, 147–166.
- Mahfouf, J. F. and Rabier, F. (2000). The ECMWF operational implementation of four-dimensional variational assimilation. Part I: Experimental results with improved physics. *Q. J. R. Meteorol. Soc.*, **126**, 1171–1190.
- Matricardi, M., Chevallier, F. and Tjemkes, S. (2001). An improved fast radiative transfer model for the assimilation of radiance observations. *ECMWF Tech. Memo. No. 345*.
- McNally, A. P. (2009). The direct assimilation of cloud affected satellite infrared radiances in the ecmwf 4d-var. *Q. J. R. Meteorol. Soc.*, **135**, 1214–1229.
- McNally, A. P., Andersson, E., Kelly, G. and Saunders, R. W. (1999). The use of raw TOVS/ATOVS radiances in the ECMWF 4D-Var assimilation system. *ECMWF Newsletter No. 83*, pp. 2–7.
- McNally, A. P. and Watts, P. D. (2003). A cloud detection algorithm for high spectral resolution infrared sounders. *Q. J. R. Meteorol. Soc.*, **129**, 3411–3423.
- Mlawer, E., Taubman, S. J., Brown, P. D., Iano, M. and Clough, S. A. (1997). Radiative transfer for inhomogeneous atmospheres: RRTM a validated correlated-k model for the longwave. *J. Geophys. Res.*, **102**, 16663–16682.

- Morcrette, J.-J. (1989). Description of the radiation scheme in the ECMWF operational weather forecast model. *ECMWF Tech. Memo. No. 165*.
- Morcrette, J.-J. (1991). Radiation and cloud radiative properties in the ECMWF operational forecast model. *J. Geophys. Res.*, **96D**, 9121–9132.
- Morcrette, J.-J. (2000). On the effects of the temporal and spatial sampling of radiation fields on the ECMWF forecasts and analyses. *Mon. Wea. Rev.*, **128**, 876–887.
- Morcrette, J.-J., Smith, L. and Fouquart, Y. (1986). Pressure and temperature dependence of absorption in longwave radiation parametrizations. *Beitr. Phys. Atmos.*, **59**, 455–469.
- Munro, R., Köpken, C., Kelly, G., Thépaut, J.-N. and Saunders, R. (2004). Assimilation of Meteosat radiance data within the 4D-Var system at ECMWF: Data quality monitoring, bias correction and single-cycle experiments. *Q. J. R. Meteorol. Soc.*, **130**, 2293–2313.
- Orr, A., Bechtold, P., Scinocca, J., Ern, M. and Janisková, M. (2010). Improved middle atmosphere climate and analysis in the ECMWF forecasting system through a non-orographic gravity wave parametrization. *J. Climate*, **23**, 5905–5926.
- Ou, S. and Liou, K.-N. (1995). Ice microphysics and climate temperature feedback. *Atmosph. Research*, **35**, 127–138.
- Pailleux, J. (1990). A global variational assimilation scheme and its application for using TOVS radiances. In *Proc. WMO International Symposium on Assimilation of Observations in Meteorology and Oceanography*, pp. 325–328, Clermont-Ferrand, France.
- Rabier, F. and Courtier, P. (1992). Four-dimensional assimilation in the presence of baroclinic instability. *Q. J. R. Meteorol. Soc.*, **118**, 649–672.
- Rabier, F., Järvinen, H., Klinker, E., Mahfouf, J.-F. and Simmons, A. (2000). The ECMWF operational implementation of four-dimensional variational assimilation. Part I: Experimental results with simplified physics. *Q. J. R. Meteorol. Soc.*, **126**, 1143–1170.
- Rabier, F., McNally, A., Andersson, E., Courtier, P., Undén, P., Eyre, J., Hollingsworth, A. and Bouttier, F. (1998). The ECMWF implementation of three dimensional variational assimilation (3D-Var). II: Structure functions. *Q. J. R. Meteorol. Soc.*, **124**, 1809–1829.
- Radnóti, G., Trémolet, Y., Andersson, E., Isaksen, L., Hólm, E. and Janisková, M. (2005). Diagnostics of linear and incremental approximations in 4d-var revisited for higher resolution. *ECMWF Tech. Memo. No. 467*.
- Saunders, R. W. and Matricardi, M. (1998). A fast forward model for ATOVS (RTATOV). In *Tech. Proc. 9th International TOVS Study Conference*, p. 11 pp, Igls, Austria, 20–26 February, 1997.
- Savijärvi, H. (1995). Error growth in a large numerical forecast system. *Mon. Wea. Rev.*, **123**, 212–221.
- Scinocca, J. F. (2003). An accurate spectral nonorographic gravity wave drag parameterization for general circulation models. *J. Atmos. Sci.*, **60**, 667–682.
- Sherlock, V. J. (1999). ISEM-6: Infrared Surface Emissivity Model for RRTOV-6. *Forecasting Research Technical Report No. 299*, available from Met Office, London Road, Bracknell, Berkshire RG12 2SZ, UK.
- Simmons, A. J. and Burridge, D. (1981). An energy and angular momentum conserving vertical finite difference scheme and hybrid coordinate. *Mon. Wea. Rev.*, **109**, 758–766.
- Simmons, A. J. and Chen, J. (1991). The calculation of geopotential and the pressure gradient in the ECMWF atmospheric model: Influence on the simulation of the polar atmosphere and on temperature analyses. *Q. J. R. Meteorol. Soc.*, **117**, 29–58.

- Smith, E. A. and Shi, L. (1992). Surface forcing of the infrared cooling profile over the Tibetan plateau. Part I: Influence of relative longwave radiative heating at high altitude. *J. Atmos. Sci.*, **49**, 805–822.
- Stark, J. D., Donlon, C. J., Martin, M. J. and McCulloch, M. E. (2007). Ostia : An operational, high resolution, real time, global sea surface temperature analysis system. *Oceans '07 IEEE Aberdeen, conference proceedings. Marine challenges: coastline to deep sea. Aberdeen, Scotland. IEEE*.
- Stoffelen, A. and Anderson, D. (1997). Ambiguity removal and assimilation of scatterometer data. *Q. J. R. Meteorol. Soc.*, **123**, 491–518.
- Sundqvist, H., Berge, E. and Kristjánsson, J. E. (1989). Condensation and cloud parameterization studies with a mesoscale numerical weather prediction model. *Mon. Wea. Rev.*, **117**, 1641–1657.
- Talagrand, O. (1997). Assimilation of observations, an Introduction. *J. Meteorol. Soc. Japan*, **75**, N.1B,191–209.
- Tavolato, C. and Isaksen, L. (2010). Huber norm quality control in the IFS. *ECMWF Newsletter No. 122*, pp. 27–31.
- Temperton, C. (1988). Implicit normal mode initialization. *Mon. Wea. Rev.*, **116**, 1013–1031.
- Temperton, C. (1989). Implicit normal mode initialization for spectral models. *Mon. Weather Rev.*, **117**, 436–451.
- Thépaut, J.-N. and Andersson, E. (2003). Assimilation of high-resolution satellite data. *ECMWF Newsletter No. 97*, pp. 6–12.
- Tomassini, M., LeMeur, D. and Saunders, R. W. (1998). Near-surface satellite wind observations of hurricanes and their impact on ECMWF model analyses and forecasts. *Mon. Wea. Rev.*, **126**, 1274–1286.
- Tompkins, A. and Janisková, M. (2004). A cloud scheme for data assimilation: Description and initial tests. *Q. J. R. Meteorol. Soc.*, **130**, 2495–2518.
- Trémolet, Y. (2003). Model error in variational data assimilation. In *Proc. ECMWF Seminar on Recent Developments in Data Assimilation for Atmosphere and Ocean*, pp. 361–367, Reading, 8–12 Sept 2003.
- Trémolet, Y. (2004). Diagnostics of linear and incremental approximations in 4D-Var. *Q. J. R. Meteorol. Soc.*, **130**, 2233–2251.
- Trémolet, Y. (2005). Incremental 4d-var convergence study. *ECMWF Tech. Memo. No. 469*.
- Uppala, S. M. *et al.* (2005). The ERA-40 re-analysis. *Q. J. R. Meteorol. Soc.*, **131**, 2961–3012.
- Vasiljevic, D., Cardinali, C. and Undén, P. (1992). ECMWF 3D-Variational assimilation of conventional observations. In *Proc. ECMWF Workshop on Variational Assimilation with Emphasis on Three-dimensional Aspects*, Reading, 9–12 November 1992.
- Veerse, F. and Thépaut, J. N. (1998). Multiple-truncation incremental approach for four-dimensional variational data assimilation. *Q. J. R. Meteorol. Soc.*, **124**, 1889–1908.
- Vialard, J., Vitart, F., Balmaseda, M., Stockdale, T. and anderson, D. (2005). An ensemble generation method for seasonal forecasting with an ocean-atmosphere coupled model. *Mon. Wea. Rev.*, **133**, 441–453.
- Warner, C. D. and McIntyre, M. E. (1996). An ultra-simple spectral parametrization for non-orographic gravity waves. *J. Atmos. Sci.*, **58**, 1837–1857.
- Washington, W. M. and Williamson, D. L. (1977). A description of the NCAR GCMs. GCMs of the atmosphere. j. chang, ed. *Methods in Computational Physics*, **17**, 111–172, Academic Press.
- Wergen, W. (1987). Diabatic nonlinear normal mode initialisation for a spectral model with a hybrid vertical coordinate. *ECMWF Tech. Report No. 59*.